

DEVELOPING A SYSTEM TO MEASURE RHEOLOGY OF CONDITIONED SOIL FOR
SOFT-GROUND TBM TUNNELING

by
Wei Hu

Copyright by Wei Hu 2020
All Rights Reserved

A thesis submitted to the Faculty and the Board of Trustee of the Colorado School of Mines in partial fulfillment of the requirements for the degree of Doctor of Philosophy (Underground Construction and Tunneling Engineering).

Golden, Colorado

Date: _____

Signed: _____

Wei Hu

Signed: _____

Dr. Jamal Rostami

Thesis Advisor and Department Head

Mining Engineering Department

Golden, Colorado

Date: _____

Signed: _____

Dr. Michael Mooney

Degree Program Director

Underground Construction and Tunnel Engineering

ABSTRACT

Driven by the unprecedented process of urbanization across the globe and rise of need in infrastructure such as transportation, water, sewer, utilities, storage space, etc., the world has witnessed rapid expansion of the tunneling and underground construction industry in the past few decades. Among all tunnel construction methods, the growth of soft-ground tunneling using Earth Pressure Balance (EPB) Tunnel Boring Machines (TBMs) has been the most significant. EPB TBMs use the excavated muck in the machine chamber as a supporting medium before moving it to the muck haulage system. This is conducted to achieve the desired functionality of the conditioned muck, such as maintaining face stability while ensuring the designed advancing rate. To modify the behaviors of the muck, soil conditioners are often injected to the tunnel face and the machine chamber so the conditioned muck will exhibit certain properties such as good balance between flowability and viscosity, low abrasiveness, and low stickiness. There is no universally accepted approach for evaluation of these properties, leading to the current industry trend of using trial-and-error evaluation approaches.

The primary purpose of this thesis was to develop a new system for large-scale measurement of the rheology of conditioned soil for application in EPB TBM tunneling. The development is presented in three phases:

1. The first phase was to evaluate the feasibility of measuring the rheology of conditioned soil using existing conventional small-scale rheometers designed for liquid testing in industries such as biological and chemical engineering. The results show that the small-scale rheometers are capable of testing the yield stress and viscosity of liquid using oscillation sweep and strain ramp methods. The gaps between the vanes and the cells of the rheometers, however, are not large enough to accommodate the free flow of soils containing coarse sand or even larger particles. The torque and axial force capacities of the rheometers are also insufficient to test firm soils. It was therefore necessary to develop a large-scale rheology measurement system for evaluating rheology of conditioned soil in the context of EPB tunneling applications.

2. The second phase was to develop a large-scale rheology measurement system and conduct preliminary testing to verify the viability of the proposed system for assessment and measurement of soil rheology. Built upon the prototype of the existing Soil Abrasion Index (SAI) testing machine, a Variable Frequency Drive (VFD) was incorporated to allow for control of the rotational speed of the propeller. The pitched propeller was used as a preliminary configuration for

assessment of the shear resistance vs. shear rate relationship for various mediums. Several steps were taken to establish the feasibility of the system, including device calibration in air and water, testing on a poorly graded sand with different water content conditions, and back analyses of rheological parameters using Computational Fluid Dynamics (CFD) modeling. The results demonstrate that the system of combining lab experiment and CFD modeling is a feasible method to determine rheology of conditioned soil. The Bingham plastic model is shown to be a suitable model to represent the rheology of conditioned soil. The operational range of the system's rotational speed for this purpose is between 3 rpm and 60 rpm. Furthermore, a parametric study using CFD modeling was conducted to evaluate the optimal configuration of the propeller. The results show that the auger geometry with a similar diameter to that of the existing pitched propeller is the optimized configuration for measurement of soil rheology.

3. The third phase was to verify the system with an auger propeller by testing various scenarios including different soil types with various water content conditions and conditioning parameters (i.e., Foaming Agent Concentration, Foam Injection Ratio, Foam Expansion Ratio), test durations, ambient pressures, and compressibility settings in CFD models. A general measurement protocol was set up for future assessment. The results proved the ability of the system in measuring the variation in the rheology of the soil mix, using different conditioning parameters.

A preliminary study was conducted to assess the preparation and rheology evaluation of conditioned clayey soils. For testing rheology of foam conditioned clay, the major challenge was to mix clay and foam homogeneously in a timely manner. Six different mixing methods were tested, and none of them proved to provide a quality clay-foam mixture for subsequent rheology testing. For clay clogging evaluation, mixtures of clayey soil at various water content levels were tested in the proposed rheometer with the goal of finding the possible impact of surcharge loading on clay clogging potential using propeller torque as an indicator. The results show high variability in torque with respect to different surcharge loading. Due to the torque limit of the rheometer, limited testing of the clay at water content near plastic limit was conducted, which showed high tendency of clogging.

With the newly developed rheology measurement system, soils with different natural compositions may be conditioned with various soil conditioning agents such as water and foam, and the rheology of the conditioned soils can be characterized. This will lead to establishing a

database of soil rheology based on soil conditioning parameters, which can be combined with CFD modeling of EPBMs to predict the machine response and optimize soil conditioning practices.

TABLE OF CONTENTS

ABSTRACT.....	iii
LIST OF FIGURES.....	ix
LIST OF TABLES.....	xiv
ACKNOWLEDGEMENTS.....	xv
CHAPTER 1 INTRODUCTION.....	1
1.1 Overview.....	1
1.2 Research objectives.....	3
1.3 Methodologies.....	3
1.4 Thesis organization.....	3
CHAPTER 2 LITERATURE REVIEW.....	6
2.1 Mixing challenge for foam conditioned soil.....	6
2.2 Evaluating the properties of conditioned soil.....	7
2.2.1 Permeability.....	7
2.2.2 Compressibility.....	8
2.2.3 Strength.....	8
2.2.4 Stickiness.....	8
2.3 Soil abrasion.....	9
2.4 Clay clogging.....	9
2.5 Rheology of conditioned soil.....	10
2.6 Real-time determination of muck behavior and machine operation.....	10
2.7 Knowledge gaps.....	12
CHAPTER 3 MEASURING RHEOLOGY OF CONDITIONED SOIL USING CONVENTIONAL SMALL-SCALE DEVICES.....	14
3.1 Abstract.....	14
3.2 Introduction.....	14
3.3 Soil samples and testing methods.....	18
3.3.1 Soil.....	18
3.3.2 Testing with ARES-G2 rheometer.....	20
3.3.3 Testing with Discovery HR-3 rheometer.....	23
3.4 Results and analysis.....	25
3.4.1 ARES-G2 rheometer testing results.....	25

3.4.2	HR-3 rheometer testing results	32
3.5	Conclusions.....	36
CHAPTER 4 A NEW METHOD TO QUANTIFY RHEOLOGY OF CONDITIONED SOIL FOR APPLICATION IN EPB TBM TUNNELING.....38		
4.1	Abstract.....	38
4.2	Introduction.....	38
4.3	Proposed soil rheology evaluation method.....	40
4.3.1	Overview.....	40
4.3.2	Preliminary testing.....	41
4.3.3	Computational Fluid Dynamics (CFD) Modeling	43
4.4	Preliminary testing and modeling results	45
4.4.1	Device calibration with air and water	45
4.4.2	Testing on sand	47
4.4.3	Back analysis of rheological parameters using CFD models.....	53
4.4.4	Comparisons of various propeller designs	56
4.5	Discussions	66
4.6	Conclusions.....	67
CHAPTER 5 DEVELOPMENT OF A SYSTEM TO MEASURE RHEOLOGY OF CONDITIONED SOIL FOR APPLICATION IN SOFT-GROUND TUNNELING.....69		
5.1	Abstract.....	69
5.2	Introduction.....	69
5.3	Background.....	72
5.3.1	General review	72
5.3.2	Rheology study of conditioned soil in EPB tunneling application.....	74
5.4	Proposed rheology evaluation method in the previous study	76
5.4.1	Overview.....	76
5.4.2	Summary of previous development	76
5.5	Current improved protocol for soil rheology measurement	78
5.5.1	Measurement system components	78
5.5.2	Testing materials.....	80
5.5.3	Sample preparation	83

5.5.4	Testing procedures	86
5.6	Results and analyses	92
5.6.1	Effect of auger geometry on torque response	92
5.6.2	Effect of ramping sequence on torque response	94
5.6.3	Effect of compressibility setting in CFD on calculated torque.....	98
5.6.4	Effect of soil type on soil rheology.....	99
5.6.5	Effect of water content on soil rheology.....	103
5.6.6	Effect of foam conditioner on soil rheology.....	106
5.6.7	Effect of passing of time on torque response.....	115
5.6.8	Effect of ambient pressure on torque response.....	115
5.7	Discussions	118
5.8	Conclusions.....	119
CHAPTER 6 ADVANCING STUDY OF RHEOLOGY OF CONDITIONED CLAY FOR APPLICATION IN EPB TBM TUNNELING.....		121
6.1	Introduction.....	121
6.1.1	Challenges for testing rheology of conditioned clay	121
6.1.2	Objectives and materials.....	122
6.2	Methods of preparation of conditioned clay	123
6.2.1	Mixing clay with liquid.....	123
6.2.2	Mixing clay with foam.....	126
6.3	Evaluation of rheology of clay and sand mixture	126
6.4	Evaluation of clay clogging potential	130
6.4.1	Consistency Index approach	130
6.4.2	Empirical Stickiness Ratio approach	131
6.4.3	Proposed evaluation approach using torque as an indicator	133
6.5	Conclusions.....	139
CHAPTER 7 CONCLUSIONS, CONTRIBUTIONS AND RECOMMENDATIONS.....		140
7.1	Conclusions from each chapter.....	140
7.2	Recommendations for future work	143
REFERENCES.....		146

LIST OF FIGURES

Figure 1.1 Overall flowchart and methodologies of the thesis.	4
Figure 3.1 Particle size distribution curve of CSM sand.	19
Figure 3.2 AR-G2 rheometer: (a) overall view; (b) sand paper to prevent wall slip; and (c) vane after testing.	22
Figure 3.3 HR-3 rheometer: (a) overall view; (b) device motor, bearing, sensor and pressure cell; (c) testing vane; and (c) pressure cell.	24
Figure 3.4 Flow sweep experiment results for CSM sand at: (a) $w=5%$ ($S_r=25%$); and (b) $w=7.5%$ ($S_r=37.5%$).	26
Figure 3.5 Averaged viscosity values and curve fitting for CSM sand at: (a) $w=5%$ ($S_r=25%$); and (b) $w=7.5%$ ($S_r=37.5%$).	27
Figure 3.6 Flow sweep experiment results for CSM sand at (a) $w=10%$ ($S_r=50%$); (b) $w=15%$ ($S_r=75%$); and (c) $w=20%$ ($S_r=100%$).	28
Figure 3.7 Stress vs. strain curve during strain ramp testing at $w=5%$ ($S_r=25%$) and shear rate=0.0003 1/s (0.018 rpm).	30
Figure 3.8 Determining yield stress from oscillation sweep results at $w=5%$ ($S_r=25%$).	32
Figure 3.9 Viscosity testing results of CSM sand at $w=10%$ ($S_r=50%$) using HR-3 rheometer: (a) raw data; and (b) averaged viscosity.	33
Figure 3.10 Averaged viscosity testing results of CSM sand at different water content and cell pressure combinations using HR-3 rheometer: (a) atmospheric condition; and (b) 4bar pressure.	34
Figure 3.11 Effect of cell pressure on the measured elastic modulus and yield stress: (a) $w=5%$ ($S_r=25%$); and (b) $w=7.5%$ ($S_r=37.5%$).	35
Figure 3.12 Effect of water content on the measured elastic modulus and yield stress: (a) atmospheric condition; and (b) 4bar pressure.	36
Figure 4.1 Configuration of the preliminary design of soil rheometer device: (a) overview; (b) new VFD unit; (c) rotational speed control panel; and (d) pitched propeller with 10 degree (deg) pitch angles.	42
Figure 4.2. Effect of the ramping factor, m	45
Figure 4.3 Torque vs. time curves at 0.1 rpm for testing in: (a) air; and (b) water.	46
Figure 4.4 Torque vs. rotational speed curves for testing in air and water.	47
Figure 4.5 A concrete mixer used to mix CSM sand and water.	48
Figure 4.6 Typical torque vs. time curves at different rotational speeds on dry CSM sand: (a) 0.1 rpm; (b) 0.5 rpm, representative for range of 0.2 rpm to 0.9 rpm; and (c) 30 rpm, representative for range of 1.0 rpm to 60 rpm.	50

Figure 4.7 Preliminary rheology testing of dry CSM sand with 10 deg pitched propeller.	51
Figure 4.8 Torque vs. rotational speed curves for rheology testing of CSM sand at various water content levels with 10 deg pitched propeller.	52
Figure 4.9 Torque vs. water content curves for testing of CSM sand with 10 deg pitched propeller. The dashed lines for different rotational speeds are not real measurements and work as illustrative purposes only.	53
Figure 4.10 CSM sand in the testing chamber at: (a) $w=20\%$; and (b) $w=15\%$	53
Figure 4.11 Simplified COMSOL model of the rheometer using 10 deg pitched propeller.	55
Figure 4.12 Simulated torque (continuous lines) based on back calculated yield stress and viscosity and experimented torque (scattered data) using 10 deg pitched propeller.	56
Figure 4.13 COMSOL CFD models for pitched propellers with three blades: (a) 10 deg; (b) 30 deg; and (c) 90 deg.	59
Figure 4.14 COMSOL CFD models for vane propellers with different blades: (a) three blades, 50.8 mm in height; (b) four blades, 50.8 mm in height; and (c) four blades, 127 mm in height.	59
Figure 4.15 COMSOL CFD models for auger propellers with different diameters, D: (a) $D=296.4\text{mm}$; (b) $D=228\text{mm}$; and (c) $D=114\text{mm}$	60
Figure 4.16 COMSOL CFD models for auger propellers with different leads, L: (a) $L=94.25\text{mm}$; (b) $L=75.4\text{mm}$; and (c) $L=62.83\text{mm}$	60
Figure 4.17 COMSOL CFD models for auger propellers with different auger heights, H: (a) $H=226.2\text{mm}$; (b) $H=188.5\text{mm}$; and (c) $H=150.8\text{mm}$	61
Figure 4.18 Sensitivity of torque to viscosity and yield stress for pitched propellers running at a rotational speed of 60 rpm: (a) $\tau_y=250\text{ Pa}$; and (b) $\mu_0=300\text{ Pa}\cdot\text{s}$	62
Figure 4.19 Sensitivity of torque to viscosity and yield stress for vane propellers running at a rotational speed of 60 rpm: (a) $\tau_y=250\text{ Pa}$; and (b) $\mu_0=300\text{ Pa}\cdot\text{s}$	62
Figure 4.20 Sensitivity of torque to viscosity and yield stress for auger propellers with different diameters running at a rotational speed of 60 rpm: (a) $\tau_y=250\text{ Pa}$; and (b) $\mu_0=300\text{ Pa}\cdot\text{s}$	63
Figure 4.21 Sensitivity of torque to viscosity and yield stress for auger propellers with different leads running at a rotational speed of 60 rpm: (a) $\tau_y=250\text{ Pa}$; and (b) $\mu_0=300\text{ Pa}\cdot\text{s}$	63
Figure 4.22 Sensitivity of torque to viscosity and yield stress for auger propellers with different heights running at a rotational speed of 60 rpm: (a) $\tau_y=250\text{ Pa}$; and (b) $\mu_0=300\text{ Pa}\cdot\text{s}$	64
Figure 4.23 Overall comparison of sensitivity of torque to changes of yield stress and viscosity with three propeller geometries: (a) $\tau_y=250\text{ Pa}$; and (b) $\mu_0=300\text{ Pa}\cdot\text{s}$	64

Figure 4.24 CFD simulated velocity field using: (a) 10 deg pitched propeller; and (b) auger with a diameter of 296 mm.	65
Figure 5.1 Illustration of EPB TBMs: (a) “Big” Bertha for SR 99 tunnel project in Seattle, the United States of America (WSDOT Flickr); (b) schematic drawing of major components of an EPB TBM (CONDAT).	73
Figure 5.2 Large single-flight auger propeller: (a) dimensions; and (b) installed auger on shaft.	79
Figure 5.3 Large double-flight auger propeller: (a) dimensions; and (b) installed auger on shaft.	79
Figure 5.4 COMSOL CFD models for large auger propellers: (a) single-flight auger; and (b) double-flight auger.	80
Figure 5.5 Particle size distribution curves for the soils in this study.	81
Figure 5.6 Foam generator in this study (Alavi, Rostami, and Talebi 2014).	84
Figure 5.7 Small single-flight auger propeller: (a) dimensions; and (b) installed auger on shaft.	88
Figure 5.8 Torque vs. time plots for testing dry CSM sand: (a) ramping up rotational speed from 3 rpm to 60 rpm; and (b) ramping down rotational speed from 60 rpm to 3 rpm.	90
Figure 5.9 Torque vs. time plots for testing foam conditioned CSM sand when $c_f=1\%$, $FER=15$, and $FIR=30\%$: (a) ramping up rotational speed from 3 rpm to 60 rpm; and (b) ramping down rotational speed from 60 rpm to 3 rpm.	91
Figure 5.10 Torque at different rotational speeds for testing CSM sand at two water content levels using the small auger.	93
Figure 5.11 Gap between the outer edge of the small auger and the chamber wall.	93
Figure 5.12 Torque at different rotational speeds for testing CSM sand at two water content levels using the large single-flight auger.	94
Figure 5.13 Comparison of measured torque between ramping up and ramping down rotational speed for: (a) dry HD Sand; and (b) dry Ottawa Sand.	95
Figure 5.14 Comparison of measured torque between ramping up and ramping down rotational speed for CSM sand: (a) $w=0\%$; and (b) $w=5\%$	96
Figure 5.15 Comparison of measured torque between ramping up and ramping down rotational speed for conditioned CSM sand: (a) $c_f=3\%$, $FER=15$, $FIR=50\%$, 0kPa, 0.25h; and (b) $c_f=5\%$, $FER=15$, $FIR=30\%$, 0kPa, 0.25h.	97
Figure 5.16 Experimented torque vs. rotational speed relationships for six dry soils using the large single-flight auger.	100
Figure 5.17 Back calculated yield stress for six dry soils.	100
Figure 5.18 Back calculated plastic viscosity for six dry soils.	103

Figure 5.19 Experimented torque vs. rotational speed relationships for testing CSM sand at different water content levels using the large single-flight auger. Note that the dashed lines are the linear fitting lines.	104
Figure 5.20 Back calculated yield stress vs. water content relationships for CSM sand.....	105
Figure 5.21 Back calculated plastic viscosity vs. water content relationships for CSM sand....	106
Figure 5.22 Measured torque vs. rotational speed relationships for foam conditioned CSM sand at different <i>FIRs</i> while keeping <i>w</i> , <i>c_f</i> and <i>FER</i> constants. The dashed lines are the best linear fitting correlations.	108
Figure 5.23 Measured torque vs. rotational speed relationships for foam conditioned CSM sand at different <i>FERs</i> while keeping <i>w</i> , <i>c_f</i> and <i>FIR</i> constants. The dashed lines are the best linear fitting correlations.	108
Figure 5.24 Measured torque vs. rotational speed relationships for foam conditioned CSM sand at different <i>c_f</i> while keeping <i>w</i> , <i>FIR</i> and <i>FER</i> constants. The dashed lines are the best linear fitting correlations.	109
Figure 5.25 Effect of <i>FIR</i> on soil rheology parameters: (a) yield stress; and (b) viscosity.	111
Figure 5.26 Effect of <i>FER</i> on soil rheology parameters: (a) yield stress; and (b) viscosity.	111
Figure 5.27 Effect of <i>c_f</i> on soil rheology parameters: (a) yield stress; and (b) viscosity.	111
Figure 5.28 Relationships among <i>FIR</i> , yield stress, and slump test results: (a) vertical slump vs. <i>FIR</i> ; (b) lateral spread vs. <i>FIR</i> ; and (c) vertical slump vs. yield stress.	112
Figure 5.29 Relationships among <i>FER</i> , yield stress, and slump test results: (a) vertical slump vs. <i>FER</i> ; (b) lateral spread vs. <i>FER</i> ; and (c) vertical slump vs. yield stress.	113
Figure 5.30 Relationships among <i>c_f</i> , yield stress and slump test results: (a) vertical slump vs. <i>c_f</i> ; (b) lateral spread vs. <i>c_f</i> ; and (c) vertical slump vs. yield stress.	114
Figure 5.31 Measured torque vs. rotational speed relationships for foam conditioned CSM sand at atmospheric pressure at different elapse of time: (a) <i>c_f</i> =3%, <i>FER</i> =15, <i>FIR</i> =50%; (b) <i>c_f</i> =3%, <i>FER</i> =15, <i>FIR</i> =40%; (c) <i>c_f</i> =3%, <i>FER</i> =15, <i>FIR</i> =30%; and (d) <i>c_f</i> =3%, <i>FER</i> =20, <i>FIR</i> =30%.	116
Figure 5.32 Measured torque vs. rotational speed relationships for foam conditioned CSM sand at different chamber pressures: (a) <i>c_f</i> =3%, <i>FER</i> =15, <i>FIR</i> =50%; (b) <i>c_f</i> =3%, <i>FER</i> =15, <i>FIR</i> =40%; (c) <i>c_f</i> =3%, <i>FER</i> =15, <i>FIR</i> =30%; and (d) <i>c_f</i> =3%, <i>FER</i> =20, <i>FIR</i> =30%.	117
Figure 5.33 Proposed application of rheological models as functions of soil conditioning.	120
Figure 6.1 Denver clay before mixing: (a) pulverized clay powder; and (b) clay lumps.	124
Figure 6.2 Tools for mixing Denver clay and liquid: (a) a concrete mixer; (b) a dough mixer; and (c) a hammer drill mixing tool.	125

Figure 6.3 Tools for mixing Denver clay and foam: (a) and (b) concrete mixers; (c) a hammer drill mixing tool; (d) a flat beater with the rheometer power; (e) a tiller mixer; (f) a continuous mixer; and (g) clogged clay in the continuous mixer.	127
Figure 6.4 Torque vs. rotational speed relationships for different mixtures of Denver clay and CSM sand.....	128
Figure 6.5 Comparison of flow capability for clay vs. sand ratio of 1:2 between: (a) $w=20\%$; and (b) $w=30\%$	129
Figure 6.6 Comparison of flow capability for clay vs. sand ratio of 2:1 between: (a) $w=30\%$; and (b) $w=40\%$	130
Figure 6.7 Evaluation of clogging potential of Denver clay based on the Consistency Index approach for EPB supporting mud (Hollmann and Thewes, 2013). Data from this study are overlaid in the graph as triangular markers.	131
Figure 6.8 Evaluation of clay clogging based on Empirical Stickiness Ratio approach: (a) testing device; and (b) weight measurement.	132
Figure 6.9 Empirical Stickiness Ratio vs. water content curve. The boundaries were suggested by Zumsteg, Plötze, and Puzrin (2013).....	133
Figure 6.10 Empirical Stickiness Ratio vs. Foaming Agent Concentration curve at $w=40\%$ while mixing Denver clay with conditioner solution.	134
Figure 6.11 Measured maximum torque vs. water content curve for Denver clay using SAI testing machine with 10 deg pitched propeller.	135
Figure 6.12 Compaction of Denver clay at the end of SAI testing without surcharge loading: (a) significant compaction at $w=23.8\%$; and (b) slight compaction and signs of plastic deformation at $w=49.4\%$	135
Figure 6.13 Compaction and UCS measurement using: (a) Proctor compaction; and (b) Penetrometer.	136
Figure 6.14 Dry unit weight vs. water content measurements using Proctor compaction.....	136
Figure 6.15 UCS vs. water content measurements using Penetrometer.	137
Figure 6.16 Torque measurement on Denver clay using SAI testing machine with surcharge loading: (a) surcharging loading component; (b) torque vs. rotational speed curves for three surcharge loading pressures at $w=27.3\%$; and (c) torque vs. water content curves for three surcharge loading pressures at a rotational speed of 60 rpm. The dashed lines indicate missing data due to limitation of the machine motor capacity.	138

LIST OF TABLES

Table 3.1 Mineralogy of CSM sand.....	19
Table 3.2 Herschel-Bulkley model fitting parameters for CSM sand.....	29
Table 3.3 Yield stress testing conditions using strain ramp method.	30
Table 3.4 Yield stress testing conditions using oscillation sweep method.....	31
Table 3.5 Yield stress of CSM sand determined by different methods and criteria.	32
Table 4.1 Bulk density of CSM sand at different water content levels.....	49
Table 4.2 Summary of back calculated soil rheology.	56
Table 4.3 Summary of COMSOL CFD modeling parameters for propeller optimization.	61
Table 5.1 Soil mineralogy, specific gravity and soil classification for the soils in this study.....	82
Table 5.2 Dry bulk density and void ratio of the six tested soils.	83
Table 5.3 Control of foam conditioning parameters for testing on foam conditioned CSM sand.....	85
Table 5.4 Summary of testing scenarios.	89
Table 5.5 Measured density change of foam conditioned CSM sand.....	98
Table 5.6 Differences of computational results between "compressible" and "incompressible" setting in COMSOL.	101
Table 5.7 Differences in calculated torque between upper and lower density settings in COMSOL.....	102
Table 5.8 Summary of effect of soil type on soil rheology parameters.	102
Table 5.9 Summary of effect of water content on soil rheology parameters.	104
Table 5.10 Summary of effect of foam conditioner on soil rheology parameters.	109
Table 6.1 Basic physical properties of Denver clay.....	123
Table 6.2 Back calculation of rheological parameters of different soil conditions.....	129
Table 7.1 Limitations of the current version of the newly developed rheology measurement system.....	144

ACKNOWLEDGEMENTS

The past four years of my life have been surreal but nice! Upon coming to the end of this terrific journey, I couldn't be more grateful to all the people who profoundly impacted me to make this adventure a success.

First of all, I am privileged to have Dr. Jamal Rostami as my advisor. He is the one-of-a-kind human being who always greets me with smile and easy approach. He is such a generous and knowledgeable professor who has always been willing and capable of giving his advice. I feel extremely fortunate to be advised by him.

I am thankful to all my committee members who have been willing and capable of giving invaluable comments throughout my thesis process. They are Dr. Jorge Sampaio, Dr. Gabe Walton, and Dr. Reza Hedayat.

I am forever indebted to Dr. Maosheng Zhang, who was my early-career mentor and provided huge encouragement for my pursue of this degree throughout.

I am grateful to all other professors and professionals who have shaped my understanding of this dynamic and promising career, specifically Dr. Mike Mooney, Dr. Priscilla Nelson, Dr. Molsen Mosleh, and Dr. Joseph Samaniuk.

I would like to appreciate all the Mines community and alumni for their generous help and advice on my research. To name a few, this includes Dr. Omid Frough, Brent Duncan, Bruce Yoshioka, Anuradha Khetwal, Muthu Vinayak Thyagarajan, Benjamin Appleby, Dr. Kamran Jahan Bakhsh, Ray Johnson, Dr. Richard Wendlandt, Dr. Katharina Pfaff, Dr. Marcelo Simoes, Dr. Masami Nakagawa, and other graduate and undergraduate students.

Other people and organizations who provided technical help and research sources are also greatly appreciated, including Guijie Sang, Jiehao Wang, The COMSOL Group, BASF, CONDAT, MAPEI, NORMET, and the anonymous reviewers of my published papers.

Lastly, this thesis is dedicated to my beloved family. I could have barely moved an inch towards this finishing line without my wife and my children's long-time support and sacrifice. I owe them countless days and nights. This achievement also goes to my parents. The family tradition of working hard that they passed on to me contributed tremendously to this achievement.

CHAPTER 1

INTRODUCTION

1.1 Overview

Primarily driven by the unprecedented transportation need and urbanization process in developing countries, as well as the infrastructure modernization demand in developed countries, the world has witnessed rapid development of the tunneling industry in the past few decades. Despite the significant advances in machine manufacturing technologies as well as construction chemicals used for modifying soil behavior in this period, tunnel construction is an industry that is still highly experience-based (Langmaack 2000). One example is that Earth Pressure Balance (EPB) Tunnel Boring Machines (TBMs) are operated based on the operator's judgement of the observed conditions and the response of machine sensory systems.

The basic function of EPB TBMs is to utilize the excavated muck as the supporting medium for maintaining face pressure to assure face stability while transferring the excavated material through excavation chamber and screw conveyor in the tunnel, which is under atmospheric pressure. To optimize this system, the muck should have certain properties such as low permeability, high compressibility, low abrasiveness, proper viscosity and strength. For instance, the viscosity and strength of the muck are expected to be neither too high, to potentially plug the machine, nor too low, to collapse readily and fail to support the tunnel face. However, it is very rare for natural soils to have the desired properties, meaning that they must be conditioned to modify their behaviors to more workable mixes based on the grain size distribution, mineralogy, clay content, water content, and surcharge/pore pressure. To facilitate the optimal operation of an EPB tunneling system, a good understanding of the behaviors of conditioned soils for all types of soil conditions is required. Evaluating these parameters by lab testing can reduce the risks of costly mistakes and delays in the field.

However, there are still gaps in proper prediction of muck behaviors in laboratory settings to reflect the site conditions. For example, there are still no well-defined standard conditioning and clogging tests for clayey soils, nor there is much information on rheology of conditioned soils (Hollmann and Thewes 2013; Galli 2016; Mori, Alavi, and Mooney 2017). Also, the details of soil movement within the cutting chamber and screw conveyor relative to the speed of excavation and the face pressure are unknown.

This thesis is focused on some aspects of EPB tunneling. The major goal of this thesis was to explore the relationship between soil conditioning parameters and resulting soil rheology. This began with a feasibility study of measuring rheology of conditioned soil in small-scale conventional rheometers designed for testing biochemical materials. Given the evident limitations of measuring rheology of conditioned soil for tunneling applications, the pertinent tests of conditioned soil were subsequently performed within the Soil Abrasion Index (SAI) testing machine chamber and modeled via Computational Fluid Dynamics (herein CFD) programs to establish relationships for prediction of soil rheology based on different settings and conditioning parameters. This includes the development of a large-scale rheology measurement system for soils and an assessment plan to evaluate various soil properties relative to water content, Foaming Agent Concentration (c_f) of the surfactant, Foam Expansion Ratio (FER), and Foam Injection Ratio (FIR). It is a system combining both experimental and numerical components. The experiments include different rotational speed and measurement of related torque and applied forces on the propeller to establish the torque vs. rotational speed charts. The modeling of the testing scenarios allows for soil yield stress and viscosity to be modified to match the observations in the laboratory, thus providing back calculated values of these parameters of conditioned soils. With more soil samples being tested in the future and development of a suitable database, a statistical analysis between rheological parameters and soil conditioning parameters will offer models for prediction of trends in soil rheology as functions of soil conditioning parameters. These models can subsequently be used to simulate the soil flow within the cutting chamber and screw conveyor of EPB machines, predict the machine response, and ultimately, optimize the machine operation and soil conditioning practice.

This thesis also includes the evaluation of methods for sample preparation of conditioned clay for rheological assessment, including means to mix clay and conditioners, clay rheology measurement, and evaluation of clogging potential. Since there was no established or standard laboratory method for preparation of conditioned clay for testing in a large-scale apparatus, several means of clay-foam mixing were examined to introduce an innovative scheme of clay conditioning for rheology testing purposes. Additional insight to available clogging evaluation methods and potential missing factors are discussed.

1.2 Research objectives

This thesis primarily aimed to develop and assess a new system for measuring the rheology of conditioned soil for application in EPB TBM tunneling. The study also explored new methods to quantify rheology and clogging potential of conditioned clay, including means to mix conditioner and clay and subsequent rheology testing of conditioned clay.

1.3 Methodologies

The overall methodology for achieving the objectives of this thesis was to use a combination of experimental work and modeling to assess the rheology of conditioned soil. For this purpose, required modifications of the SAI testing machine were planned and implemented, and an experimental testing plan was developed. Pertinent tests were conducted in various soils by considering soil type, water content, and soil conditioning parameters, in addition to the various propeller geometries, propeller rotational speeds, test durations, and various pressures in the chamber. In parallel, modeling of the system was conducted to understand the anticipated behavior of the system in various soil types with different rheological properties. The modeling was also used for optimization of the configuration of the propeller. The test results were compared to the modeling results to backcalculate the viscosity and yield stress of the samples from observed shear stress vs. shearing rate of the conditioned soil. Some tests were conducted on available smaller rheometers. The combination of these tests allowed for verification of the thesis hypotheses. These include the assumptions that small-scale conventional rheometers are ill-suited for rheology measurement of conditioned soils containing coarse-grained particles, and rheological responses of conditioned soils follow Bingham plastic model. These tests also validated capabilities of the proposed testing system to estimate a unique set of yield stress and viscosity of conditioned soils by combining experimental work and numerical modeling, and to establish prototype relationship between soil rheology and soil conditioning parameters with sufficient sensitivity. The methodologies in this thesis are shown in the overall flowchart in Figure 1.1.

1.4 Thesis organization

This thesis consists of seven chapters. Following this introductory chapter (Chapter 1), Chapter 2 details and summarizes the existing literature on the characterization of conditioned soils in the context of EPB tunneling. The literature review validates the knowledge gaps and research motivations.

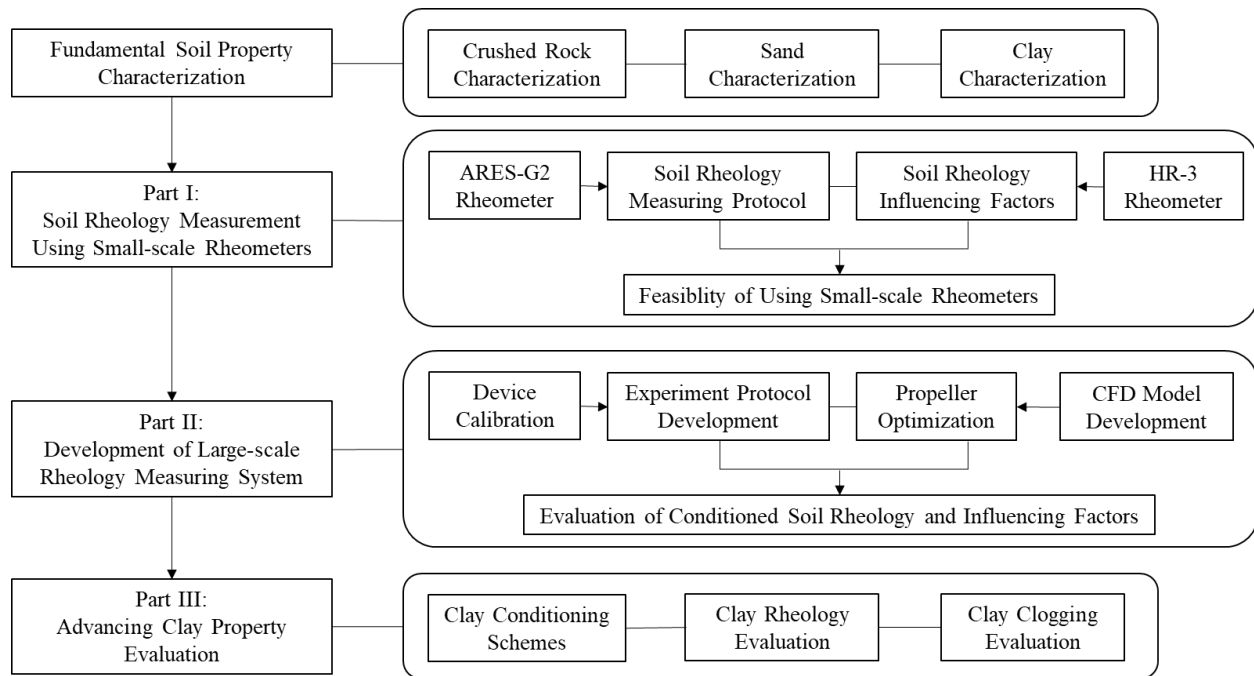


Figure 1.1 Overall flowchart and methodologies of the thesis.

Chapter 3 focuses on measuring rheology of conditioned soil using conventional small-scale devices. It presents the experimental results on the rheology of a conditioned sand using two small-scale conventional rheometers. It demonstrates the limitations of such small-scale devices for EPB tunneling applications and the necessity to develop a new large-scale rheology measurement system.

Chapter 4 is modified from a paper entitled “A new method to quantify rheology of conditioned soil for application in EPB TBM tunneling”. This paper was published in *Tunneling and Underground Space Technology* and focuses on the preliminary development of a new rheology measurement system, including rotational speed control, torque calibration, identification of the rheological model for conditioned soils, feasibility of determining soil rheological parameters using back-calculation, and propeller optimization using CFD modeling.

Chapter 5 is modified from a paper under preparation, titled “Development of a system to measure rheology of conditioned soil for application in soft-ground tunneling”. This paper will be submitted to *Tunneling and Underground Space Technology*. The chapter focuses on the full development of the proposed rheology measurement system for conditioned soil. This includes the development of the measurement protocol with the optimized auger propeller, the establishment

of the relationship between soil rheology and soil conditioning parameters, and the effects of several influencing factors on soil rheology.

Chapter 6 discusses the study of rheology of conditioned clay for application in EPB TBM tunneling. This chapter presents the challenges of characterizing rheology of conditioned clay, including lack of means to generate homogeneous foam and clay mixture for research purpose, lack of rheology data on foam conditioned clay, and lack of consideration of the pressure condition in clay clogging potential assessment in current approaches used for dealing with soil clogging. These works are presented to generate more interest in research in this important field.

Chapter 7 contains the summary of the major findings and contributions in this thesis and provides recommendations for future work.

CHAPTER 2

LITERATURE REVIEW

This chapter summarizes the most relevant literature related to this thesis, including conditioning challenges for sand and clay, evaluation of conditioned soil properties, evaluation of soil abrasion, evaluation of clay clogging, rheology evaluation of conditioned soil, and real-time determination of muck behavior and machine operation. Each of the following chapters will elaborate on the literature directly associated with their topics.

2.1 Mixing challenge for foam conditioned soil

In practice, soils with particle size ranging from clay to silt, sand, and gravel have been conditioned to enable EPB tunneling, as indicated in the publication “Specification and guidelines for the use of specialist products for mechanized tunneling (TBM)” (EFNARC 2005) released by European Federation of National Associations Representing producers and applicators of specialist building products for Concrete (herein EFNARC). To date, however, the majority of lab-scale soil conditioning studies have been focused on granular soil or sand (e.g. Psomas 2001; Alavi 2013; Galli 2016; Mori 2016). This is due to the ease of mixing sand and conditioners (in most cases, foam). Because of clay structural constraints and the density contrast between foam and clay, mixing these two materials homogeneously for lab studies is extremely challenging. Although some publications reported preparation of conditioned clay samples when studying clay clogging issues (Merritt 2004; Ball et al., 2009; Zumsteg et al., 2012; Zumsteg and Puzrin 2012; Plötze et al., 2013; Zumsteg et al., 2013; Peila et al., 2016; Oliveira et al., 2017), there are still doubts on the suitability of using pure clay samples, as well as the homogeneity of the conditioned clay used in testing.

Testing of natural clayey soil containing randomly scattered gravels has been made possible by the introduction of a large-scale testing system for conditioned soil, formerly known as the Soil Abrasion Index testing machine (Rostami et al., 2012; Alavi et al., 2014). This unit is currently at Colorado School of Mines’ EMI laboratory. While the testing of conditioned clay in this unit is possible, the remaining challenge lies in proper mixing of clay and foam. In fact, the studies on material mixing are crucial for not only EPB tunneling, but also many other applications such as food processing, mineral processing, and wastewater treatment. The success of mixing lies in both mixing time and the degree of homogeneity (Paul et al., 2004). Although the mechanisms

of mixing have been long identified as convective mixing, shear mixing, diffusive mixing, or any combination of thereof, the methods to study specific mixing modes have only advanced rapidly in the last two decades thanks to the improvements in both instrumentation and computer modeling technique, such as visualization techniques and CFD modeling (Nazem 2017). Despite of these advances, soil-foam mixing studies in the EPB tunneling application are still rare, with just one recent publication on the use of a unique visualization technique to observe the mixing and migration process of sand and foam at the lab scale (Nazem et. al., 2018). Otherwise, little is known about the real mixing process and effectiveness inside the EPB machine, especially when dealing with clay.

Therefore, very limited studies have focused on clay conditioning and there are many unknowns about the applicability of current mixing theories for clay and water in industrial practices. Some mixing trials in the current study also have shown their inability in mixing of foam and clay for conditioning. In addition, experienced engineers working with suppliers of chemicals for clay conditioning practices have doubts about the efficiency of mixing of foam and clay, as a lack of a reliable solution to prevent the clogging in EBP tunneling is evident by examples of machines being stuck in sticky clay that is reflected in the literature (Rostami and Hu, 2019). To advance clay conditioning practice, clay-water-chemical mixing studies need to be attempted until a viable solution is reached.

2.2 Evaluating the properties of conditioned soil

Evaluation of conditioned soil properties is essential for understanding and improving EPB machine operation. Some of the critical input parameters and pertinent testing methods for characterization of unconditioned natural soils as well as conditioned soil are as follows:

2.2.1 Permeability

The permeability of conditioned soil is very important in maintaining face pressure and limiting the mobility of water in the mix in the screw conveyor (Duarte 2007). Some studies have proposed a permeability value of 10^{-5} m/s or less for conditioned soil to be considered acceptable to prevent significant seepage flow, tunnel face collapse, and related ground settlement (Quebaud et al., 1998; Borio and Peila 2010). These authors utilized constant head permeability tests to measure the permeability of conditioned soil.

2.2.2 Compressibility

The conditioned soil should also be compressible to enable flexible adjustment of chamber pressure so as to adjust to the changing face pressure requirement. A pressurized testing chamber was proposed to test the compressibility of conditioned soil (Mori et al., 2015). During the test, the chamber was pressurized without air outlet. The e -log(p) plot was drawn showing the existence of a transitional void ratio. Above this threshold, the foam bubbles govern the compressibility of the conditioned soil, while below it, particle-to-particle contacts in the conditioned soil control the behavior of the medium. Other researchers mainly used conventional oedometers in their studies (Duarte 2007; Djeran-Maigre et al., 2018).

2.2.3 Strength

Soil strength should also be low to allow muck movement with the minimum resistance from adjacent soil particles. Direct shear boxes and vane shear boxes are the two most common devices used in exploring the strength of conditioned soil (Duarte 2007; Messerklinger et al., 2011; Mori et al., 2015).

In applying these tests, one should take ample caution to assure their applicability to conditioned soil. For example, water flow could wash out the foaming agent, and as a result, the results of permeability tests may not be representative of the true permeability of the conditioned soil. Additionally, the test duration is not standardized, and for long running tests, the foam may very likely be degraded (Mori 2016). Therefore, the above-mentioned testing schemes may not be practical in characterizing conditioned soil in all applications, although the three aforementioned properties are important to soil conditioning assessment.

2.2.4 Stickiness

Stickiness of clayey contents could lead to EPB machine clogging and downtime if the ground is not well-characterized and inappropriately conditioned. To characterize soil stickiness, many approaches have been proposed, such as the lateral adhesion test (Peila et al., 2016), the cone pull-out test (Feinendegen et al., 2011), the Empirical Stickiness Ratio method (Zumsteg and Puzrin 2012; Zumsteg et al., 2013; Plötze et al., 2013), and the consistency-based clogging potential diagram method (Hollmann and Thewes 2013; Thewes and Hollmann 2016). The soils used in these studies were pure commercial clay. However, it is rare to encounter pure clay condition in real tunneling projects. Instead, natural clayey ground usually consists of diverse grain sizes (though dominated by clayey particles). Therefore, more studies on complex natural clayey

soils should be conducted to verify the applicability of above-mentioned methods. Recently, stickiness of mixed ground conditions has been reported in some studies (Roby and Willis 2014; Oliveira et al., 2017), although the volume of work on clay is very limited.

2.3 Soil abrasion

Soil abrasion is a critical issue in soft-ground tunneling because it can cause severe primary and secondary machine and tool wear and related downtime (Alavi et al., 2011). It has become a research focus in the past few decades due to severe damage to the machines in some soft-ground tunnel projects around the world. Several approaches were proposed to characterize soil abrasiveness and tool wear, such as NTNU/SINTEF Soil Abrasion Test (Nilsen et al., 2007; Jakobsen et al., 2013), LCPC Abrasivity Test (Thuro, K., and Singer 2007), Torino Soil Abrasion Test (Peila et al., 2012), Soil Abrasion Index Testing (Rostami et al., 2012), and others (Barzegari et al., 2013; Jakobsen et al., 2013). For studies on the effect of soil conditioning on soil abrasiveness, all the reported studies were conducted in sand due to ease of sample preparation (Alavi et al., 2013; Alavi et al., 2014).

2.4 Clay clogging

In clayey soil, clogging occurs in certain water content conditions, which can be worsened by inappropriate conditioning and operating pressure. In the past, clogging evaluation was equated to stickiness assessment, which was summarized in the literature (Thewes and Burger 2004; Feinendegen et al., 2011; Zumsteg et al., 2013; Hollmann and Thewes 2013; Hollmann 2014; Thewes and Hollmann 2016), while the impacts of machine parameters, including thrust force, face pressure, and RPM, were ignored. To advance clogging studies, some fundamental questions should be answered. These include development of a quantifiable definition of clogging, evaluation of the clogging mechanism, and detailed assessment of influencing factors. Recently, a method based on site monitoring of the apparent density of the conditioned soil was proposed to evaluate the clogging issue. In this approach, an apparent density above the virgin soil density was used to indicate the existence of plugging issues in the machine (Mori et al., 2017). Not much analysis on interrelationship between machine operation parameters and clay density nor quantification on the impacts of machine operation parameters on clogging is available in the literature. Nevertheless, this method appears to be promising for use in future clogging research, because density change takes into account the impact of the machine operation.

2.5 Rheology of conditioned soil

While abrasiveness and stickiness are relevant properties for gravel/sandy and clayey soils, respectively, flow properties are more critical and applicable properties for all types of soils in the context of EPB tunneling applications. The slump test has been adopted from concrete pumping applications and is widely utilized to assess the plastic flowability of conditioned soil due to its simplicity. However, the slump test is considered to be an index test, which is run at atmospheric pressure, while the soils at the face and in the working chamber are under variable pressures (Meng et al., 2011). Meng et al. (2011) pointed out that the slump value shows a good correlation with the yield stress, while not being responsive to impacts of changing strain rate on the stress–strain behavior of the conditioned soil. Recently, several authors have advanced the studies into a more rigorous and scientific set of rheological parameters, involving yield stress and viscosity. Some of the representative cases include: Meng et al. (2011) studied the rheological response of foam conditioned sand to different chamber pressures and *FIRs*; Djeran-Maigre et al. (2018) studied the viscosity reduction between unconditioned and conditioned sand; Galli (2016) developed a Ball Measuring System that tests yield stress and viscosity features of foam conditioned sand with different grain size distributions and conditioning parameters, and explored the correlation of these parameters with slump values.

While some studies on the topic of soil rheology have been conducted in the past, all of the studies were focused on granular soil or sand. Also, the rheological testing devices used were small and unable to accommodate soil samples containing randomly scattered gravels from the project sites. In addition, all of the studies in the past were simply proposed to test soil rheology with no consideration for EPB tunneling applications and related issues. Therefore, there is a need to study the rheological behavior of soil in a more comprehensive manner to include fine-grained plastic clays through coarse-grained gravel-laden soil and everything in between, for tunneling applications. The priority, however, is to develop a suitable rheology measurement system for EPB tunneling applications.

2.6 Real-time determination of muck behavior and machine operation

Although studies on the rheology of conditioned sand have shed light on advancing EPB soil conditioning practice, the optimal operation of an EPB tunneling system requires a good understanding of the behavior of conditioned soil for all types of soil and operational conditions. Therefore, there is a need to study the rheological behavior of soil in a more comprehensive manner

to include fine-grained plastic clay all the way to coarse-grained gravel laden soil. Several European institutions have built up lab-scale EPB screw conveyor systems to incorporate the study of the movement features of clayey muck inside the conveyor (Merritt 2004; Merritt and Mair 2006; Peila et al., 2007; Merritt and Mair 2008; Vinai et al., 2008). However, this type of approach is very expensive and hence, very limited data is available. Overall, for study of muck behaviors, the available experimental systems are far from sufficient to generate information on soil movement relative to the conditioning parameters. Also, the details of soil movement within the chamber relative to speed and pressure in various locations are rarely known.

Instrumenting and measuring the relevant parameters require time-consuming lab testing. To avoid costly mistakes and delays in the field, it is best if a smaller-scale test could be conducted to allow for quantification of the impacts of various conditioning parameters on rheological behavior of muck. EPB machines are primarily operated based on the operator's experience and a trial-and-error process, i.e., feedback and learning from real-time monitoring of the machine data and ground responses (Godinez et al., 2015). The function of Geotechnical Baseline Report (GBR) is limited to providing qualitative descriptions of soil types and general soil properties, and no guidance is provided on the machine design and operation based on changing ground conditions. When encountering unexpected under-defined geological conditions, the conventional approach is a passive means of mitigation response and not flexible enough to provide adequate guidance on operation. It has caused costly downtimes for machine repair or for mitigation of the surface settlements. As one of the proactive mitigation measures, extensive rheology testing of conditioned soil will lead to establishing the relationship between conditioning parameters and its rheological behavior, hence allowing for optimizing the conditioning parameters to quickly react to changing ground conditions.

As such, there is a need for a proactive study of muck behavior and the rheology of conditioned muck/soil. This could facilitate the development of an intelligent EPB tunneling system which can address the deficiencies of traditional trial-and-error based selection of conditioning parameters and reduce the dependency on individual judgements. The system will be capable of predicting the soil conditioning needs before the operation start, while offering a means for evaluating/adjusting the conditioning parameters in a real-time manner. An evaluation methodology that can consider both muck properties and machine operational parameters is necessary to meet these goals. Soil rheology is a discipline that can offer such potential capability.

Computational Fluid Dynamic (CFD) simulations based on soil rheology have shown potential to offer a realistic simulation of the muck movement within the EPB machine cutting chamber and screw conveyor, and to predict EPB machine performances (Talebi et al., 2015). The current gaps lie in verification of a CFD model of a lab-scale rheometer that can be scaled to real EPB TBMs.

2.7 Knowledge gaps

Some of the major knowledge gaps in the property characterizations of conditioned soils and their tunneling applications are as follows:

1. A universal set of parameters or approaches to characterize all types of unconditioned and conditioned soils, relative to the performance of EBP machines is needed. While the rheological properties including yield stress and viscosity seem to be sufficient to describe soil behavior in this application, there is a need to set logical rheological boundaries for optimally conditioned, adequately conditioned, not-well conditioned, and natural conditions of the soil in the cutting chamber for EPB tunneling application.

2. The relationships between soil rheological parameters (i.e., yield stress and viscosity) and soil conditioning properties commonly used by the tunneling industry (water content, abrasiveness, stickiness, slump value, c_f , FER , FIR , shear strength, etc.) need to be explored.

3. Limited CFD modelling of the muck flow in the cutting chamber and screw conveyor of EPB machines has been conducted, mainly due to lack of rheological properties of conditioned soil. This approach appears to be promising to simulate behavior of conditioned soil in practical application. At this stage, for a particular soil conditioning setting, the soil rheological parameters can be back calculated by CFD modeling, but the complexity of the operation can impact the accuracy of the calculated rheological parameters.

4. A method for measurement of rheology of conditioned soil needs to be developed to enable the CFD modeling of the EPB machine for a variety of end applications. Incorporating soil rheology and CFD models to simulate the muck flow inside the cutterhead chamber and the screw conveyor can be very critical in optimal operation of the machine in the field, but at this time none of the available system is capable of accurate measurement of rheology of conditioned soil.

5. None of the existing soil abrasion testing systems incorporate realistic stress conditions, nor do they explore the correlation between soil abrasiveness and soil rheology.

6. There are critical challenges in conducting lab-scale evaluation of conditioned soils with various conditioning schemes. For instance, the amount of work on natural sticky clayey soil has been limited and there is a need for a proper testing protocol to be developed for clay and sticky soil. The same is true for larger-grained soils and the clayey/sandy soils consisting of randomly scattered gravels. As such, a testing protocol for various soil types for the Soil Abrasion Index testing machine needs to be developed.

7. Clay stickiness does not necessarily correspond to clogging, and there is a need for a quantifiable measure for both properties relative to water content, surcharge loading, pore pressure, etc.

These knowledge gaps have been considered in developing the scope for this study to address some of the problems related to clay conditioning approaches, measurement of rheology of conditioned soil, and relationship between soil rheology and soil conditioning parameters.

CHAPTER 3

MEASURING RHEOLOGY OF CONDITIONED SOIL USING CONVENTIONAL SMALL-SCALE DEVICES

3.1 Abstract

The excavated muck in the excavation chamber and the screw conveyor of Earth Pressure Balance (EPB) Tunnel Boring Machines (TBMs) is utilized as the supporting medium to maintain the face pressure before being transported to the conveyor belt. To realize this function, the muck is often conditioned to bear certain target properties such as low permeability, high compressibility, proper yield stress and viscosity. Characterization of soil rheology plays a critical role in controlling the desired characteristics of the conditioned muck. However, soil rheology testing is still a new perspective among all means of property characterizations of conditioned soils, and consequently, no universally accepted characterizing approach has been offered. In this chapter, small-scale rheometers, which are widely accepted in biological and chemical engineering, were utilized to test conditioned soils. The goals were to investigate the feasibility of using these devices to characterize rheology of conditioned soil for EPB tunneling application and to verify the need to develop a new large-scale rheometer for tunneling application. Two small-scale rheometers were used to test a sand with different water content and cell pressure conditions. The experimental trials confirm two major assumptions. First, strain ramp procedure and oscillation sweep method are appropriate for estimation of viscosity and yield stress of conditioned sand. Second, both water content and cell pressure have impacts on the soil rheology. In addition, the results also reveal two shortcomings of the small-scale rheometers, i.e., limited torque and axial force capacities when dealing with firm soils, and insufficient flow channel between the vane and the cell to accommodate the sand with coarse grains. Consequently, the available test data is insufficient to make general conclusions regarding behavior of conditioned soil and there is a need to develop a new large-scale rheometer for application in EPB tunneling.

3.2 Introduction

Rheology is a classical topic in fluid mechanics, dealing with the deformation and flow properties of materials, primarily liquids, corresponding to changes of environmental settings such as stress and temperature. The rheological behaviors of materials are critical in many industries such as food processing, mineral processing, petroleum/oil/gas drilling, concrete pumping,

biochemical engineering and production (e.g., Ferraris 1999; Wright et al., 2001; Samaniuk et al., 2012; Vipulanandan and Mohammed 2014). The focus of rheological studies in many of these applications is the viscosity of the medium under various environmental parameters. The geo-materials such as slurries and clay pastes that are encountered in the tunneling industry usually exhibit the so-called viscoplastic behavior, which is identified by a threshold stress, i.e., yield stress (τ_y), below which the material does not flow (Papanastasiou 1987; Mitsoulis 2007). These materials with yield stress are also called non-Newtonian materials. Numerous non-Newtonian rheological models have been developed and applied. The most common models include the ideal Bingham plastic model and the subsequent modifications, the Herschel-Bulkley model, and the Casson model (Mitsoulis 2007).

A rheometer is a device to measure the non-Newtonian material rheology. The common theme of a rheology measurement system is its capability to rotate a form of propeller inside the target medium with various speeds and measure the resistance of the fluid against the movement of the propeller, and consequently, determine yield stress and viscosity (μ_0) of the fluid medium. Different types and sizes of rheometers have been introduced for different applications, with some common stirring geometries being concentric cylinders (Ewoldt et al., 2015), augers, and vane blades (Samaniuk et al., 2014). Among them, the most common rheometers are small devices designed for testing liquid materials in industries such as food engineering, biological engineering and chemical engineering.

Despite the importance of muck rheology in operation of EPB TBMs, very limited studies have been conducted to characterize soil rheological behaviors under conditions similar to those presented in this application. Among these attempts, one of the most widely accepted approaches is the slump test. Adopted from concrete industry, the slump test has been widely utilized to assess the plastic flow ability of conditioned soil for EPB tunneling application. This is primarily due to its simplicity and familiarity of many civil engineers with this test. However, the slump test is considered as an index test which is carried out at atmospheric pressure while the soil at the tunnel face and in the working chamber of an EPB machine is under variable pressure and shear rate, depending on the location (Meng et al., 2011). It is reported that slump value offers good correlation with yield stress, while not being responsive to changing strain rate on the stress–strain behavior of the conditioned soil (Roussel and Coussot, 2005; Meng et al., 2011). Recently, several studies have been published with more rigorous and scientific set of rheological parameters, i.e.,

yield stress and viscosity to describe behavior of the soil in cutting chamber of EPB machines. Some of the representative cases are as follows. Meng et al. (2011) studied the rheological response of foam conditioned sand to different chamber pressures and *FIRs*. Djeran-Maigre et al. (2018) studied the viscosity reduction between unconditioned and conditioned sand. Galli (2016) developed a Ball Measuring System that tested yield stress and viscosity features of foam conditioned sand with different grain size distributions and conditioning settings, explored the correlation of these parameters with slump values and hence, introduced a comprehensive model to be used for potential EPB tunneling application. Freimann et al. (2017) examined the flow behaviors of conditioned sand by using the Ball Measuring System and the outlook for upscaling the results of laboratory studies to EPB tunneling.

Nearly all of the studies on rheology of conditioned soil in the past have been focused on granular soil or sand and rarely did they include testing in fine-grained soils and clay. Often the existing rheology testing devices were small, meaning lack of ability to accommodate coarse soils, not to mention to test real site soil samples containing randomly scattered gravels. In addition, all of these studies were merely proposed to test soil rheology in atmospheric conditions, instead of simulating the true conditions in EPB tunneling such as variable surcharge loading and pore pressure.

Another important factor in the study of soil rheology is that in EPB machine applications, some forms of soil conditioning are applied. This could range from as simple as adjusting the water content (w) of the soil for improving its characteristics, to injection of clay, various chemicals, surfactants, polymers, even cellulose into the cutting chamber for modifying the behavior of the soil. The most common form of soil conditioning is foam. It is a surfactant that increases the surface tension of the water and allows for formation of the bubbles, which in turn allows for easier flow of the material, while maintaining certain viscosity in the mix to allow for pressure control in the cutting chamber and screw conveyor. The conditioning process with the foam involves selection of the proper settings including the following parameters:

(1) Foaming Agent Concentration (c_f). It is defined as:

$$c_f = m_{surfactant} / m_{foam\ solution} \times 100\% \quad (3.1)$$

where $m_{surfactant}$ is the mass (kg) of surfactant in foaming solution and $m_{foam\ solution}$ is the mass (kg) of foaming solution, which is the blend of water and surfactant (EFNARC 2005). It is revealed that surfactant density is within the range between 0.95 g/cm³ and 1.0 g/cm³, regardless

of the storage environment (Bhattacharai, Chatterjee, and Niraula 2013). Together with the chemical suppliers' recommendations, the density of surfactant in this thesis was equated with that of water. Therefore, the mass ratio between surfactant and foaming solution is equivalent to the corresponding volume ratio.

(2) Foam Expansion Ratio (*FER*). It is defined as:

$$FER = V_{foam}/V_{foam\ solution} \quad (3.2)$$

where V_{foam} is the volume (m³) of foam at working pressure and $V_{foam\ solution}$ is the volume (m³) of foaming solution (EFNARC 2005).

(3) Foam Injection Rate (*FIR*). It is defined as:

$$FIR = V_{foam}/V_{soil} \times 100\% \quad (3.3)$$

where V_{foam} is the volume (m³) of foam at working pressure and V_{soil} is the volume (m³) of in situ soil to be excavated (EFNARC 2005).

While it is well known that these parameters control soil rheology, and in the field, they are adjusted based on the ground conditions to allow more efficient operation of the machine, their impacts on various soil types under different surcharge loading and pore pressure conditions are not known. Although the studies on the rheology of conditioned sand have shed some light on advancing soil conditioning practice in EPB tunneling, the optimal operation of an EPB tunneling system requires an in-depth understanding of the behavior of conditioned soil for all types of settings. Several European institutions have built lab-scale EPB screw conveyor systems to incorporate the study of the movement features of clayey muck inside the conveyor (Merritt, 2004; Merritt and Mair, 2006; Peila et al., 2007; Merritt and Mair, 2008; Vinai et al., 2008). However, this type of approach is very expensive and hence, very limited databases on the test results are available. An evaluation methodology that can consider both muck properties and machine operational parameters is in demand. Soil rheology is a discipline that can offer such potential capability. Measured or estimated yield stress and viscosity of conditioned soil, combined with Computational Fluid Dynamic (CFD) modeling, have shown the potential for modeling muck movement within EPB machine cutting chamber and screw conveyor, and for prediction of EPB machine performance (Talebi et al., 2015). The current gap lies in providing the input parameters for CFD modeling based on well-established models to estimate pertinent machine operation parameters. The critical input parameters could be obtained from a rheometer that can simulate working conditions of EPB machine for a given project.

Therefore, study on the rheological behaviors of the conditioned soil in a setting close to the working conditions of an EPB machine as well as study of the behaviors of fine-grained plastic clays seemed to be critical and much needed. As such, development of a soil rheology evaluation method was considered to be a priority in order to answer the aforementioned questions. To begin with this development process, two commonly used small-scale rheometers in chemical and biological engineering practices were utilized to establish the viscosity and yield stress testing protocols on conditioned soils, to study the general rheological patterns with regard to changes of water content and cell pressure, and more importantly, to explore the feasibility of using the small rheometers to test samples of conditioned sand and verify the necessity to develop a new large-scale rheometer.

3.3 Soil samples and testing methods

3.3.1 Soil

The soil used throughout this thesis is a sand produced by crushing rock, named CSM sand. It was produced in a quarry by crushing process and commercially available in Denver, Colorado, USA. The particle size distribution curve of CSM sand was obtained by sieve analysis, as shown in Figure 3.1. Fine (0.074 mm - 0.42 mm), medium (0.42 mm - 2.0 mm), and coarse (2.0 mm - 4.76 mm) sand particles comprise roughly 27%, 60%, and 13% of CSM sand, respectively. Based on Unified Soil Classification System, CSM sand is classified as poorly graded sand (SP) (ASTM International, 2017). The water content of air-dried CSM sand was found to be 0.2%, meaning the sand in the CSM lab condition can be considered as nearly dry. The specific gravity of the sand, G_s , defined as the ratio of the density of the soil solid particles to that of the water, was estimated to be 2.69.

The mineralogy of CSM sand was tested by using QemScan technology, as summarized in Table 3.1. It is shown that quartz and feldspar (i.e., plagioclase and orthoclase) comprise 40.5% and nearly 48% of CSM sand, respectively. While the quartz content is less than typical quartz-rich sand such as silica sand, this composition is similar to some typical natural sands with limited weathering process (Nelson 2006). Because ground conditions along the tunnel could vary, it is unrealistic to find and test a universal soil candidate to represent all possible ground conditions. Instead, extensive testing on different types of soils are needed to find trends in ground behavior and derive soil classification for tunneling applications.

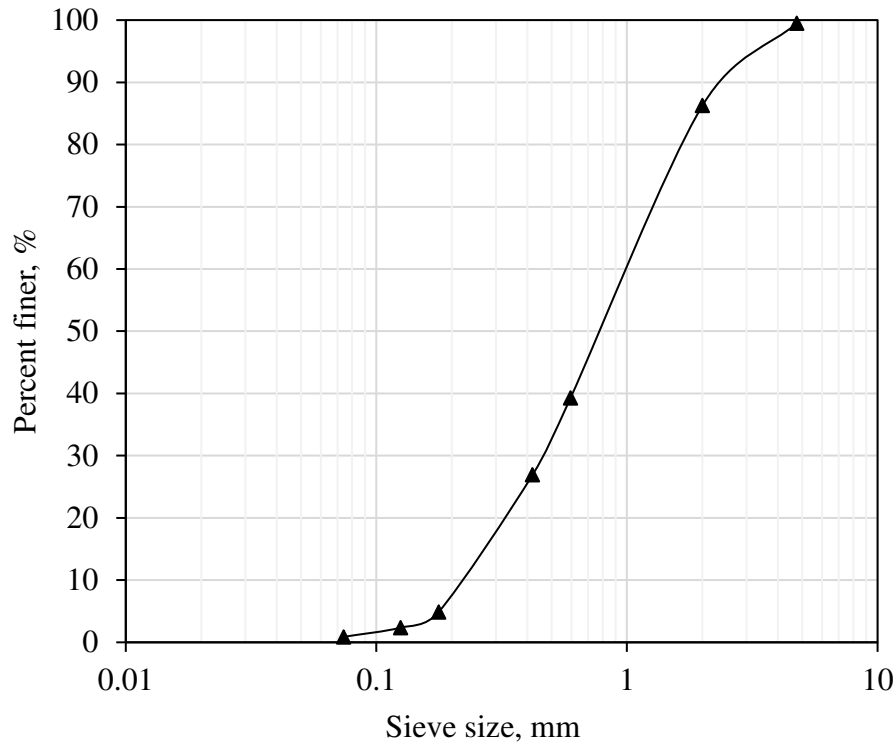


Figure 3.1 Particle size distribution curve of CSM sand.

Table 3.1 Mineralogy of CSM sand.

Property	CSM Sand
Mineral by mass (%)	Quartz 40.5%;
	Plagioclase 28.8%;
	Orthoclase 19.0%;
	Fe Oxides 4.1%;
	Mafic Minerals 3.6%;
	Mica 2.6%;
	Others 1.5%
USCS classification	SP

Note that mineralogy is one of the multiple factors to influence soil behaviors during EPB tunneling (Rostami et al. 2012). According to Lu et al. (2006), the interparticle forces of clay are primarily attributed to the physicochemical component of the suction stress among particles, which

is sensitive to the types of clay minerals. While for granular soil, the interparticle forces are mainly a result of surface tension at air-water interface. Therefore, mineralogy has limited influence on the sand properties. Instead, sand behavior is more influenced by other factors such as particle size distribution, angularity, water content, etc. While limited literature is available on the response of sand behaviors to soil conditioning with regard to mineralogy change, soil mineralogy is expected to impact the conditioning results. As such, mineralogy of CSM sand is provided to indicate the sample composition for future reference and comparison with future tests.

Water content is a dominant factor in controlling soil properties. In this study, CSM sand was adjusted to different water content levels before rheology testing. Approximately 60 g of the air-dried sand was put in an evaporating dish and dried for 10 min in an oven pre-heated to 150 °C. Afterwards, tap water was instilled into the sand to adjust the water content to designated values including 5%, 7.5%, 10%, 15%, and 20%. Previous tests indicated that 100% degree of saturation in this sand is at the water content of 20%, and as such, the above-mentioned water content levels refer to degree of saturation of 25%, 37.5%, 50%, 75%, and 100%, respectively. The wet sand was sealed and kept in a container ready for testing while adjusting the rheometer set-up.

3.3.2 Testing with ARES-G2 rheometer

Two small rheometers were used in the study presented in this chapter, namely ARES-G2 rheometer and Discovery HR-3 rheometer. Both rheometers were manufactured by TA Instruments. The ARES-G2 magnetic bearing rheometer, as shown in Figure 3.2 (a), is a rotational rheometer mounted with a maximum torque capacity of 200 mN·m and a maximum axial force capacity of 20 N (TA Instruments 2017). The built-in vane is 28 mm in length and 15 mm in diameter. The cup diameter is 29.36 mm. This renders a gap between the vane and the cup of roughly 7.5 mm. To reduce the wall-slip effect between the sample and the cup, a piece of sand paper was curled and glued to the cup, as shown in Figure 3.2 (b), which further reduces the available gap down to roughly 6.5 mm.

CSM sand with the designated water content was loaded into the cell using a laboratory spatula. The volume of the loaded sand was set to be roughly 35 ml so that the vane was entirely covered by the sand after being lowered into the testing position. It is important to keep the soil structure loose so that the vane can be lowered in place. The viscosity and yield stress measurement utilized different testing modules in the affiliated TA Instruments software called TRIOS. For viscosity measurement, flow sweep procedure was implemented meaning that the shear rate of the

testing was controlled in a stepwise fashion. For each shear rate, the device made five readings which were averaged to record a value for plotting the shear stress-shear rate curve. For this vane geometry, the shear rate range was fixed between 0.01 1/s (0.6 rpm) and 200 1/s (12,000 rpm). This covers a normal range of possible shear rate on the excavated muck in EPB tunneling. A total of five sweeps were implemented, including an initial mixing sweep ramping up shear rate from 0.01 1/s (0.6 rpm) to 200 1/s (12,000 rpm). Subsequently, the shear rate was ramped up and down twice, respectively, between 0.01 1/s (0.6 rpm) and 200 1/s (12,000 rpm). This operation ensured sufficiently stable soil structure and repeatable data sets of each soil condition.

Once viscosity testing was completed, the vane was lifted up, as shown in Figure 3.2 (c), and the soil structure inside the cup was restored by stirring it with a lab spatulas. This would allow for the subsequent yield stress measurements on the same soil structure. There are different means of determining yield stress such as stress ramp, strain ramp, oscillation sweep, and multiple sweep (Tianhong 2000; Malvern Instruments Worldwide 2016). In this study, two methods were implemented and compared, namely strain ramp and oscillation sweep methods. In strain ramp method, the strain rate was fixed at a certain value for each testing and the cumulative strain was systematically controlled until either a soil softening behavior was observed or a maximum of 4% cumulative strain was reached. The shear stress corresponding to either the end of the elastic deformation portion or the 4% strain was taken as the yield stress. Note that the 4% strain criterion was selected based on a study on isotropic polymers (Farrokh and Khan 2010). Compared with polymers, CSM sand has more loose structure and is expected to yield at a lower strain. Therefore, the yield stress obtained from 4% strain criterion is expected to be the upper bound limit, as will be shown in the later comparison.

In the oscillation sweep method, the vane was initiated in an oscillatory fashion until the vane endured large rotational displacement. Akin to that of the strain ramp method, there were also two yield criteria for consideration. That is, either the point with the initially drastic drop in the measured elastic modulus (G') curve, or the crossover point between the elastic modulus and the loss modulus (G'') curves was taken as the yield point. The yield stress results obtained from these two methods were compared to determine a reliable measurement method.

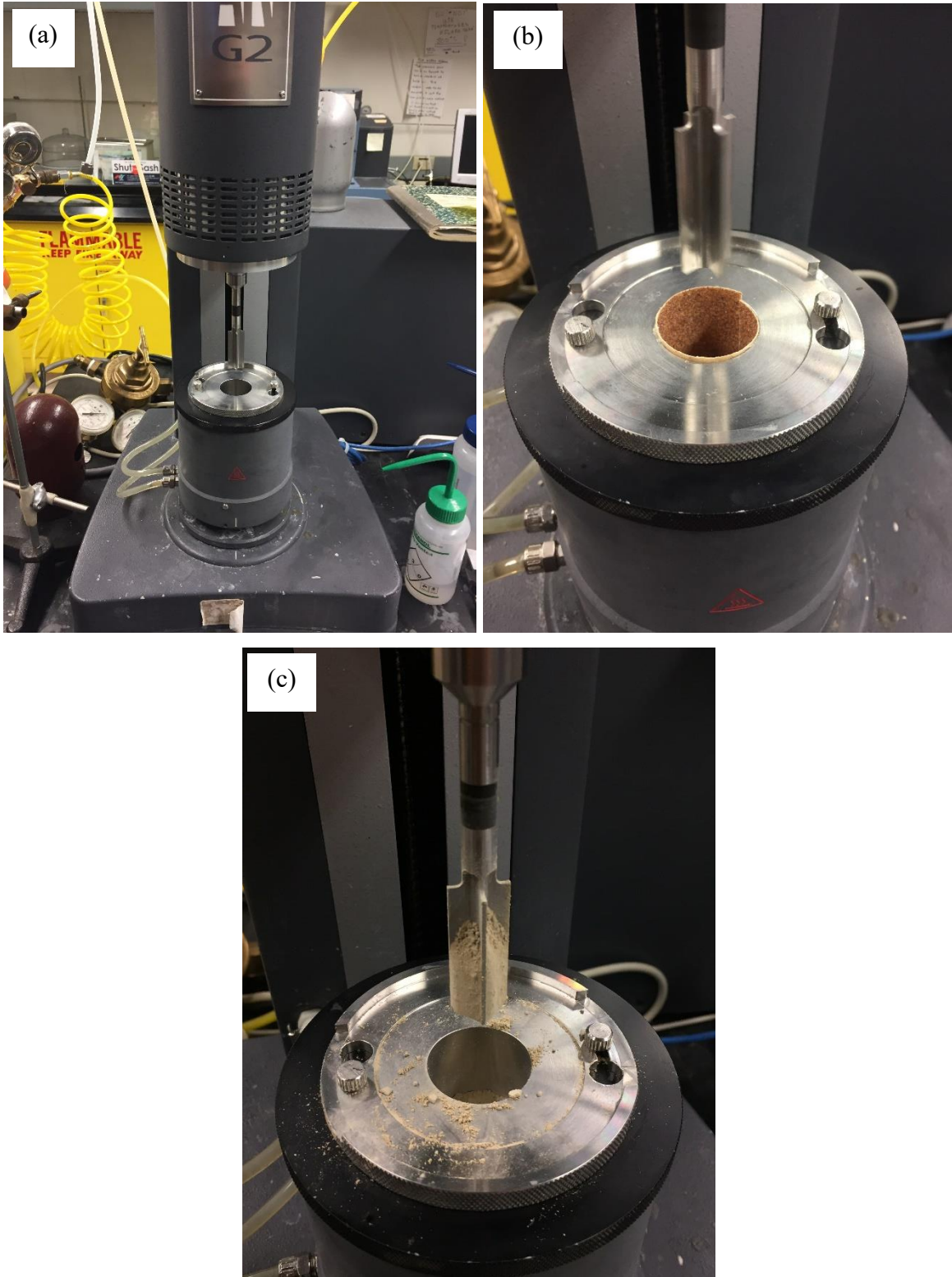
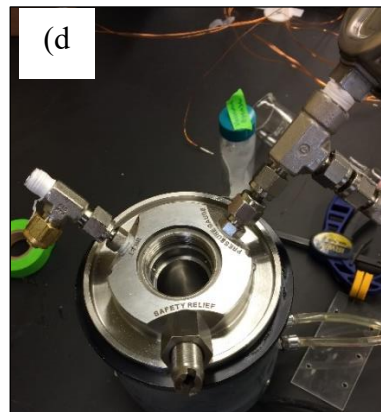
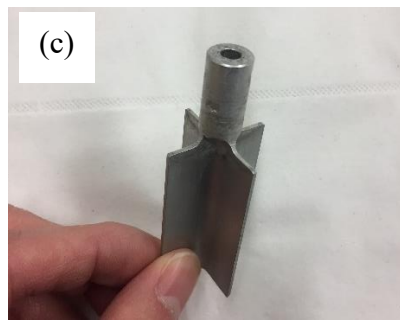
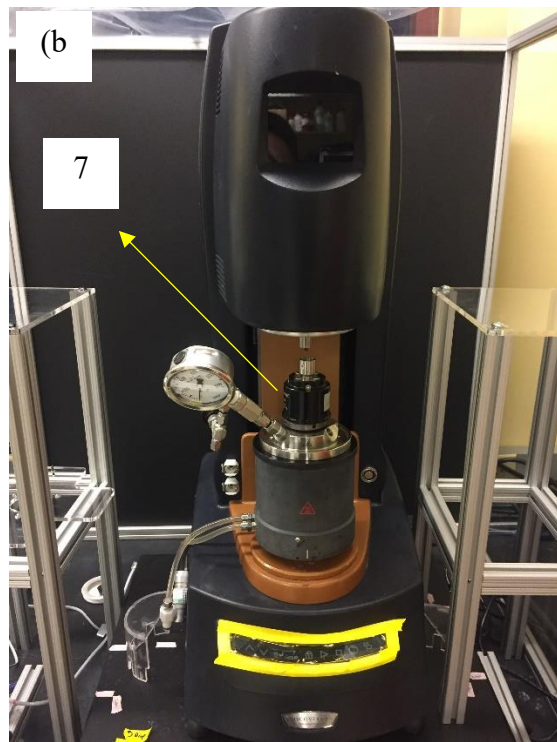
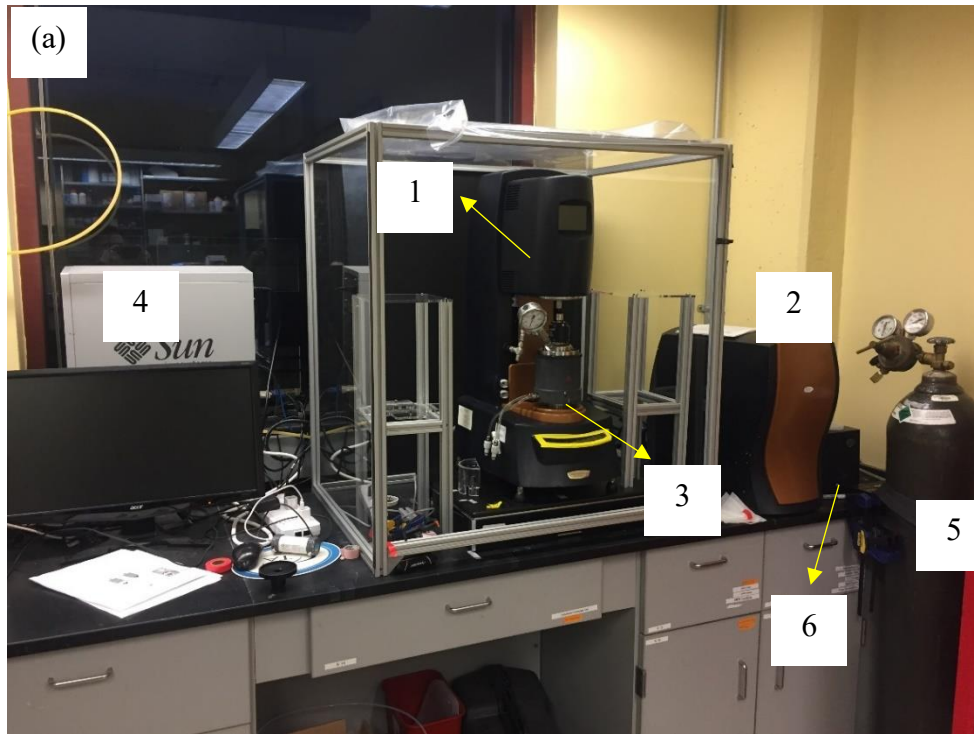


Figure 3.2 AR-G2 rheometer: (a) overall view; (b) sand paper to prevent wall slip; and (c) vane after testing.

3.3.3 Testing with Discovery HR-3 rheometer

The ARES-G2 is not equipped with a pressurized cell and is only capable of testing in atmospheric condition. To explore the rheology testing procedure under pressurized conditions, further experiments were carried out with another small-scale rheometer equipped with a pressurized cell, namely Discovery HR-3 rheometer. As shown in Figure 3.3, HR-3 is one of the most advanced single-head rotational rheometers with a maximum torque capacity of 200 mN·m and a maximum axial force of 50 N. Compared with ARES-G2 rheometer, it offers better torque sensitivity and a pressurized testing cell enabling rheology testing at a pressure up to 138 bar (TA Instruments 2019). The aluminum vane is 43 mm in length and 26 mm in diameter. The pressure cell is 56 mm in depth and 28 mm in diameter. Compared with the dimensions of the ARES-G2 device, the gap between the vane and the cell in HR-3 is only 1 mm, casting doubt on the feasibility of using this device for rheology testing of CSM sand. Note that the primary goal of these tests was to explore the potential impact of pressure on sand rheology, not the absolute measurement of rheological parameters of the conditioned CSM sand. Therefore, a NO. 40 sieve with the opening of 0.42 mm was used to sieve CSM sand and the particles finer than 0.42 mm were selected for testing.

The selected fine sand samples at four water content levels, including 5%, 7.5%, 10%, and 15%, were prepared with the procedure akin to the testing with ARES-G2 rheometer. Before loading the cell with soil, the device was calibrated for system inertia before connecting with any geometry and by rotational mapping when connecting with the geometry. An estimated 35 ml of sand was then loaded into the cell before closing the cell lid and installing the cell on the rheometer ready for each testing. For testing in atmospheric cell condition, the viscosity and yield stress testing procedures followed the same flow sweep and oscillation sweep procedure described in ARES-G2 testing. Testing at an elevated cell pressure of 4 bar required the disassembly of the pressure cell and restoration of the soil structure before putting back the pieces together again and connecting the cell with a pressure tank. Once the 4-bar pressure was applied on the cell, the testing followed the same procedure.



Note: 1. Motor, bearing and sensor module; 2. Motor control module; 3. Pressure cell; 4. TRIOS module; 5. Compress air; 6. Temperature control pump; 7. Magnetic connector.

Figure 3.3 HR-3 rheometer: (a) overall view; (b) device motor, bearing, sensor and pressure cell; (c) testing vane; and (d) pressure cell.

3.4 Results and analysis

3.4.1 ARES-G2 rheometer testing results

Similar to other soil properties, the rheology of soil is also greatly influenced by water content. A total of five water content conditions, including 5%, 7.5%, 10%, 15%, and 20%, were selected for rheology testing. The viscosity as a function of the shear rate was found to follow two modes. The first mode, as shown in Figure 3.4, occurs at water content of 5% and 7.5%. It is observed that within the same water content the curves differentiate little between different sweeps, indicating the material structure was stable after the initial pre-mix step. Hence, the testing procedure may be shortened to include only one cycle of ramping up and ramping down the shear rate.

It should be noted that the torque was also measured during the flow sweep. Hence, the yield stress can be obtained via model fitting technique (Malvern Instruments Worldwide 2016). In this chapter, however, yield stress will be measured by different testing methods on the same materials. The model fitting technique will be utilized in the following chapters when developing the new rheometer.

Due to the limited deviation, the viscosity values of the four sweeps for the same shear rate were averaged to obtain the average viscosity vs. shear rate response for these two water content conditions, as shown in Figure 3.5. It is observed that the viscosity vs. shear rate curves for water content of 5% and 7.5% follow a power law shear thinning pattern with satisfactory coefficient of determination (R^2) of 0.9976 and 0.9954, respectively.

The second mode of the viscosity function was found at water content levels of 10%, 15%, and 20%, as shown in Figure 3.6. The scattered logarithmic viscosity data no longer show monotonic linearly decreasing trend as the shear rate increases logarithmically. Instead, three separate portions can be found, i.e., a Newtonian plateau portion at a shear rate lower than 1 1/s (60 rpm), a power law shear thinning portion at a shear rate between 1 1/s (60 rpm) and around 40 1/s ~ 50 1/s zone (2,400 rpm ~ 3,000 rpm), and a shear thickening portion when the shear rate exceeds 50 1/s (3,000 rpm).

In addition, akin to that of the water content of 5% and 7.5%, the viscosity curves also show insignificant deviation between different sweeps.

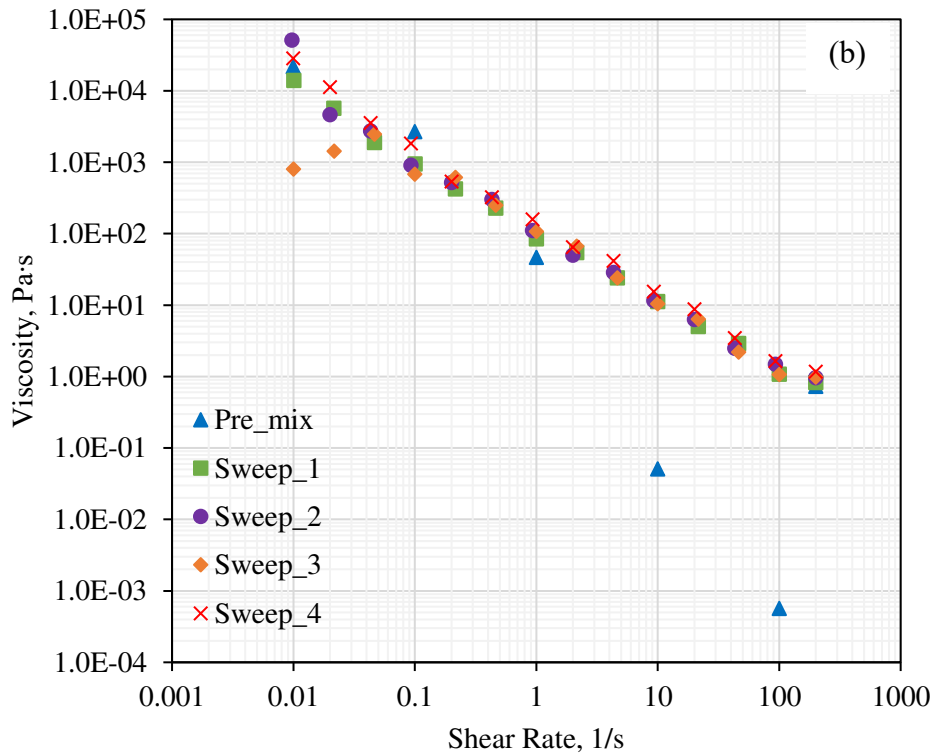
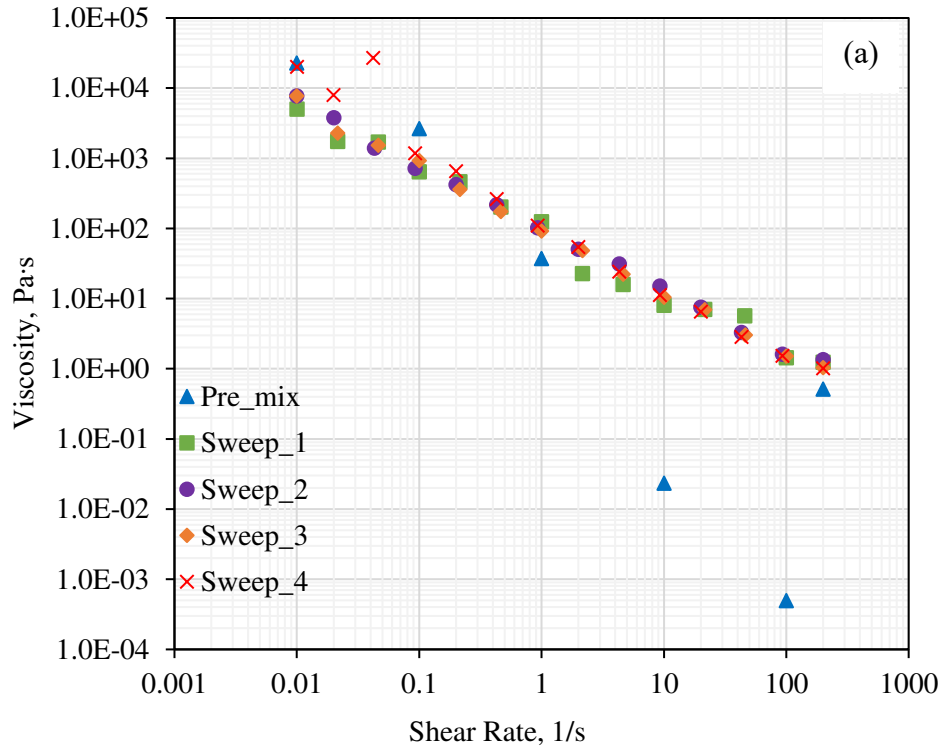


Figure 3.4 Flow sweep experiment results for CSM sand at: (a) $w=5\%$ ($S_r=25\%$); and (b) $w=7.5\%$ ($S_r=37.5\%$).

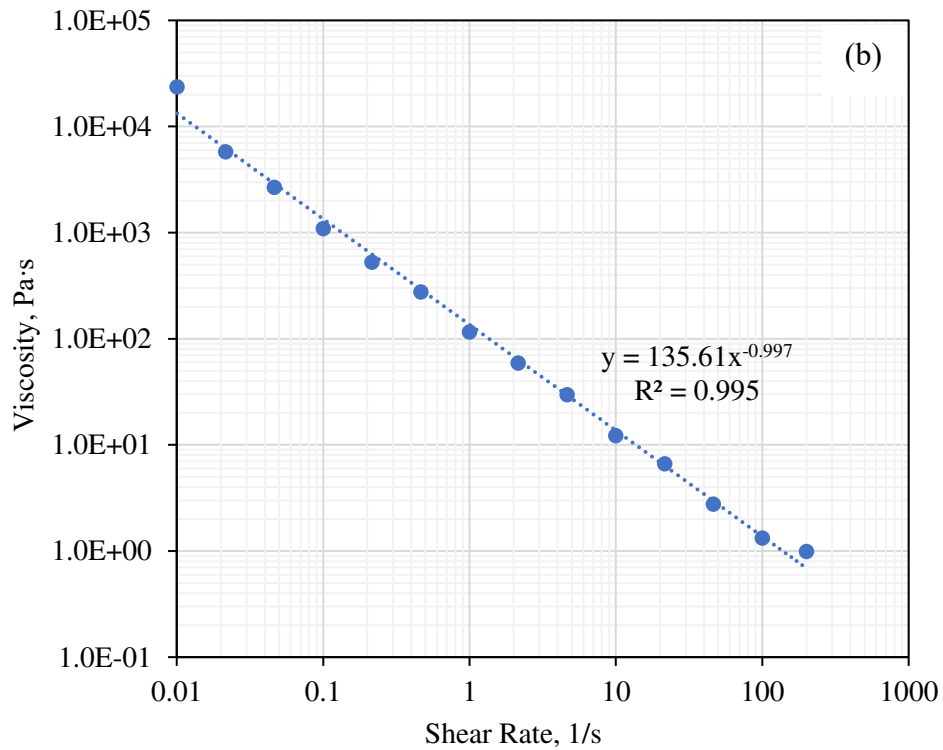
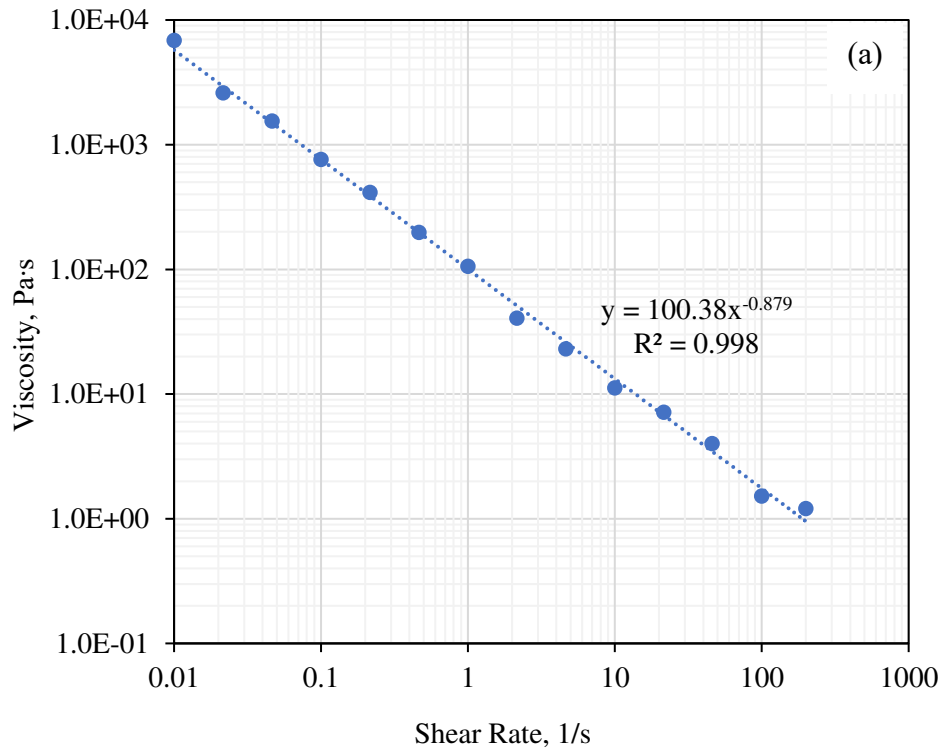


Figure 3.5 Averaged viscosity values and curve fitting for CSM sand at: (a) $w=5\%$ ($S_r=25\%$); and (b) $w=7.5\%$ ($S_r=37.5\%$).

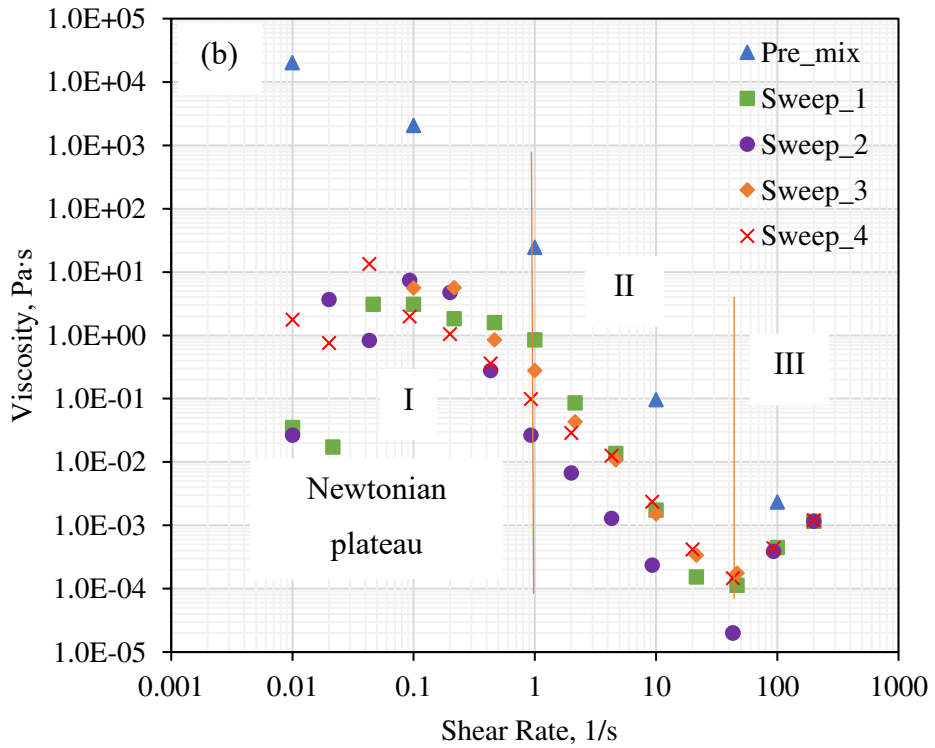
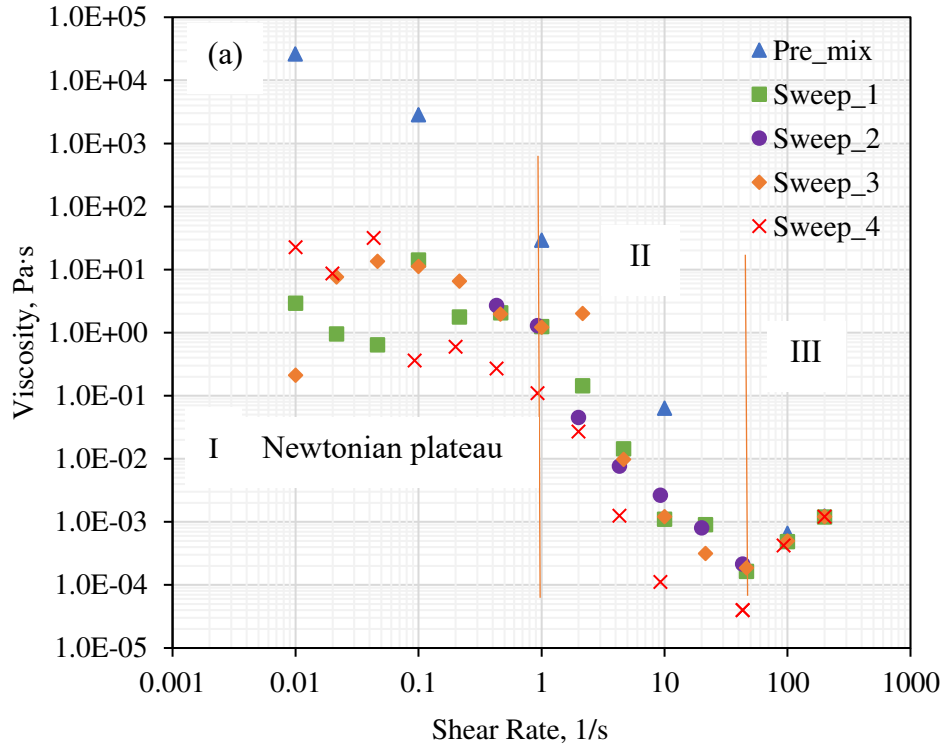


Figure 3.6 Flow sweep experiment results for CSM sand at (a) $w=10\%$ ($S_r=50\%$); (b) $w=15\%$ ($S_r=75\%$); and (c) $w=20\%$ ($S_r=100\%$).

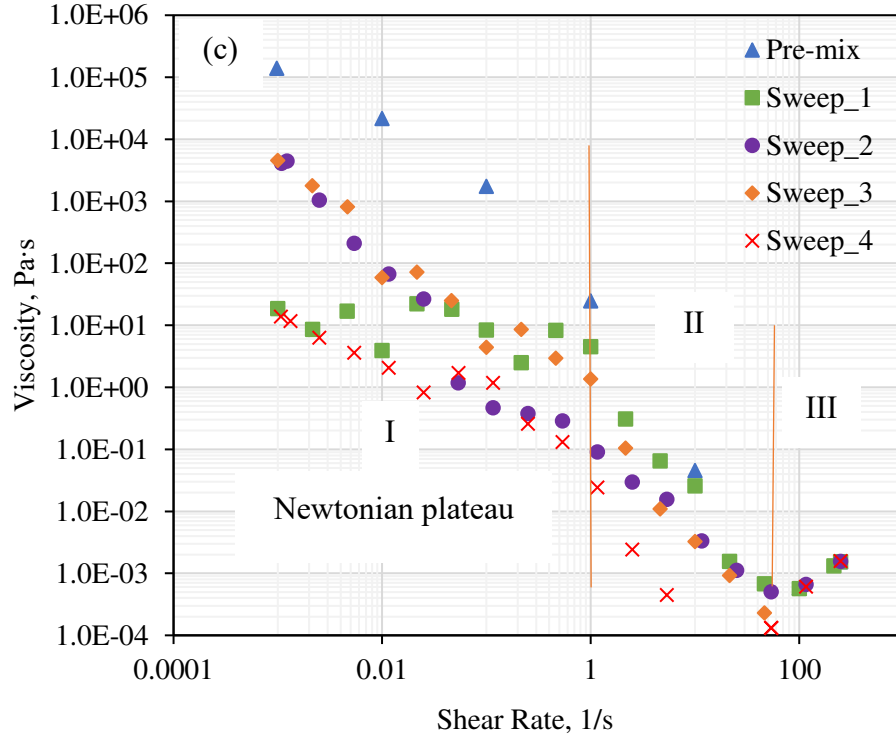


Figure 3.6 Continued.

The above-mentioned power law model of the viscosity data is the well-known shear thinning Herschel-Bulkley model. Eq. (3.4) and Eq. (3.5) are two different ways of presenting the model where the shear stress and viscosity are functions of the shear rate, respectively. The fitting coefficients of the Herschel-Bulkley model for water content of 5% and 7.5% are summarized in Table 3.2.

$$\tau(\dot{\gamma}) = \tau_y + K \cdot \dot{\gamma}^n \quad (3.4)$$

$$\mu(\dot{\gamma}) = \frac{d\tau(\dot{\gamma})}{d\dot{\gamma}} = n \cdot K \cdot \dot{\gamma}^{n-1} = k \cdot \dot{\gamma}^{n-1} \quad (3.5)$$

where “ τ ” is shear stress (Pa), “ μ ” is viscosity (Pa·s), “ τ_y ” is yield stress (Pa), “ $\dot{\gamma}$ ” is shear rate (1/s). In addition, k , n and K are model fitting parameters.

Table 3.2 Herschel-Bulkley model fitting parameters for CSM sand.

w (%)	S_r (%)	k (Pa)	n	K (Pa)
5	25	100.4	0.121	829.6
7.5	37.5	135.6	0.003	45203.3

Yield stress of the above-mentioned CSM sand at different water content levels were measured using two methods, i.e., strain ramp method and oscillation sweep method. In the testing using strain ramp method, three different shear rate levels were conducted for all water content conditions except 15%, as shown in Table 3.3. This is to examine whether yield stress of the sand would be impacted by changes of shear rate, and if so, to obtain a reasonable range of yield stress. A typical stress vs. strain curve of the strain ramp testing is shown in Figure 3.7. Two criteria were used to pinpoint the yield stress, i.e., the elasticity criterion and the 4% strain criterion. The elasticity criterion suggests that the material starts yielding at the end the elastic deformation portion which usually comes at around 1% strain or less, while the 4% strain criterion allows the material to deform as much as 4% strain before yielding. As is explained earlier, the yield stress obtained from 4% strain criterion is expected to be on the upper bound limit.

Table 3.3 Yield stress testing conditions using strain ramp method.

w (%)	S_r (%)	Shear rate (1/s)	Shear rate (rpm)
5	25	0.0003, 0.0005, 0.001	0.018, 0.03, 0.06
7.5	37.5	0.0001, 0.0003, 0.0005	0.006, 0.018, 0.03
10	50	0.0002, 0.001, 0.1	0.012, 0.06, 6
15	75	0.01	0.6
20	100	0.0002, 0.0003, 0.0005	0.012, 0.018, 0.03

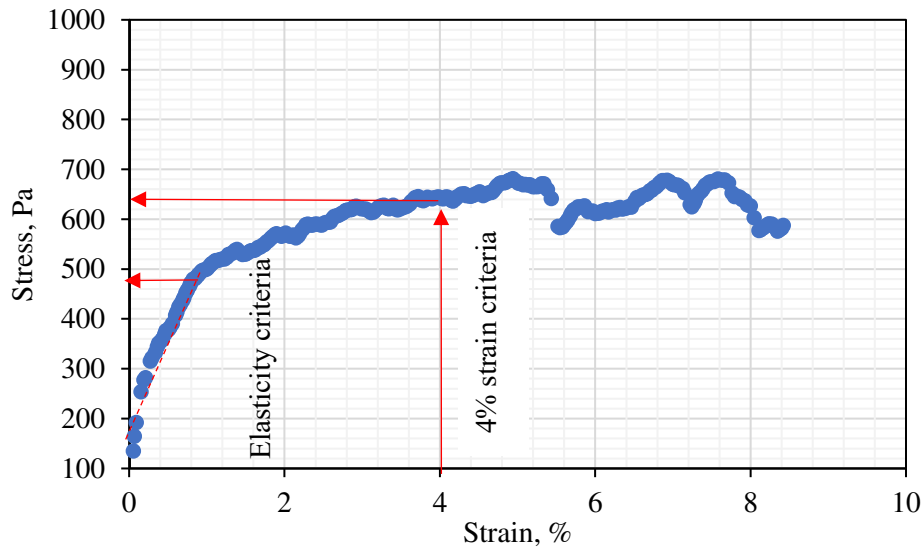


Figure 3.7 Stress vs. strain curve during strain ramp testing at $w=5\%$ ($S_r=25\%$) and shear rate=0.0003 1/s (0.018 rpm).

In oscillation sweep method, the oscillation frequency was universally set as 1 Hz, as shown in Table 3.4. Also shown in Table 3.4, the oscillation stress range for each water content condition was set based on some trial testing.

Table 3.4 Yield stress testing conditions using oscillation sweep method.

w (%)	S_r (%)	Oscillation frequency (Hz)	Oscillation stress range (Pa)
5	25	1	0.01-1000
7.5	37.5	1	0.01-1100
10	50	1	0.01-1300
15	75	1	0.01-1300
20	100	1	0.01-1400

The transient elastic modulus (G') and loss modulus (G'') values with respect to oscillation stress increase within the designated stress range were recorded during the test. Figure 3.8 shows typical modulus vs. oscillation stress relationships. It can be observed that the modulus values are sporadically scattered at oscillation stress less than 0.1 Pa. This is considered to be related to measurement precision of the device. After the oscillation stress exceeds 0.1 Pa, the modulus values stay at stable levels with unnoticeable change until 100 Pa when the G' curve starts to drop, indicating structural breakdown. This corresponds to one measure of the yield point. The other yield point is the one when the G' and G'' curves crossover each other, representing the transition from solid to liquid-like behavior. It is estimated around 400 Pa for the sand shown in Figure 3.8. The zone spanning these two points is referred to as the yield zone (Malvern Instruments Worldwide 2016).

The yield stress values estimated from both strain ramp and oscillation sweep methods using different yield criteria are summarized in Table 3.5. As shown in this table, it is confirmed that the 4% strain criterion generated the highest yield stress values in all water content conditions. Overall, it is hard to designate a fixed value of yield stress for certain condition. As such, it is more appropriate to specify a yield zone.

Overall, the above-presented results confirm the suitability of using flow sweep procedure to test viscosity of soils. Both strain ramp and oscillation sweep methods offer a zone of yield stress of materials even though the range differ significantly. It is suggested that the oscillation sweep method be adopted due to its clearer physical definition of the yield point.

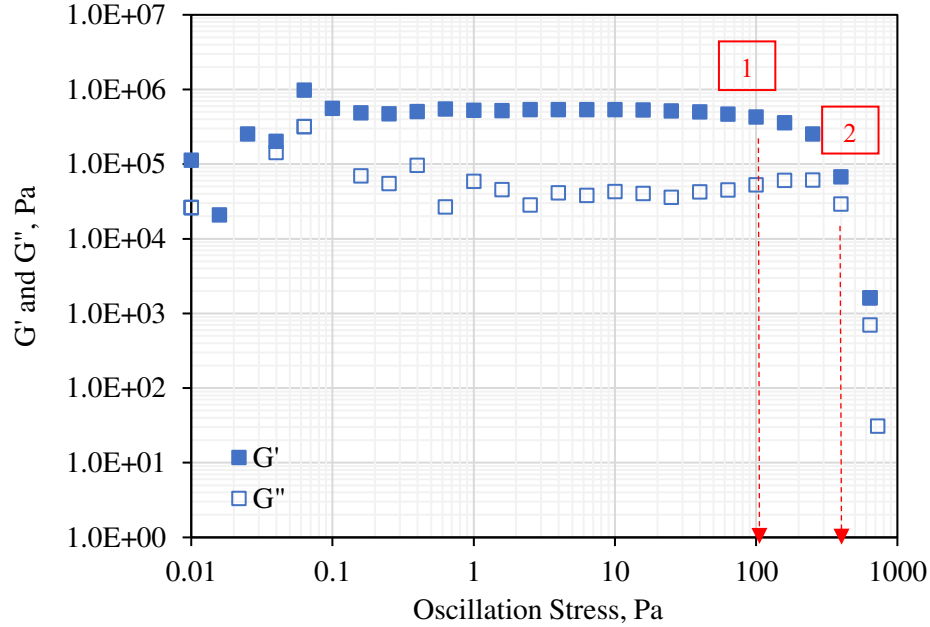


Figure 3.8 Determining yield stress from oscillation sweep results at $w=5\%$ ($S_r=25\%$).

Table 3.5 Yield stress of CSM sand determined by different methods and criteria.

w (%)	S_r (%)	Yield stress using strain ramp method (Pa)		Yield stress using oscillation sweep method (Pa)	
		Elasticity criterion*	4% strain criterion*	Initial G' drop criterion	G'/G'' crossover criterion
5	25	1000	1163	100	400
7.5	37.5	1650	1900	400	630
10	50	593	727	250	400
15	75	1500	3400	250	630
20	100	750	983	250	630

*. The values in these two columns were obtained by averaging the yield stress for different shear rates shown in Table 3.3 within the same water content.

3.4.2 HR-3 rheometer testing results

The sieved fine sand from CSM sand at four water content levels were tested using HR-3 rheometer. For each water content, two different cell pressure conditions were applied to test the viscosity response. Typical viscosity testing results are presented in Figure 3.9 (a). As is shown, the deviation between the different sweeps within the same cell pressure group is not substantial.

This allows for the operation of averaging the viscosity values at different sweeps to derive an averaged curve, as shown in Figure 3.9 (b). This figure also demonstrates that the viscosity values under a cell pressure of 4 bar increase to twice as much as that of the atmospheric condition. This means that cell pressure plays an important role in the viscosity of the soil.

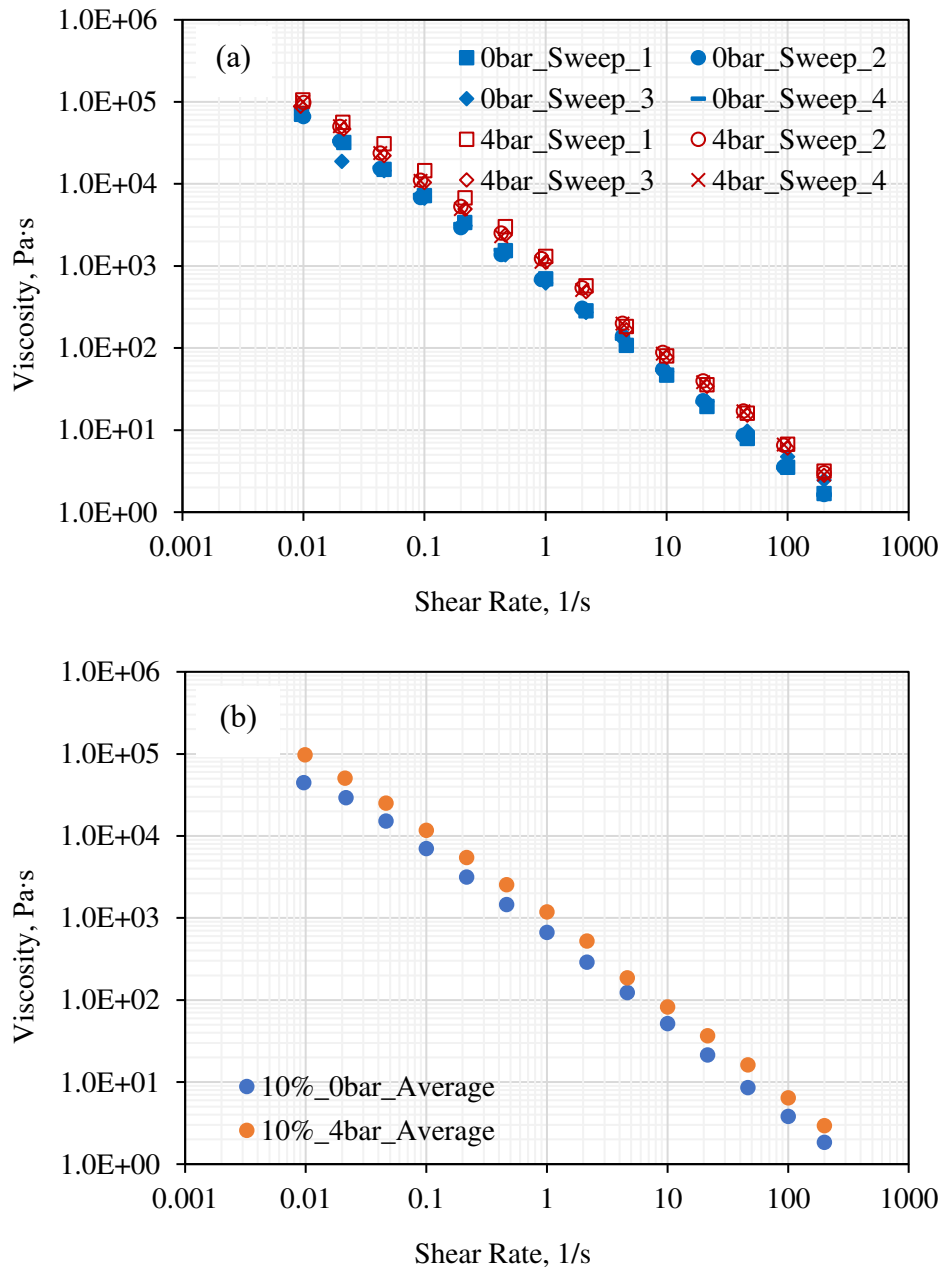


Figure 3.9 Viscosity testing results of CSM sand at $w=10\%$ ($S_r=50\%$) using HR-3 rheometer: (a) raw data; and (b) averaged viscosity.

The effect of water content on viscosity of the fine sand was also studied by comparing the viscosity response at four different water content levels, as shown in Figure 3.10. When it is under atmospheric condition, as seen in Figure 3.10 (a), the viscosity reaches maximum at water content of 5%, followed by 15%, 7.5%, and 10%. Quantitatively, the overall drop of viscosity from 5% to 10% is 2.12 times. When the cell pressure was increased to 4 bar, the deviation of viscosity decreased as shown in Figure 3.10 (b). These two scenarios reveal that both water content and ambient pressure play important roles in rheological behaviors of the fine sand, with the latter factor being more dominant in the soil used in this study.

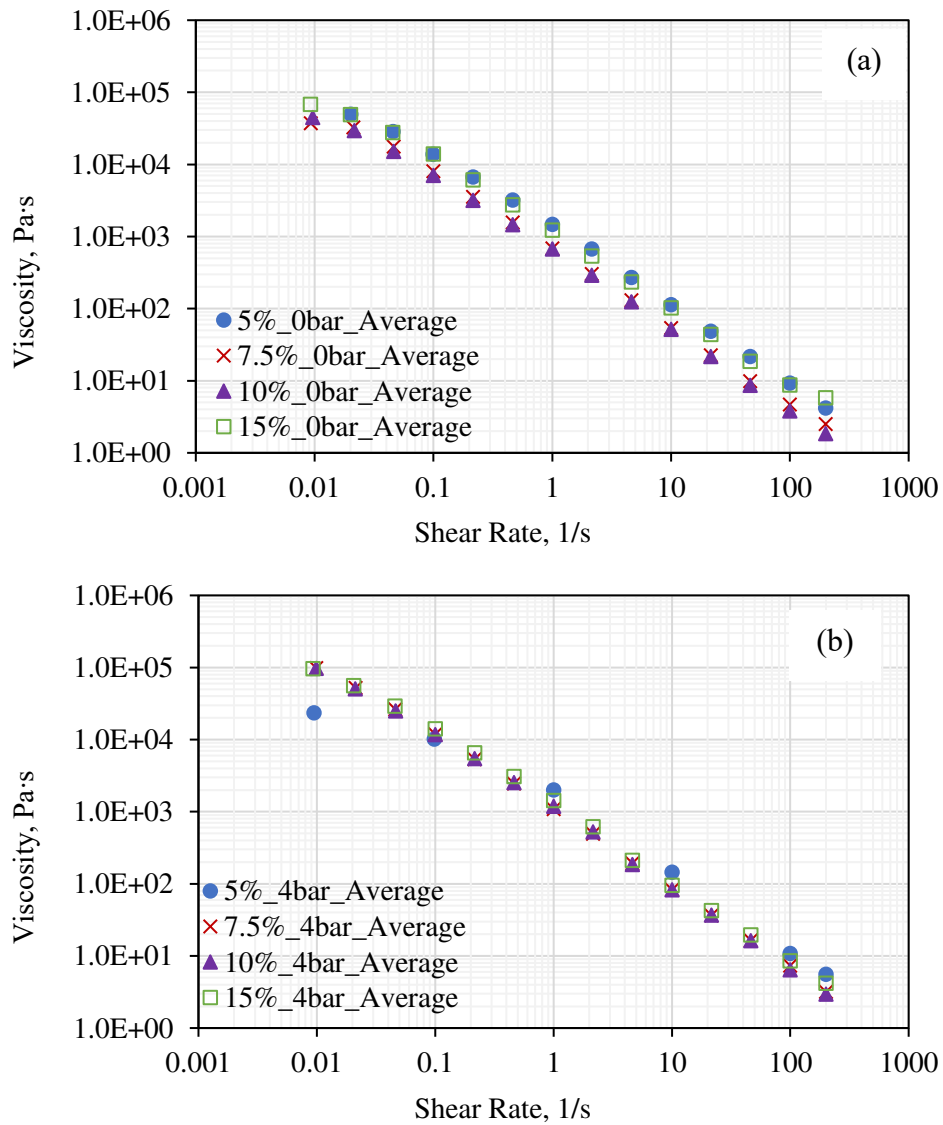


Figure 3.10 Averaged viscosity testing results of CSM sand at different water content and cell pressure combinations using HR-3 rheometer: (a) atmospheric condition; and (b) 4bar pressure.

Yield stress of the fine sand at water content of 5% and 7.5% were measured using oscillation sweep method. Unlike what occurred in viscosity when changing water content and cell pressure, the directly measured elastic modulus curves were found not to be sensitive to these changes in the pressure ranges below 400 pa, as shown in Figure 3.11 and Figure 3.12.

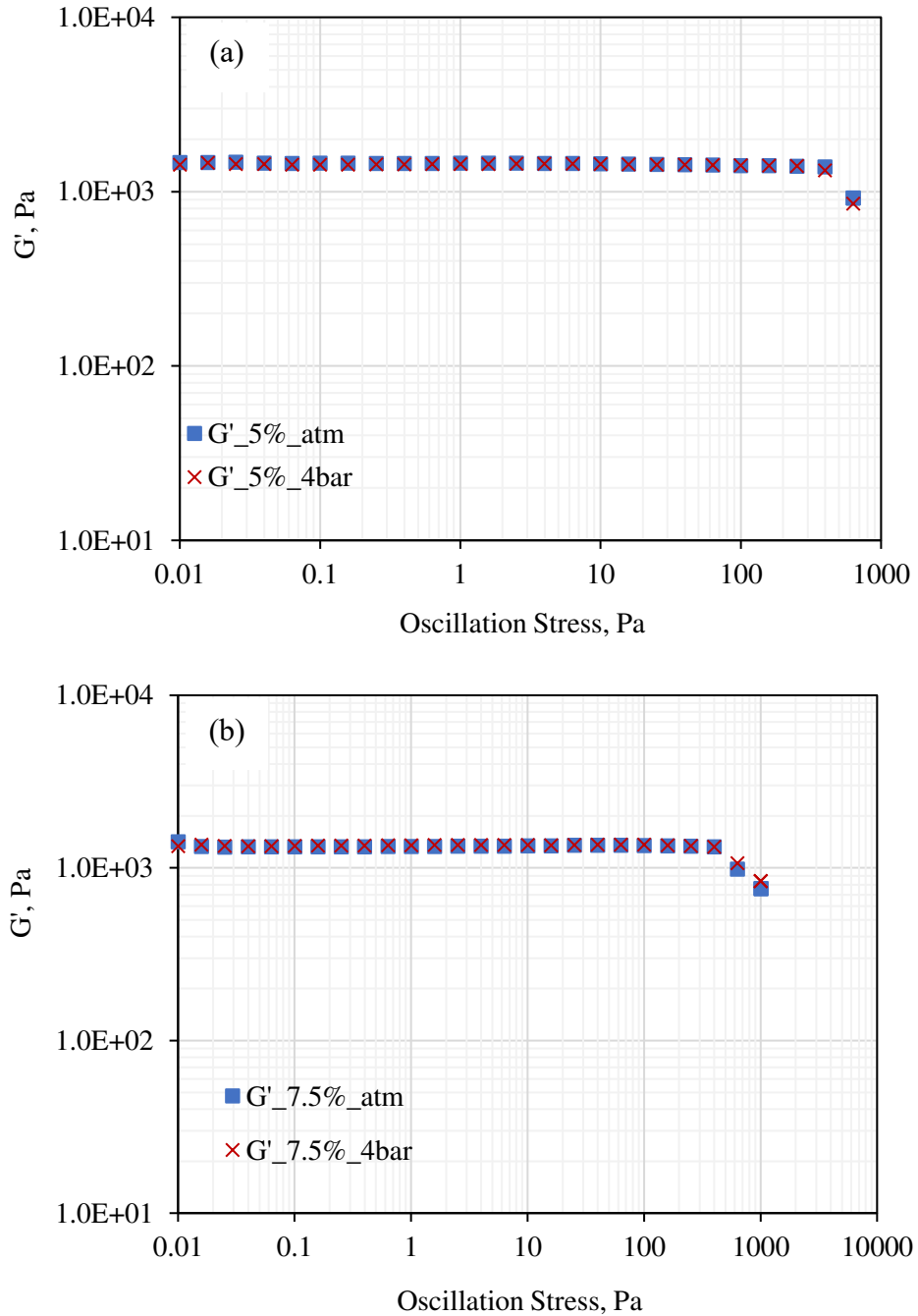


Figure 3.11 Effect of cell pressure on the measured elastic modulus and yield stress: (a) $w=5\%$ ($S_r=25\%$); and (b) $w=7.5\%$ ($S_r=37.5\%$).

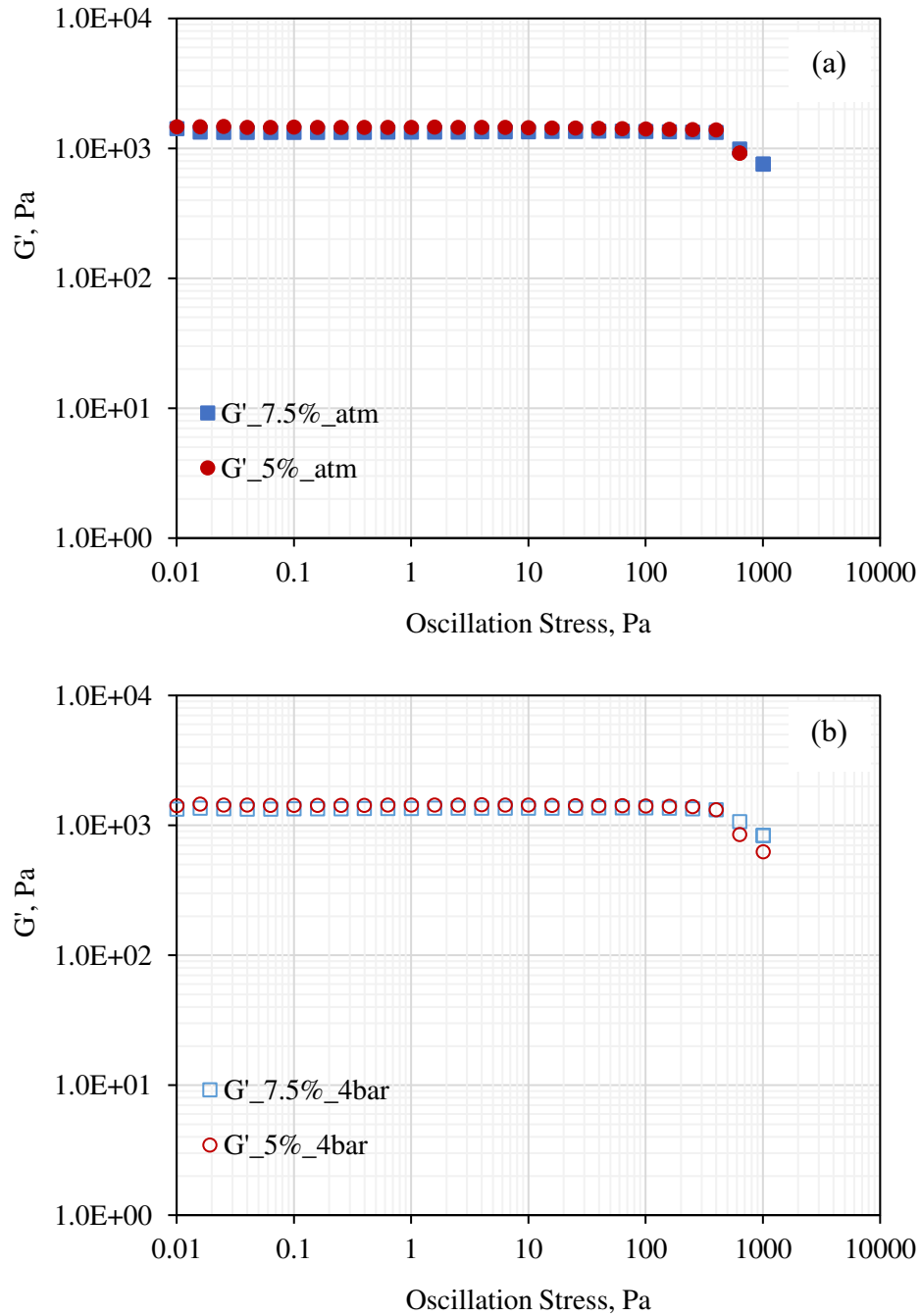


Figure 3.12 Effect of water content on the measured elastic modulus and yield stress: (a) atmospheric condition; and (b) 4bar pressure.

3.5 Conclusions

The experimental programs in this chapter were designed to serve as a preliminary phase of rheology characterization of conditioned soils for application in EPB tunneling. The ARES-G2 and HR-3 rheometers manufactured by TA Instruments belong to the category of small-scale

rheometers. They are widely used in rheology characterization of materials for application in food science, petroleum engineering, biological and chemical engineering, etc. In these industries, the materials tested in the small-scale devices are primarily liquid with homogeneous matrix. They have not been used to test soils with particles containing coarse sand. The experimental practice and results in this chapter verify the concern of the feasibility of using these small-scale rheometers to test soils for EPB tunneling purposes. That is, with the flow channel in these devices being in the millimeter scale, soils containing particles in the similar scale would have trouble to move around freely and the testing results may not exhibit true free flow behavior. The ratio between the flow channel and the largest material particles, as a rule of thumb, should be no less than 10:1 to prevent material from clogging (Zhong 2019). In other words, in order to obtain reliable test results with ARES-G2 and HR-3 rheometers, the soil particles should be limited to smaller than 0.5 mm and 0.1 mm, respectively.

Preliminary studies on the potential effect of water content and operation pressure on soil rheology were carried out and the results verify that both factors can impact soil rheology. In addition, shear thinning behaviors were observed in some soil samples and the Herschel-Bulkley model was applied to describe these behaviors. Overall, however, the observations show that the rheological responses of soil at various water content levels were not consistent and consequently, a practical rheological model for coarse-grained soils could not be developed.

To further address these problems, a large-scale rheometer, as will be discussed in the following chapters, is deemed necessary. With such a rheometer, soils containing particles as large as gravels can be tested. The effects of many potential influencing factors on soil rheology including water content, cell pressure, and foam conditioning parameters will be explored. Effort will also be made to investigate the possibility of using a linear model such as the Bingham plastic model to define rheology of such mediums.

CHAPTER 4

A NEW METHOD TO QUANTIFY RHEOLOGY OF CONDITIONED SOIL FOR APPLICATION IN EPB TBM TUNNELING

Modified from a paper published in *Tunneling and Underground Space Technology*

Wei Hu^{1,*} and Jamal Rostami¹

4.1 Abstract

The muck in the excavation chamber and the screw conveyor of Earth Pressure Balance (EPB) TBM, which comprises soil and rock fragments, is often conditioned to adjust its properties for more efficient operation of the machine. The target properties of the conditioned soil include low permeability, high compressibility, proper viscosity, and low abrasiveness, which are controlled to allow for maintaining face pressure, and to facilitate reduced torque and less wear of machine components. For instance, the viscosity and yield stress of the muck are expected to be neither too high to potentially plug the machine, nor too low to cause an uncontrollable flow or drop of the needed pressure to support the tunnel face. Among the critical properties, soil rheology plays a major role in offering desired characteristics in the conditioned soil. Rheology measurement of conditioned soil allows for optimizing the conditioning parameters and modeling of the muck flow through the machine. In this chapter, a new device for evaluation of soil rheology under specific settings of the conditioned soil in soft-ground tunneling is introduced and the preliminary results of the proposed testing method are discussed. The initial process of optimizing the configuration of the device for higher accuracy and sensitivity to rheological properties of conditioned soil through computational models are explained. The results of numerical modeling using CFD simulation to identify the preferred configuration of the new soil rheology measurement device are discussed. The feasibility of using the proposed system for quantification of the soil rheology for tunneling applications is examined.

4.2 Introduction

The basic function of the EPB TBM is to utilize the excavated muck as the supporting medium to maintain tunnel face stability while transporting the cuttings from the face through

Modified with permission of *Tunneling and Underground Space Technology*, 2020, 96, 103192.

¹ Earth Mechanics Institute, Colorado School of Mines, Golden, CO, 80401, United States.

* Corresponding author and editor. Direct correspondence to whwhuhw@hotmail.com.

excavation chamber and screw conveyor to the tunnel conveyance system in atmospheric pressure. To perform this function, the muck should have certain properties and show desired behaviors, such as low permeability, high compressibility, reasonable viscosity or flow-ability, and strength. For instance, the viscosity and yield stress of the muck are expected to be neither too high to potentially plug the machine, nor too low to cause an uncontrollable flow or drop of the needed pressure to support the tunnel face. Meanwhile, to minimize the downtime due to tool wear and machine clogging, the muck also needs to be within acceptable range of abrasiveness and stickiness. However, it is extremely rare for natural soil to exhibit these desired properties and often the muck, including soil and rock fragments, must be conditioned to modify its natural behavior. Typical conditioning agents for EPB tunneling include water, foam, polymer, and bentonite. To facilitate the optimal operation of an EPB tunneling system, a good understanding of the behavior of conditioned soil for all types of soil settings is essential.

Evaluating these parameters requires time-consuming lab testing processes to avoid costly mistakes and delays in the field. There is no universally accepted test for evaluating muck behaviors. However, some methods for evaluating the behaviors of conditioned soil have been adopted from other geotechnical and structural engineering tests, such as mixing test, slump test, permeability test, compressibility test, adhesion test, cone penetration test, soil abrasion test, vane shear test, among others (Messerklinger et al., 2011; Rostami et al., 2012; Zumsteg and Puzrin, 2012; Alavi et al., 2014; Galli and Thewes, 2014; Peila, 2014; Budach and Thewes, 2015; Galli and Thewes, 2016; Peila et al., 2016; Galli and Thewes, 2019).

In addition to being influenced by soil conditioning parameters, muck behavior is also impacted by other factors. This includes operating pressure, TBM operational parameters such as thrust force and rotational speeds of both the cutterhead and the screw conveyor. EPB machines must be operated with proper rotational speeds and thrust force for specific geological conditions to provide appropriate face support, facilitate muck transportation, maintain acceptable torque and energy consumption, and eventually offer maximum productivity. To date, it is still challenging to take into account both geology and machine operation when predicting muck behaviors. In other words, there are still gaps in proper prediction of muck behaviors as functions of conditioning parameters to reflect the site conditions. For example, there is no standardized soil abrasion test for sandy soils, nor a well-defined standard conditioning and clogging tests for clayey soils. Furthermore, there is limited information on soil rheology relative to the conditioning parameters.

Also, the details of soil movement within the chamber relative to the configuration of the cutterhead, cutting chamber, and screw conveyor, cutterhead speed, and pressure in various locations are unknown.

This is why tunneling is still a highly experience-based industry, despite the significant advances in machine manufacturing technologies as well as construction chemicals used for modifying soil behavior in the past few decades (Langmaack 2000). One example is that the EPB TBMs are operated based on the operator's judgement of the observed conditions and the response of machine sensory systems. While some people argue that a detailed geotechnical investigation program and well-defined Geotechnical Baseline Report (GBR) together with experience of crew are enough to ensure successful tunneling, there are cases where unexpected under-defined geological conditions have caused costly downtimes for machine repair or extreme measures for mitigation of the surface settlements. Therefore, an on-site intelligent EPB shield operating system with both predictive and real-time assessment capabilities could help manufacturers to design optimal configurations of cutterhead and excavation chamber, screw conveyor, and conditioning system. It also allows contractors to reasonably predict machine operational parameters before the start of tunneling. Such an intelligent system can ideally assist the operators to make proper decisions about machine operational and soil conditioning parameters. With such intelligent systems together with experienced crews, EPB machine advance rate is expected to greatly improve due to reduced downtime.

This chapter presents the importance and intricacies of rheology of conditioned soil and the necessity to properly characterize soil rheology. A newly developed soil rheology evaluation method and the initial steps towards the development of a device for measurement of rheology of conditioned soil will be discussed. It introduces the preliminary results of developing a new system for evaluation of rheology of conditioned soil. The system involves a properly scaled rheometer that allows for observation of the shear stresses under different shear rates for samples of conditioned soil at given pressure, c_f , FER , FIR , and w , in conjunction with CFD modeling to back calculate yield stress and viscosity.

4.3 Proposed soil rheology evaluation method

4.3.1 Overview

The proposed soil rheology evaluation method is a combination of lab testing and computer modeling. The lab testing component is modified from the Soil Abrasion Index testing device

(Rostami et al., 2012), by adding a Variable Frequency Drive (VFD) unit and optimized propellers. This device measures torque at various rotational speeds of the propeller, thus allows for establishing a relationship between torque as representative of shear stress, and rotational speed that is the indicator of shear rate, for different soil settings and machine operational parameters. The corresponding soil rheology parameters, i.e., yield stress and viscosity, are still unknown, but they can be directly calculated if a simple propeller geometry such as a vane is used to connect micro-scale rheology parameters to macro-scale torque.

For more general scenarios and more complex propeller geometries, the yield stress and viscosity can be back calculated in CFD models. That is, parameters including yield stress, plastic viscosity, and rotational speed will be used as input parameters for corresponding CFD models to estimate torque values. In this way, a unique torque vs. rotational speed curve can be established for a particular combination of yield stress and plastic viscosity. By fitting the simulated curve to the tested scattered data, a unique set of yield stress and plastic viscosity values can be found for corresponding soil settings. In other words, for a given setting of soil conditioning, pressure, and other environmental control parameters, a unique set of rheological parameters can be assigned.

By repeating this process for different scenarios of soil type, soil conditioning, and machine operation, a comprehensive soil rheology chart can be established. For each unique set of soil settings, including soil types and conditioning schemes, there is only one set of soil rheology parameters that offers the best fit for matching the torque vs. rotational speed response of the testing unit. The model can then be upscaled to EPB machines to predict the anticipated flow behavior of the soil under given machine operating conditions.

4.3.2 Preliminary testing

The testing component of the proposed soil rheological study, or rheometer was developed on the basis of the Soil Abrasion Index testing machine, shown in Figure 4.1 (a). It consists of a cylindrical testing chamber 330 mm in inner diameter and 450 mm in height, enabling testing of soil with various particle size distributions, up to gravel-size particles. A pitched propeller with three blades is mounted at the lower end of the drive shaft and spins inside the chamber containing the soil under desired conditions (moisture content, conditioning, pressure, etc.). The propeller is powered by a 3.7 kW drive unit. When testing, the chamber is filled with soil to 300 mm of the chamber height, rendering 150 mm of soil depth both above and below the propeller. The soil can be prepared with different water content conditions and conditioning parameters, and tested under

selected surcharge loading and ambient pressures, representing the column of soil above the tunnel and pore pressure, respectively. The torque, which is the integration of the shearing force in the horizontal planes in the soil, is directly measured by two force sensors attached to the chamber. The axial force imposed on the soil by the spinning pitched propeller is not measured. This is because the tray table under the chamber is designed to be free spinning and consequently, the axial force will not add extra friction to the system. Compressed air valves are connected to the top lid of the chamber and can simulate various pressures, including tunneling conditions with pore pressure or surcharge loading up to 1000 kPa. Details of the device can be found in literatures (Rostami et al., 2012; Alavi et al., 2013; Hedayatizadeh et al., 2017).

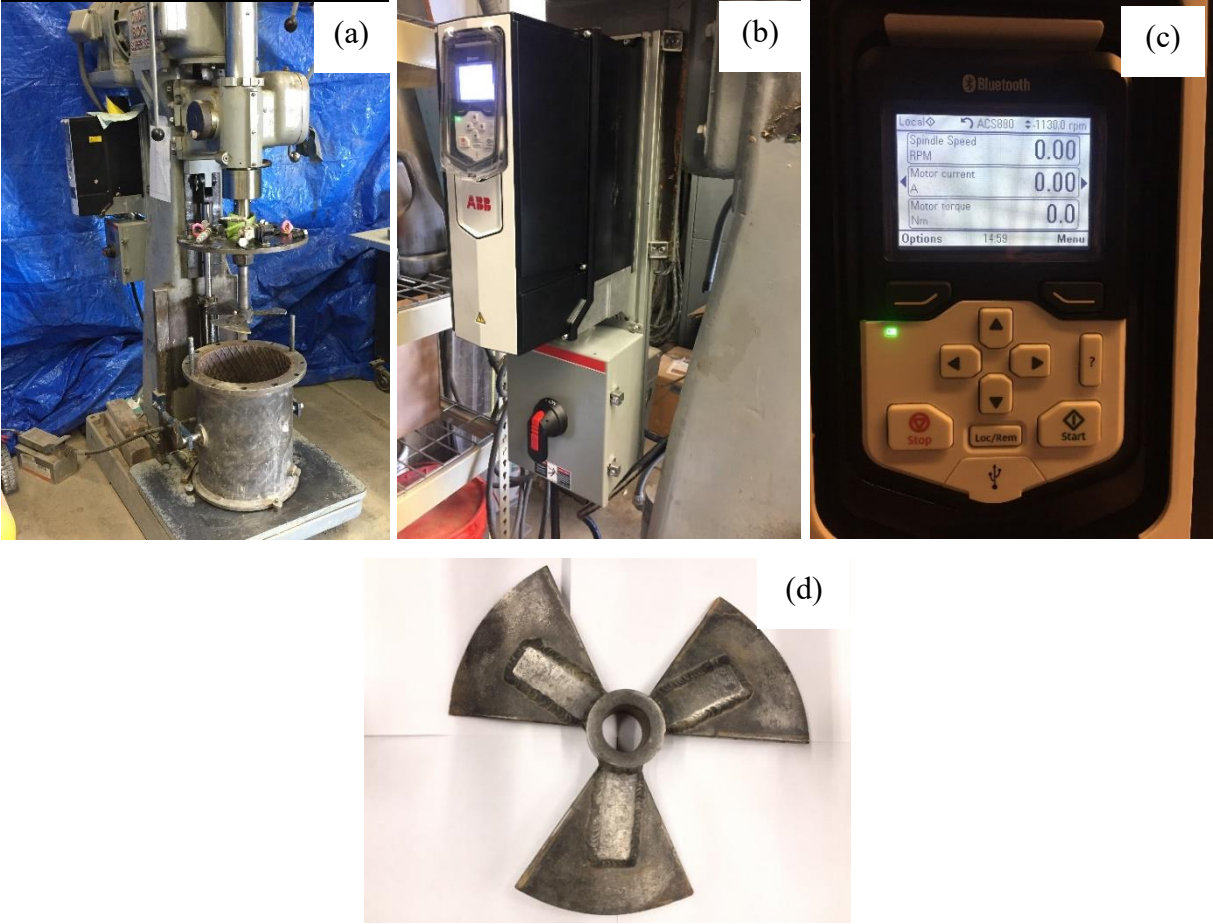


Figure 4.1 Configuration of the preliminary design of soil rheometer device: (a) overview; (b) new VFD unit; (c) rotational speed control panel; and (d) pitched propeller with 10 degree (deg) pitch angles.

The original design of the machine allowed for operation at 60 rpm, designed for expediting tool wear measurement in the laboratory. A VFD controller, as shown in Figure 4.1 (b), was added

in this study to allow various propeller rotational speeds between 0 rpm and 1000 rpm, through a control panel as shown in Figure 4.1 (c). The control panel also shows estimated torque and power draw of the drive unit that can be utilized in future versions of the device for pertinent calculations.

While the current propeller can offer the torque vs. rotational speed relationship for conditioned soil, the possibility of using a different propeller geometry or an optimal design that could offer higher sensitivity and accuracy in calculation of rheological parameters was examined in this study. For initial testing and calibration of the models, the existing 10 deg pitched propeller, as shown in Figure 4.1 (d), was used to carry out some preliminary rheology testing on CSM sand and some clay samples. The initial testing allowed for verification of the CFD modeling for simulation of the working conditions of the propeller in the chamber, which would subsequently be used to predict the behavior of various propeller geometries in the similar working conditions. This exercise allowed for selection of the optimal propeller geometry for the rheometer unit.

4.3.3 Computational Fluid Dynamics (CFD) Modeling

The CFD modeling is governed by Navier-Stokes equations which consist of the mass continuity equation and the momentum balance equation denoted as Eq. (4.1) and (4.2), respectively.

$$\frac{\partial \rho}{\partial t} + \nabla \cdot (\rho \mathbf{u}) = 0 \quad (4.1)$$

$$\rho \frac{\partial \mathbf{u}}{\partial t} = -\nabla p + \nabla \boldsymbol{\tau} + \rho \mathbf{g} \quad (4.2)$$

where ρ is the fluid density (kg/m^3), t is the time (s), \mathbf{u} is the velocity tensor, $\boldsymbol{\tau}$ is the viscous stress tensor, \mathbf{g} is the acceleration (Oliva et al. 2015). In Eq. (4.2), the term on the left side of the equilibrium denotes the momentum convection, whereas the terms on the right side of the equilibrium denote surface force, viscous force, and mass force, respectively. The Navier-Stokes equations are highly non-linear partial differential equations which require numerical tools to solve under reasonable simplifications for particular applications (Kundu, Cohen, and Dowling 2012).

The determination of the rheological parameters of the conditioned soil was conducted with the Rotating Machinery interface in the CFD module in COMSOL Multiphysics V5.4 (Comsol Inc 2018). The modeling began with the geometrical setting of the test chamber and the propeller. Soil was added to the chamber as a non-Newtonian fluid (Meng et al., 2011; Galli and Thewes, 2019) and divided into the rotating domain and the stationary domain connected by sliding meshes. The rotation module of the program allowed for rotation of the propeller in the chamber and calculation

of the torque on the propeller. Assigned yield stress, viscosity, and rotational speed were the primary input parameters of the model to calculate torque on the propeller as a primary output.

To achieve optimal balance between computational accuracy and cost, the following simulation settings and considerations in the CFD models were implemented:

(1) Laminar flow. This is because the Reynold number was estimated to be less than 100.

(2) Frozen rotor approach. This method adopts the pseudo-stationary concept to simulate rotating devices without rotating them as if the rotating parts were “frozen” in position. The feasibility of this approach was validated by the experimental results that the flow and the torque in the chamber stabilized after some time for all propeller speeds. This method reduces computational time and required resources significantly, and meanwhile is appropriate in mixers without baffles (Kinnane, 2013).

(3) Soil density values at different water content levels were set up as those values adopted from laboratory measurements.

(4) The Bingham-Papanastasiou (B-P) plastic model (Papanastasiou 1987) was used. The B-P plastic model is written as $\eta = \mu_0 + \frac{\tau_y}{|\dot{\gamma}|} [1 - \exp(-m|\dot{\gamma}|)]$, where:

(1) “ η ”: dynamic viscosity (Pa·s). It is defined as $\eta = \frac{\tau}{|\dot{\gamma}|}$.

(2) “ μ_0 ”: plastic viscosity (Pa·s). It is defined as $\mu_0 = \frac{\Delta\tau}{|\dot{\gamma}|}$.

(3) “ τ_y ”: yield stress (Pa).

(4) “ $|\dot{\gamma}|$ ”: shear rate (1/s).

(5) “ m ”: ramping factor (s). When m approaches infinity, the B-P model becomes the

$$\text{Bingham model } \eta = \mu_0 + \frac{\tau_y}{|\dot{\gamma}|}$$

Note that the B-P plastic model was used instead of direct implementation of the Bingham model due to computational convenience (Papanastasiou 1987). The exponential term, called the ramping factor, m , facilitates convergence at extremely low shear rate so that one continuous function would be adequate to describe the yield stress phenomenon instead of using a step function. The ramping technique is a powerful iteration tool in COMSOL. With this feature the computational results of a smaller m value can be used as the initial conditions for solving the following iteration with a higher m value. For each iteration, m is a constant, and hence, reducing

the total number of unknowns of the B-P plastic model to two, i.e., μ_0 and τ_y . Therefore, the two unknowns can be solved with two shear rate values and two equations.

Figure 4.2 provides an illustration of this ramping concept where μ_0 and τ_y are 100 Pa·s and 800 Pa, respectively. As illustrated in Figure 4.2, the dynamic viscosity is constant when m equals 0, which is unable to describe the yield point. As m increases, the curve approaches the ideal Bingham plastic model. As long as m is large enough, the modeled curve will be reasonably close to the theoretical model. In this case, when m reaches 100, the curve already overlaps with that of $m=1000$. Meanwhile, the computational time should also be considered meaning that m shall not go to infinity. In this thesis, m value was set to increase from 0 to 1, and to 10 for each computational model. A larger m value such as 100 was not used throughout because the increased accuracy was considered marginal, as shown in Figure 4.2, while the computational time was significantly increased. The computational time increased from approximately 1.5 h for $m=10$ to roughly 2.5 h for $m=100$ for most of the modeling cases, with some extreme scenarios unable to converge for $m=100$. Meanwhile, the corresponding computational torque results were found to be within 2% difference between that of $m=10$ and $m=100$.

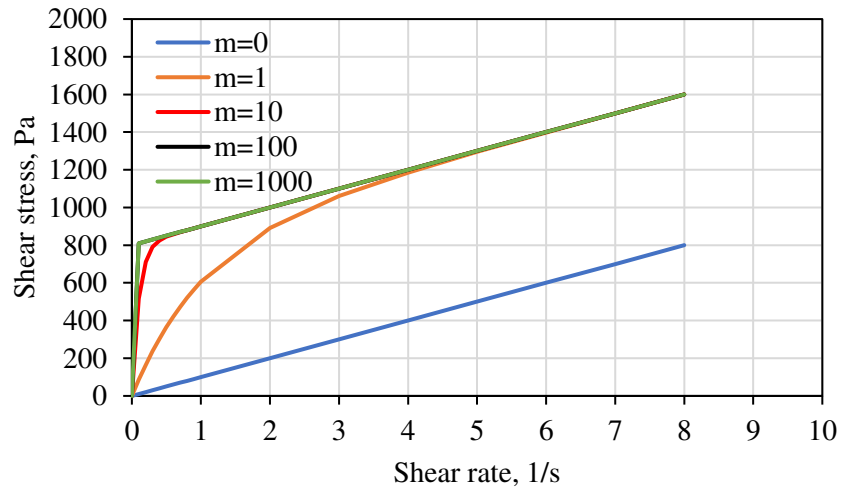


Figure 4.2. Effect of the ramping factor, m .

4.4 Preliminary testing and modeling results

4.4.1 Device calibration with air and water

To calibrate the internal mechanical efficiency of the device and accuracy in controlling the rotational speed, some calibration tests were conducted with air and water as the testing materials. The rotational speed started from 0.1 rpm to 60 rpm, with 0.1 rpm interval between 0.1 rpm and 1.0 rpm. At 0.1 rpm, the spindle was observed with some stick-slip behavior, which was

also reflected by the approximate 18 second-long steps in the torque vs. time curves as shown in Figure 4.3, indicating that controlling 0.1 rpm is beyond the machine sensory capacity. As such, future testing excluded running at 0.1 rpm. Note that the graphs describe sinusoidal behavior for roughly half turn, while the measured torque are low but within the range of accuracy of the torque sensor. The torque vs. rotational speed curves, derived by choosing the absolute average torque value at each rotational speed and shown in Figure 4.4, show that the torque in either air or water is within 5 N·m error, and hence, coincides with the zero shear resistance hypothesis for air and water. In other words, these values reflect the resistance to the rotation through the bearing and seal system that attaches the upper lid to the chamber, and in low viscosity fluids, can be used as adjustment for pre-existing device resistance to rotation. Subsequent testing in soil proved that the low value of torque and inherent machine resistance could be ignored in comparison to high torque requirement of moving the propeller in most of conditioned soil samples.

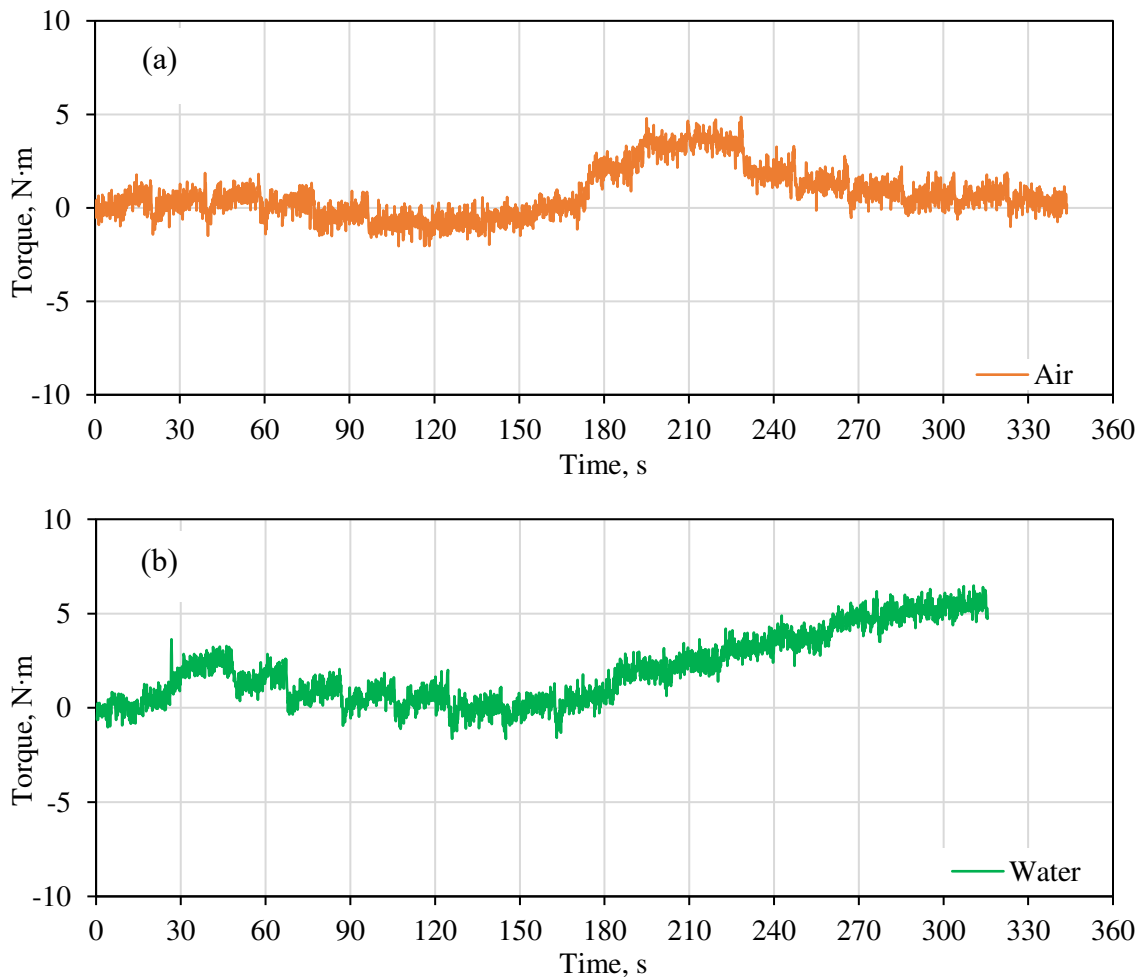


Figure 4.3 Torque vs. time curves at 0.1 rpm for testing in: (a) air; and (b) water.

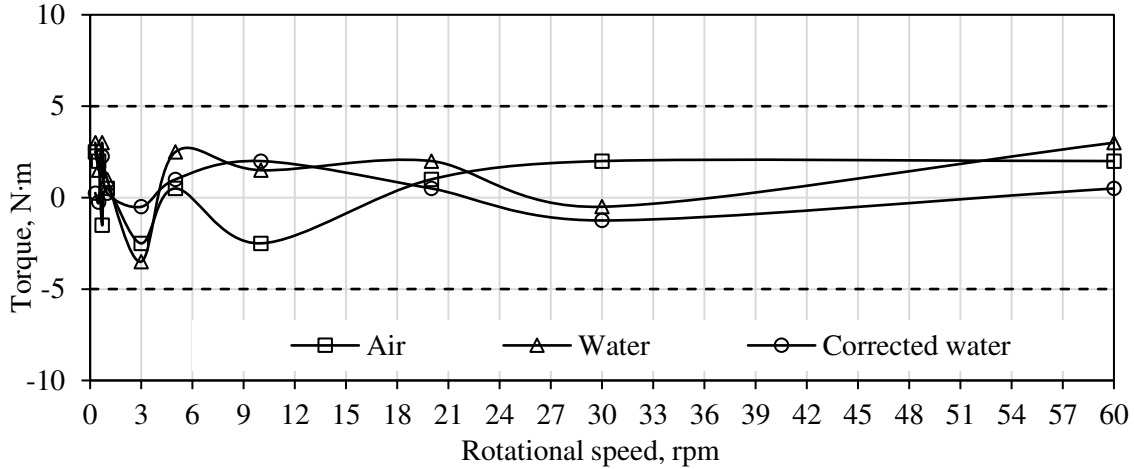


Figure 4.4 Torque vs. rotational speed curves for testing in air and water.

4.4.2 Testing on sand

CSM sand continued to be used in this study. The particle size distribution and mineralogy information are presented in Figure 3.1 and Table 3.1 in Chapter 3, respectively. Because of the dry weather and low relative humidity in the Greater Denver area, the indoor air-dried CSM sand was measured to bear water content of only 0.2% in different seasons of the year. This level of water content can be considered as nearly dry and the sand was ready for testing.

For each test of the dry condition, 42 kg of air-dried sand was loaded into the testing chamber. When properly flattened at the surface, this amount of at-rest dry CSM sand occupied 300 mm of the chamber height. The bulk density of the dry sand was subsequently calculated as:

$$\rho_{dry} = \frac{m_s}{V} = \frac{m_s}{0.25 \cdot \pi \cdot D^2 \cdot H} = \frac{42 \text{ kg}}{0.25 \cdot \pi \cdot (0.33 \text{ m})^2 \cdot (0.3 \text{ m})} = 1636 \text{ kg} \cdot \text{m}^{-3} \quad (4.3)$$

where ρ_{dry} is the bulk density of the dry sand ($\text{kg} \cdot \text{m}^{-3}$), m_s is the mass of the dry sand (kg), V is the bulk volume of the loaded sand (m^3), D is the inner diameter of the testing chamber (m), and H is the height of the loaded sand in the chamber (m).

To verify this method of estimating bulk density, a parallel measurement was conducted by using a standard Proctor. The Proctor was filled up with CSM sand until the sand overtopped. A ruler was used to scratch and flatten the sand surface to be at the same level with the top edge of the Proctor container. The density was calculated as $1552 \text{ kg} \cdot \text{m}^{-3}$, calculated from the soil weight divided by the volume. The error of density measured by these two methods is about 5% and was deemed acceptable for this thesis. Therefore, soil density was estimated during sample loading stage for the rest of the thesis. Furthermore, the void ratio of the dry sand can be calculated as:

$$e = \frac{V_v}{V_s} = \frac{V - V_s}{V_s} = \frac{0.25 \cdot \pi \cdot D^2 \cdot H - m_s / (G_s \cdot \rho_w)}{m_s / (G_s \cdot \rho_w)} = \frac{0.25 \cdot \pi \cdot (0.33\text{m})^2 \cdot (0.3\text{m}) - \frac{42\text{kg}}{2.69 \cdot 1000\text{kg} \cdot \text{m}^{-3}}}{\frac{42\text{kg}}{2.69 \cdot 1000\text{kg} \cdot \text{m}^{-3}}} = 0.64 \quad (4.4)$$

where e is void ratio (unitless), V_v is the volume of the void (m^3), V_s is the volume of the particle (m^3), G_s is the specific gravity of the soil particle (unitless), ρ_w is the density of pure water ($\text{kg} \cdot \text{m}^{-3}$), and the rest symbols are the same as previously defined.

A concrete mixer with 0.11 m^3 tank volume and 0.37 kW motor, as shown in Figure 4.5, was used to mix air-dried CSM sand and water to designated water content conditions. Subsequently, the mixture was loaded into the testing chamber to the same height, i.e., 300 mm . It was observed that the corresponding weight of air-dried sand in the wet conditions to reach 300 mm of chamber height was 42 kg , indicating negligible change of the void ratio when the sand became wet. The bulk density of the wet sand can be calculated as:

$$\rho_{wet} = \frac{m_s + m_w}{V} = \frac{m_s + m_s \cdot w}{V} \quad (4.5)$$

where ρ_{wet} is bulk density of the wet sand ($\text{kg} \cdot \text{m}^{-3}$), m_w is mass of the water (kg), w is mass water content (%), and the rest symbols are the same as previously defined. Based on Eq. (4.5), the bulk densities of CSM sand at designated water content levels were calculated and presented in Table 4.1.



Figure 4.5 A concrete mixer used to mix CSM sand and water.

Table 4.1 Bulk density of CSM sand at different water content levels.

Water content, w (%)	Bulk density, ρ_{wet} ($\text{kg} \cdot \text{m}^{-3}$)
0	1636
5	1716
7.5	1757
10	1798
15	1879
20	1961

Because the quantification of tool wear was not the focus of this study, tungsten carbide covers were mounted on the propeller blades as a means of protecting the blades to avoid damage of the propeller.

To develop the standard rheology testing protocol, some preliminary testing was conducted to verify the appropriate sequence and range of rotational speed operation. Three sets of tests on dry sand with the proposed rotational speed ranging from 0.1 rpm to 60 rpm were carried out, with 0.1 rpm interval between 0.1 rpm and 1.0 rpm. Other rotational speed steps were set as 1 rpm, 2 rpm, 3 rpm, 5 rpm, 7 rpm, 10 rpm, 15 rpm, 20 rpm, 30 rpm, 40 rpm, 50 rpm and 60 rpm.

To examine the proper sequence of rotational speed ramping (increasing or decreasing), Set 1 was conducted by decreasing rotational speed from 60 rpm down to 0.1 rpm. Set 2 had the same sequence of rotational speed changes as that of Set 1, with the difference being soil loosening was not exercised during the transition between adjacent rotational speeds, meaning continuous running from one rotational speed to the next. In Set 3, the rotational speed was increased from 0.1 rpm up to 60 rpm. Soil was loosened to break any compaction effects on the soil under the propeller and assure same soil settings for the tests at different rotational speeds. It was observed that the spindle rotated differently for each range of rotational speed. For 0.1 rpm, the spindle rotated inconsistently with stick-slip behavior, resulting in the stepwise force curves as shown in Figure 4.6 (a). Similar to the testing for air and water, this stick-slip behavior is due to the accuracy limitation of the gearbox and coupler between the motor and gearbox, i.e., the machine cannot be consistently run at or below 0.1 rpm. For rotational speed ranging from 0.2 rpm to 0.9 rpm, the spindle accelerated upon the start of the VFD control, followed immediately by static loading status. A typical force curve for this condition is presented in Figure 4.6 (b), in which the dashed

line is the extrapolated section representing the expected lasting static condition. Although the device is able to control speed at this range, as indicated by the tests in air and water, the resistance provided by soil particles is greater than the spinning propulsion of the bearing. Once the rotational speed reached above 1.0 rpm, the spindle rotated consistently and accurately as intended, evidenced by both the infrared tachometer reading and the force curves, as shown in Figure 4.6 (c).

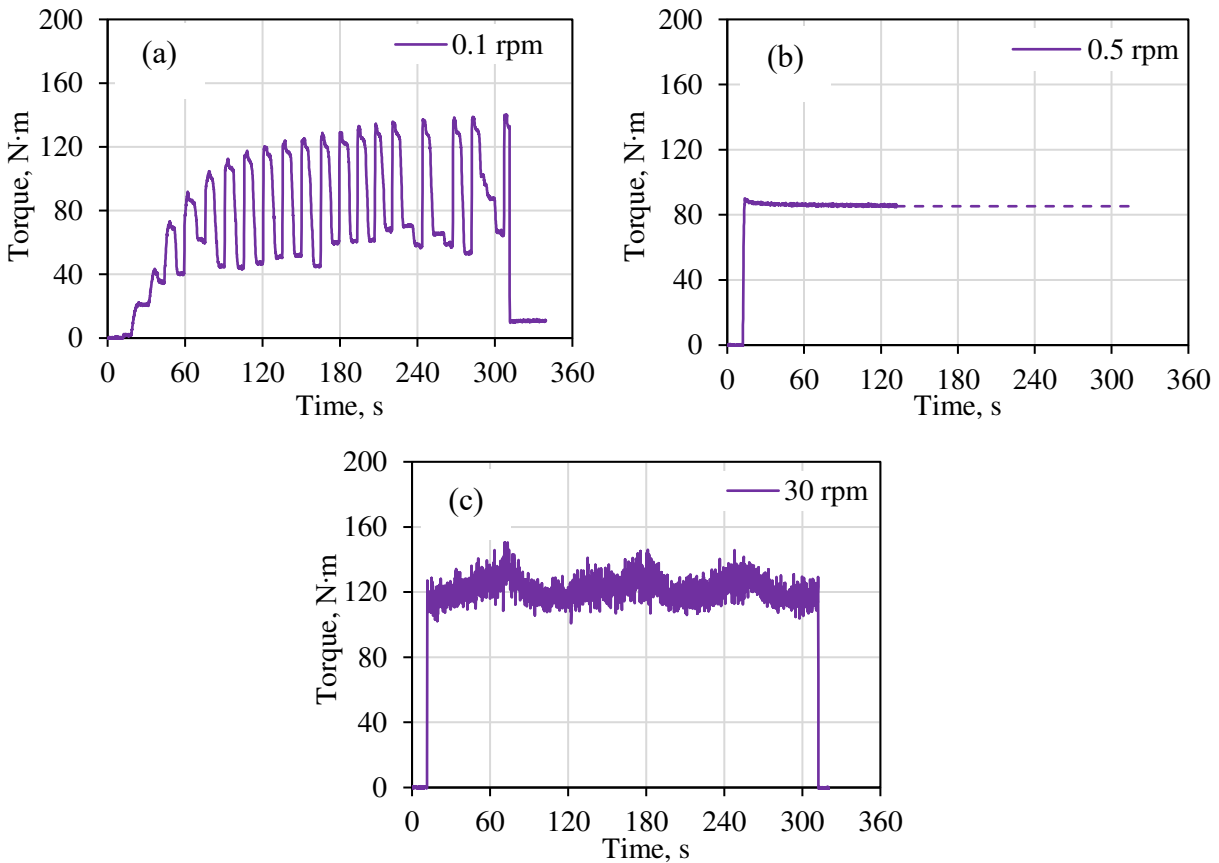


Figure 4.6 Typical torque vs. time curves at different rotational speeds on dry CSM sand: (a) 0.1 rpm; (b) 0.5 rpm, representative for range of 0.2 rpm to 0.9 rpm; and (c) 30 rpm, representative for range of 1.0 rpm to 60 rpm.

The results of the three sets of tests are shown in Figure 4.7. As is shown, the general trends and magnitudes of torque for these three sets of tests are similar. It is notable, however, that the curve for Set 2 is more fluctuating, meaning that loosening soil after each rotational speed is necessary with the 10 deg pitched propeller in order to restore the soil structure after compaction during the tests. This is because the inclined propeller blades have the tendency to compact the soil below them as the propeller spins clockwise (Mosleh et al., 2019). On the contrary, both curves

of ramping up and ramping down rotational speed, as indicated by Set 1 and Set 3 in Figure 4.7, do not show evident fluctuations when the rotational speed is greater than 3 rpm. Therefore, if the three-blade pitched propeller is to be used as the base for the rheometer, the soil structure must be loosened and restored during the test to improve the accuracy of the tests, especially in stiffer soil samples at low water content and without foam conditioning. Curves of Set 1 and Set 3 in Figure 4.7 also demonstrate that the torque climax at 1.0 rpm before plunging to lower torque values at 3.0 rpm. When the rotational speed exceeds 3.0 rpm, the curves follow linearly increasing patterns as the rotational speed increases, indicating that the proposed Bingham plastic rheological model is applicable to rotational speed greater than 3.0 rpm. For the purpose of rheology study herein, the lower limit of rotational speed is set as 3.0 rpm.

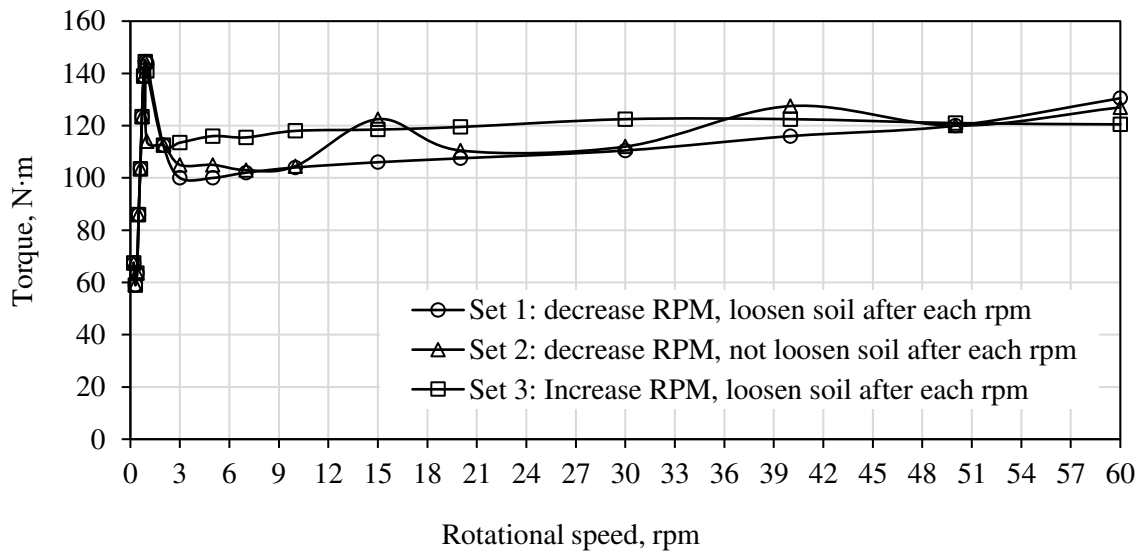


Figure 4.7 Preliminary rheology testing of dry CSM sand with 10 deg pitched propeller.

With the pre-determined test settings, more rheology tests were carried out on CSM sand with various water content conditions using the 10 deg pitched propeller. The results are shown in Figure 4.8. The curves follow linear patterns, meaning that using the Bingham fluid model is acceptable. It should also be noted that the curves for saturated conditions dip down as the rotational speed increases. The reason is unknown at this stage. Possible hypotheses include liquefaction and centrifugal effects at high rotational speeds, and consequently, the material density surrounding the propeller and the material strength become lower (Samaniuk et al. 2012; Pei et al. 2017; Hu 2019). Meanwhile, torque vs. water content relationships at various rotational speeds were also plotted, as shown in Figure 4.9. The maximum torque was expected and observed to

occur when the water content was between 5% and 10%, as illustrated by the dashed lines for each rotational speed in Figure 4.9, indicating the highest torque would occur at certain water content within this range. Note that the location of the exact peak is unknown due to the limitation of the motor power. Therefore, the dashed lines are only for illustrative purposes. This trend corresponds to the most severe wear scenario found in the previous soil abrasion studies (Alavi et al., 2013). The explanation of the mechanisms for this trend can also be found in this literature. As shown in Figure 4.10, the free standing water at the surface of the sand at water content of 20% in the testing chamber indicates that the sand had reached full saturation, while no free water was observed in the sand at water content of 15%, although local saturation could be seen. However, the torque does not decrease after the water content reached 15%, as shown in Figure 4.8, meaning that the sand at water content of 15% had similar, if not the same, rheological responses to that of the fully saturated sand.

The change of particle size distribution of the sand and its potential impact on soil rheology were not particularly investigated in this study. A similar investigation had been conducted in a previous study on the changes of particle size distribution curves for gravel, sand and clay during soil abrasion testing using the similar setting (Alavi et al., 2011). The results show that the change of grain size distribution of sandy soils was negligible at different testing durations. This negligible change in grain size distribution was also observed when water content was changed.

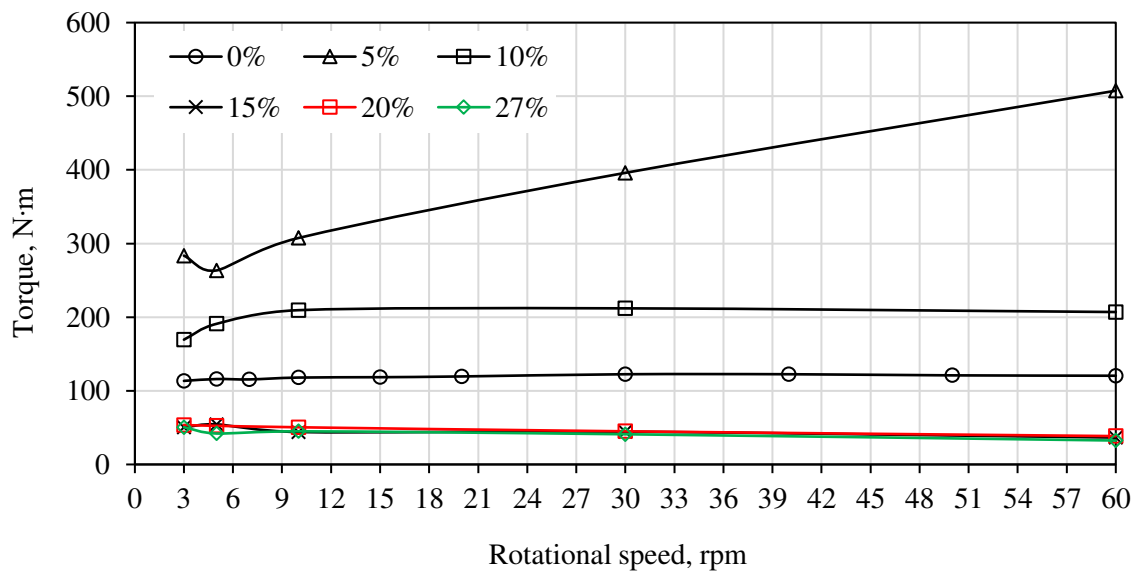


Figure 4.8 Torque vs. rotational speed curves for rheology testing of CSM sand at various water content levels with 10 deg pitched propeller.

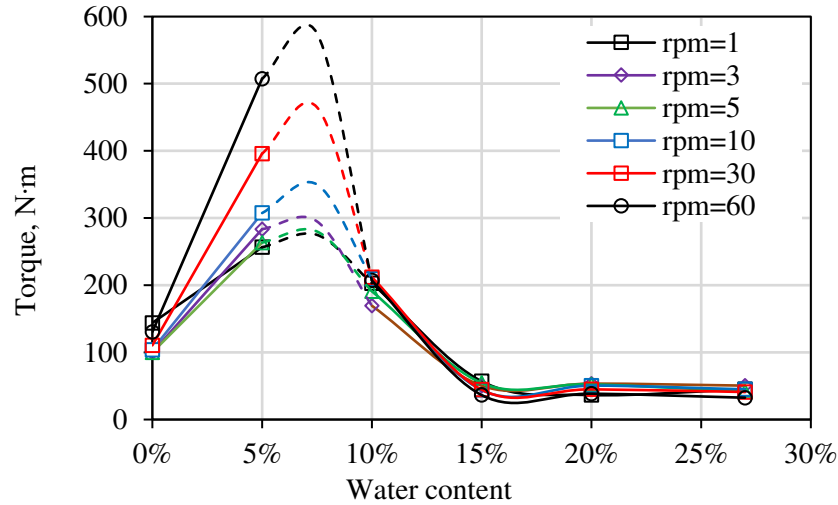


Figure 4.9 Torque vs. water content curves for testing of CSM sand with 10 deg pitched propeller. The dashed lines for different rotational speeds are not real measurements and work as illustrative purposes only.

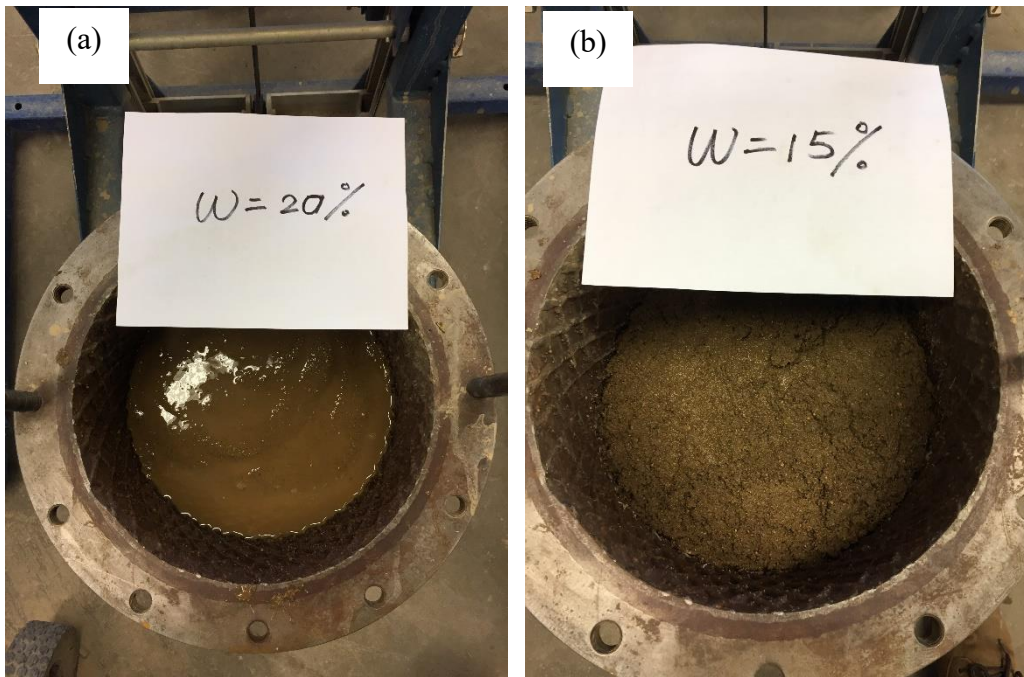


Figure 4.10 CSM sand in the testing chamber at: (a) $w=20\%$; and (b) $w=15\%$.

4.4.3 Back analysis of rheological parameters using CFD models

After lab testing, CFD simulations were carried out using COMSOL Multiphysics. The determination of yield stress and viscosity was based on the back calculation of these parameters by fitting the result of numerical modeling with that of the experimental measurements. In a

rotational rheometer such as the one in this study, torque and shear stress are correlated and can be written as

$$\tau = K_{\tau} \cdot T \quad (4.6)$$

where τ is the shear stress (Pa), K_{τ} is the geometry dependent factor ($1/m^3$), and T is the torque ($N \cdot m$). Meanwhile, propeller angular velocity and strain rate are correlated and can be written as

$$\dot{\gamma} = K_{\dot{\gamma}} \cdot \Omega \quad (4.7)$$

where $\dot{\gamma}$ is the shear rate (1/s), $K_{\dot{\gamma}}$ is the geometry dependent factor (1/rad), and Ω is the propeller angular velocity (rad/sec) which can be easily converted to *rpm*, i.e., rotational speed, using the following equation:

$$\Omega = \frac{\pi}{30} \cdot rpm \quad (4.8)$$

The two geometry dependent factors are proven to be constants for a particular geometry. Therefore, the constitutive model between shear stress and shear rate such as the Bingham model, which is a linear function, can be directly formulated to describe the relationship between system torque and rotational speed. The Bingham model is written as follows:

$$\tau = \tau_y + \mu_0 \cdot \dot{\gamma} \quad (4.9)$$

Substituting Eq. (4.6), Eq. (4.7) and Eq. (4.8) into Eq. (4.9), results in:

$$T = \frac{\tau_y}{K_{\tau}} + \frac{K_{\dot{\gamma}}}{K_{\tau}} \cdot \mu_0 \cdot \frac{\pi}{30} \cdot rpm \quad (4.10)$$

To facilitate the back calculation of yield stress and viscosity for the tested sand with the 10 deg pitched propeller, the following settings were further implemented:

(1) Building the model geometry based on 1/3 of the entire chamber due to full symmetry of the propeller. This operation reduced model size and computational time.

(2) Simplifying the model geometry by ignoring minor geometry details of the propeller (i.e., negligible retaining pins, cover thickness, edge chamfers). This operation demonstrated to generate results close enough to the original model while avoiding computational difficulties (Christian Wollblad, 2018).

(3) Using partitioning to refine mesh in regions with steep gradients around the propeller.

(4) Using ramping technique to identify better initial conditions, i.e., gradually increasing m from 0 to 1000 to approach the ideal Bingham model. Since the error of torque for $m = 10$ and $m = 1000$ was within 2%, $m = 10$ was used to save on computational time.

(5) Setting the damping factor $\alpha = 0.1$ in the Solver, enabling the Newton-Raphson iteration to converge for all highly non-linear models.

The model is shown in Figure 4.11. Different combinations of yield stress and plastic viscosity were used as fluid properties to calculate torque and compare the results with observed test data. The combinations of yield stress and viscosity with the least errors were chosen as the back calculated soil rheology parameters, as shown in Figure 4.12 and Table 4.2. Note that the test results at saturated conditions, i.e., water content of 15%, 20%, and 27%, cannot be fitted by the Bingham model due to other dominant factor, i.e., liquefaction and centrifugal effects at high rotational speeds. In addition, the variation of torque to the change of rotational speed at water content of 10% was so low that a satisfactory best fit curve with acceptable correlation factors could not be found. Based on the back analysis, the variation in yield stress is significant with the lowest of 11,200 Pa at dry condition and the highest of 27,000 Pa at water content of 5%, while the materials exhibit evident change in viscosity as well. Based on these results, one can speculate that the natural CSM sand behave as solid rather than fluid, and consequently foam conditioning treatment is required to transform the sand into an acceptable muck for EPB tunneling. Also, it should be noted that the yield stress and viscosity values reported here are expected to be on the high end because of the compaction effect on the sand during experiments. In the next section, a parametric study will be presented in which CFD modeling would find the optimized propeller configuration, offering improved performance including less compaction effect.

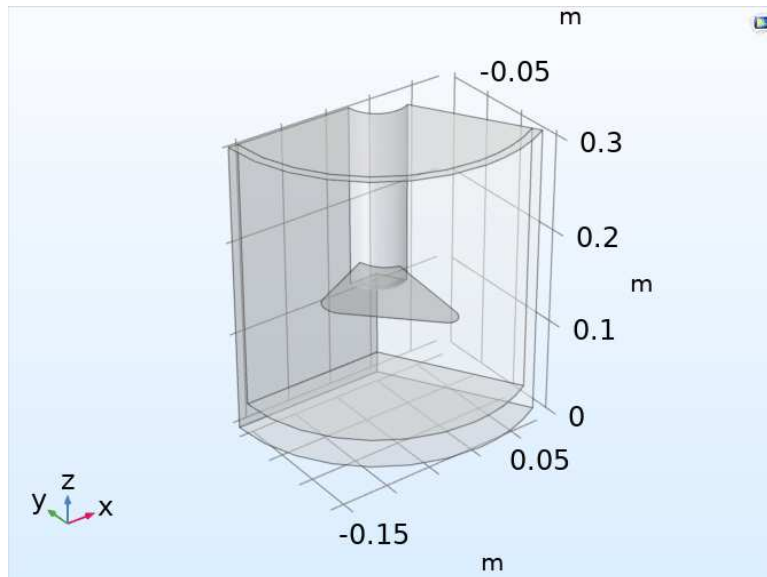


Figure 4.11 Simplified COMSOL model of the rheometer using 10 deg pitched propeller.

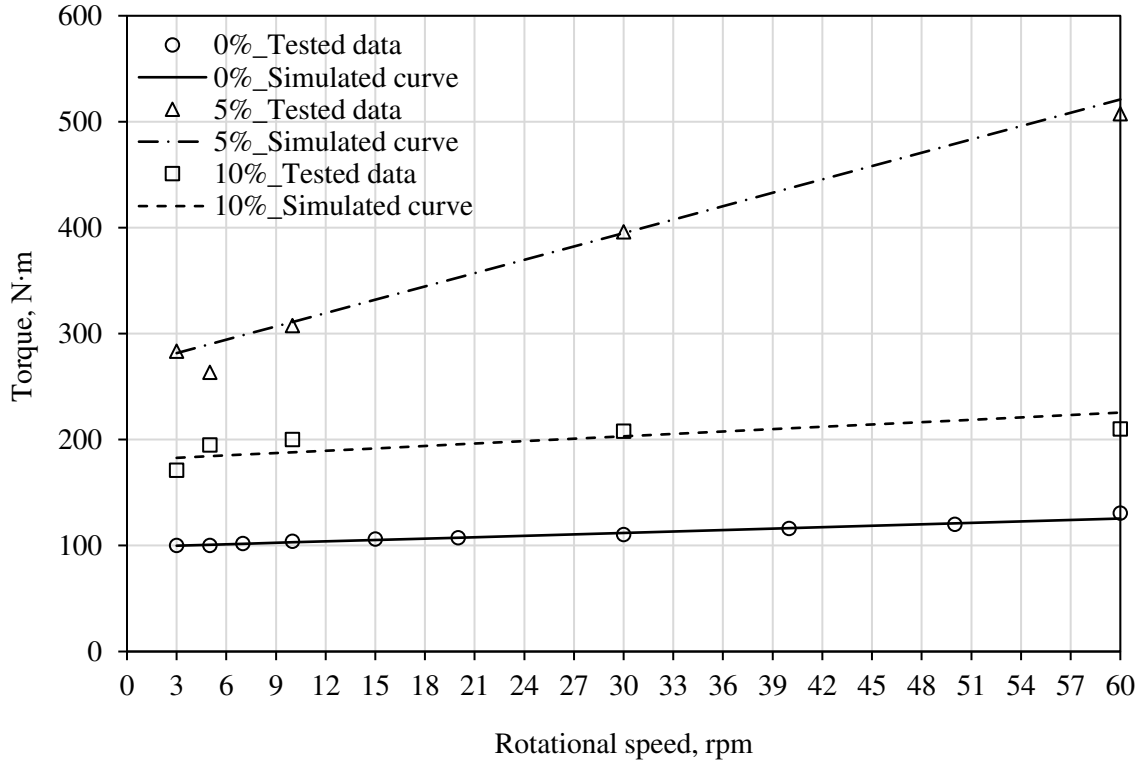


Figure 4.12 Simulated torque (continuous lines) based on back calculated yield stress and viscosity and experimented torque (scattered data) using 10 deg pitched propeller.

Table 4.2 Summary of back calculated soil rheology.

w (%)	S_r (%)	τ_y (Pa)	μ_0 (Pa·s)	$T \sim rpm$	R^2
0	0	11200	60	$T=0.483 \cdot (rpm)+98.05$	0.971
5	25	27000	1200	$T=4.172 \cdot (rpm)+261.49$	0.986
10	50	21000	60	$T=0.467 \cdot (rpm)+186.72$	0.512

4.4.4 Comparisons of various propeller designs

As mentioned before, the preliminary testing and modeling results confirm the validity of the proposed idea of determining soil rheology using the soil chamber concept. However, the proposed method still has room for improvements. One of the reasons is the possibility of using different propeller geometries to increase the sensitivity of the testing unit with regard to the changes of soil rheological parameters and rotational speed. In addition, the test unit was originally designed for soil abrasion testing, thus the 10 deg pitched propeller has intrinsic compaction effect to create significant contact stress between the propeller and the tested soil. This inherently causes high degree of compaction in soil, depending on soil type and moisture content. This effect was

observed both in sand and some preliminary tests on clay with various water content conditions, where the clay samples at water content close to the plastic limit was compacted/consolidated significantly below the propeller. The negative impact of the change of soil density due to compaction can cause potential inconsistency of torque pattern and inaccuracy of back analysis, even though this could be a good measure for studying clogging of clay.

The complex geometry of the pitched propeller does not allow for the direct manual calculation of yield stress from torque, as for in situ shear strength determination from vane shear test or yield stress evaluation from auger rheometer (Samaniuk et al. 2014). To avoid the soil compaction and allow potential direct measurement of yield stress, CFD simulations of different propeller geometries were conducted. In addition to the 10 deg pitched propeller, investigated geometries also included 30 deg and 90 deg pitched propellers (Figure 4.13), vane propellers with three geometries (Figure 4.14), and auger propellers with various dimensions (Figure 4.15, Figure 4.16, Figure 4.17). The baseline auger geometry in this study had a diameter of 228 mm, a lead (defined as the axial advance of a helix during one complete turn, or 360° of revolution) of 75.4 mm, and a total height of 188.5 mm, as shown in Figure 4.15 (b), Figure 4.16 (b), and Figure 4.17 (b). Then this baseline geometry was adjusted by changing the diameter, D (Figure 4.15 (a) and (c)), the lead, L (Figure 4.16 (a) and (c)), and the height, H (Figure 4.17 (a) and (c)). Table 4.3 summarizes the matrix of modeling configurations for this study. The magnitudes of yield stress and plastic viscosity values were selected in the vicinity of those for conditioned soil in the literature (Talebi et al. 2015).

The effectiveness of each propeller was compared based on the following six criteria:

- (1) The resultant torque should be sensitive to the changes of soil rheological properties, i.e., yield stress and viscosity.
- (2) The propeller should have insignificant effect, if any, on the density change of the soil.
- (3) The propeller should be able to generate satisfactory degree of mobilization and circulation of the soil flow within the chamber.
- (4) The resultant torque must be within the power capacity of the existing motor, i.e., 3.7 kW.

(5) The potential wall-slip effect should be minimized, if any, on the boundaries of the testing system such as the surface of the propeller and the gap between the propeller and the chamber interior wall.

(6) The propeller must be easy to be loaded and operated.

Among these, criteria (1), (2) and (3) were explored based on CFD modeling and the results will be presented in this section. This will lead to a preliminary conclusion for a proposed optimized propeller. Furthermore, criteria (4), (5) and (6) were further investigated via lab experiments. The corresponding results will be introduced in Chapter 5 based on which the final development of the propeller in the measuring system will be reached.

The settings at a rotational speed of 60 rpm were adopted for different propellers to facilitate comparison among them. In addition, yield stress $\tau_y = 250$ Pa was chosen to compare the sensitivity of torque to viscosity (μ_0) for different propellers, while viscosity $\mu_0 = 300$ Pa·s was selected to compare the sensitivity of torque to yield stress (τ_y). The results are shown in Figure 4.18 through Figure 4.22. As is shown, the torque is differentiable to the changes of viscosity within the same propeller category, while being insensitive to the changes of yield stress for all propellers.

The most sensitive case in each category was then selected to be further compared. As shown in Figure 4.23, the auger with a diameter close to the existing pitched propeller (D=300 mm) was found to offer the highest torque sensitivity with regard to the changes of viscosity and yield stress. To verify criteria (2) and (3) for optimization of the propeller geometry, the velocity fields for the 10 deg pitched propeller and the auger with similar diameter were compared, as shown in Figure 4.24. The comparison shows that the 10 deg pitched propeller stirs soil in the limited vicinity of the propeller, echoing the observed compaction effect from lab experiments. As a comparison, the auger propeller is capable of mobilizing soil in the entire chamber to generate circulation and avoid compaction. To allow for enough flow path between the propeller and the chamber wall, and hence, to allow for use of this system in soil that contain gravel size particles, an auger with a slightly reduced diameter is proposed for further optimization of the rheometer design, which will be introduced in Chapter 5.

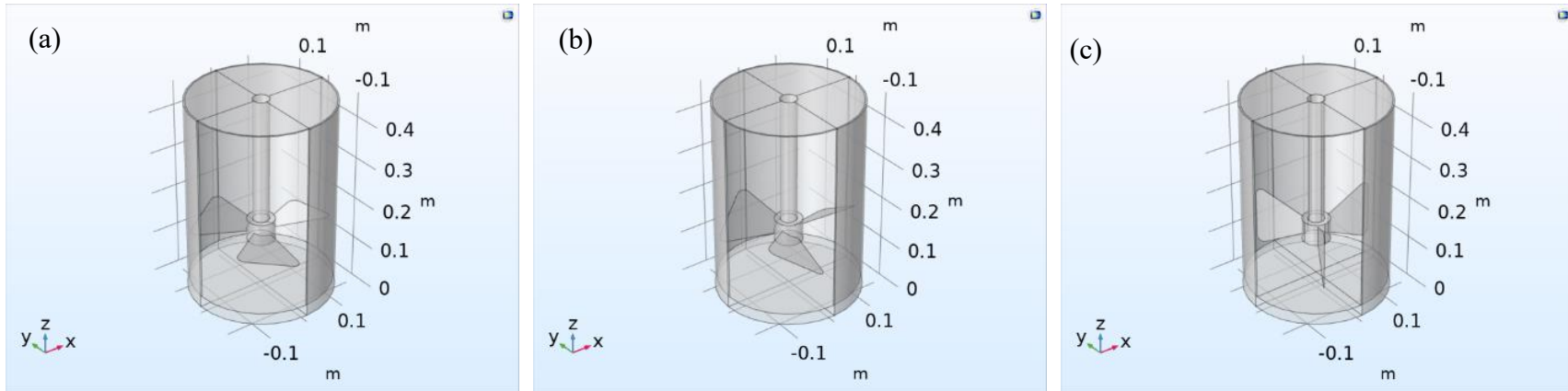


Figure 4.13 COMSOL CFD models for pitched propellers with three blades: (a) 10 deg; (b) 30 deg; and (c) 90 deg.

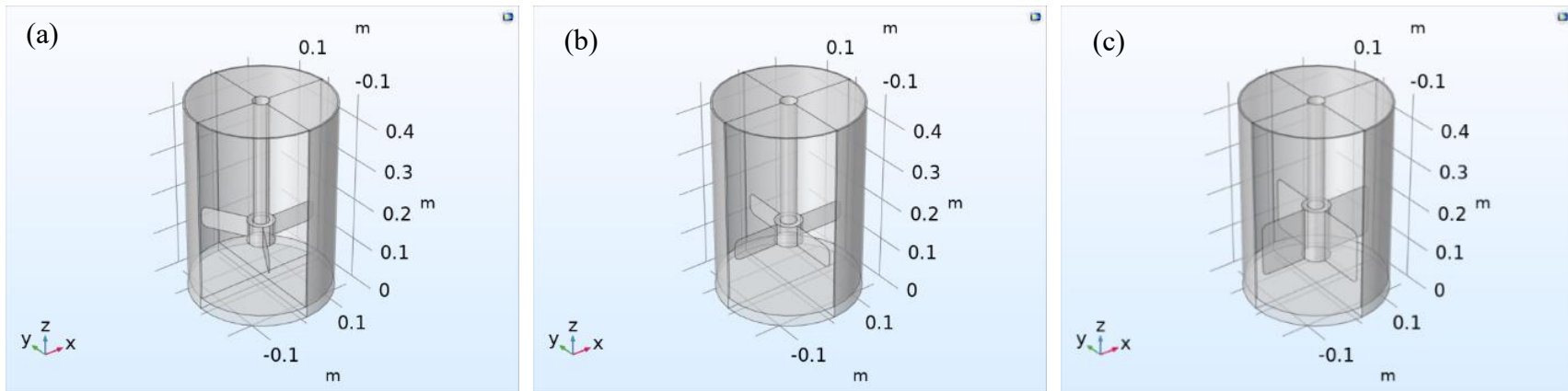


Figure 4.14 COMSOL CFD models for vane propellers with different blades: (a) three blades, 50.8 mm in height; (b) four blades, 50.8 mm in height; and (c) four blades, 127 mm in height.

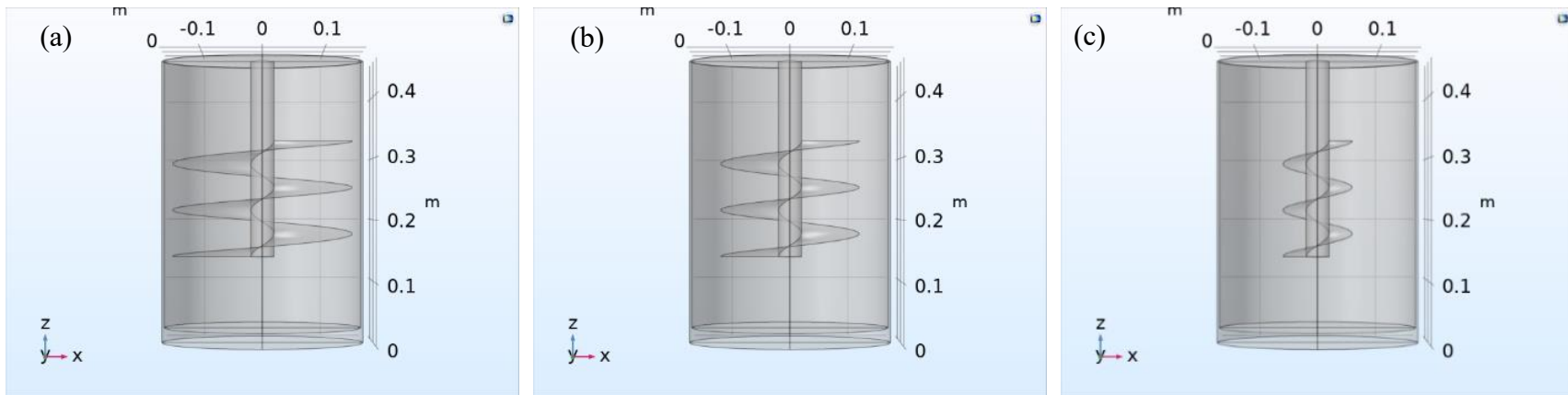


Figure 4.15 COMSOL CFD models for auger propellers with different diameters, D : (a) $D=296.4\text{mm}$; (b) $D=228\text{mm}$; and (c) $D=114\text{mm}$.

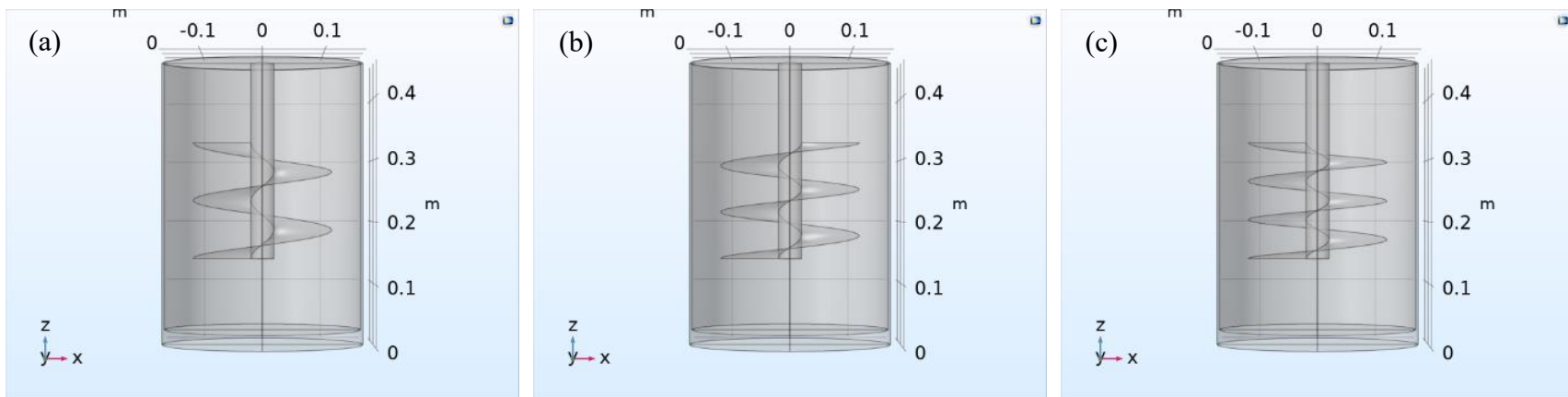


Figure 4.16 COMSOL CFD models for auger propellers with different leads, L : (a) $L=94.25\text{mm}$; (b) $L=75.4\text{mm}$; and (c) $L=62.83\text{mm}$.

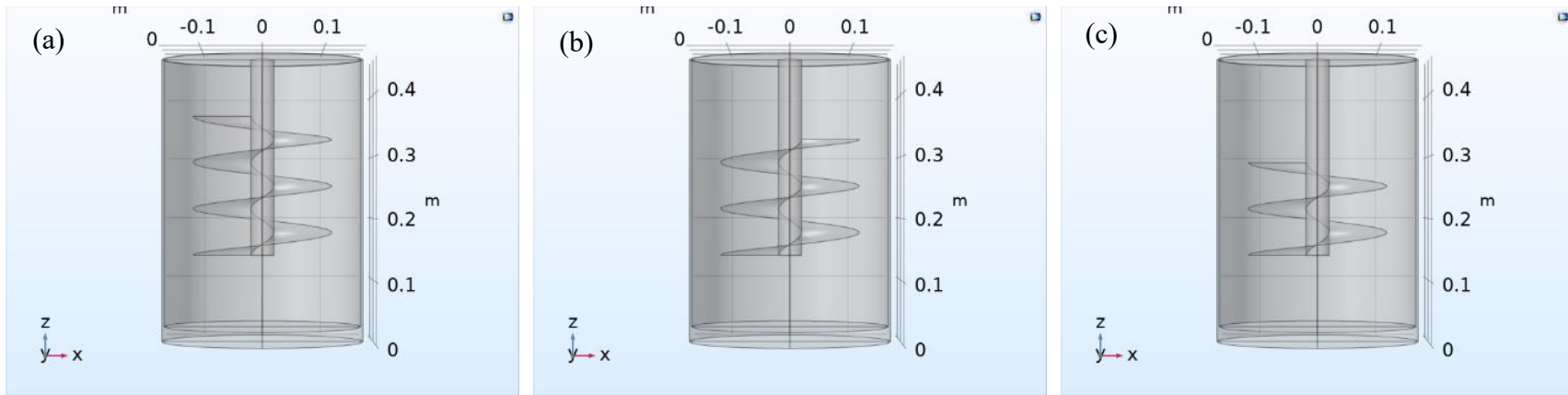


Figure 4.17 COMSOL CFD models for auger propellers with different auger heights, H: (a) H=226.2mm; (b) H=188.5mm; and (c) H=150.8mm.

Table 4.3 Summary of COMSOL CFD modeling parameters for propeller optimization.

Propeller shape	Model input		
	Yield stress, τ_y (Pa)	Plastic viscosity, μ_0 (Pa·s)	Rotational speed, (rpm)
10 deg pitched propeller with three blades	10, 50, 150, 250, 350	100, 200, 300, 400	1,5,10,20,30,60
30 deg pitched propeller with three blades	10, 50, 150, 250, 350	100, 200, 300, 400	1,5,10,20,30,60
90 deg pitched propeller with three blades	10, 50, 150, 250, 350	100, 200, 300, 400	1,5,10,20,30,60
Vane (3 blades, 50.8 mm high)	10, 50, 150, 250, 350	100, 200, 300, 400	1,5,10,20,30,60
Vane (4 blades, 50.8 mm high)	10, 50, 150, 250, 350	100, 200, 300, 400	1,5,10,20,30,60
Vane (4 blades, 127 mm high)	10, 50, 150, 250, 350	100, 200, 300, 400	1,5,10,20,30,60
Auger (change diameter)	10, 50, 150, 250, 350	100, 200, 300, 400	1,5,10,20,30,60
Auger (change lead)	10, 50, 150, 250, 350	100, 200, 300, 400	1,5,10,20,30,60
Auger (change height)	10, 50, 150, 250, 350	100, 200, 300, 400	1,5,10,20,30,60

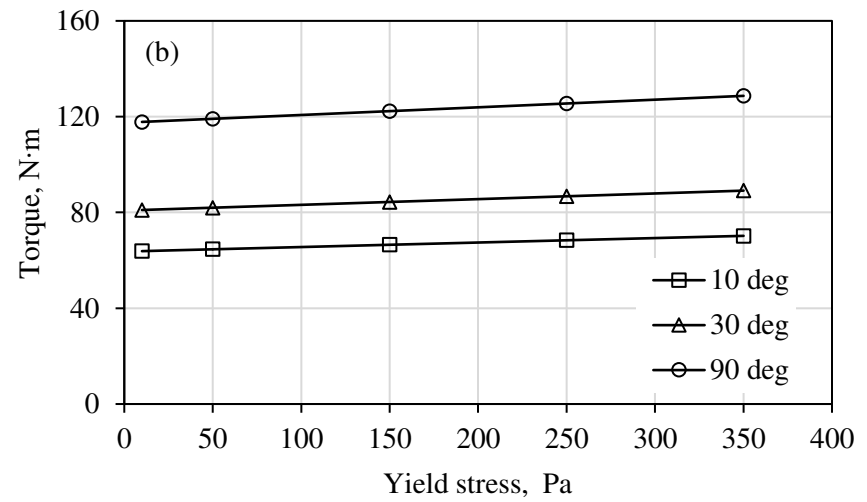
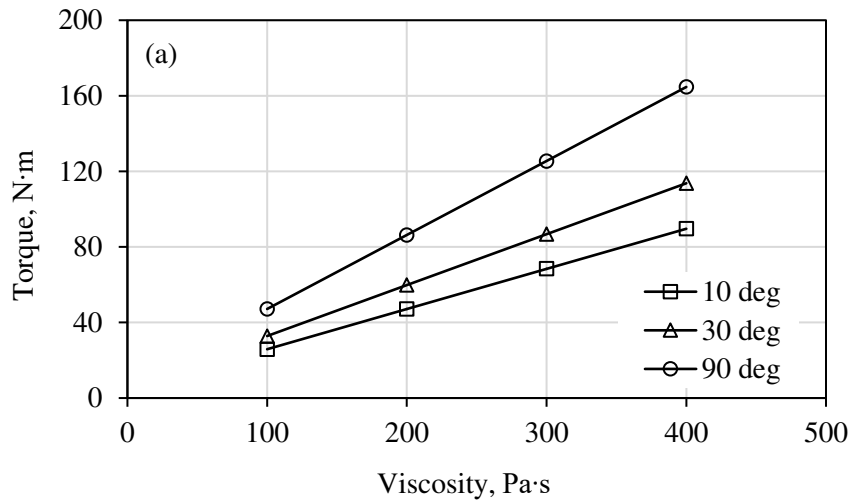


Figure 4.18 Sensitivity of torque to viscosity and yield stress for pitched propellers running at a rotational speed of 60 rpm: (a) $\tau_y=250$ Pa; and (b) $\mu_0=300$ Pa·s.

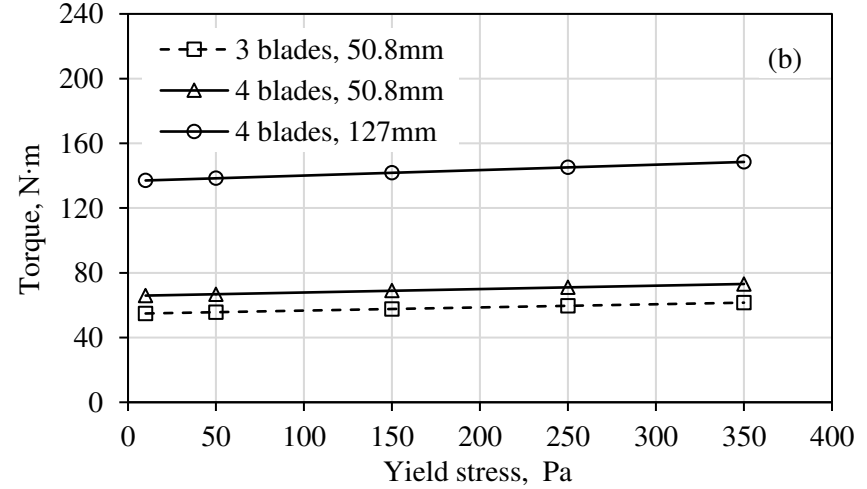
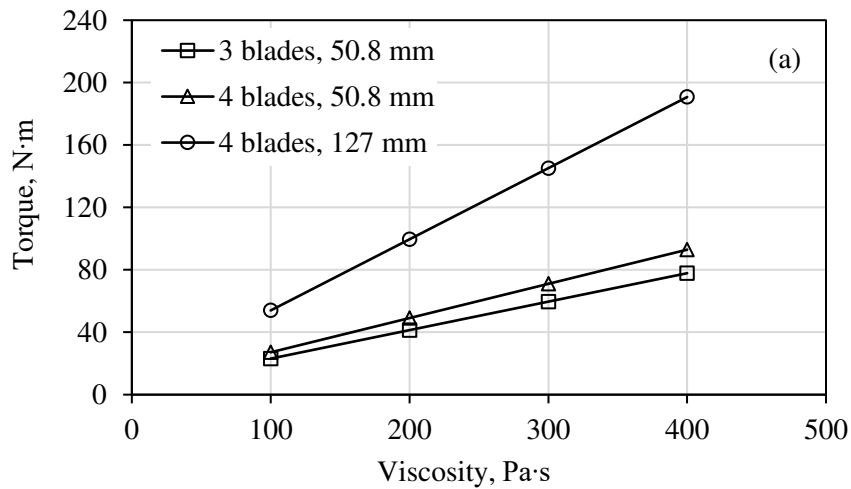


Figure 4.19 Sensitivity of torque to viscosity and yield stress for vane propellers running at a rotational speed of 60 rpm: (a) $\tau_y=250$ Pa; and (b) $\mu_0=300$ Pa·s.

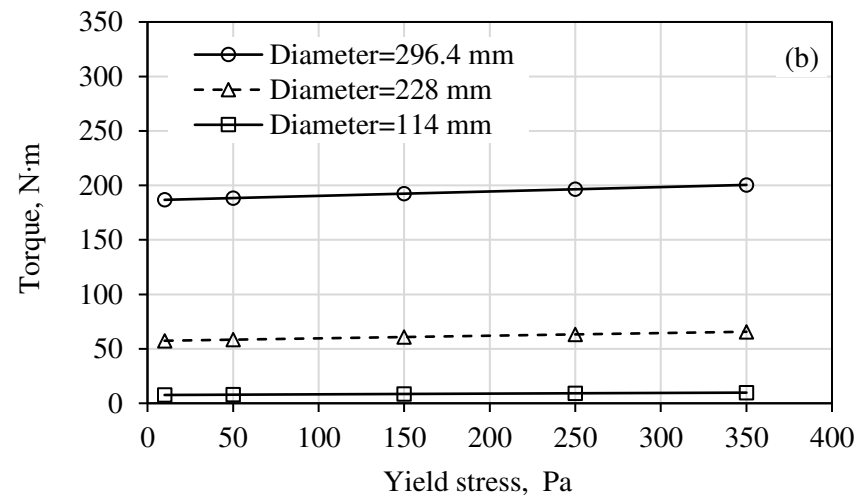
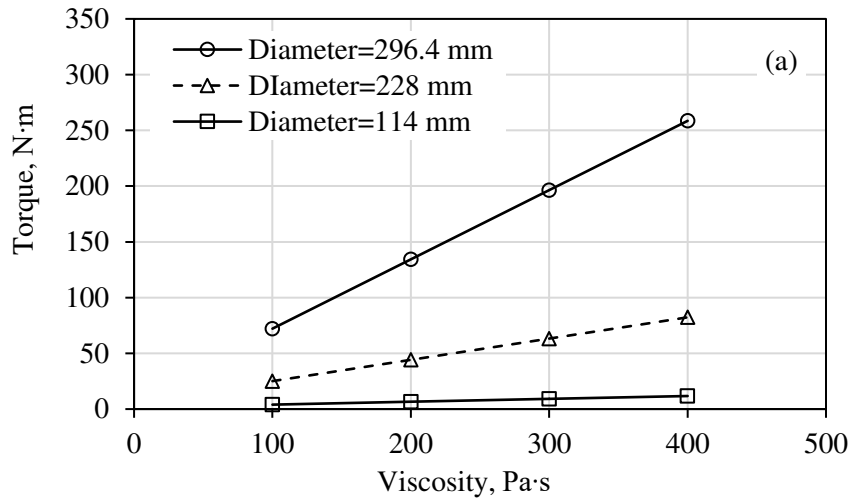


Figure 4.20 Sensitivity of torque to viscosity and yield stress for auger propellers with different diameters running at a rotational speed of 60 rpm: (a) $\tau_y=250$ Pa; and (b) $\mu_0=300$ Pa·s.

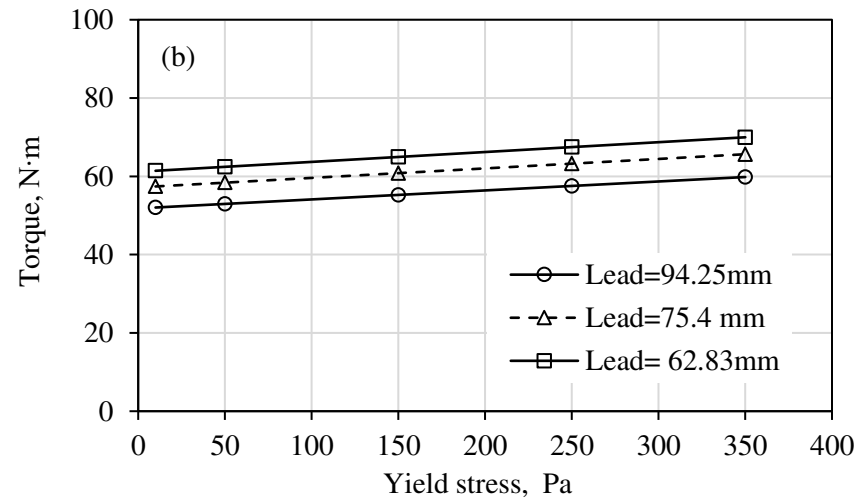
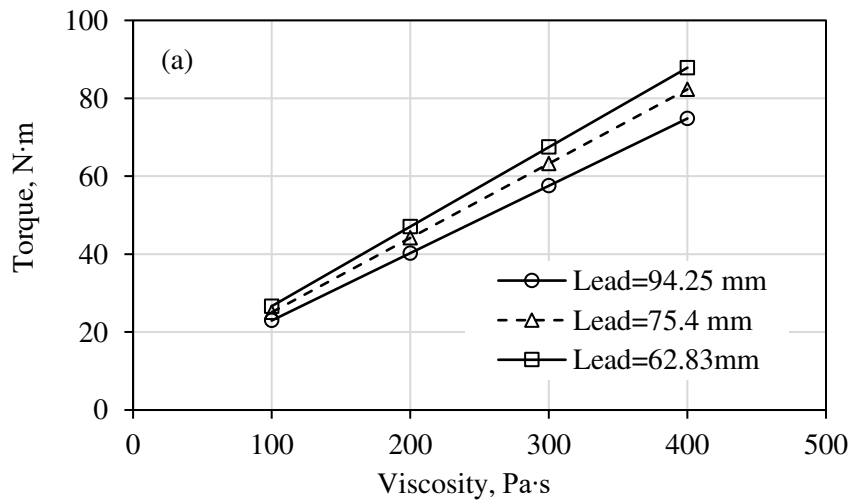


Figure 4.21 Sensitivity of torque to viscosity and yield stress for auger propellers with different leads running at a rotational speed of 60 rpm: (a) $\tau_y=250$ Pa; and (b) $\mu_0=300$ Pa·s.

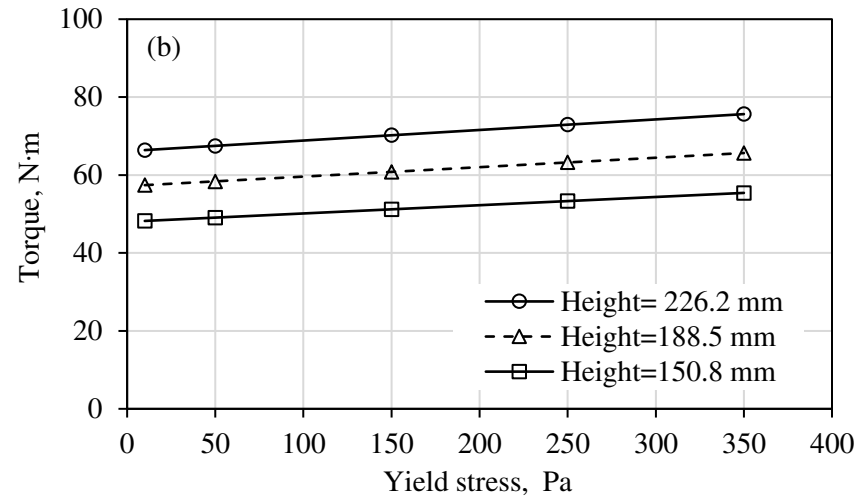
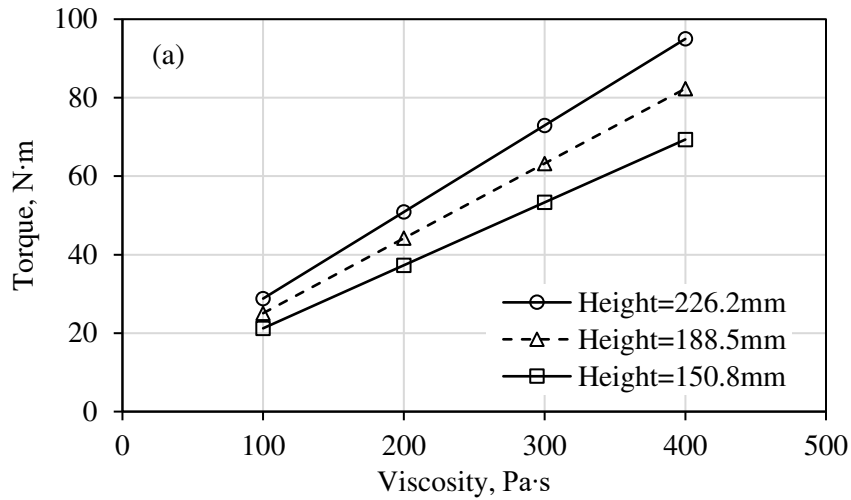


Figure 4.22 Sensitivity of torque to viscosity and yield stress for auger propellers with different heights running at a rotational speed of 60 rpm: (a) $\tau_y=250$ Pa; and (b) $\mu_0=300$ Pa·s.

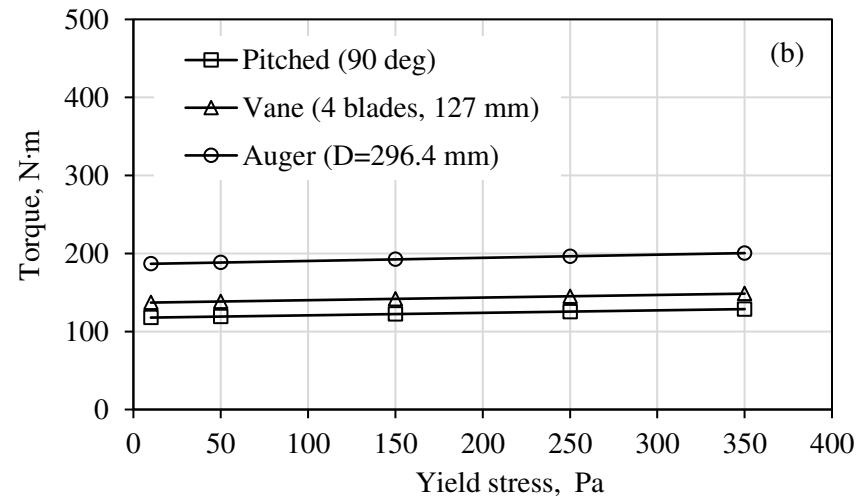
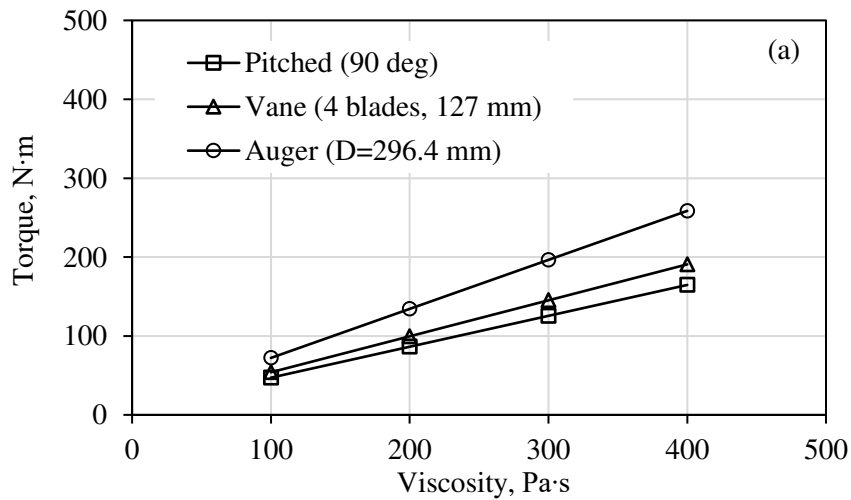


Figure 4.23 Overall comparison of sensitivity of torque to changes of yield stress and viscosity with three propeller geometries: (a) $\tau_y=250$ Pa; and (b) $\mu_0=300$ Pa·s.

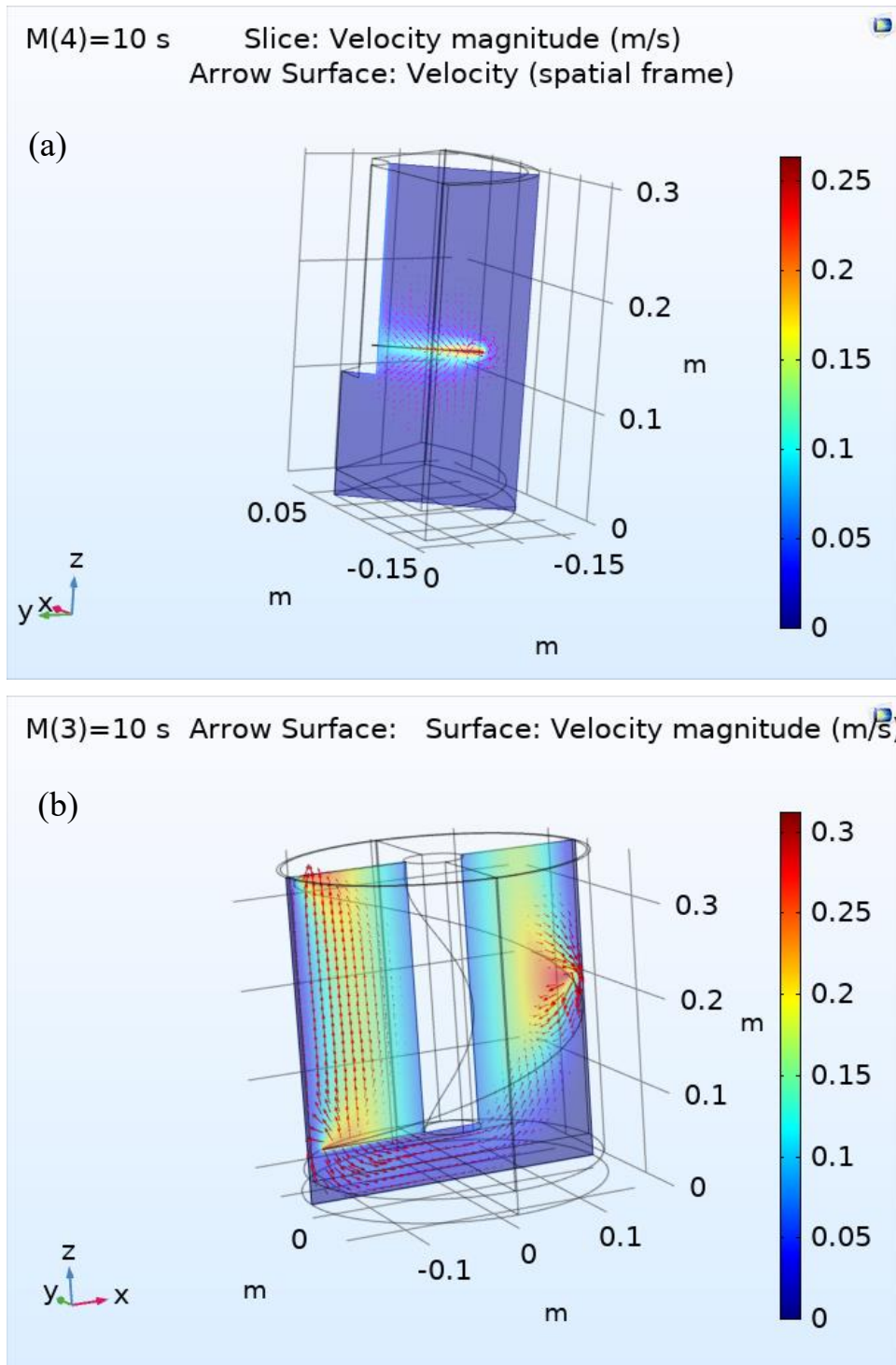


Figure 4.24 CFD simulated velocity field using: (a) 10 deg pitched propeller; and (b) auger with a diameter of 296 mm.

4.5 Discussions

To develop a universal and valuable method to measure and quantify soil rheology, several aspects of the testing device need to be improved. For ultimate design of the large-scale soil rheometer, the auger-shaped propeller, which was found to be the best geometry via CFD modeling, can be used to improve the sensitivity of the rheometer to variations in soil conditioning. Compared with the pitched propeller, the auger propeller with proper lead and clearance should have less impact on soil density during testing because it allows for easier vertical material flow within the testing chamber, as demonstrated in the velocity field in corresponding CFD modeling. Although a preliminary auger diameter slightly smaller than that of the existing pitched propeller is proposed for further rheometer design, one should also bear in mind the magnitude of the resultant torque when testing different unconditioned and conditioned soils to assure the ability of the rheometer to turn the propeller, given the limitations of motor power of the testing unit. Meanwhile, the diameter of the fully-developed auger should not be too small where the gap between the auger and the chamber wall is too big and consequently, deformation of the soil in the annular space adsorbs the energy and the resultant torque variation is too low to be measured by the torque sensors.

To date, most soil conditioning studies have been conducted on sandy materials due to the readiness of mixing sand with foaming agents. On the contrary, studies on conditioned clay were limited because of the difficulties of uniform mixing of clay with foam. These difficulties further resulted in the use of small-scale testing setups for the limited studies on conditioned clay where dry clay powder was used to mix with water and foam (Zumsteg and Puzrin, 2012; Zumsteg et al., 2013; Hollmann and Thewes, 2013; Thewes and Hollmann, 2016). In EPB tunneling in clayey ground, however, clay clumps and chips as well as gravels are commonly seen in the excavated muck meaning that large-scale laboratory devices such as the one in this chapter are essential to investigate the efficiency of clay conditioning and to evaluate the properties of conditioned clay. Some efforts were made to develop large-scale laboratory devices to study conditioned clay (Merritt and Mair, 2006; Merritt and Mair, 2008; Peila et al., 2016). However, whether the conditioned clay samples in the literatures reached satisfactory mixing conditions were not clearly reported. Therefore, acceptable method to mix clay and foam homogeneously need to be developed to provide a satisfactory mixing within limited time (to avoid foam degradation).

With the improved optimized propeller geometry and mixing scheme, systematic soil rheology testing needs to be conducted. This includes testing on both sand and clay with different combination of soil conditioning parameters. Testing sand, for example, requires sensible combinations of machine operation parameters such as rotational speed and surcharge loading, as well as soil conditioning parameters including w , c_f , FER , and FIR . The limits of these conditioning parameters will be determined by practical specifications used in the tunneling industry (EFNARC 2005). With the evaluation method presented in the previous sections, the relationships between soil rheology and soil conditioning settings can be further established. This means that this concept allows for examination of variation in yield stress and viscosity of conditioned soil as functions of w , c_f , FER , and FIR for a variety of soil types. Such relationships would allow for modeling of material flow in the EPB machines and help for optimization of proper soil conditioning and machine operations for practical applications.

The goal of studying soil rheology and soil conditioning is to predict EPB machine performance and optimize machine operations. The aforementioned concept and model correlating soil conditioning settings and soil rheology will be further extended to modeling EPB machine cutterhead and screw conveyor response during certain machine operations. That is, with the input of soil yield stress and viscosity based on soil type, anticipated w , c_f , FER , and FIR or alternatively as measured by the proposed device, the software can determine the required torque on the cutterhead and screw conveyor. It can also monitor pressure and flow velocity of the muck at various locations in the machine, predict contact stress between the muck and machine components, and offer optimal operating conditions for the machine.

4.6 Conclusions

The soil rheology can provide the link between soil property and EPB TBM operation and is very important in the optimization of soil conditioning to achieve better machine performance. Despite its importance, characterization of soil rheology in the context of EPB tunneling applications is still not as advanced as it should be. This chapter examined the feasibility of developing a new soil rheology evaluation method. The concept is to combine laboratory testing and CFD simulation to measure yield stress and viscosity of conditioned soil. The use of this concept allows for establishing the relationships between soil rheology and soil conditioning parameters and machine operations, which can be eventually used in EPB cutterhead and screw conveyor simulations. A preliminary rheometer was developed by modifying an existing SAI

testing device. The testing unit can run at rotational speeds between 0 rpm and 1000 rpm. For rheology testing purposes, preliminary testing results demonstrate that the rotational speed range between 3 rpm and 30 rpm should offer sufficient information to measure yield stress and viscosity of conditioned soil. The preliminary testing and modeling of CSM sand samples with various water content conditions allow back calculation of yield stress and viscosity of the materials tested.

Different propeller geometries were simulated using CFD modeling tool. The results indicate that the auger shaped propeller with certain lead and diameter being the optimal design for the proposed rheometer. This auger geometry would eliminate soil compaction problems and offer the highest sensitivity of torque response of the testing unit to the changes of yield stress and viscosity. The proposed methodology allows for more comprehensive study of soil rheology, and testing on various soil types and with different conditioning parameters can offer relationships between soil rheological parameters, including yield stress and viscosity, and soil type as well as conditioning parameters.

CHAPTER 5
DEVELOPMENT OF A SYSTEM TO MEASURE RHEOLOGY OF CONDITIONED SOIL
FOR APPLICATION IN SOFT-GROUND TUNNELING

5.1 Abstract

This chapter reviews the existing soil rheology measurement systems ranging from small-scale rheometers to large-scale screw conveyor models, including review of the large-scale rheology testing system developed and introduced in the previous chapter. The optimal new auger propeller geometry suggested by CFD simulation was incorporated into the measurement system. The results show that the optimized auger propeller meets the six criteria for propeller selection and verified by the previous CFD simulation results. Impacts of several potential factors on rheology measurement using the proposed system were examined. This includes ramping sequence of the rotational speed, compressibility setting in the CFD models, soil type, passing of time, and ambient pressure. Moreover, rheological responses of soil with different water content levels and foam conditioning parameters were investigated with the optimized measurement system. The study shows the interdependency between soil conditioning and rheological parameters in the conditioned soil. The measured rheological parameters of conditioned soil can be used in the simulation of muck flow within the cutterhead and screw conveyor of an EPB machine.

5.2 Introduction

The demand for mechanized soft-ground tunneling has been increasing globally. This is partially due to the unprecedented urbanization process in the Asia-Pacific region, especially China, and partially due to the redevelopment needs in Europe and North and South America. Based on one global survey in 2010 (Alavi 2013), the number of operational soft-ground TBM units increased from 144 during 1995-2000 to 353 during 2005-2010. A recent discussion with some of the leading manufacturers of TBM showed that in 2018, an estimated total of over 500 TBMs were manufactured (Rostami, 2019). Meanwhile, the EPB tunneling system was the dominant type of soft-ground tunneling machines, comprising 88% of the total during 2005-2010. No open literatures have revealed the latest figure on the global market on mechanized soft-ground tunneling in the last decade, but the estimated ratio of 90% seemed to be still through for percentage of EPB machines relative to the total number of shielded soft-ground machines manufactured in recent years. The tendency of overall growth as well as the dominance of EPB

machines in soft-ground tunneling are expected to continue as the underground construction industry is undergoing expansion to respond to the demand in additional underground space for urban infrastructure.

The concept of the EPB TBM is to use the excavated muck as the supporting medium to maintain face stability by adjusting face pressure at different locations of the tunnel alignment while transporting the cuttings from the face through excavation chamber and screw conveyor to the tunnel conveyance system in atmospheric pressure. To realize this operational goal, the excavated muck should have certain properties and exhibit proper behavior. This includes low permeability, high compressibility, low abrasiveness, low stickiness, and reasonable balance between flow capability and viscosity. Only when a good balance is reached among these properties the efficient EPB tunneling operation can be achieved, such as reduction of the cutterhead and screw conveyor torque, regulation of the face pressure, efficient mucking, and desired advance rate. In reality, it is rare for natural soil to exhibit such ideal properties and the muck must be artificially conditioned to achieve the desired behavior in the mix. The common soil conditioners used in EPB tunneling include water, foam, polymer, and bentonite. Depending on the in situ soil conditions such as soil type, particle size distribution, and water content, single or multiple conditioners should be used. The behavior of the conditioned soil for a certain formation and relative to conditioning parameters should be investigated to achieve the optimal results.

Laboratory evaluation must be considered to avoid costly mistakes and unexpected delays during construction. This refers to examination of properties of conditioned soil during the geotechnical investigation stage, which may be complemented by empirical observations in the past projects. Some methods for evaluating the behavior of conditioned soil have been adopted from other geotechnical and structural engineering tests, such as mixing test, slump test, permeability test, compressibility test, adhesion test, cone penetration test, soil abrasion test, vane shear test, among others (Psomas, 2001; Duarte, 2007; Messerklinger et al., 2011; Zumsteg and Puzrin, 2012; Galli and Thewes, 2014; Peila, 2014; Budach and Thewes, 2015; Galli and Thewes, 2016; Peila et al., 2016; Mori, 2016; Galli and Thewes, 2019). Unlike the well-established testing protocols for natural soil properties, the universal set of approaches to characterize all type of conditioned soils relative to the performance of EPB tunneling is yet to be established. This is especially true for the rheology of conditioned soil.

Samples of the conditioned soil in most laboratory experiments are not representative of the anticipated conditions unless the dimension ratio between the apparatus and the soil particles is within a proved range, i.e., a rule of thumb of a minimum of 10:1 ratio (Zhong 2019). A common feature of most laboratory devices currently used for testing conditioned soil is their relatively small scale. When studying well-graded soils containing coarse sand or even gravel particles, these devices may run into difficulties unless the natural particle size distribution of the muck is altered. To address these problems, some researchers have introduced large-scale EPB screw conveyor models (Merritt, 2004; Peila et al., 2007; Vinai et al., 2008). With these devices a limited amount of data has been collected relative to soil conditioning and flow parameters within the device. In addition, these testing devices are considered to be expensive and offer limited applicability.

In addition to being influenced by soil conditioning parameters and testing devices, muck behavior is also impacted by machine operational parameters. These include operating pressure, machine thrust force and rotational speeds of both the cutterhead and the screw conveyor. To date, it is still challenging to properly predict muck behaviors as functions of conditioning and machine operational parameters to reflect the site conditions. For example, there is limited information on soil rheology relative to the conditioning parameters, nor the details of soil movement within the chamber relative to the configurations of the cutterhead, cutting chamber, and screw conveyor, cutterhead speed, and pressure in various locations.

This is why EPB tunneling is still applied by trial and error to some extent, meaning the EPB machines are operated heavily based on the operator's judgement of the observed conditions and the response of machine sensory systems. Due to the intricate uncertainties and variations of geological conditions, under-defined geological conditions are always inevitable which have caused costly downtimes for machine repair or extreme measures for mitigation of the surface settlements. Therefore, an intelligent EPB machine operating system with both predictive and real-time assessment capabilities can help manufacturers to design the optimal cutterhead and mucking configuration, as well as conditioning system. It can also allow contractors to reasonably predict machine operational parameters before the start of operation and during the course of tunneling. Such system can intelligently assist the operators to make proper decisions about machine operational and soil conditioning parameters. With such intelligent systems together with experienced crews, EPB machine advance rate is expected to greatly improve due to reduced downtime.

This chapter presents the importance and intricacies of dealing with rheology of conditioned soil and the necessity to properly characterize soil rheology. Based on the preliminary development in the previous chapter, an improved new system to measure the rheology of the conditioned soil and the effects of several factors on the rheology measurement of the conditioned soil will be presented. Moreover, some relationships between soil conditioning parameters and rheology of conditioned soil developed based on the proposed rheometer will be examined.

5.3 Background

5.3.1 General review

The word “rheology” means the study of flow. It deals with the deformation of solid and the flow properties of liquids. Rheology of materials is influenced by several factors including the inner structure, the morphology, the stress condition and the temperature. Rheology is a critical property in many industries such as food processing, petroleum engineering, and biochemical engineering (Ferraris, 1999; Wright et al., 2001; Samaniuk et al., 2012; Vipulanandan and Mohammed, 2014), etc., where the materials in question are primarily liquids. In EPB tunneling, the excavated muck is three-phase mix but often investigated by traditional soil mechanics approaches such as compression and shear experiments. However, the expectation for the excavated muck to behave as toothpaste means that it is more relevant to study the mixture from rheology perspective.

In most cases, the rheology of material is characterized by two variables, i.e., plastic viscosity (μ_0) and yield stress (τ_y). Depending on whether an initiating stress is required to overcome the yield stress and mobilize the deformation/flow, a material is called a Newtonian fluid, which has no yield stress, or a non-Newtonian fluid, which is identified by yield stress (Papanastasiou, 1987; Mitsoulis, 2007). The focus of rheological studies in many of the traditional applications is on Newtonian fluids such as water, oil, gas, glycerin, etc, and hence, the viscosity of the mediums under various environmental parameters are measured to represent rheology of the fluid mediums. The geo-materials such as slurries and clay pastes that are encountered in the tunneling industries usually exhibit the so-called viscoplastic behaviors, which is identified by yield stress, below which the materials do not flow. When the stress exceeds the yield stress, the flow behaviors of the geo-materials are primarily governed by viscosity. Both yield stress and viscosity of the muck are required to be kept within certain range to generate sufficient material

flow in the cutterhead chamber and screw conveyor, as well as to maintain efficient mucking in the conveyor system, as illustrated in Figure 5.1.

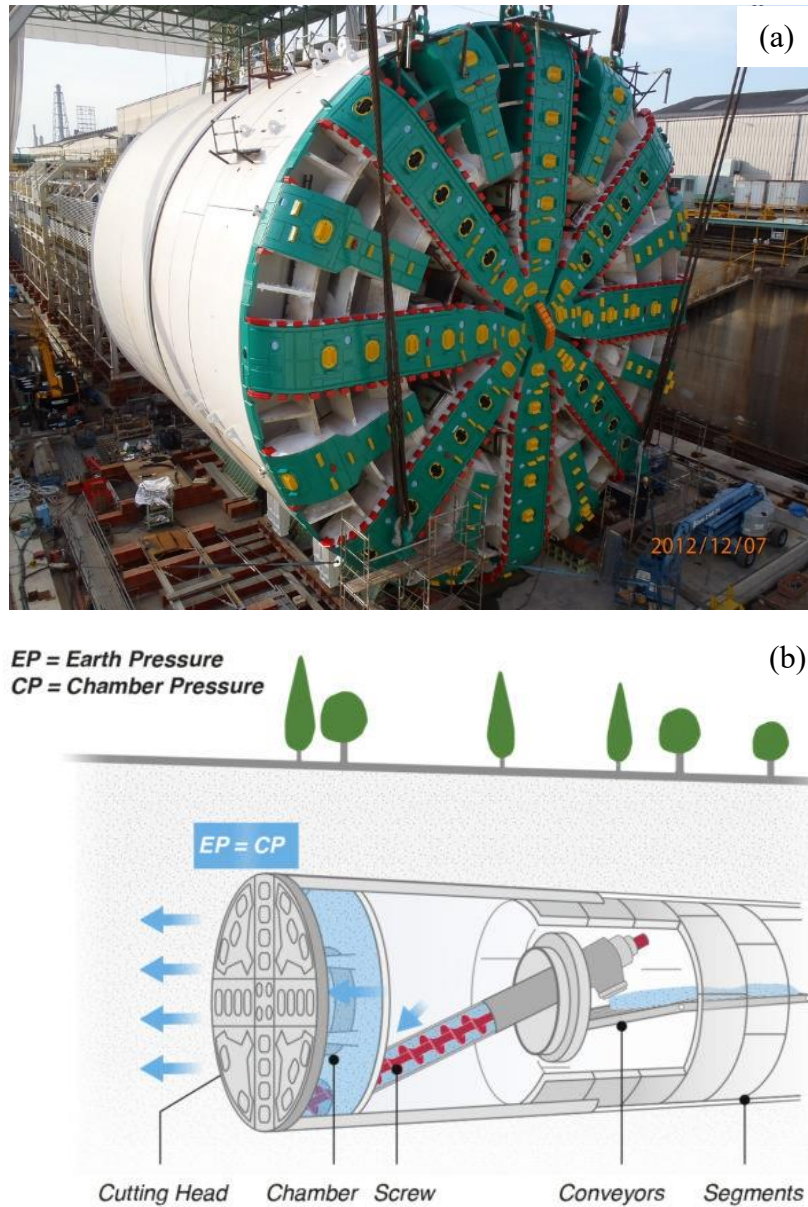


Figure 5.1 Illustration of EPB TBMs: (a) “Big” Bertha for SR 99 tunnel project in Seattle, the United States of America (WSDOT Flickr); (b) schematic drawing of major components of an EPB TBM (CONDAT).

Several non-Newtonian rheological models have been developed and applied to describe the soil mixes in the EPB machines. The most common models include the ideally linear Bingham plastic model and the subsequent modifications, the Herschel-Bulkley model, and the Casson model (Mitsoulis 2007). To determine which model fits into the unknown material, laboratory

testing is necessary, which is usually conducted in a rheometer. The general idea of a rheometer is to spin a form of propeller inside the target medium with different speeds and measure the resistance of the fluid against the movement of the propeller, and consequently, determine yield stress and viscosity of the fluid. Various types and sizes of rheometers have been introduced for different applications, with some common stirring geometries being concentric cylinders (Ewoldt, Johnston, and Caretta 2015), augers, and vanes (Samaniuk et al. 2014). It is noted that these rheometers have been developed for other applications such as food industry, chemical engineering, and biological engineering. The fluids in these industries are either pure liquids or fine-grained solids, or biomaterials. Therefore, their devices are usually too small to accommodate soil particles or to simulate the other conditioning parameters and ground pressures of the tunneling applications.

5.3.2 Rheology study of conditioned soil in EPB tunneling application

In the past, most of the studies on the properties of the conditioned muck in EPB tunneling concentrated on common geotechnical perspectives such as permeability, compressibility, and shear strength. In contrast, despite the importance of muck rheology in the operation of EPB TBMs, much less studies have been conducted to characterize soil rheological behavior under conditions similar to those present in this application.

Currently, the slump test is the most dominant form of testing for rheology characterization of conditioned soil. Adopted from concrete industry, the slump test has been widely utilized to assess the plastic flow ability of conditioned soil for EPB tunneling application. This is primarily due its simplicity and familiarity of many civil engineers with this test. However, the slump test is considered as an index test which is carried out at atmospheric pressure while the soil at the tunnel face and in the working chamber of an EPB machine is under variable pressure and shear rate, depending on the location (Meng, Qu, and Li 2011). It is reported that slump value offers good correlation with yield stress, while not being responsive to changing strain rate on the stress–strain behavior of the conditioned soil (Roussel and Coussot, 2005; Meng et al., 2011).

Recently, several studies have been published with more rigorous and scientific set of rheological parameters, i.e., yield stress and viscosity, to describe behavior of the soil in the cutting chambers of EPB machines (Meng et al., 2011; Galli 2016; Freimann et al., 2017). Often these rheological testing devices were small, meaning that they could not accommodate well-graded soil samples containing gravels without alternating the natural particle size distribution. Other limitations of the these studies include: (1) the tested soils were mainly sandy soils, and hence, the

rheological properties and behaviors of clayey soils are yet to be explored; (2) all of these studies were merely proposed to test soil rheology in atmospheric conditions, instead of simulating the true conditions in EPB tunneling such as variable surcharge loading and pore pressure.

Building large-scale EPB TBM models are worthwhile to study the impacts of soil conditioning and machine operational parameters on soil movement and flow behaviors within the machines. Several institutions have built lab-scale EPB screw conveyor systems to incorporate the study of the movement features of clayey muck inside the conveyor (Merritt, 2004; Merritt and Mair, 2006; Peila et al., 2007; Vinai et al., 2008; Merritt and Mair, 2008). However, this type of approach is very expensive and hence, very limited databases on the test results are available. Therefore, the impacts of ground conditioning and machine operation parameters on the muck rheology are still not well-known, and consequently, the optimal operation of an EPB machine based on the ground conditions including soil conditioning is not established.

From practical perspective, there is a gap for the above-mentioned studies to be applied in muck flow prediction in EPB machines. Measured or estimated yield stress and viscosity of conditioned soil, combined with Computational Fluid Dynamic (CFD) modeling have shown the potential for modeling muck movement within EPB machine cutting chamber and screw conveyor, and for prediction of EPB machine performance (Talebi et al. 2015). However, the input parameters for CFD modeling in this paper, i.e., yield stress and viscosity, are backcalculated from the site monitoring torque and are limited to that particularly studied project (Talebi et al. 2015). To a broader sense, there is a gap correlating the input soil rheology and the soil conditioning parameters such as Foaming Agent Concentration (c_f), Foam Expansion Ratio (FER), and Foam Injection Rate (FIR) for a given project.

Therefore, an evaluation methodology that can consider both muck properties and machine operational parameters was direly needed. With such a new methodology, the rheological behavior of the conditioned soil in a setting close to the working conditions of EPB machines as well as real-time EPB tunneling operation prediction would be possible. Hu and Rostami (2020) introduced such a methodology with the preliminary results of the measurement concept, experimental components and numerical optimization. This chapter offers additional details on the proposed method and follow-up steps in development of the measuring system with optimized propeller geometry and experiment protocols for examination of rheology of conditioned soil. The

system allows for evaluating the effects of different factors such as w , c_f , FER , FIR , soil density (ρ), and soil type on soil rheology.

5.4 Proposed rheology evaluation method in the previous study

5.4.1 Overview

The new soil rheology measurement method is a combination of experimental work and computer modeling as presented in the previous chapter. The experimental component comprises a modified drill press used for soil abrasion testing (Rostami et al., 2012; Mosleh et al., 2019) and a Variable Frequency Drive (VFD) unit. This device allows for controlled rotational velocity of a propeller that moves in conditioned soil, while the system measures torque at various rotational speed of the propeller, thus allows for establishing a relationship between torque as representative of shear strength, and rotational speed that is the indicator of shear rate, for different mediums. The corresponding soil rheology parameters, i.e., yield stress and viscosity, can be back calculated by CFD models with input parameters that can match the torque vs. rotational speed measurement. That is, parameters including soil density, yield stress, plastic viscosity, and rotational speed are used as input parameter for corresponding CFD models to estimate torque values at different propeller rotational speeds. In this way, a unique torque vs. rotational speed curve can be established for a particular combination of yield stress and viscosity. By fitting simulated curves to tested scattered data, unique sets of yield stress and plastic viscosity values can be found for corresponding soil settings. In other words, for a given setting of soil conditioning, pressure, and other environmental control parameters, a unique set of rheological parameters can be calculated.

By repeating this process for different soil types, conditioning, and machine operation scenarios, a comprehensive soil rheology chart can be established, which shows the variations of viscosity and yield stress as functions of conditioning parameters. For each unique set of soil settings, including soil types and conditioning schemes, there is only one set of soil rheology parameters that offer the best fit for matching the torque vs. rotational speed response of the testing unit. The model can then be used to simulate flow of the materials through an EPB machine to predict the machine operating conditions, including pressure and velocity of the muck at any given point within the muck chamber and screw conveyor.

5.4.2 Summary of previous development

The preliminary study utilizing the evaluation method was conducted in a poorly graded sand and presented in the previous chapter, with the following summary of major findings.

- (1) Calibration of the internal mechanical efficiency of the device and its accuracy in controlling the rotational speed was conducted by spinning the 10 deg pitched propeller in air and water. The rotational speed was tested from 0.1 rpm to 60 rpm. The results show the torque in either the air or water is within 5 N·m error which is a negligible value compared to the resistance of moving the propeller in most conditioned soils. Therefore, the resistance to rotation due to the bearing, seal system, and the tray table underneath the chamber is negligible.
- (2) Three sets of testing on dry CSM sand were carried out with the 10 deg pitched propeller. Although the rotational speed was operated within the same range from 0.1 rpm to 60 rpm, the three sets of testing followed different procedures in terms of whether ramping up or ramping down rotational speed, and whether restoring the soil structure after each rotational speed. The results indicate that the rotational speed should be higher than 3 rpm to ensure the applicability of the Bingham plastic model for the purpose of rheology studies. When using the pitched propeller, the soil structure must be restored after each rotational speed run to counteract the impact of compaction. In addition, the torque difference between ramping up and ramping down rotational speed is negligible, and consequently, an average of torque for ramping up and ramping down rotational speed will be used in the subsequent study.
- (3) The baseline torque vs. rotational speed curves for CSM sand at six different water content levels were obtained by using the confirmed testing protocol in dry CSM sand. All of the curves observe linear relationships between torque and rotational speed indicating that the Bingham plastic model is applicable to all of the soil conditions. The maximum torque is expected and observed to occur when the water content is between 5% and 10%. This finding was used as a guide to select the range for examining the effect of foam conditioners afterwards, which will be presented in the rest of this chapter.
- (4) Back calculation of yield stress and viscosity of CSM sand at different water content levels were achieved by comparing CFD simulated torque values with experimental ones. The results show significant variation of both yield stress and viscosity with the change of water content. One can speculate that natural CSM sand behave as solid

rather than fluid, and consequently soil conditioning treatment is required to transform it into an acceptable muck for EPB tunneling.

- (5) An optimization study was conducted in COMSOL to find the optimal propeller geometry for follow-up studies as discussed in chapter 4. The auger with a diameter of 296.4 mm was found to offer the best sensitivity of torque to the changes of yield stress and viscosity, as shown in Figure 4.23.

5.5 Current improved protocol for soil rheology measurement

While establishing the validity of the approach for evaluation of the rheology of conditioned soil, the previous work in this thesis did not include testing on conditioned soils using foaming agents as well as other factors influencing soil rheology. The follow-up work presented in this thesis deals with the development of the measurement system with the optimized propeller geometry and experiment protocols. The effects of different factors on soil rheology such as w , c_f , FER , FIR , soil density (ρ), and soil type were also examined and will be presented.

5.5.1 Measurement system components

The measurement system includes experimental or testing unit and numerical simulation tools. Compared to previous settings, the current experiments were conducted using a new auger geometry, identified as the most sensitive configuration by the previous CFD optimization study. An off-the-shelf alloy steel auger bit 296 mm in diameter and 762 mm in length was procured and modified to fit into the existing testing chamber and mounted on the shaft, as shown in Figure 5.2 (a). The remaining auger flight and the steel pipes were then welded so that the new auger shape propeller can slide into the machine shaft and be fixed by the shear pin through the existing hole in the shaft, as shown in Figure 5.2 (b). This configuration yields sufficient clearance between the auger and the testing chamber to allow for the material flow, including 27 mm gap between the auger outer edge and chamber wall, 108 mm from the auger top edge to the chamber lid, as well as 58 mm gap from the auger lower edge to the bottom of the chamber.

The geometry of a single-flight auger was used for testing on unconditioned soils. For conditioned soils by foam, another flight was added to form a double-flight auger, as shown in Figure 5.3 (a) and (b). This change ensured that the torque response for each scenario would be adequately sensible to back calculate soil rheology.

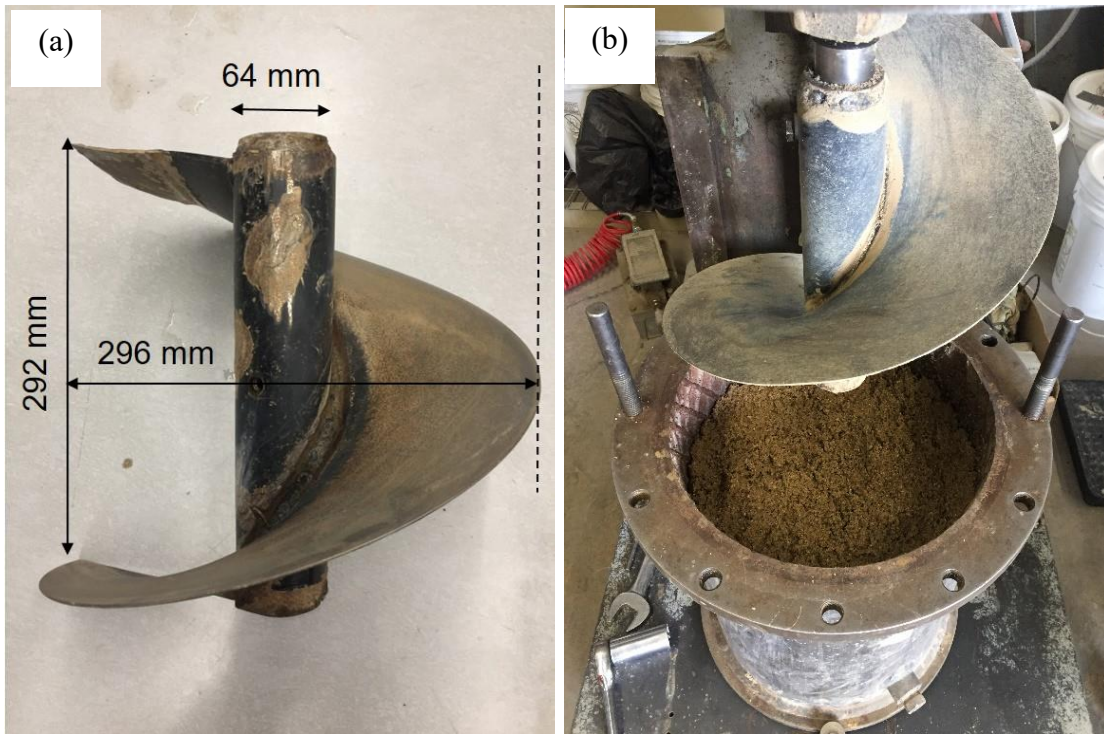


Figure 5.2 Large single-flight auger propeller: (a) dimensions; and (b) installed auger on shaft.

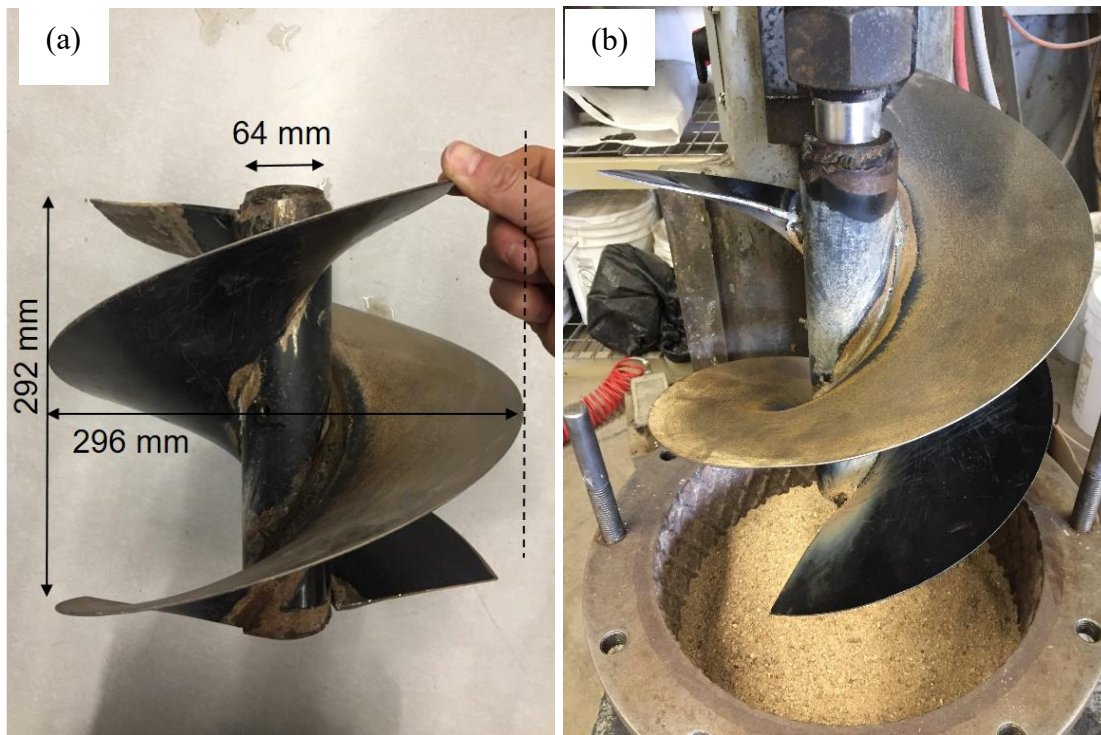


Figure 5.3 Large double-flight auger propeller: (a) dimensions; and (b) installed auger on shaft.

Meanwhile, two CFD models for both auger propellers were generated in COMSOL Metaphysics, as shown in Figure 5.4. The rest of the model setting were the same as discussed in the previous chapter.

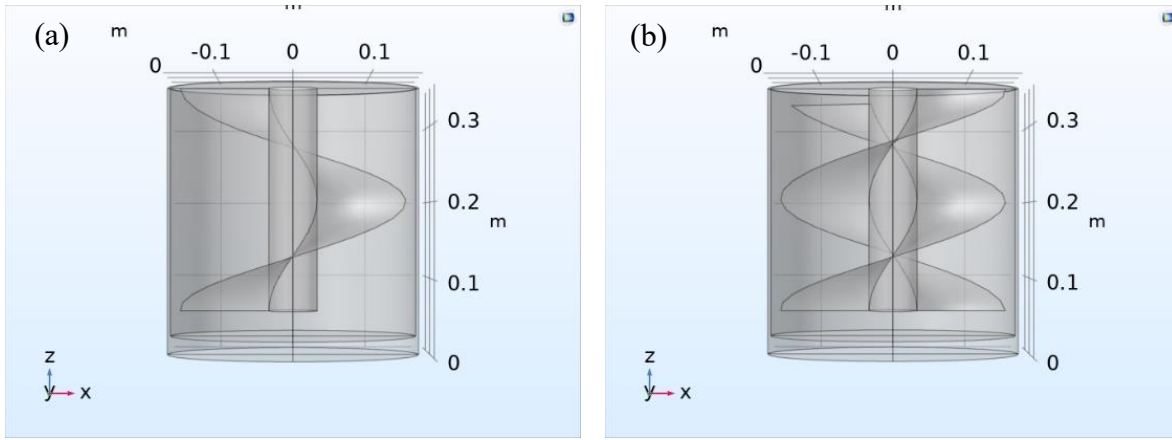


Figure 5.4 COMSOL CFD models for large auger propellers: (a) single-flight auger; and (b) double-flight auger.

5.5.2 Testing materials

CSM sand from the previous chapter was used as the main soil for this investigation. In addition, to examine the effect of soil type on soil rheology, five other soils and crushed rocks were also included in this study, namely Denver clay, HD sand, Ottawa sand, crushed CSM shale, and crushed Mexico rock. They were obtained through various sources. HD sand and Ottawa sand were off-the-shelf products and purchased from a local Home Depot store. Denver clay was obtained from a local construction site in Golden, CO. Crushed CSM shale and crushed Mexico rock refer to the crushed rock products of the original rocks sent to Earth Mechanics Institute (EMI) at Colorado School of Mines (CSM) for testing.

The particle size distribution curves of all the six materials are shown in Figure 5.5. Note that hydrometer method was used to measure the distribution curve of fine-grained Denver clay. The mineralogy of the soils and crushed rocks, as shown in Table 5.1 were assessed through various means. These include existing data source for Ottawa sand and Mexico rock, macroscopic assessment of CSM shale and Mexico rock, X-ray Diffraction (XRD) for Denver clay, and QEMSCAN for CSM Sand. There was no data source for the minerals of HD Sand. Additional details on material properties can be found in the literature (Mosleh, Hu, and Rostami 2019). In addition, the specific gravity and soil classification of the six samples were also obtained through different testing and empirical means, as shown in Table 5.1. Based on the same measurement

procedure presented in section 4.4.2, as well as Eq. (4.3) and Eq. (4.4), the dry bulk density and void ratio of each soil were calculated, as shown in Table 5.2. Note that because the specific gravity of solids of crushed Mexico rock, crushed CSM shale, and HD sand are unknown, the corresponding values of void ratio are missing.

Five types of the selected soils/crushed rocks belong to the sand category. They were selected to represent relatively uniform particle size distribution for a wide variety of sandy soils with varying mineralogy and angularity. Because the propeller geometry and final testing protocol had not been fully developed yet, no gravel material was tested. This needs to be addressed in the future study. In addition, as a preliminary trial for the following chapter specified on clay rheology study, Denver clay was tested at dry condition at this stage.

The foam conditioner used in this study was the anti-wear MasterRoc SLF 47 provided by BASF Group. The product is designed to improve soil plasticity, reduce permeability, and lower inner friction and abrasiveness of the soil. The optimal dosage of the chemical is recommended to be 2% to 3% in water with general range from 2% to 6% (BASF, 2018). The storage and handling requirements in the product technical data sheet were rigorously followed to ensure testing quality.

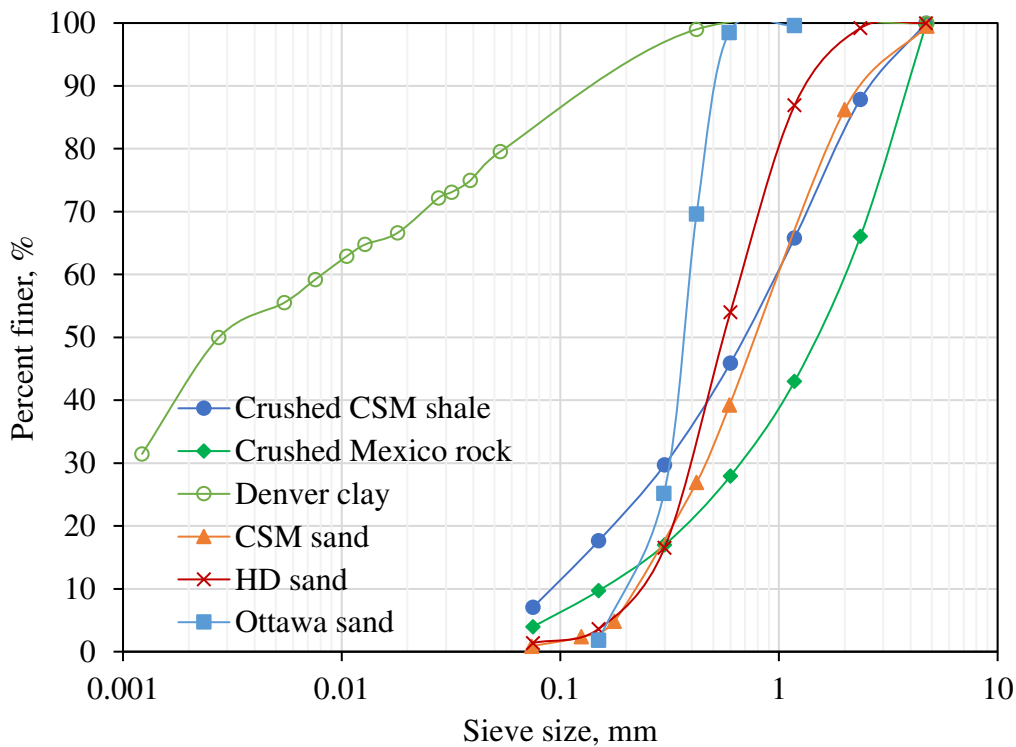


Figure 5.5 Particle size distribution curves for the soils in this study.

Table 5.1 Soil mineralogy, specific gravity and soil classification for the soils in this study.

Property	Samples used in experimental program					
	Crushed CSM shale	Crushed Mexico rock	Denver clay	Ottawa sand	HD sand	CSM sand
Mineral by mass (%)	N/A, expected to be clay minerals.	N/A; dominant minerals include pyrite, galena, chert, clay minerals, etc.	Quartz 58%; Smectite 15%; Illite 10%; Kaolinite 9%; Calcite 3%; Potassium feldspar 3%; Sodium feldspar 2%	Quartz 99.7%; Aluminum Oxide 0.06%; Iron Oxide 0.02%; Titanium Dioxide 0.01%	N/A	Quartz 40.5%; Plagioclase 28.8%; Orthoclase 19.0%; Fe Oxides 4.1%; Mafic Minerals 3.6%; Mica 2.6%; Others 1.5%
Specific gravity, G_s	NA	NA	2.72	2.58	NA	2.69
USCS classification	SW	SW	CH	SP	SP	SP

Table 5.2 Dry bulk density and void ratio of the six tested soils.

Soil type	Dry bulk density, ρ_{dry} ($\text{kg} \cdot \text{m}^{-3}$)	Void ratio, e
Crushed CSM shale	1396	NA
Crushed Mexico rock	1571	NA
Denver clay	1280	1.12
Ottawa sand	1533	0.68
HD sand	1609	NA
CSM sand	1636	0.64

5.5.3 Sample preparation

The dry samples in this study were prepared based on particle-dependent procedures. CSM sand, HD sand, Ottawa sand, as well as blocks of uncrushed CSM shale and Mexico rock were air-dried in the EMI lab environment for 5 to 7 days. An industrial fan was used to expedite this process, especially for initially wet samples. Air drying, however, was insufficient to dry fine-grained Denver clay samples. Therefore, the clay was dried in an industrial size oven set at an average temperature of 110 °C.

Dried Denver clay lumps, CSM shale and Mexico rock blocks were further crushed in a sequence by a jaw crusher and if needed, a roller crusher to obtain the desired grain size distribution. That is, the clay lumps and rock blocks were first hammered or cut into chunks of maximum diameter of 8 cm to 10 cm before being fed into a jaw crusher. After several crushing passes, the jaw crusher further reduced the lumps to less than 1 cm to be ready for the roller crushing. The roller crushing also involved multiple passes, starting from an initial roller gap of 6 mm to 8 mm, to a final gap around 2 mm. The soil and crushed rock samples were sieved through a U.S Standard NO. 4 size sieve with the opening of 4.76 mm. The entire sample preparation process rendered soil and crushed rock grain size distributions as shown in Figure 5.5. The grain size distribution of Denver clay was measured by hydrometer method for fine-grained soils.

The wet CSM sand samples in this study were prepared by adding calculated amount of water to 45 kg of dry sand and mixing them in the mixer shown in Figure 4.5. This amount of material ensured that the auger was fully in soil sample during testing. The rest of the preparation followed the same procedure as that presented in section 4.4.2.

The foam conditioned CSM sand samples were prepared by mixing dry CSM sand, pure water and foam in the same mixer shown in Figure 4.5. The preparation of seven batches of foam conditioned sand in this study is summarized in Table 5.3 and is detailed as follows.

First, 45 kg of dry CSM sand (Column (A)) and initial amount of pure water (Column (B)) were mixed to generate wet CSM sand. The amount of water was less than what was needed to adjust to the overall water content of 7.5% because additional water contained in the upcoming foam would be added later.

Second, a foam generator shown in Figure 5.6 was used to generate the required mass of foam based on the desired foaming parameters, i.e., c_f , FER , and FIR . Note that the inlet compress air pressure connecting to the foam solution tank was set as a value between 3 bar and 3.5 bar to achieve consistent air and liquid ratio and ensure security. Meanwhile, the masses of surfactant and water contained in the generated foam were calculated. Subsequently, the ultimate water content of each batch of foam conditioned sand was calculated and confirmed to be 7.5%.



Figure 5.6 Foam generator in this study (Alavi, Rostami, and Talebi 2014).

Table 5.3 Control of foam conditioning parameters for testing on foam conditioned CSM sand.

Dry sand	Initial w	c_f	Atm. FER	Atm. FIR	Initial water	Delta foam	Surfactant	c_{fs}	Delta water	Total water	Total w
g	%	%	-	%	g	g	g	%	g	g	%
(A)	(B)	(C)	(D)	(E)	(F)=(A)·(B)	(G)	(H)=(C)·(G)	(I)=(H)/(A)	(J)=(G)-(H)	(K)=(F)+(J)	(L)=(K)/(A)
45000	5.5	3	15	50	2475	942.5	28.3	0.063	914.3	3389.3	7.5
45000	5.9	3	15	40	2655	754.0	22.6	0.050	731.4	3386.4	7.5
45000	6.3	3	15	30	2835	565.5	17.0	0.038	548.6	3383.6	7.5
45000	5.7	3	10	30	2565	848.3	25.4	0.057	822.9	3387.9	7.5
45000	6.6	3	20	30	2970	424.1	12.7	0.028	411.4	3381.4	7.5
45000	6.3	1	15	30	2835	565.5	5.7	0.013	559.8	3394.8	7.5
45000	6.3	5	15	30	2835	565.5	28.3	0.063	537.2	3372.2	7.5

Thirdly, the generated mass of fresh foam was immediately added to the wet CSM sand obtained in the first step and mixed in the mixer for a cumulative duration of 2 min until homogeneous mixing was achieved. Note that the mixer chamber was covered by a transparent lid during the mixing process to avoid mixture spill and inaccurate mixture recipe.

Lastly, the well-mixed foam conditioned sand was transport and loaded into the rheometer testing chamber to fill 340 mm of chamber height for torque measurement. Because the mixture structure became fluffy after adding foam, there was always unused foam conditioned sand remained in the mixer. The weight of redundant mixture was measured to determine the weight of mixture in the chamber, and consequently, to estimate the density of the mixture. A small portion of the mixture was also obtained for slump test. Note that this loading process and slump test were conducted in a fast manner to minimize the effect of foam degradation. For all seven batches of testing, the duration between foam generation and commencement of rheology testing was well-controlled to be 15 min.

5.5.4 Testing procedures

Table 5.4 summarizes the testing scenarios in current study. It started with the comparison of two single-flight auger geometries with different dimensions. One is the optimized large auger shown in Figure 5.2 and the other is an auger with reduced dimensions, as shown in Figure 5.7 (a) and (b). The small auger is 203 mm in diameter and 184 mm in height. It has the shaft size of 51 mm in outer diameter and 38 mm in inner diameter. When mounted to the machine shaft, the clearance between the auger and the testing chamber will allow for the material flow, if generated, including 72 mm gap between the auger outer edge and the chamber wall, 146 mm from the auger top edge to the chamber lid, as well as 127 mm gap from the auger lower edge to the bottom of the chamber. The purpose of this comparison was to validate the use of the large auger as the optimized option. Subsequently, the single-flight large auger was used to test soils without foam conditioning, including CSM sand at five different water content levels of 0%, 5%, 7.5%, 10%, and 15%, as well as five other dry soils namely HD sand, Ottawa sand, Denver clay, crushed CSM shale, and crushed Mexico rock. Due to the possibility of low torque response in foam conditioned CSM sand using the single-flight large auger, another flight was added to the large auger to form a double-flight auger as shown in Figure 5.3. With this double-flight auger, a set of testing including seven conditioning scenarios was carried out to study the influence of foam conditioning parameters on soil rheology. The detailed process of how to generate the desired mixture was already presented

in Table 5.3. For each individual conditioning scenario, the chamber pressure was elevated to 150 kPa and 300 kPa to investigate the potential influence of ambient pressure on soil rheology. Lastly, the testing was repeated at different time after foam generation to evaluate the effect of passing of time on soil rheology.

Unlike the previous pitched propeller which tends to compact the soil, the new auger propeller does not compact the soil during testing and hence, minimizes the change of density due to compaction. In fact, the auger propeller simulates the screw conveyor auger in the EPB machine. Once the soil is transported above the auger it will automatically fall down through the gap between the auger and the chamber wall, and feed back to the fluid system.

The basic rotational speed values for each testing were 3 rpm, 5 rpm, 10 rpm, 20 rpm, 30 rpm, 40 rpm, 50 rpm, and 60 rpm. One exception was the experiment at wet CSM sand with water content of 7.5% where the torque was very high and the motor was struggling. Therefore, to avoid potential damage to the motor, the maximum rotational speed was set as 40 rpm for testing at water content of 7.5%. For testing on the unconditioned soils, i.e., soils without foam conditioning, the testing started with ramping up rotational speed from 3 rpm to 60 rpm with 2 min at each rotational speed and 1 min of intermediate stop between two adjacent speeds to adjust the rotational speed on the control panel. Subsequently, a separate testing was conducted by ramping down rotational speed from 60 rpm to 3 rpm with the same testing duration and intervals. For unconditioned soil, it was assumed that the sequence of ramping up and ramping down would not impact the torque vs. rotational speed curves because of little soil structure change. The typical torque data of testing on unconditioned soils with the passing of time for both ramping up and ramping down spinning speed are shown in Figure 5.8 (a) and Figure 5.8 (b), respectively.

Testing on foam conditioned soils usually started 15 min after foam generation. The lag was caused by foam and soil mixing, slump test, soil loading and machine set up. The rotational speed was first ramped up and then ramped down for each testing. This operational sequence was rigorously followed due to the concern of early soil structure disturbance at early high rotational speed and that the measurements at subsequent low rotational speeds would be inaccurate. By operating in this sequence, at least one series of data, i.e., the ramping up curve, would be useful. The rotational speed values were the same as those testing in unconditioned soils. However, the testing duration at each rotational speed was reduced to 1 minute and the interval between neighboring speeds was kept at 1 min. This led to the combined testing duration for both ramping

up and ramping down speed be limited to 30 min, as shown in Figure 5.9 (a) and Figure 5.9 (b), respectively.

A representative torque value was obtained for each rotational speed by averaging the corresponding portion of the curve at the residual stage. This resulted in a scattered torque vs. rotational speed relationship for both ramping up and ramping down cycle. Finally, the torque values at the same rotational speed for the two cycles were averaged to generate the representative experimental torque vs. rotational speed curve ready for rheology back calculation. It is demonstrated that the torque and the rotational speed are correlated positively, i.e., the torque increases and decreases as the rotational speed increases and decreases, respectively. Note that the torque curves have the tendency to vibrate more and more as the rotational speed increases beyond 30 rpm. The vibration is especially significant when the speed is 60 rpm. However, this vibration effect impacts torque measurement for all speeds and is compensated by averaging the torque data obtained for each speed for calculating yield stress and viscosity.

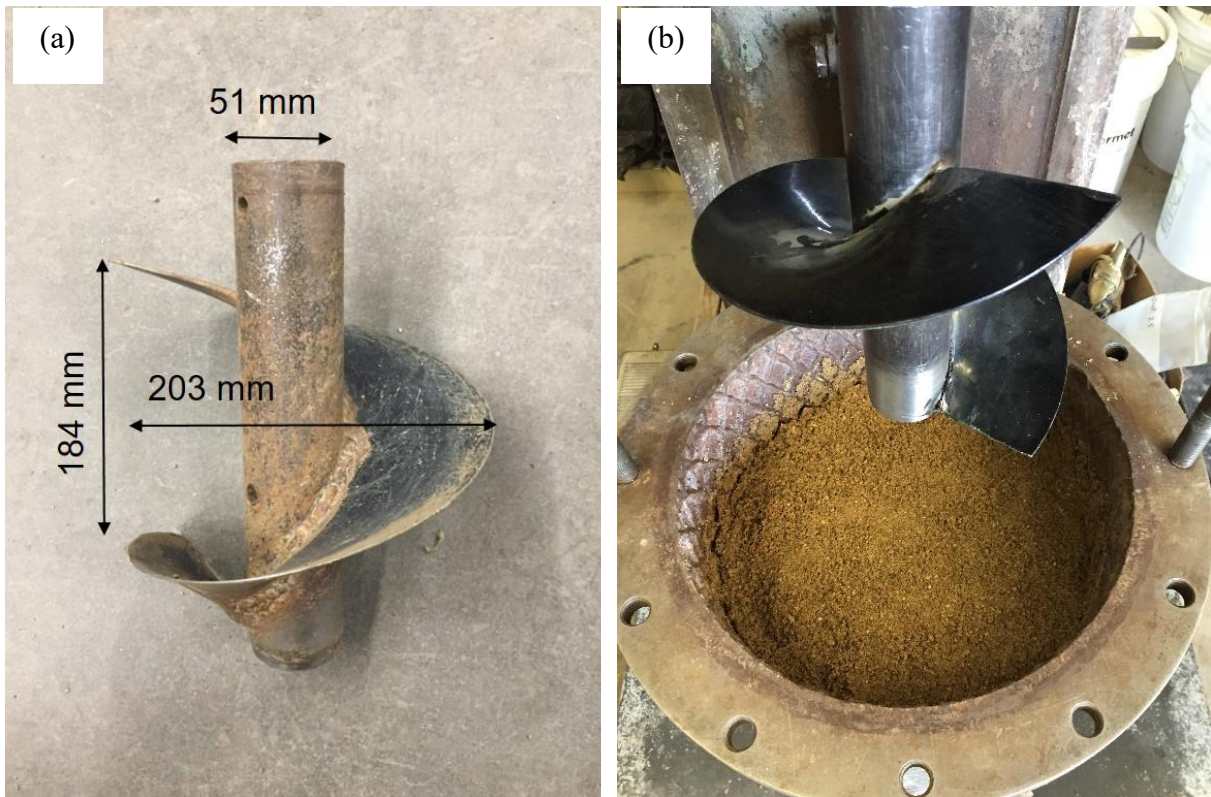


Figure 5.7 Small single-flight auger propeller: (a) dimensions; and (b) installed auger on shaft.

Table 5.4 Summary of testing scenarios.

Propeller geometry	Soil	Conditioning parameters			
		w (%)	c_f (%)	FER	FIR (%)
Small auger	CSM sand	5, 15	NA	NA	NA
Single-flight large auger	CSM sand	0, 5, 7.5, 10, 15	NA	NA	NA
Single-flight large auger	HD sand	0	NA	NA	NA
Single-flight large auger	Ottawa sand	0	NA	NA	NA
Single-flight large auger	Denver clay	0	NA	NA	NA
Single-flight large auger	Crushed CSM shale	0	NA	NA	NA
Single-flight large auger	Crushed Mexico rock	0	NA	NA	NA
Double-flight large auger	CSM sand	7.5	3	15	50
Double-flight large auger	CSM sand	7.5	3	15	40
Double-flight large auger	CSM sand	7.5	3	15	30
Double-flight large auger	CSM sand	7.5	3	10	30
Double-flight large auger	CSM sand	7.5	3	20	30
Double-flight large auger	CSM sand	7.5	1	15	30
Double-flight large auger	CSM sand	7.5	5	15	30

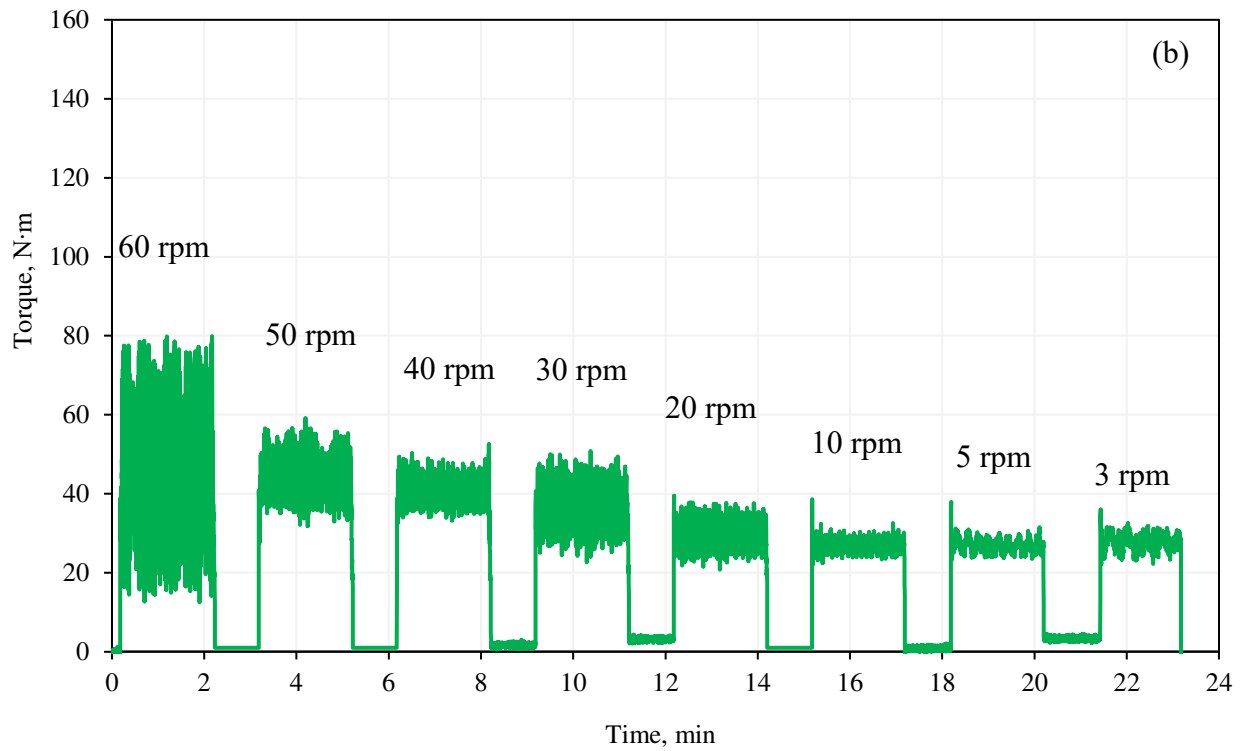
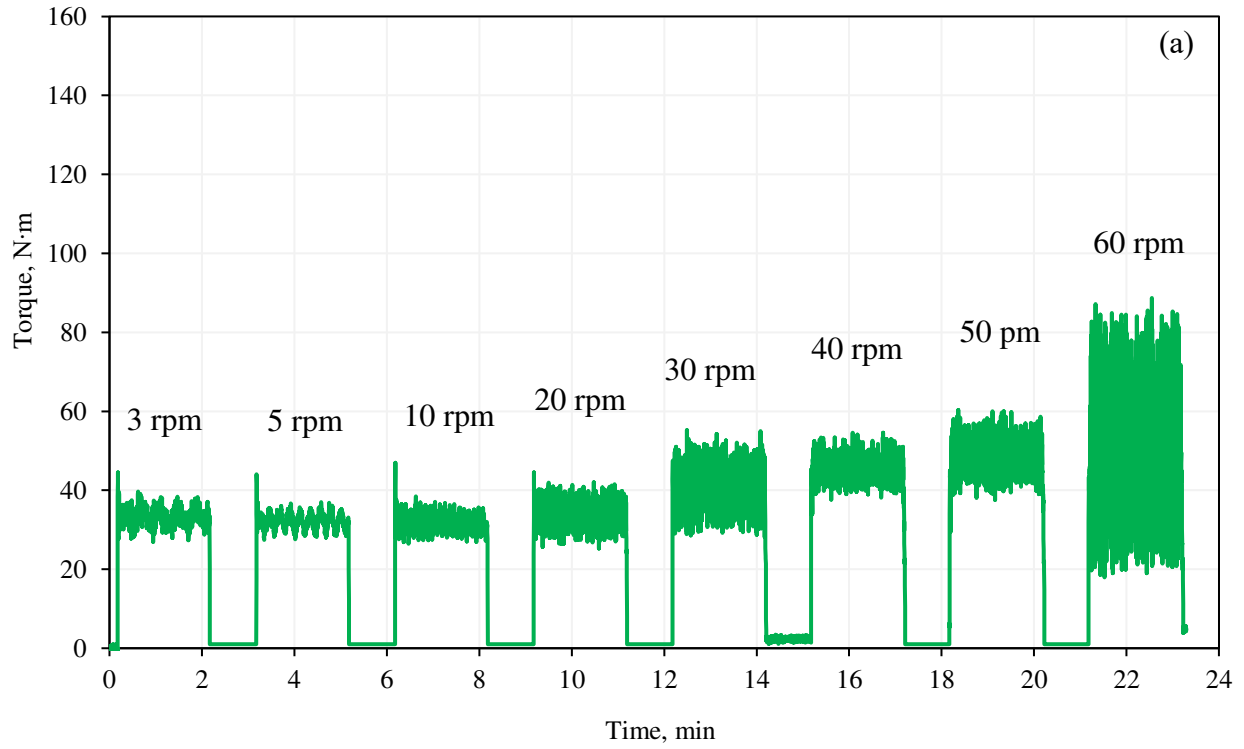


Figure 5.8 Torque vs. time plots for testing dry CSM sand: (a) ramping up rotational speed from 3 rpm to 60 rpm; and (b) ramping down rotational speed from 60 rpm to 3 rpm.

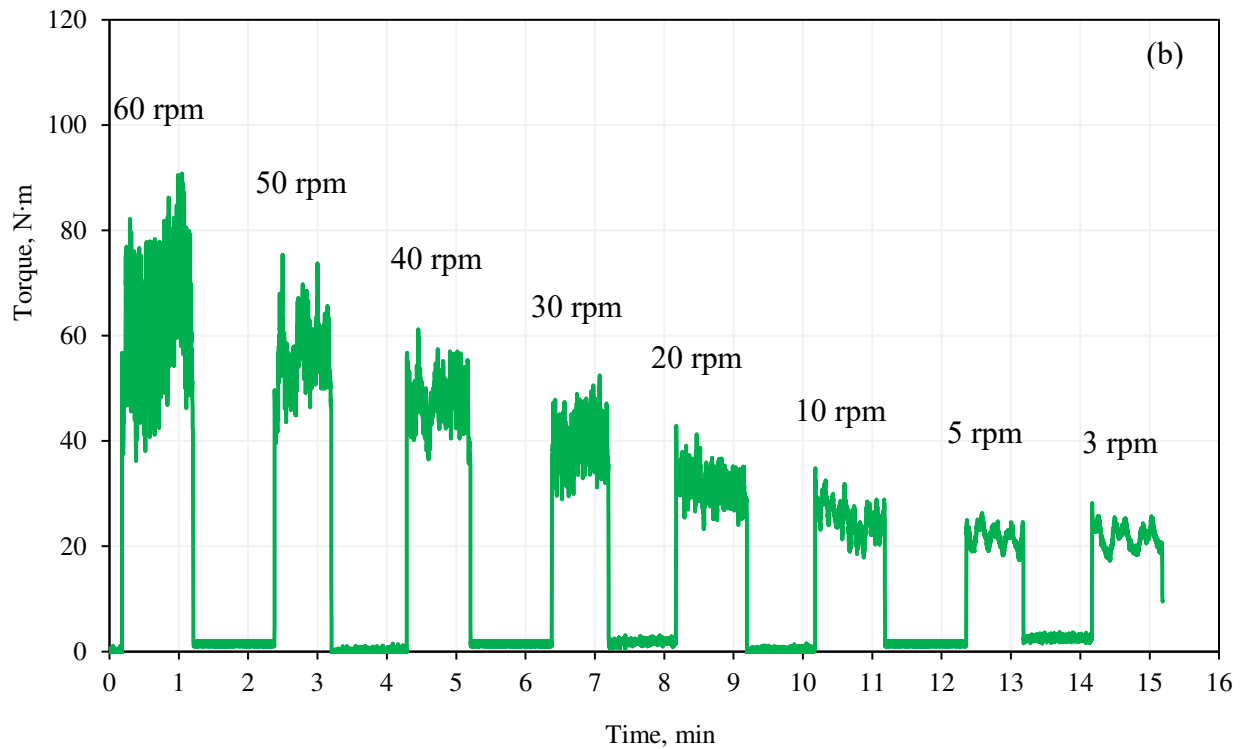
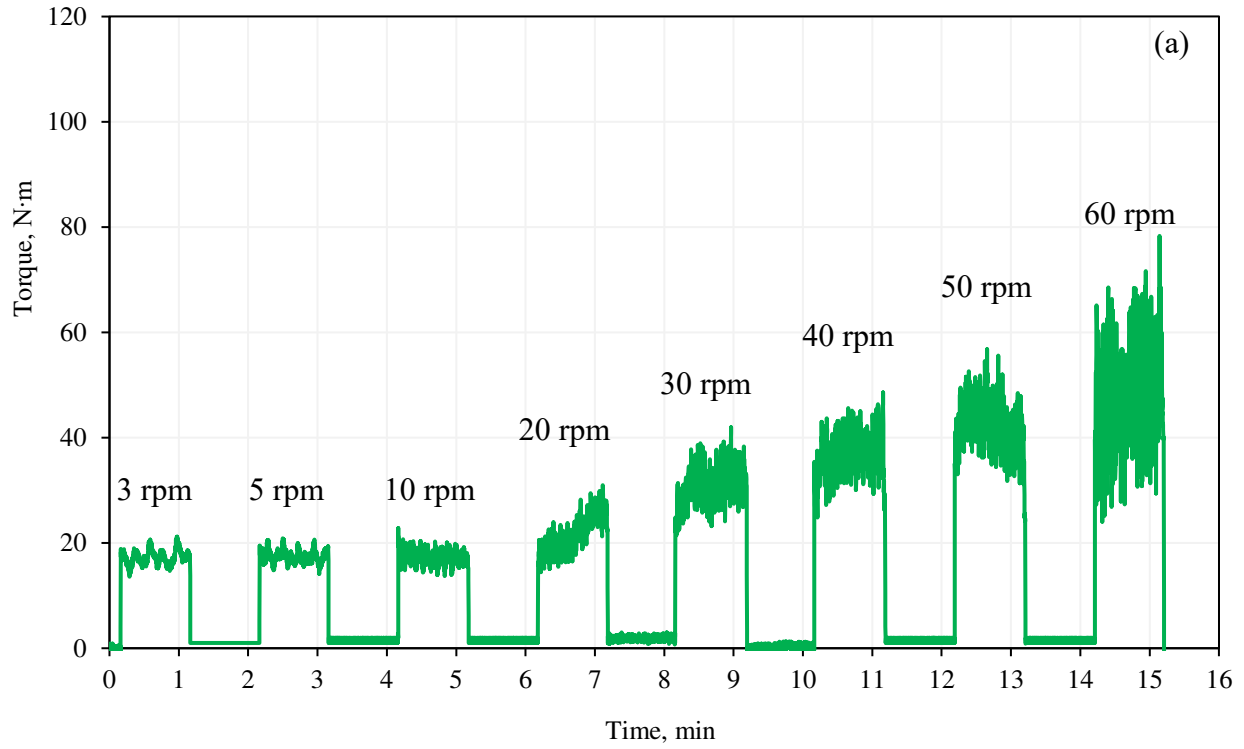


Figure 5.9 Torque vs. time plots for testing foam conditioned CSM sand when $c_f=1\%$, $FER=15$, and $FIR=30\%$: (a) ramping up rotational speed from 3 rpm to 60 rpm; and (b) ramping down rotational speed from 60 rpm to 3 rpm.

5.6 Results and analyses

As indicated in Table 5.4, several factors influencing soil behavior were selected to study their impacts on soil rheology. This includes the auger geometry, water content, soil type, Foaming Agent Concentration, Foam Expansion Ratio, and Foam Injection Ratio. For the conditioned samples, the testing was repeated several times so that the torque vs. rotational speed curves were obtained at different passing of time. This included 0.25 h, 2 h, 5 h, and 24 h. In addition, the chamber pressure was elevated to 150 kPa and 300 kPa to test the corresponding rheology response of conditioned soil. The results and analyses will be discussed in the following section.

5.6.1 Effect of auger geometry on torque response

The optimized propeller geometry in the previous study was found to be an auger of 296 mm in diameter through CFD modeling. This process saved repetitive and laborious lab experiment work. The recommendation from CFD modeling was primarily based on the torque sensitivity to the variations of the yield stress and viscosity, together with magnitude of soil density change, material flow capability, and soil loading viability. However, two more factors were missing from the previous study, i.e., potential wall slip issue for using certain propellers and the power capacity limitation of the machine motor. This is because the CFD model assumed no-slip boundary condition between the fluid and the chamber wall as the surface of the interior wall was purposefully fabricated to be rough to transmit torque. Also, the CFD models had no upper limit for the calculated torque. To address these issues, a small auger shown in Figure 5.7 was tested in conjunction with the optimized auger shown in Figure 5.2 to confirm and finalize the auger geometry and examine the wall slip phenomenon.

The soils used in this comparison were CSM sand at two water content levels, i.e., 5% and 15%, to represent viscous and flowable soil, respectively. The torque responses when changing rotational speed using the small auger are shown in Figure 5.10. It is clearly seen that the torque values fluctuate in the vicinity of zero, similar to the testing responses in air and water (Hu and Rostami 2020). This could mean that either the rotational movement of the small auger generate little torque, or due to the large gap between the auger bit and the chamber wall, the torque cannot properly propagate to the force sensory arms attached to the two sides of the chamber, as shown in Figure 5.11 (Rostami et al. 2012). In summary, the small auger with a diameter of 203 mm was unable to offer measurable torque values.

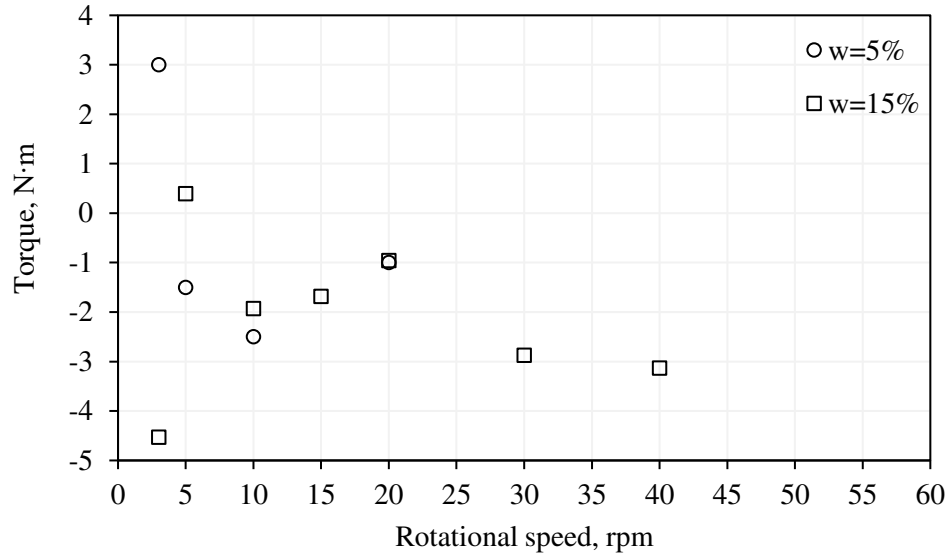


Figure 5.10 Torque at different rotational speeds for testing CSM sand at two water content levels using the small auger.



Figure 5.11 Gap between the outer edge of the small auger and the chamber wall.

In contrast, the similar experiments by using large single-flight auger with 296 mm in diameter demonstrated the suitability of the auger. As shown in Figure 5.12, the torque values were in a range indicating not only efficient torque transmission from the propeller to the sensory system but also reasonable utilization of the motor power. In addition, best fit curves with high correlation coefficients could be found using the Bingham plastic model. Therefore, the lab testing confirmed

the viability of using the large auger as the optimized geometry, as previously indicated in auger optimization via CFD modeling.

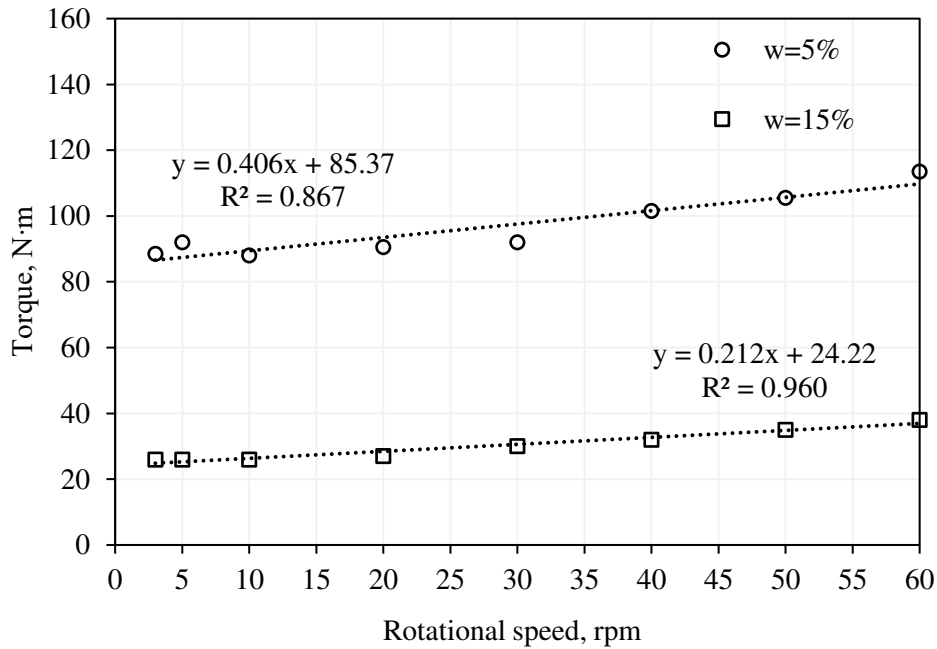


Figure 5.12 Torque at different rotational speeds for testing CSM sand at two water content levels using the large single-flight auger.

5.6.2 Effect of ramping sequence on torque response

As discussed earlier in Section 4.4, the torque vs. rotational speed data used for rheology back calculation were averaged from the data of ramping up and ramping down operation for each testing condition. To validate this procedure, the torque variations between ramping up and ramping down testing were studied for all the testing scenarios in Table 5.4. The representative results are shown in Figure 5.13, Figure 5.14, and Figure 5.15. In some scenarios, the torque differences between ramping up and ramping down are negligible such as the ones shown in Figure 5.14. In others where there are measurable differences, the averaging process can eliminate the odd points and smooth the curve for modeling and best fit calculations, as shown in Figure 5.15. In practice, however, it is recommended that the testing should start with lower speed and increase in selected increments in a ramping up process, followed by ramping down. The benefits of this sequence of operation are that, starting with low rotational speed means that ramping up would eliminate the risk of high initial torque and the potential damage to the device, and this sequence would minimize the potential disturbance from high rotational speeds at the beginning of the testing and ensure the acquisition of reliable data from operation at low rotational speeds.

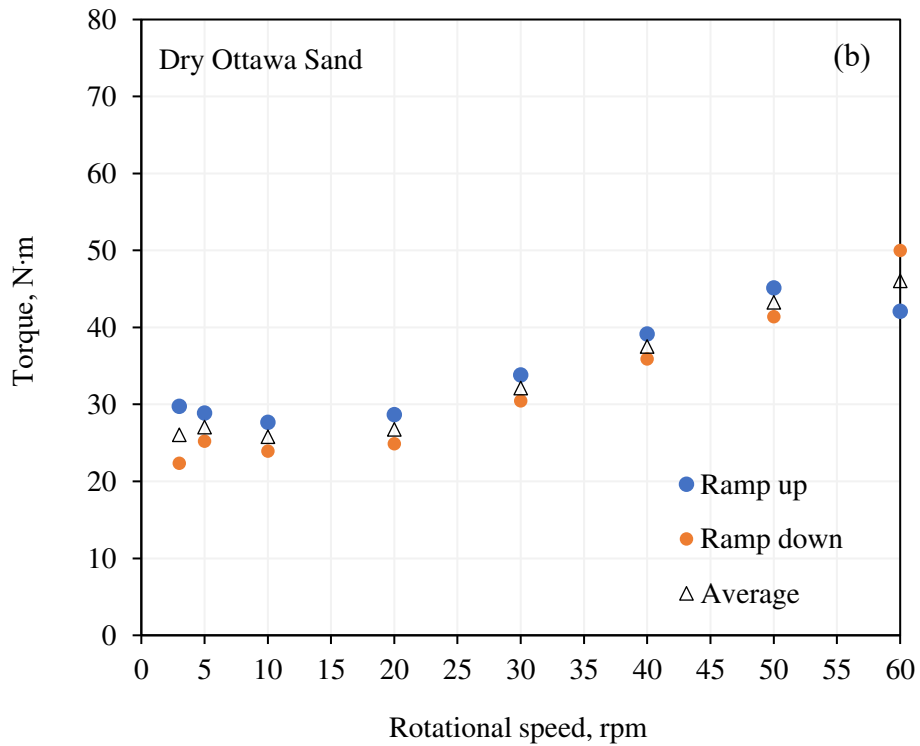
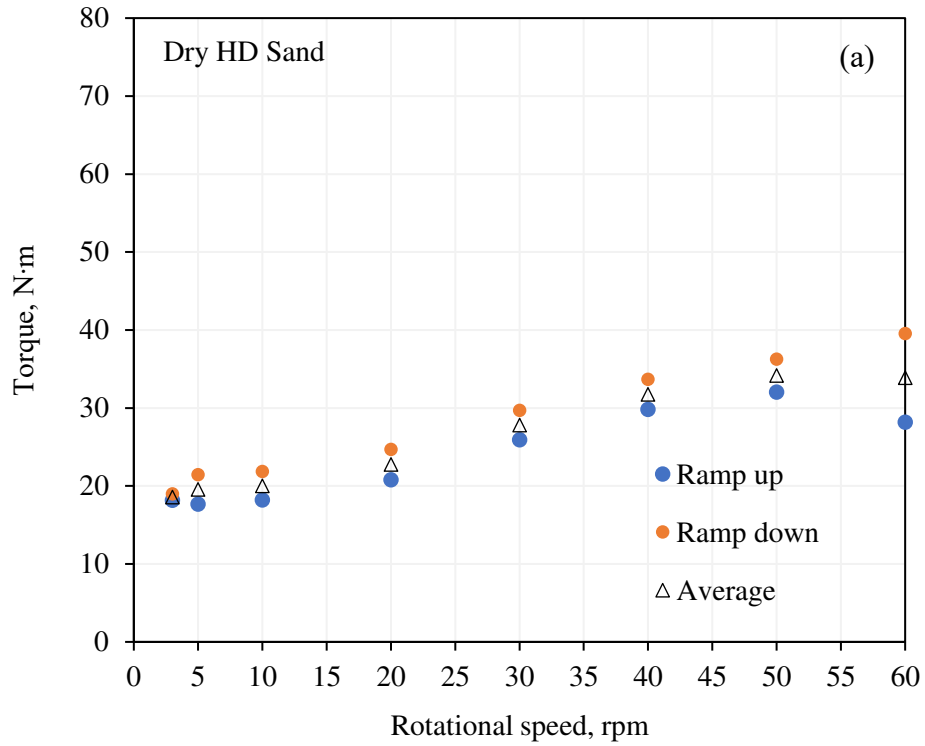


Figure 5.13 Comparison of measured torque between ramping up and ramping down rotational speed for: (a) dry HD Sand; and (b) dry Ottawa Sand.

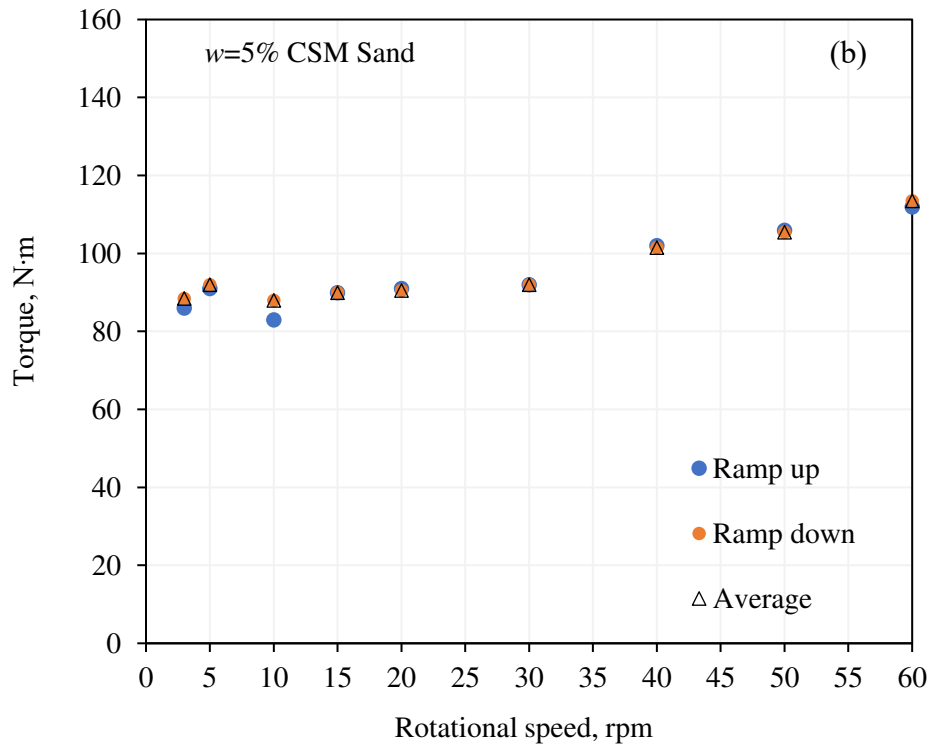
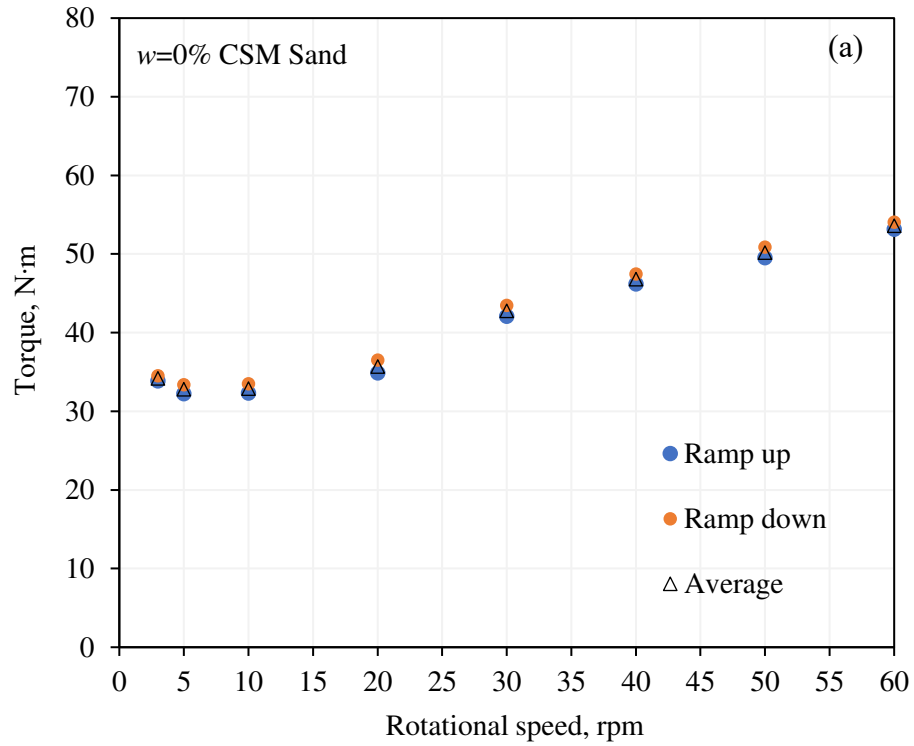


Figure 5.14 Comparison of measured torque between ramping up and ramping down rotational speed for CSM sand: (a) $w=0\%$; and (b) $w=5\%$.

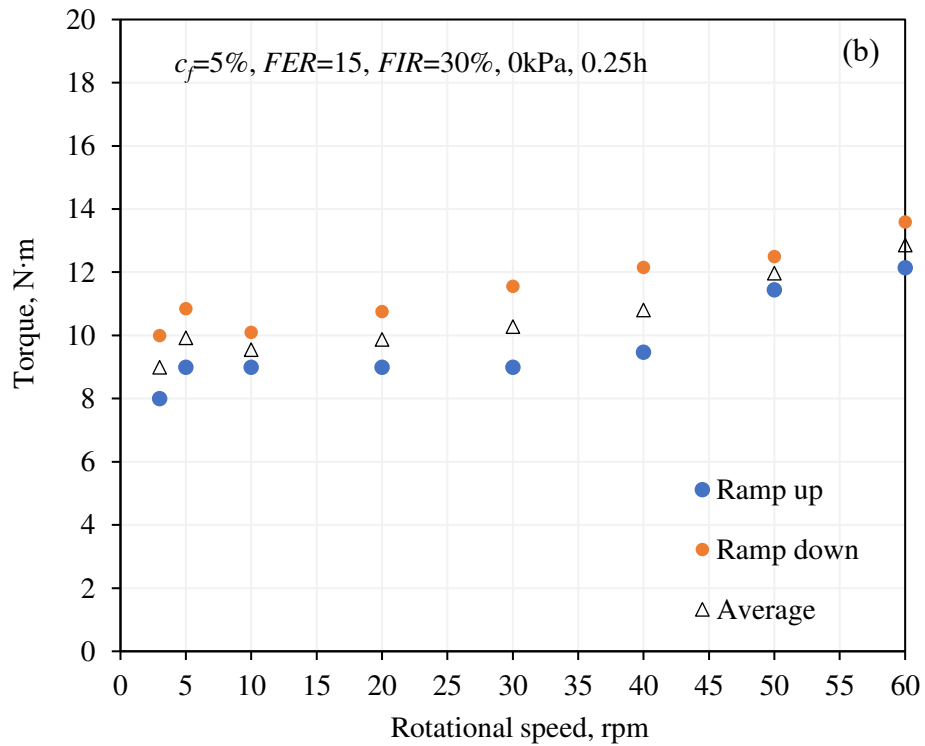
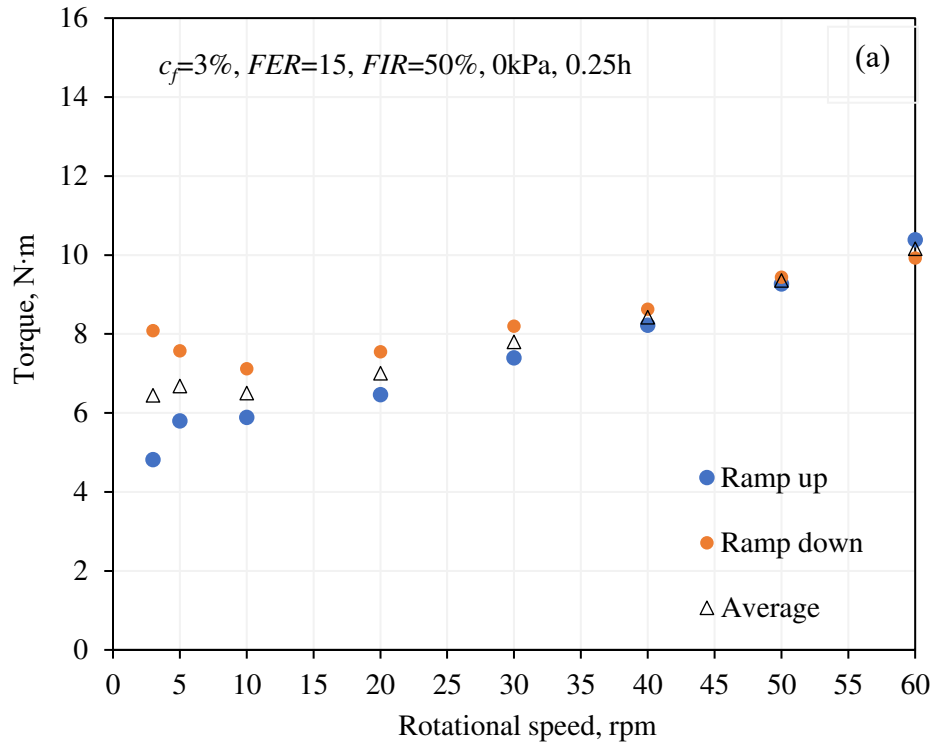


Figure 5.15 Comparison of measured torque between ramping up and ramping down rotational speed for conditioned CSM sand: (a) $c_f=3\%$, $FER=15$, $FIR=50\%$, 0kPa , 0.25h ; and (b) $c_f=5\%$, $FER=15$, $FIR=30\%$, 0kPa , 0.25h .

5.6.3 Effect of compressibility setting in CFD on calculated torque

One of the desired functions of the foam conditioned soil is the high compressibility. With high compressibility, the chamber pressure can be readily adjusted to counterbalance the changing face pressure without inducing undesired torque. This is usually achieved by adjusting the rotational speeds of the cutterhead and the screw conveyor so that the amount of materials removed from the chamber is adjusted. In this study of the soil rheology, the conditioned CSM sand was used to examine the impact of compressibility setting in CFD models on the calculated torque. For this purpose, the density of the conditioned soil was measured both before rheology testing and after 24 h, as shown in Table 5.5. The results show that the density of conditioned soils increased for all the conditioning scenarios ranging from 2.64% to 25.76%, which confirmed the high compressibility assumption.

Table 5.5 Measured density change of foam conditioned CSM sand.

w	c_f	FER	FIR	Density of fresh mixture	Density after 24h	Average density	Density increase	Density increase
%	%		%	kg/m ³	kg/m ³	kg/m ³	kg/m ³	%
7.5	3	15	50	1351	1698	1525	348	25.76%
7.5	3	15	40	1514	1647	1581	133	8.79%
7.5	3	15	30	1561	1602	1582	41	2.64%
7.5	3	20	30	1494	1675	1584	180	12.06%
7.5	3	10	30	1564	1607	1586	43	2.78%
7.5	5	15	30	1481	1596	1538	115	7.77%
7.5	1	15	30	1438	1587	1513	149	10.39%

On the other hand, the core of CFD modeling is to solve the Navier-Stokes equations, which consist of the mass continuity equation and the momentum balance equation denoted as Eq. (4.1) and Eq. (4.2), respectively. Because the Navier-Stokes equations are highly non-linear partial differential equations which require numerical tools to solve under reasonable simplifications for particular applications (Kundu, Cohen, and Dowling 2012), any unnecessary variables in the equations will significantly increase the computational difficulties such as increased computational time and even divergence of the numerical solution.

In addition, little was known about how the density changed as a function of time. Therefore, the density of the conditioned soil in the CFD modeling in this study was still implemented as a constant equivalent to that of the fresh mixture. The following will validate that it is a worthy trade-off to represent ρ with a constant value while not sacrificing the computational accuracy nor requiring excessive computational time.

The computational process and results of “Compressible flow” and “Incompressible flow” settings in CFD were compared. Table 5.6 shows the CFD modeling results of two conditioning scenarios, i.e., $c_f=3\%$, $FER=15$, $FIR=50\%$, and $c_f=1\%$, $FER=15$, $FIR=30\%$. The results demonstrated that the torque differences between the two flow settings are within 1.5%. As a comparison, the differences of computational time can be more significant such as these presented in the last two rows in Table 5.6. However, the computational time for compressible setting was within one hour, which was acceptable considering the time for other soil conditions. Therefore, incompressible flow setting was implemented in COMSOL.

Both the upper and lower bound of the density in Table 5.5 were implemented in CFD models to compare the resulting torque values. Note that yield stress and viscosity were assumed to be the same for both density conditions. As shown in Table 5.7, the torque differences between two density conditions are negligible indicating that the measured variations of density have little impact on the calculated torque values, and consequently, little on the back calculated yield stress and viscosity. Therefore, the density values of the fresh conditioned soil were used in this study.

5.6.4 Effect of soil type on soil rheology

To investigate the effect of soil type on soil rheology, five other types of dry soils were selected in addition to the dry CSM sand shown in Table 5.4. Figure 5.16 shows the torque responses for these six dry soils at eight rotational speeds. It was found that the data for five soils form a cluster while the torque values for crushed Mexico rock are significantly higher. Table 5.8 shows that the relationships between torque and rotational speed are linear, with high R^2 values. The back calculated yield stress and viscosity are also shown in Table 5.8 and compared in Figure 5.17 and Figure 5.18, respectively. It is concluded that yield stress is sensitive to soil types with the highest of 1,750 Pa in crushed Mexico rock and the lowest of 270 Pa in Denver clay, while the viscosity values are low and remain in the range of 30 Pa·s to 50 Pa·s. This is expected to be the aggregate results of variation of soil structure and formation, primarily particle size distribution, particle roundness, and particle interlock. One can compare Ottawa sand and crushed Mexico rock

to explain the impact of grain shape. Because Ottawa sand is a poorly-graded and rounded soil (Alavi 2013), there is little interparticle locking to resist the movement of the soil particles. On the contrary, the crushed Mexico rock is observed to be rich in well-graded and angular particles, and consequently, required significant force to counteract the interlocking structure and mobilize flow.

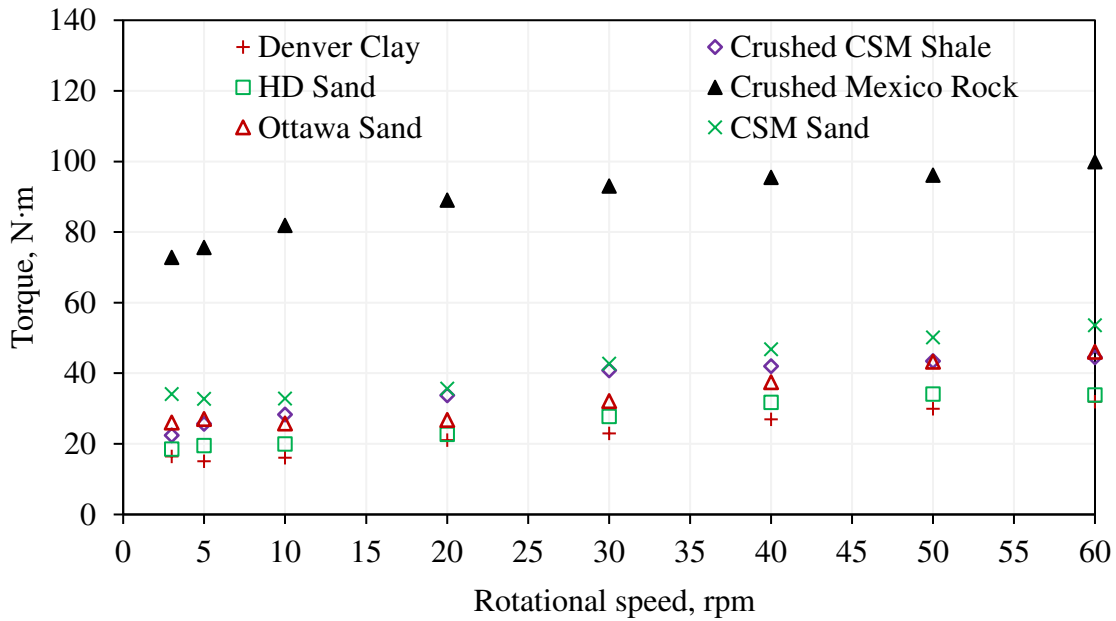


Figure 5.16 Experimented torque vs. rotational speed relationships for six dry soils using the large single-flight auger.

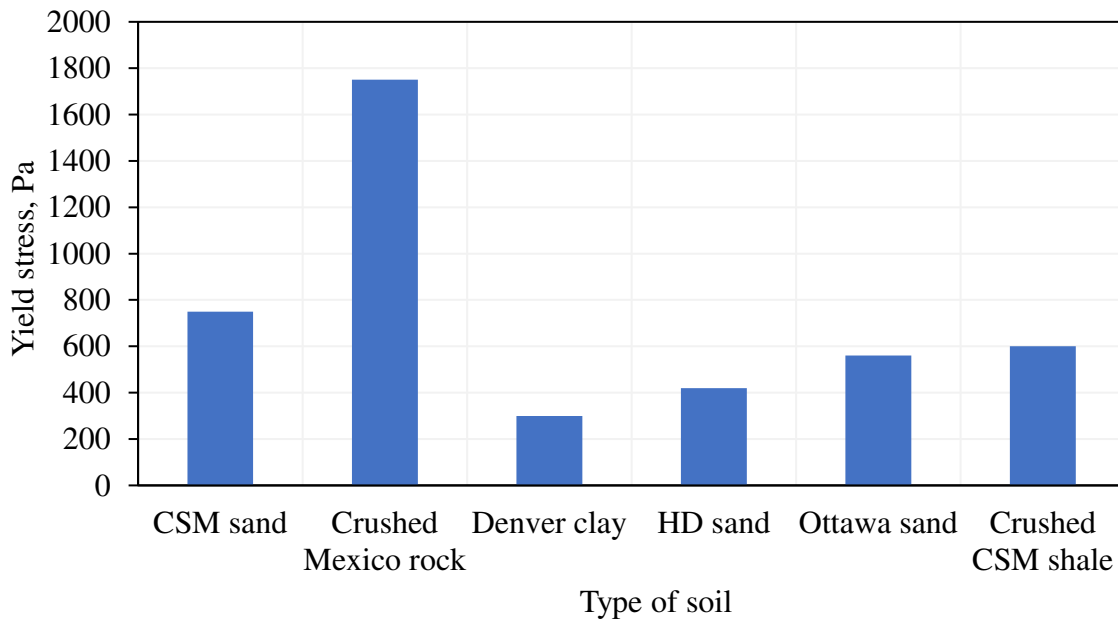


Figure 5.17 Back calculated yield stress for six dry soils.

Table 5.6 Differences of computational results between “compressible” and “incompressible” setting in COMSOL.

Conditioning parameters	rpm	τ_y	μ_0	ρ	Propeller	Compressibility	Torque	Torque Difference	Computational time
	1/min	Pa	Pa·s	kg/m ³			N·m	%	
$c_f=3\%$, $FER=15$, $FIR=50\%$	30	120	5	1351	Double-flight auger	Incompressible	7.7136	1.45%	49min
	30	120	5	1351	Double-flight auger	Compressible	7.6020		50min
	40	120	5	1351	Double-flight auger	Incompressible	8.4307	1.41%	50min
	40	120	5	1351	Double-flight auger	Compressible	8.3117		51min
$c_f=1\%$, $FER=15$, $FIR=30\%$	30	400	45	1438	Double-flight auger	Incompressible	37.4540	1.31%	33min
	30	400	45	1438	Double-flight auger	Compressible	36.9650		47min
	40	400	45	1438	Double-flight auger	Incompressible	43.3710	1.20%	10min
	40	400	45	1438	Double-flight auger	Compressible	42.8500		47min

Table 5.7 Differences in calculated torque between upper and lower density settings in COMSOL.

<i>w</i>	<i>c_f</i>	<i>FER</i>	<i>FIR</i>	Torque in fresh mixture, N·m		Torque after 24h, N·m	
%	%		%	30 rpm	40 rpm	30 rpm	40 rpm
7.5	3	15	50	7.7136	8.4307	7.7120	8.4282
7.5	3	15	40	13.5680	14.9880	13.5680	14.9880
7.5	3	15	30	22.3840	23.8760	22.3840	23.8750
7.5	3	20	30	22.3840	23.8760	22.3830	23.8750
7.5	3	10	30	12.3540	12.4490	12.3520	12.4470
7.5	5	15	30	10.6958	11.2738	10.6940	11.2719
7.5	1	15	30	37.4540	43.3710	37.4530	43.3690

Table 5.8 Summary of effect of soil type on soil rheology parameters.

<i>Soil</i>	<i>T~rpm</i>	<i>R</i> ²	<i>τ_y</i> (Pa)	<i>μ₀</i> (Pa·s)
CSM sand	$T=0.384 \cdot (rpm)+30.66$	0.967	750	30
Crushed Mexico rock	$T=0.447 \cdot (rpm)+75.84$	0.895	1750	50
Denver clay	$T=0.541 \cdot (rpm)+11.82$	0.907	270	50
HD sand	$T=0.304 \cdot (rpm)+17.78$	0.961	420	30
Ottawa sand	$T=0.372 \cdot (rpm)+22.97$	0.936	560	30
Crushed CSM shale	$T=0.390 \cdot (rpm)+24.52$	0.907	600	33

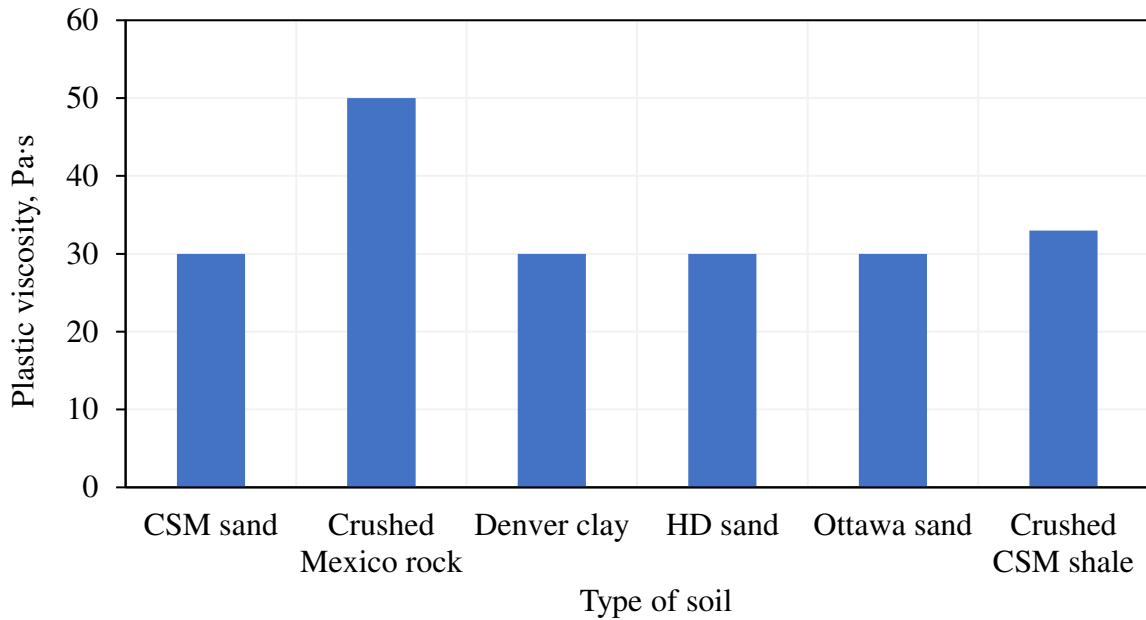


Figure 5.18 Back calculated plastic viscosity for six dry soils.

Except for CSM sand, there were limited sources of other soil/crushed rock samples at this stage of study and consequently, only dry samples were tested. Other influential factors, including water content and foam conditioning parameters need to be investigated in the future.

5.6.5 Effect of water content on soil rheology

The engineering properties and behaviors of soil are significantly influenced by water content (Lu et al., 2006; Alavi et al., 2013). In some ground conditions, only water is used as the conditioner to modify the rheology of the excavated muck. In order to reveal the impact of water content on soil rheology, dry CSM sand and water were mixed to obtain five batches of wet sand at water content of 0%, 5%, 7.5%, 10%, and 15%, as shown in the second row in Table 5.4. The rheological properties of these soils were tested and back calculated, including the two conditions in Figure 5.12. In general, the tests were conducted by spinning the auger between 3 rpm and 60 rpm, as discussed in Section 5.5.4. One exception is that a maximum rotational speed of 40 rpm was used for testing wet CSM sand at water content of 7.5%. This is because the machine motor had limited power and further increase of rotational speed could lead to permanent damage to the testing unit. Figure 5.19 shows the tested torque vs. rotational speed data for the five scenarios. The relative magnitude of the five conditions demonstrates that the most and the least resistant conditions occur at water content of 7.5% and 15%, respectively. This confirms the predicted water content where peak torque would occur in Chapter 4. The linear fitting results, presented in Table

5.9, indicate that the experimental data follow linear relationships with high R^2 . Because of the linear correlations between torque and stress, and between rotational speed and strain rate, as shown in Section 4.4.3, it is verified that the soil rheology follows the proposed Bingham model.

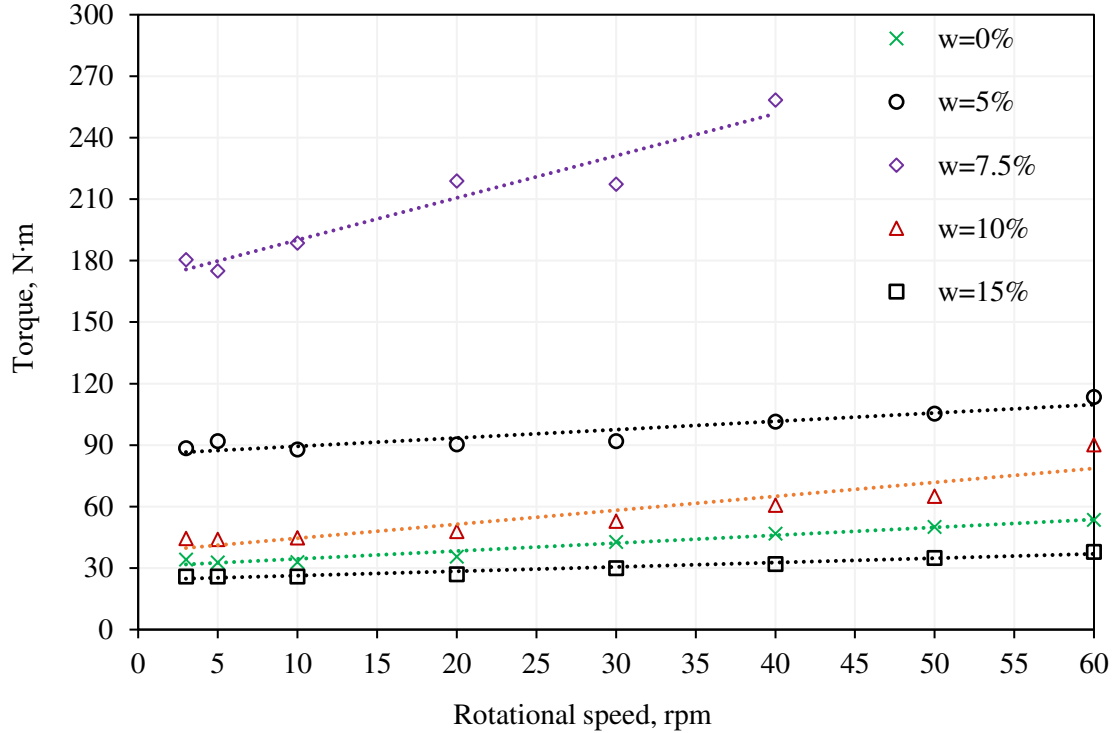


Figure 5.19 Experimented torque vs. rotational speed relationships for testing CSM sand at different water content levels using the large single-flight auger. Note that the dashed lines are the linear fitting lines.

Table 5.9 Summary of effect of water content on soil rheology parameters.

w (%)	$T \sim rpm$	R^2	τ_y (Pa)	μ_0 (Pa·s)
0	$T=0.384 \cdot (rpm)+30.66$	0.967	750	30
5	$T=0.406 \cdot (rpm)+85.37$	0.867	2150	40
7.5	$T=2.054 \cdot (rpm)+169.55$	0.929	4200	170
10	$T=0.681 \cdot (rpm)+37.77$	0.848	900	60
15	$T=0.212 \cdot (rpm)+24.22$	0.960	550	25

Yield stress and viscosity were back calculated in the CFD module in COMSOL, and were plotted against water content, as shown in Figure 5.20 and Figure 5.21, respectively. Note that the dashed lines in both figures are not meant to provide definitive model fitting curves to the scattered

data. Instead, the lines are meant to remind the readers of the overall trend with regards to increase of the water content. While the water content increases from dry to saturated, both yield stress and viscosity initially increase to reach a peak at water content of 7.5%, followed by a decrease when the water content approaches 15%, i.e., saturation point. This overall trend is similar to Proctor compaction test results and comparable to the relationship between tool wear vs. water content indicated in the literature (Alavi, Qiu, and Rostami 2013). The mechanism of this trend can be summarized as follows. When the water content increases from dry to approximately 7.5%, which is lower than the optimum water content, the aggregate soil suction stress increases which can be attributed to the change of surface tension forces, cementation forces, and physicochemical forces (Lu et al. 2006), resulting in higher shear strength and stiffness of the particle assemblage. This increase in strength and stiffness further augments the frictional resistance between soil particles. Beyond $w=7.5\%$, a decrease in torque is observed due to lubricating effects of water kicking in, resulting in lower shear strength and stiffness. The decrease in strength and stiffness reduces the frictional resistance and contact pressure on the propeller blades as they rotate in the soil samples.

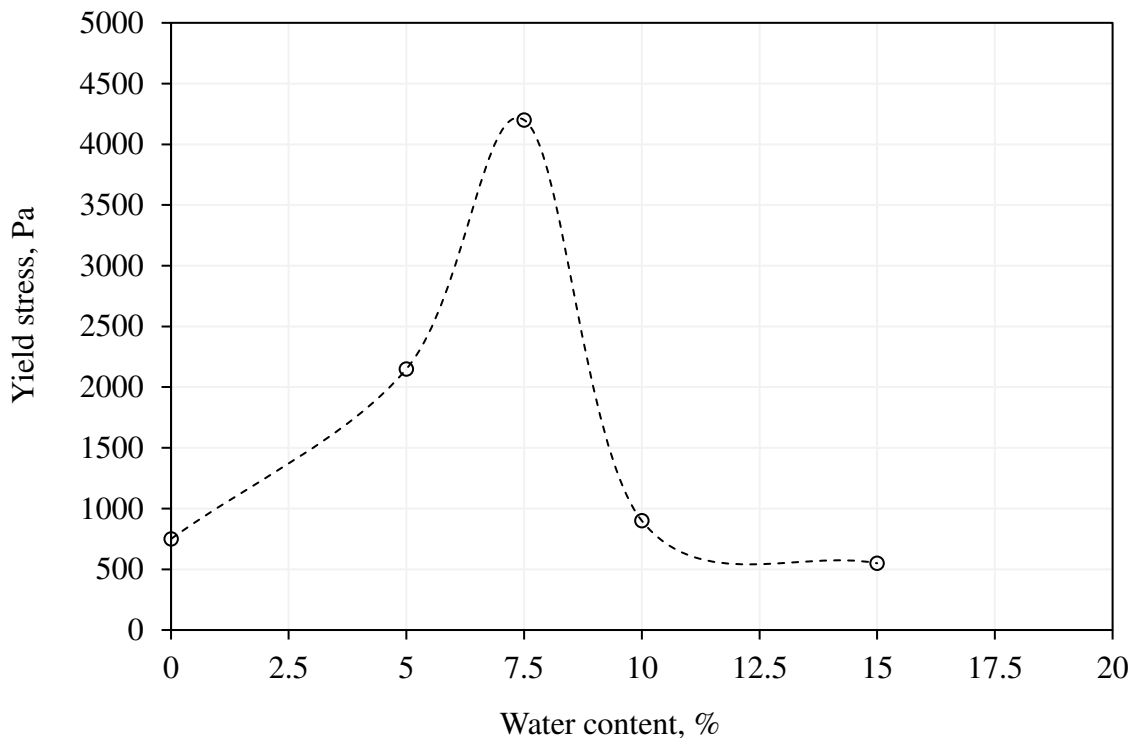


Figure 5.20 Back calculated yield stress vs. water content relationships for CSM sand.

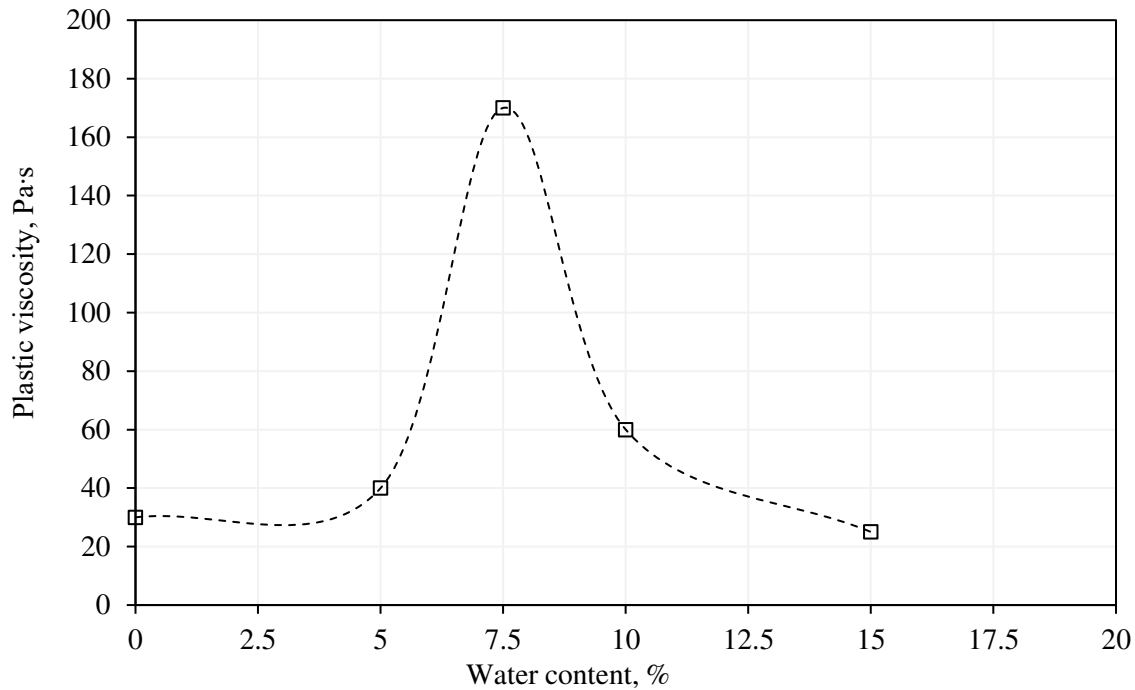


Figure 5.21 Back calculated plastic viscosity vs. water content relationships for CSM sand.

Note that the yield stress and viscosity values shown in this study differ from those presented in Chapter 4 and the literature (Hu and Rostami 2020) at the same water content, i.e., the rheological parameters derived from previous study using the pitched propeller are much higher than the ones using the current auger propeller. This contrast is especially significant for yield stress. In fact, it is an expected distinction due to the contrasting interactive mechanisms between the propeller and the soil. The pitched propeller has continuous compaction effect on the soil during rotation and hence, the soil becomes denser and stronger over the testing course. On the contrary, the auger propeller is capable of circulating the soil without densifying the original soil structure. Therefore, yield stress and viscosity measured by the current auger propeller are considered more appropriate. To eliminate the potential errors in the back calculated data, however, more testing on the same soil conditions can be conducted in the future to assign statistically reasonable data set and confirm the results.

5.6.6 Effect of foam conditioner on soil rheology

In EPB tunneling, soil conditioning measures, typically a foam is injected to the tunnel face and cutting chamber to modify the flowability and viscosity of the excavated muck. To investigate the effect of foam as a soil conditioner on soil rheology, seven foam conditioned CSM sand

samples with different foam conditioning parameters were tested and modeled in the current measurement system, as shown in Table 5.4. The variables controlling foaming effect include w , c_f , FER , and FIR . Note that 7.5% in the bottom seven rows in Table 5.4 refers to the designated ultimate water content of the sand and foam mixture. This value was kept the same to exclude the influence of water content on soil rheology of these foam conditioned samples. It was chosen because the yield stress and viscosity of wet CSM sand peak at this level of water content, as shown in Figure 5.20 and Figure 5.21. Consequently, this universal setting of ultimate water content can best demonstrate the contrast of rheology and the effect of foam conditioning once foam is added.

The propeller used in this testing category was the double-flight auger shown in Figure 5.3. The reason to use double-flight auger instead of the single-flight one, as shown in Figure 5.2, was due to the concern that the single-flight geometry may not be able to generate sufficient torque in well-conditioned soil, and hence, lead to difficulties in back calculating yield stress and viscosity.

Another important factor taken into consideration was the time constraint due to the inherent nature of foam collapse and degradation over time. Therefore, the duration between foam generation and the beginning of rheology testing was rigorously kept as 0.25 h (15 min) throughout the seven experiments. This was found to be sufficient to carry out activities including mixing sand and foam, slump test, loading conditioned soil into the testing chamber, chamber assembly, and data acquisition preparation.

Figure 5.22, Figure 5.23 and Figure 5.24 show the experimented torque vs. rotational speed relationships for each foam conditioning recipe. It is demonstrated that these curves shift as the foam conditioning parameters change respectively. At the same rotational speed, the torque value decreases with respect to the increase of FIR and c_f , while the torque value decreases as FER decreases within the selected range. A linear Bingham plastic rheological model can be observed in these charts. The linear function offered high correlations except for one condition, i.e., $w=7.5\%$, $c_f=3\%$, $FIR=30\%$, $FER=10$, as shown in Table 5.10. This is because the foam with low FER was too wet and the corresponding conditioned soil provided little resistance to auger rotation. Liquefaction at high rotational speeds may also contribute to bending down the overall curve and resulting in the low correlation.

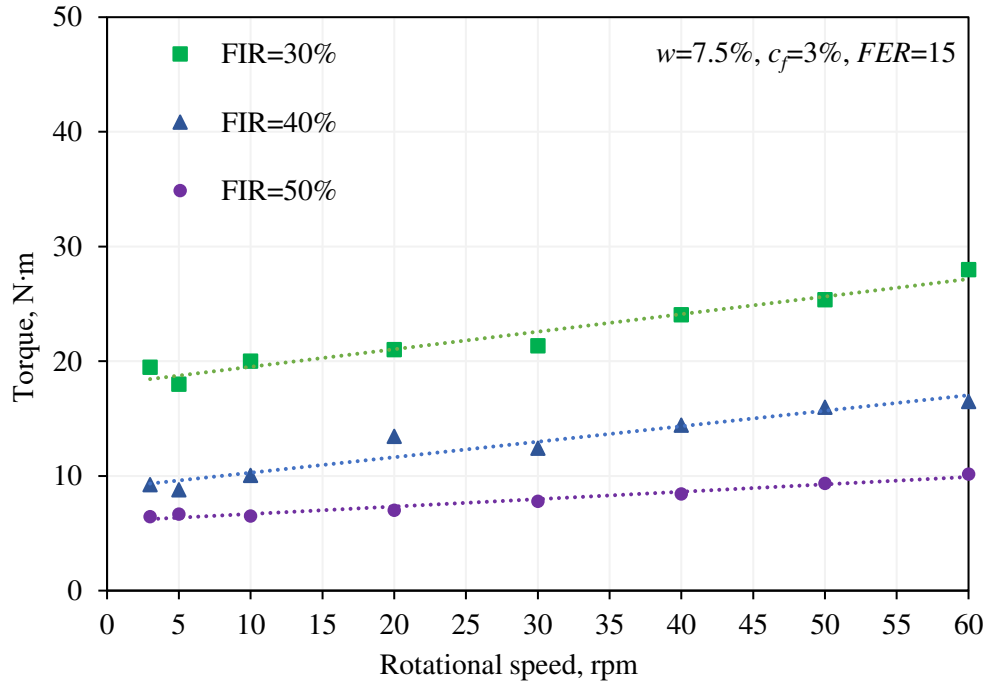


Figure 5.22 Measured torque vs. rotational speed relationships for foam conditioned CSM sand at different FIR s while keeping w , c_f and FER constants. The dashed lines are the best linear fitting correlations.

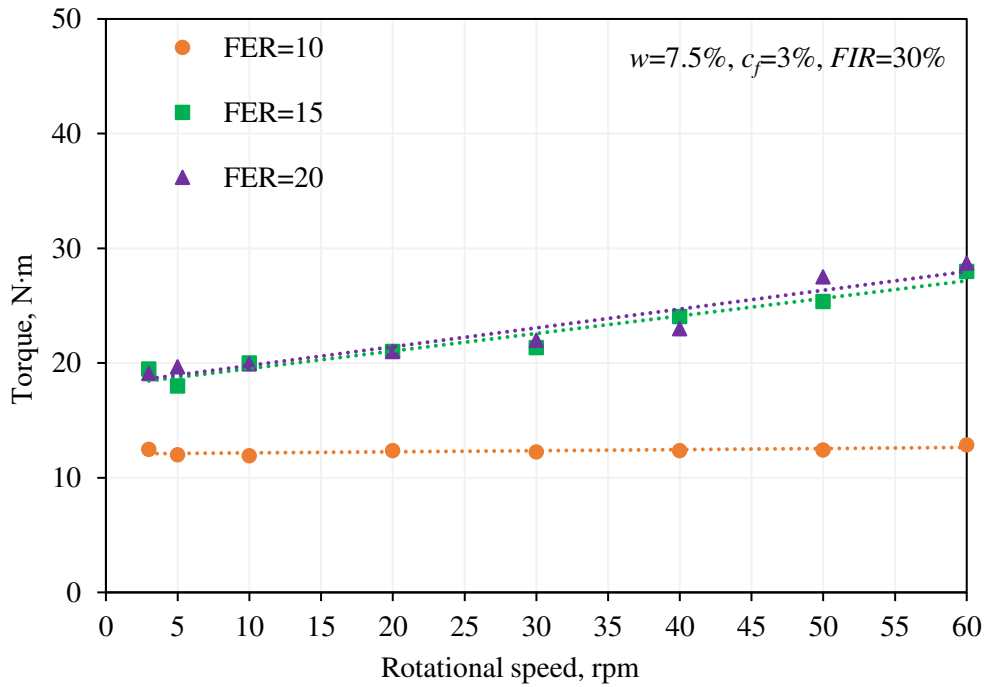


Figure 5.23 Measured torque vs. rotational speed relationships for foam conditioned CSM sand at different FER s while keeping w , c_f and FIR constants. The dashed lines are the best linear fitting correlations.

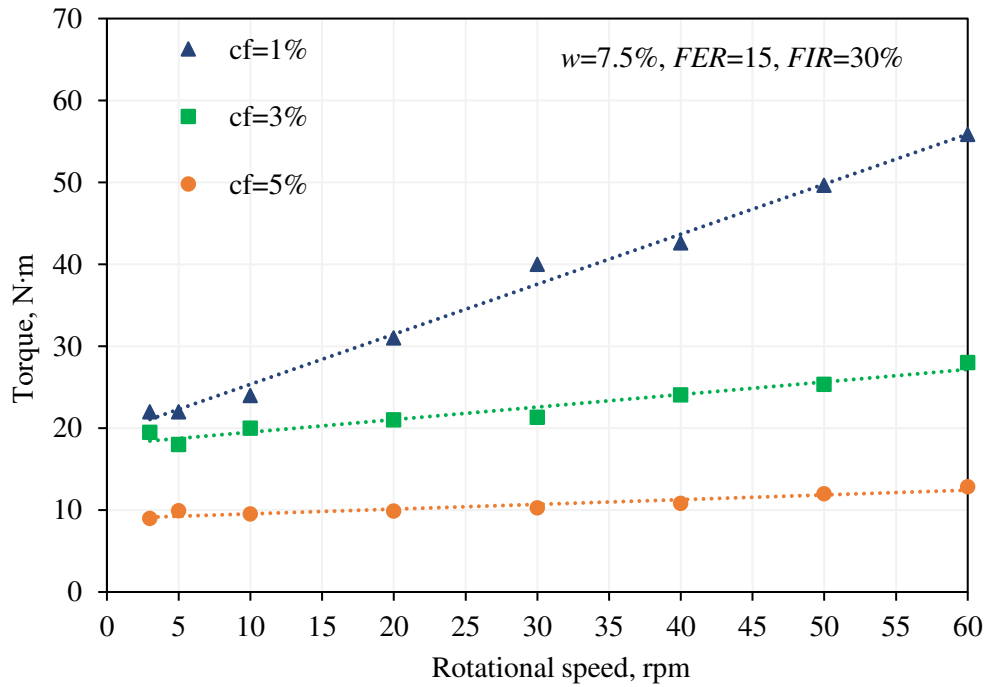


Figure 5.24 Measured torque vs. rotational speed relationships for foam conditioned CSM sand at different c_f while keeping w , FIR and FER constants. The dashed lines are the best linear fitting correlations.

Table 5.10 Summary of effect of foam conditioner on soil rheology parameters.

w (%)	c_f (%)	FER	FIR (%)	$T \sim rpm$	R^2	τ_y (Pa)	μ_0 (Pa·s)
7.5	3	15	50	$T=0.065 \cdot (rpm)+6.04$	0.969	120	5
7.5	3	15	40	$T=0.135 \cdot (rpm)+8.93$	0.925	200	10
7.5	3	15	30	$T=0.153 \cdot (rpm)+17.98$	0.947	390	10
7.5	3	10	30	$T=0.010 \cdot (rpm)+12.07$	0.485	260	5
7.5	3	20	30	$T=0.164 \cdot (rpm)+18.14$	0.927	390	11
7.5	1	15	30	$T=0.611 \cdot (rpm)+19.25$	0.992	400	45
7.5	5	15	30	$T=0.058 \cdot (rpm)+8.96$	0.905	200	5

The overall trends are more clearly quantifiable when the yield stress and viscosity are back calculated and related to the conditioning parameters, including FIR , FER , and c_f , as shown in Figure 5.25, Figure 5.26, and Figure 5.27, respectively. It is concluded that both yield stress and viscosity decrease with differentiable magnitudes as FIR increases, as FER decreases, and as c_f increases. This verifies the capability and sensitivity of the new rheology measurement system in establishing the relationships between soil rheological parameters and foam conditioning parameters for foam conditioned CSM sand. In the future, rheology of more conditioned soils with densified intervals of soil conditioning parameters can be measured in similar ways. The existing relationships for foam conditioned CSM sand presented herein will work as prototypes for establishing the relationships between soil rheological parameters and foam conditioning parameters of these soils in a more statistical and quantifiable way. In the end, a database of rheology of conditioned soil as functions of soil conditioning parameters can be established for EPB tunneling applications.

Compared with the testing results of the CSM sand at $w=7.5\%$ without foam, as shown in Figure 5.20 and Figure 5.21, the corresponding yield stress and viscosity of the foam conditioned sand decrease for more than an order of magnitude. That is a decrease of yield stress from 4,200 Pa to the range of 120 to 400 Pa, and a reduction of viscosity from 170 Pa·s to the range of 5 to 15 Pa·s, with one exception at $w=7.5\%$, $c_f=1\%$, $FER=15$, and $FIR=30\%$. This is partially due to the fact that this c_f value lies beyond the recommended product dosage by the manufacturer (BASF, 2018), which was evidenced by inconsistent bubble sizes during foam generation. This condition was tested merely for the purpose of studying the effect of c_f . In practice, it is strongly recommended that c_f should be controlled within the chemical supplier's recommended range.

Slump tests were conducted before the conditioned samples were charged into the chamber for rheology testing. The results are shown in Figure 5.28, Figure 5.29, and Figure 5.30. It is concluded that slump test parameters, i.e., vertical slump and lateral spread, correlate with soil conditioning parameters and yield stress, and consequently, can be used as indicators for assessing the flowability of conditioned soil. However, yield stress and viscosity are considered more advantageous because they are more physically sound, more capable of assessing rheology during material motion, as well as more suitable as CFD model inputs to simulate the EPB machine response.

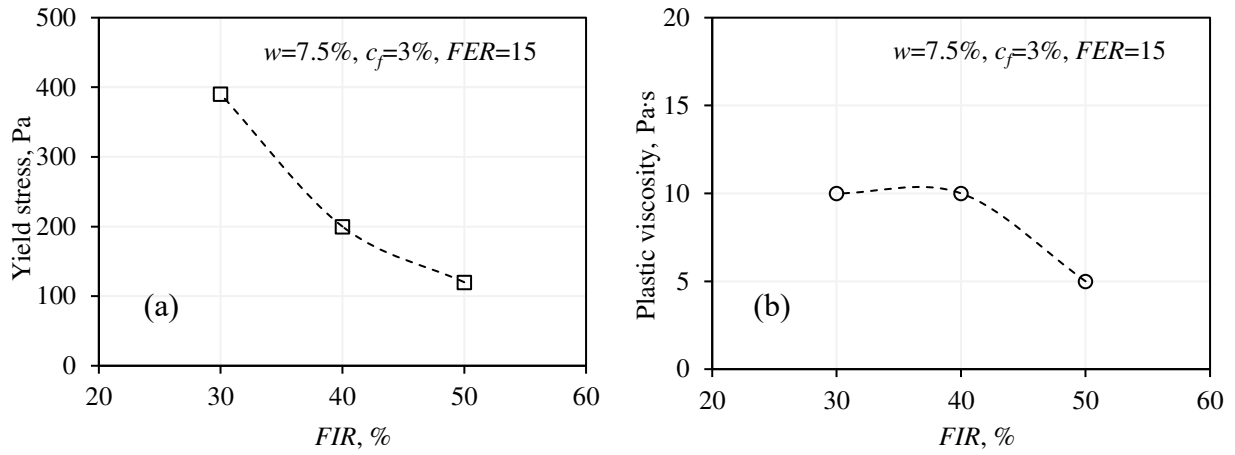


Figure 5.25 Effect of FIR on soil rheology parameters: (a) yield stress; and (b) viscosity.

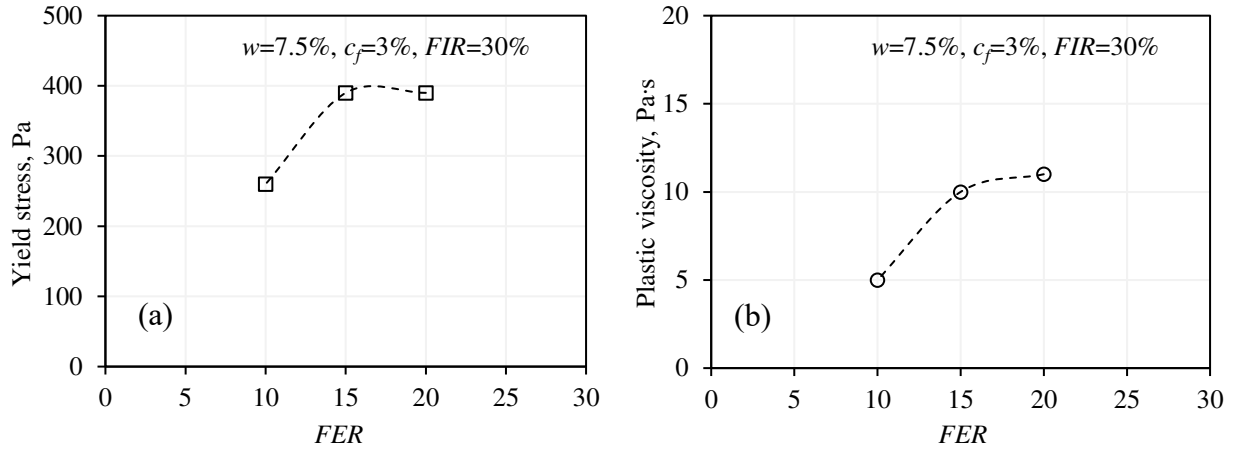


Figure 5.26 Effect of FER on soil rheology parameters: (a) yield stress; and (b) viscosity.

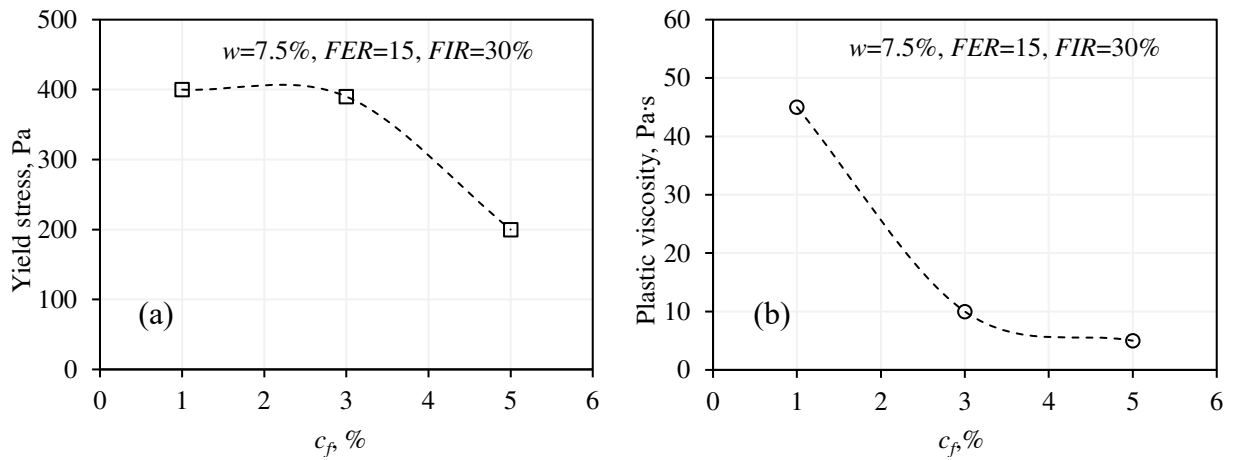


Figure 5.27 Effect of c_f on soil rheology parameters: (a) yield stress; and (b) viscosity.

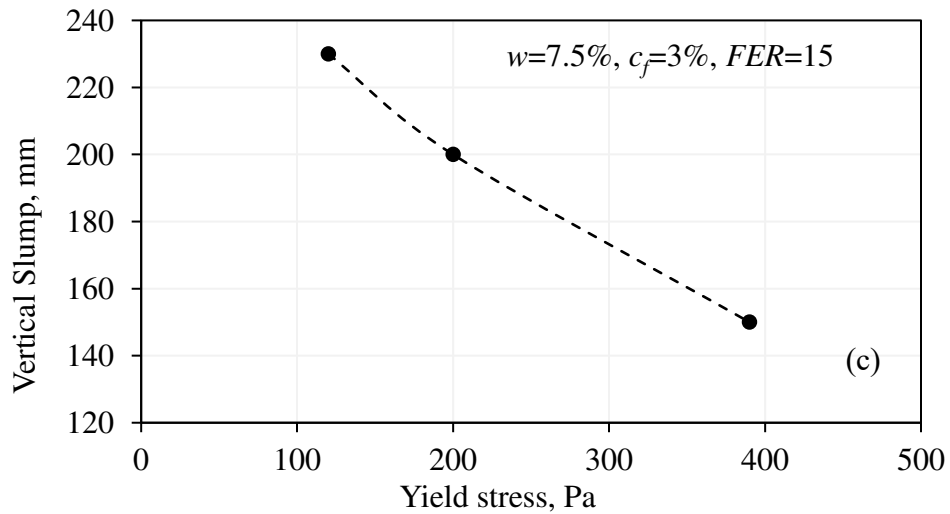
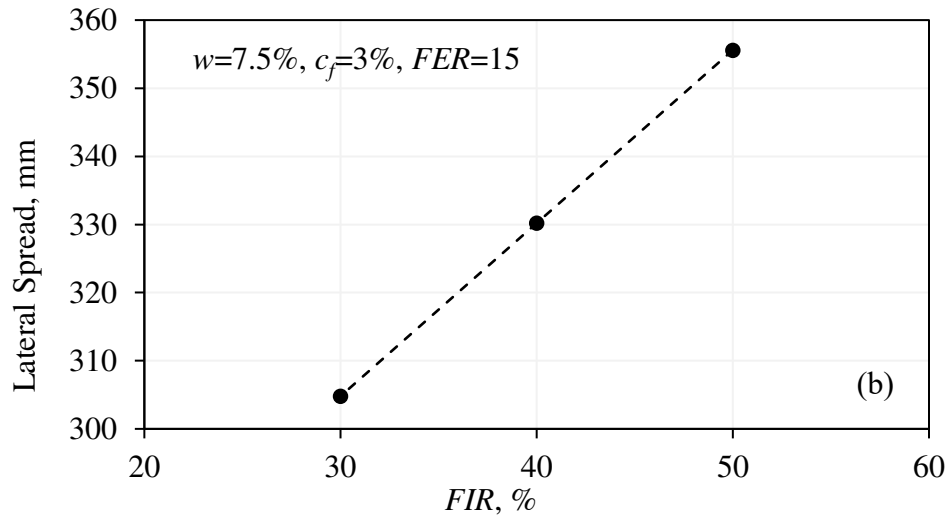
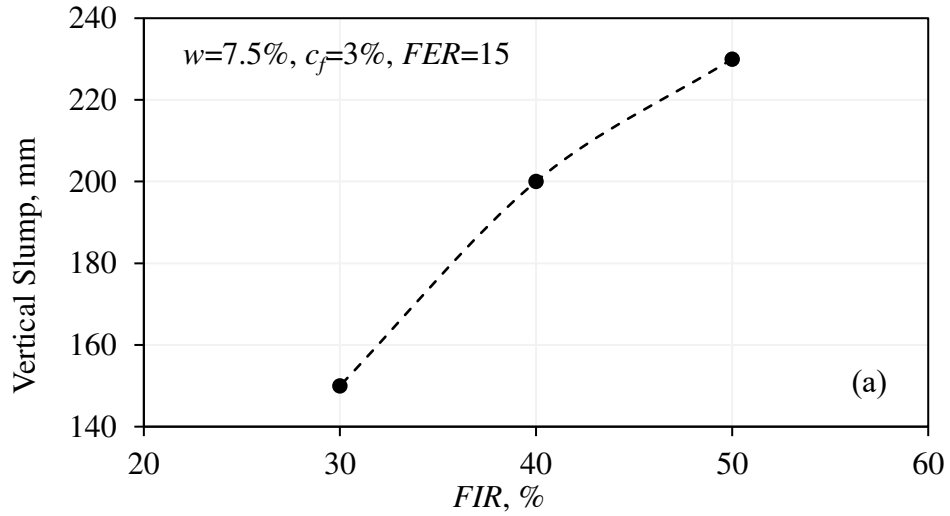


Figure 5.28 Relationships among *FIR*, yield stress, and slump test results: (a) vertical slump vs. *FIR*; (b) lateral spread vs. *FIR*; and (c) vertical slump vs. yield stress.

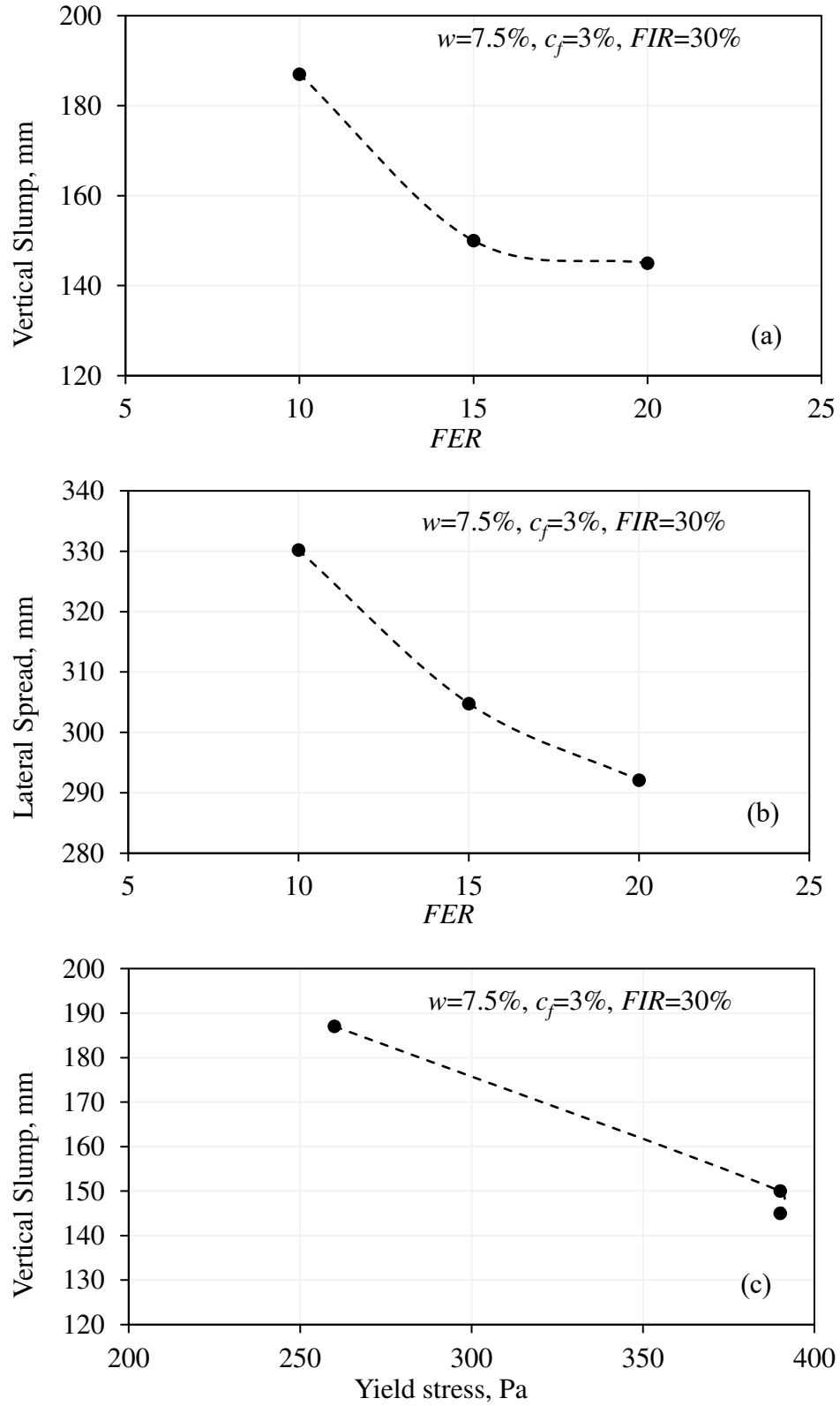


Figure 5.29 Relationships among FER , yield stress, and slump test results: (a) vertical slump vs. FER ; (b) lateral spread vs. FER ; and (c) vertical slump vs. yield stress.

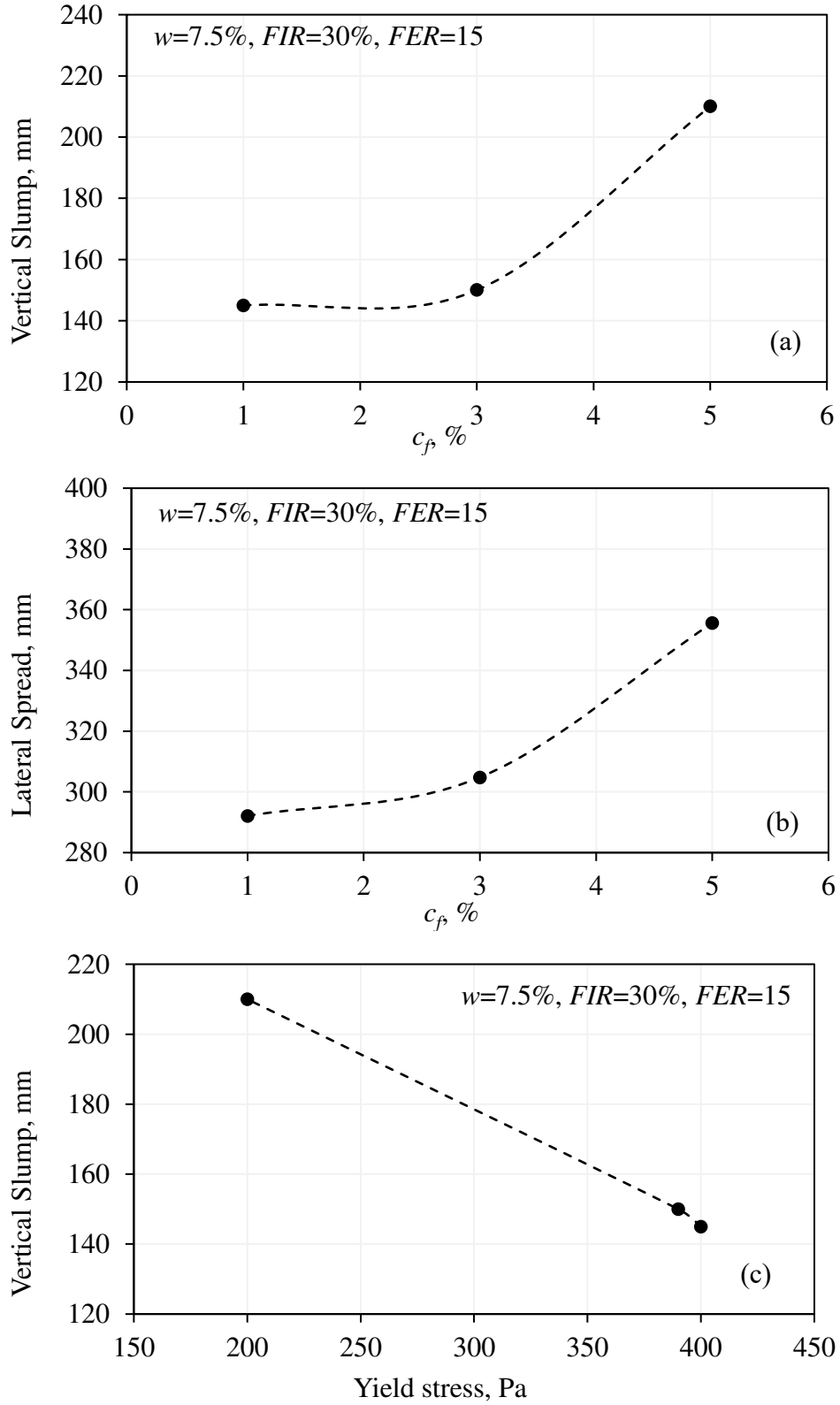


Figure 5.30 Relationships among c_f , yield stress and slump test results: (a) vertical slump vs. c_f ; (b) lateral spread vs. c_f ; and (c) vertical slump vs. yield stress.

5.6.7 Effect of passing of time on torque response

Foam shows signs of degradation over time and the structure of conditioned soil appears to be sensitive to time (Wu 2018). This ultimately influences the engineering properties and behaviors of foam conditioned soil, including yield stress and viscosity. To assure that the tests were within the acceptable time frame and valid, the seven foam conditioned soils were repeatedly tested at three or four different times at atmospheric chamber pressure. Experimental results of four of the representative samples are shown in Figure 5.31. Note that the testing time mentioned in these graphs mean the elapsed time after foam generation and was rigorously recorded to be within ± 2 min error. From these graphs it is observed that the torque values more or less overlapped for those measurements within 2 h, while starting to have measurable increase between 2 h and 5 h. The torque values then increased significantly after 24 h of foam generation. This finding suggests that the foam conditioned soil sustained its rheological behavior for sufficient amount of time, and consequently, allowed for the testing window to be extended for testing different impacting factors with the same batch of conditioned soil.

5.6.8 Effect of ambient pressure on torque response

Face pressure during EPB tunneling usually varies to provide required face support at different locations of the tunnel alignment. The transmitted pressure on the conditioned muck in the cutterhead chamber and screw conveyor acts as total stress that is shared by the soil grains and the pore liquid and foam bubbles. Understanding the overall behavior of this multiphase media is complex and requires unsaturated soil mechanics theory to quantify such a system due to a combination of factors such as geology, advance rate, and machine dimensions. There are also times when compressed air is applied at the face to carry out hyperbaric interventions to inspect, maintenance, and replace cutting tools. During these occasions, the engineering responses of the conditioned muck are expected to differ from those under atmospheric conditions (Meng et al., 2011; Wu, 2018).

Preliminary effort has been made to investigate the impact of elevated pressure on the rheological response of conditioned soil. The chamber pressure was elevated to 150 kPa and 300 kPa and torque vs. rotational speed data were measured. Figure 5.32 shows the torque vs. rotational speed responses of four representative conditioned soils at different chamber pressures. It is demonstrated that torque generally increases as the chamber pressure increases, while the threshold pressure of such an evident increase differentiates for different batch of conditioned soil. Note that

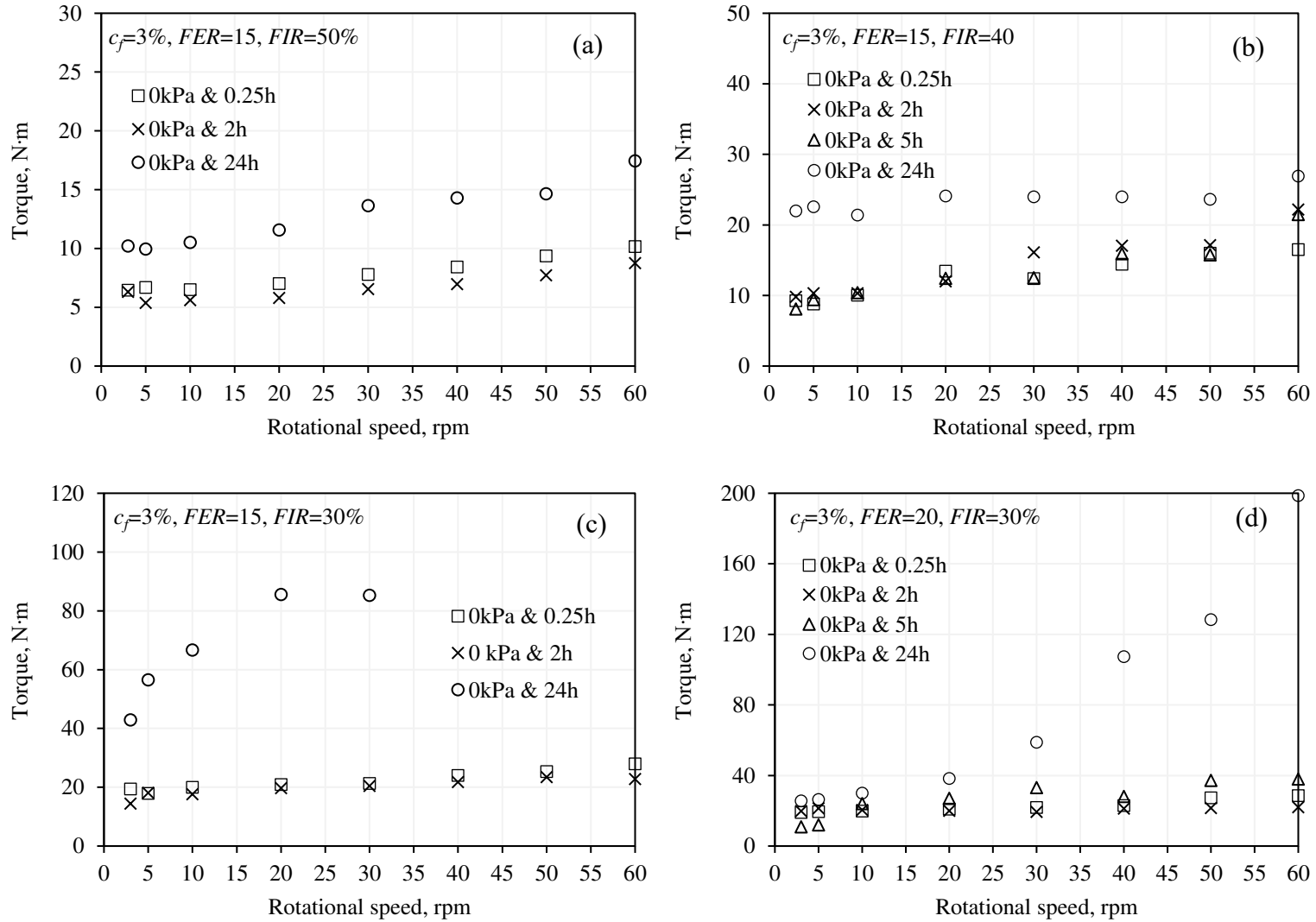


Figure 5.31 Measured torque vs. rotational speed relationships for foam conditioned CSM sand at atmospheric pressure at different elapse of time: (a) $c_f=3\%$, $FER=15$, $FIR=50\%$; (b) $c_f=3\%$, $FER=15$, $FIR=40\%$; (c) $c_f=3\%$, $FER=15$, $FIR=30\%$; and (d) $c_f=3\%$, $FER=20$, $FIR=30\%$.

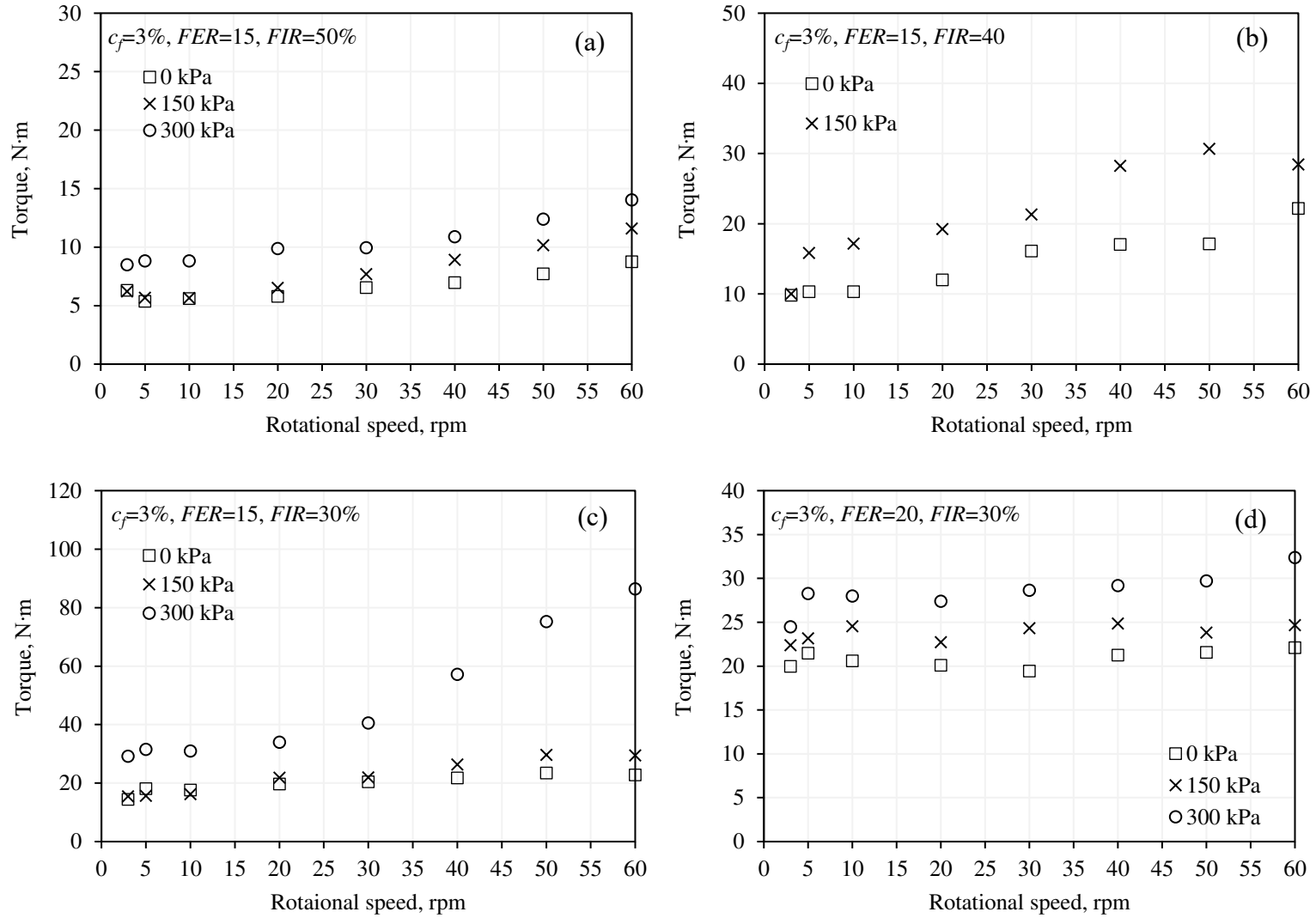


Figure 5.32 Measured torque vs. rotational speed relationships for foam conditioned CSM sand at different chamber pressures: (a) $c_f=3\%$, $FER=15$, $FIR=50\%$; (b) $c_f=3\%$, $FER=15$, $FIR=40\%$; (c) $c_f=3\%$, $FER=15$, $FIR=30\%$; and (d) $c_f=3\%$, $FER=20$, $FIR=30\%$.

the applied chamber pressure was directly connected with the pores of the conditioned soils and should be viewed as pore pressure. Therefore, the increase in torque is expected to be resulted from the decrease of void ratio due to bubble shrinking and collapse, and consequently, densification of the soil structure. However, to simulate the real EPB chamber pressure, the apparatus needs to be modified to apply total stress on the conditioned soil which will be explored in future studies.

5.7 Discussions

The new rheology evaluation system shows its potential to be used for measurement of soil rheology in various working conditions. The auger with a diameter of 296 mm has been tested in various soil and machine operational conditions and the effects of various geotechnical and soil conditioning factors have been investigated. The results indicate that the proposed method to measure and quantify rheology of conditioned soil is greatly improved by using optimized propeller configuration. A set of prototype relationships between soil rheology and soil conditioning parameters of the soil has been established. However, there are still challenges to be addressed in the near future to advance the method towards ultimate EPB tunneling applications.

One of the remaining challenges is to obtain the rheology of foam conditioned clay or clayey soil. As discussed in the previous chapter and the literature (Hu and Rostami 2020), studies on the engineering behaviors of foam conditioned clay samples with similar volume as presented in this study are limited because of the difficulties of uniform mixing of clay with foam. The authors have conducted some preliminary mixing trials with regard to mixing sticky clay with water and foam for testing in the presented rheometer in this study. The tools used for mixing were the concrete mixer with 0.11 m³ tank volume mentioned in section 4.2, a dough mixer with 0.06 m³ bowl volume, a hammer drill mixing tool, a tiller mixer, and a ToughTek CM-40 continuous mixer (Graco 2019). None of these systems provided a satisfactory mix within five minutes (to avoid foam degradation). The details of this series of mixing tests will be presented in the following chapter. As such, more mixing methods are under consideration.

Meanwhile, more rheology testing of different types of soils at various water content and foam conditioning settings need to be conducted. This includes not only obtaining new types of soils for rheology testing but also extending the existing ranges of foam conditioning parameter to investigate the rheological boundary, as well as repeating experiments of existing conditions to attribute statistical meaning to the rheology data. With more and more data and enriched rheology database, the relationships between soil rheology, i.e., yield stress and viscosity, and soil

conditioning settings such as w , c_f , FER , FIR can be further explored. Subsequently, classification of conditioned soils based on soil rheology database is expected to be achieved.

Although the proposed rheology measurement system with the optimized auger geometry is analogous to the screw conveyor configuration in a real EPB machine, the measurement system does not include continuous muck feeding attachment. This gap, however, can be bridged by using a surcharge loading component on top of the soil in the chamber to apply needed ground loading conditions.

Furthermore, the established relationships between soil rheology and soil conditioning settings should also be cross checked with tunneling monitoring data. Such improved relationships will allow for modeling of material flow in the EPB machines and help for optimization of proper soil conditioning and machine operations for practical applications. As depicted in Figure 5.33, with the input of soil yield stress and viscosity either estimated from the established models based on soil type and anticipated w , c_f , FER , and FIR , or alternatively measured by the presented measurement system, the CFD modeling software can determine the required torque on the cutterhead and screw conveyor. It can also monitor pressure and flow velocity of the muck at various locations in the machine, and contact stress between the muck and machine components. This allows for predicting EPB machine performance in different ground conditions and for optimization of soil conditioning. While being used in conjunction with field monitoring data, the presented method can further optimize machine operation and provide real-time guidance to the operators for soil conditioning.

5.8 Conclusions

EPB TBMs are the dominant machines in soft-ground tunneling. To optimize EPB machine operation where the excavated muck works as the supporting medium, the muck needs to be properly conditioned with foam or other additives. To optimize soil conditioning practice and achieve better machine performance, soil rheology of the excavated muck should be well understood. With the soil rheology as functions of soil conditioning parameters, the flow of muck in the EPB machine cutterhead and screw conveyor together with machine responses such as torque and stress can be predicted.

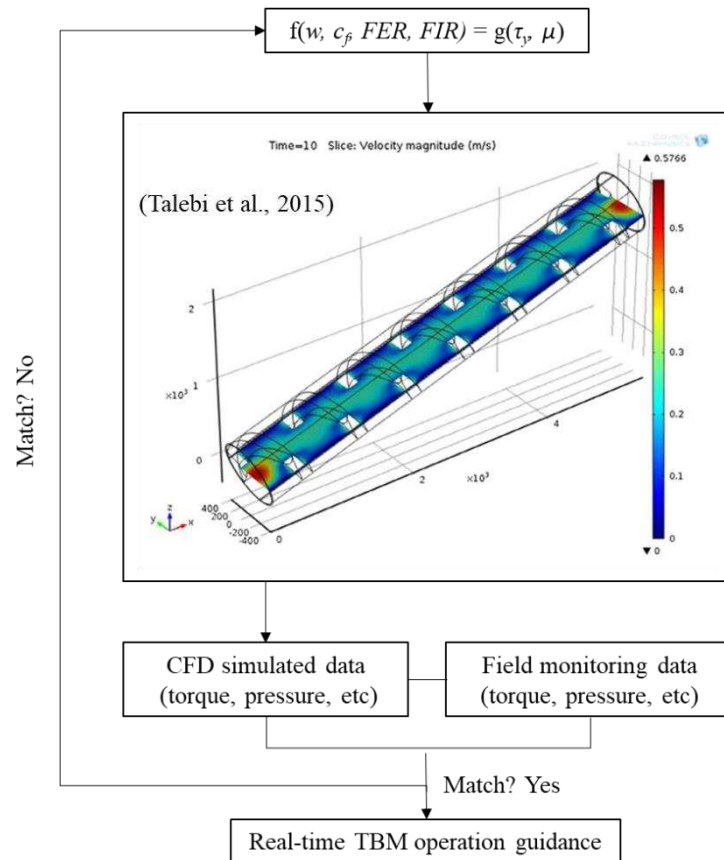


Figure 5.33 Proposed application of rheological models as functions of soil conditioning.

Despite its importance, characterization of rheology of conditioned soil for EPB tunneling applications is still not as advanced as it should be. This chapter adopted the proven concept of rheology measurement by combining lab experimental work and CFD simulation and introduced a new auger propeller for soil rheology testing. Correspondingly, a measurement protocol for soil was introduced. Seven foam conditioned soil samples were tested and the rheological properties were quantified. The relationships between soil rheology, i.e., yield stress and viscosity, and soil conditioning parameters such as w , c_f , FER , and FIR were explored. In addition, the impacts of passing of time and ambient pressure on rheology measurement were investigated.

The rheology measurement of foam conditioned clay is still a challenge due to mixing difficulties. In the future, efforts need to be made to measure the rheology of more types of soils in different soil conditioning and machine operational parameters. The database of the rheology of conditioned soils as functions of soil conditioning parameters in the context of EPB tunneling can be established and used for soil conditioning optimization and machine performance prediction.

CHAPTER 6

ADVANCING STUDY OF RHEOLOGY OF CONDITIONED CLAY FOR APPLICATION IN EPB TBM TUNNELING

6.1 Introduction

So far, the rheology studies in this thesis primarily used granular soils as the testing materials. Only dry clay powder was tested to examine the effect of soil type on rheology, as shown in Chapter 5. Neither wet clay nor foam conditioned clay was included in the previously shown studies due to several challenges as follows.

6.1.1 Challenges for testing rheology of conditioned clay

One of the biggest challenges in the studies of conditioned clay is to prepare homogeneous foam conditioned clay samples. Note that “homogeneous” in the context of this thesis is related to a problem’s geometric scale. While fist-sized clay lumps after foam conditioning are often seen and acceptable in some EPB tunneling projects where the machine diameters could be several meters, they are not considered homogeneous mixing products for lab scale research purposes such as using the newly developed rheometer (D. Peila et al. 2016). To date, most of soil conditioning studies have been conducted on sandy materials due to the readiness of mixing sand with foaming agents. On the contrary, studies on conditioned clay were limited because of the difficulties of uniform mixing of clay with foam. This difficulty further resulted in the use of small-scale testing setups for the limited studies on conditioned clay where dry clay powder was used to mix with water and foam (Zumsteg and Puzrin, 2012; Zumsteg et al., 2013; Hollmann and Thewes, 2013; Thewes and Hollmann, 2016). In EPB tunneling in clayey ground, however, clay clumps and chips as well as gravels are commonly seen in the excavated muck (D. Peila et al. 2016). Some efforts were made to develop large-scale laboratory devices to study conditioned clay (Merritt and Mair, 2006; Merritt and Mair, 2008; Peila et al., 2016). However, whether the conditioned clay samples in the literatures reached satisfactory mixing conditions were not clearly reported.

In addition to the lack of effective mixing protocol for foam and clay, there is limited study on direct measurement of rheological parameters of conditioned clay. It has been shown in the previous chapters that the existing studies focused on testing rheology of granular soils (Meng et al., 2011; Galli 2016; Galli and Thewes 2016; Freimann et al., 2017; Djeran-Maigre et al., 2018; Hu and Rostami 2020).

Rheology is the major perspective and direct measurement to study the flowability and viscosity of clay. In addition, two other aspects also reflect the flowability and viscosity of the clay namely clay stickiness and clay clogging. While the studies on the rheology characterization of conditioned clay are limited, studies of clay stickiness and clay clogging are abundant. One of the pioneering work in this area is the study on the mechanisms causing stickiness and clogging of fine-grained soil and clay which was investigated in details by Thewes (1999). This includes adhering, bridging, cohering, and no dissolving. The subsequent experimental work on clay stickiness and clay clogging was conducted by a few research groups in terms of static and dynamic adhesion test (Peila et al., 2016), cone pull-out test (Feinendegen et al., 2011), Empirical Stickiness Ratio test (Zumsteg et al., 2013), improved Empirical Stickiness Ratio test with additional ATUR device (Oliveira 2018), vane shear test (Messerklinger et al., 2011; Zumsteg et al., 2012), and consistency diagram (Hollmann and Thewes 2013; Thewes and Hollmann 2016). Among them, the consistency diagram approach has gained more popularity in the industry practice, mainly the application in the clay clogging potential evaluation in GBRs. The problem with the current consistency diagram is that it is conducted under atmospheric pressure condition while how the clogging behaviors would change under elevated face pressure in different soil types is unknown.

6.1.2 Objectives and materials

In this chapter, some investigations to advance rheology testing of conditioned clay and clay clogging evaluation will be presented to address some of the above-mentioned challenges.

The fat clay used in this study, namely the blue/gray clay from Denver metropolitan area, is a natural soil and has high plasticity, as shown in Table 6.1. Particle size analyses by both sieving and hydrometer methods show that fine particles smaller than 0.075 mm dominate 80% of the clay, while randomly scattered gravels occupy less than 10% of the soil sample. The mineralogy of the clay was also analyzed via XRD, as shown in Table 5.1, indicating a total of 34% of the clay are water-sensitive minerals including smectite, illite and kaolinite. These minerals result in the apparent strong stickiness and clogging of the clay. Note that XRD is optimally suited for mineral identification and is not a best option for quantifying the mineral content of the sample. But it offers a reasonable approximation in terms of percentage of constituent minerals. The accuracy of estimated mineral content by XRD depends on many factors including grain size, preferred grain orientation, solid solution, order-disorder, etc., thus the estimates provided herein should be considered semi-quantitative.

The foaming conditioner used in this study was the BASF MasterRoc ACP 127. It is a liquid polymer especially designed for conditioning clayey soils with high clogging and adhesion potential. In a real TBM tunneling project, it is used as aqueous solution with 3% to 5% concentration. The typical *FER* ranges from 8 to 20 and the typical *FIR* from 30% to 80%. More technical details can be found in the product data sheet (BASF 2018).

Table 6.1 Basic physical properties of Denver clay.

Parameter	Value
Specific gravity, G_s	2.72
Air-dried water content, w (%)	3.9
Air-dried at-rest bulk density, ρ_{dry} ($\text{kg} \cdot \text{m}^{-3}$)	1280
Plastic limit, PL (%)	23
Liquid limit, LL (%)	50
Plastic index, IP	27
USCS	CH

6.2 Methods of preparation of conditioned clay

To advance schemes to prepare homogeneous conditioned clay for rheology testing in the large-scale rheometer, some mixing methods were tested and evaluated. This consists of two phases as follows.

6.2.1 Mixing clay with liquid

Firstly, the likelihood of mixing clay with liquid, i.e., water or foaming solution, was explored. The original particle size varied from crusher-pulverized Denver clay with the particle size distribution shown in Figure 5.5 in Chapter 5 and in Figure 6.1 (a), to clay lumps with the average chunk size of 5 cm, as shown in Figure 6.1 (b). The original water content of the clay ranged from air-dried state (around $w=4\%$) to the plastic limit state ($w=23\%$).

The mixing tools used include the concrete mixer with 0.11 m^3 container volume, a dough mixer with 0.06 m^3 bowl volume, and a hand-held drill mixing tool, as shown in Figure 6.2. The results show that when the original clay is air-dried, it is critical to reduce the particle size and avoid large clay lumps to reach an acceptable mixing. For instance, the concrete mixer is unable to mix water and dry clay lumps. The degree of mixing clay lumps and water was increased using the dough mixer or the hand-held drill mixing tool while there were still clay lumps existing in the

mixture. When the original water content is close to the plastic limit, the effect of the size of clay lump is less severe because the interparticle physicochemical bond is significantly lower than that at the air-dried water content (Lu et al. 2006). For standard practice in the future, it is recommended that the clay should be oven dried or air dried followed by pulverization. Depending on the availability of the beater in different labs, either a large size dough mixer or a hand-held drill mixing tool can be used for the mixing task. A possible benefit of this tool is that no time restraint is imposed, and hence, it is possible to mix clay with anti-clogging foaming solution.



Figure 6.1 Denver clay before mixing: (a) pulverized clay powder; and (b) clay lumps.



Figure 6.2 Tools for mixing Denver clay and liquid: (a) a concrete mixer; (b) a dough mixer; and (c) a hammer drill mixing tool.

6.2.2 Mixing clay with foam

Unlike mixing clay with liquid, the potential method for mixing clay with foam must not only provide satisfactory homogeneity of the mixture, but also finish the process in a quick fashion. This is due to the intrinsic time-sensitive feature of the foam (Wu 2018). The main problem is the difference in density of soil solid particles and foam. Foam is much lighter than even water and has the tendency to move above the mix. In this context, smaller density contrast of soil and water and the surface tension of the water are the reasons for higher success in mixing of soil with water.

A total of six mixing methods were tested. This includes the same concrete mixer for mixing clay and liquid with additional lid to prevent mixture splash, the drill mixing tool used for mixing clay and liquid, a concrete mixer with different inner blade configuration, a flat beater mixing using the large-scale rheometer power drive, a tiller mixer, and a Graco CM-40 continuous mixer, as shown in Figure 6.3.

The mixing results show that none of the tools generated satisfactory homogeneity of the foam and clay mixture, i.e., notable amount of foam was observed to stand separately from the clay at different mixing durations. Unlike mixing sand and foam where the foam is capable of penetrating into the sand void, the permeability of clay is orders of magnitude lower (Lu and Likos 2004). Together with the drastic density contrast between clay and foam, the foam would always come to float atop of the clay. Because of these two reasons, extending the mixing time did not improve degree of mixing. On the contrary, the foam showed the tendency to collapse in this mixing process with the tested mixing methods.

In EPB tunneling practice in clayey ground, homogeneous mixing between clay and foam may not be rigorously required to reach millimeter level as long as the muck is able to provide face pressure and does not plugged the machine. However, the lab studies on foam conditioned clay do require an acceptable homogeneity of the mixture to facilitate examination of the impact of conditioning parameters on the behaviors of the mix. More studies are needed in the future before advancing to test the rheology of foam conditioned clay.

6.3 Evaluation of rheology of clay and sand mixture

Although homogeneous clay and foam mixture for the large-scale rheology testing has not been generated, Denver clay was mixed with CSM sand to achieve acceptable flowability and the corresponding rheological properties were measured.



Figure 6.3 Tools for mixing Denver clay and foam: (a) and (b) concrete mixers; (c) a hammer drill mixing tool; (d) a flat beater with the rheometer power; (e) a tiller mixer; (f) a continuous mixer; and (g) clogged clay in the continuous mixer.

Denver clay and CSM sand at air-dried condition were mixed at different weight ratio before adding certain weight of water to adjust the mixture to designated water content conditions, as shown in Table 6.2. The gaps of water content between dry and 20% for clay vs. sand ratio of 1:2, and between dry and 30% for clay vs. sand ratio of 2:1, are due to the fact that the mixtures in these in-between water content conditions were too sticky to be tested using the proposed rheometer. The experimental torque vs. rotational speed results are shown in Figure 6.4. As comparison, the results from dry Denver clay and dry CSM sand are also included. Back calculation using CFD modeling was subsequently conducted to obtain the yield stress and viscosity of each soil mixture, as shown in Table 6.2. For the mixture with clay vs. sand ratio of 1:2, the yield stress is 1,014 Pa at water content of 20% before falling to 100 Pa at water content of 30%. Based on past experience (Talebi et al. 2015) and on-site observations, as shown in Figure 6.5, it is suggested that the rheology of the mixture reaches the ideal situation when the water content is close to 30%. For the mixture with clay vs. sand ratio of 2:1, the yield stress is 1,208 Pa at water content of 30% before dropping to 290 Pa at water content of 40%. Observational comparison, as shown in Figure 6.6, also demonstrates that the rheology at water content around 40% is deemed optimal for soil at higher clay content in this study. As such, the higher clay vs. sand ratio, the higher water content is required to achieve the optimal rheological response of the mixture.

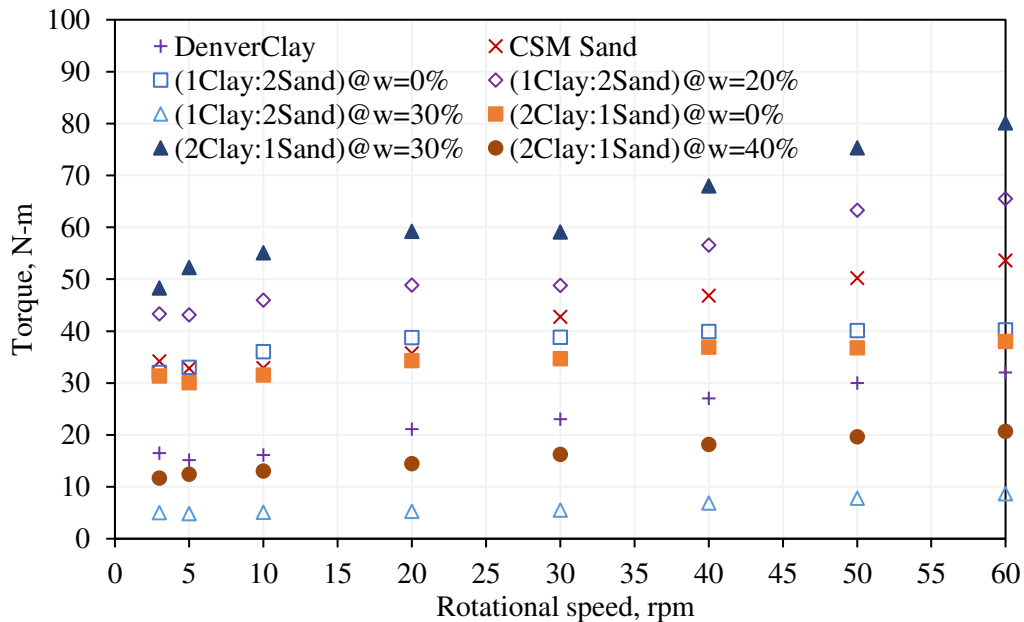


Figure 6.4 Torque vs. rotational speed relationships for different mixtures of Denver clay and CSM sand.

Table 6.2 Back calculation of rheological parameters of different soil conditions.

Soil	w (%)	Clay vs. sand ratio	$T \sim rpm$	R^2	τ_y (Pa)	μ_0 (Pa·s)
Pure Clay	4	1:0	$T=0.304 \cdot (rpm)+14.30$	0.983	300	30
Pure Sand	0	0:1	$T=0.384 \cdot (rpm)+30.66$	0.967	750	30
Mixture	0	1:2	$T=0.135 \cdot (rpm)+33.67$	0.774	845	15
Mixture	20	1:2	$T=0.402 \cdot (rpm)+40.95$	0.953	1014	34
Mixture	30	1:2	$T=0.065 \cdot (rpm)+4.35$	0.920	100	10
Mixture	0	2:1	$T=0.133 \cdot (rpm)+30.56$	0.928	770	10
Mixture	30	2:1	$T=0.518 \cdot (rpm)+48.05$	0.964	1208	40
Mixture	40	2:1	$T=0.160 \cdot (rpm)+11.43$	0.995	290	13

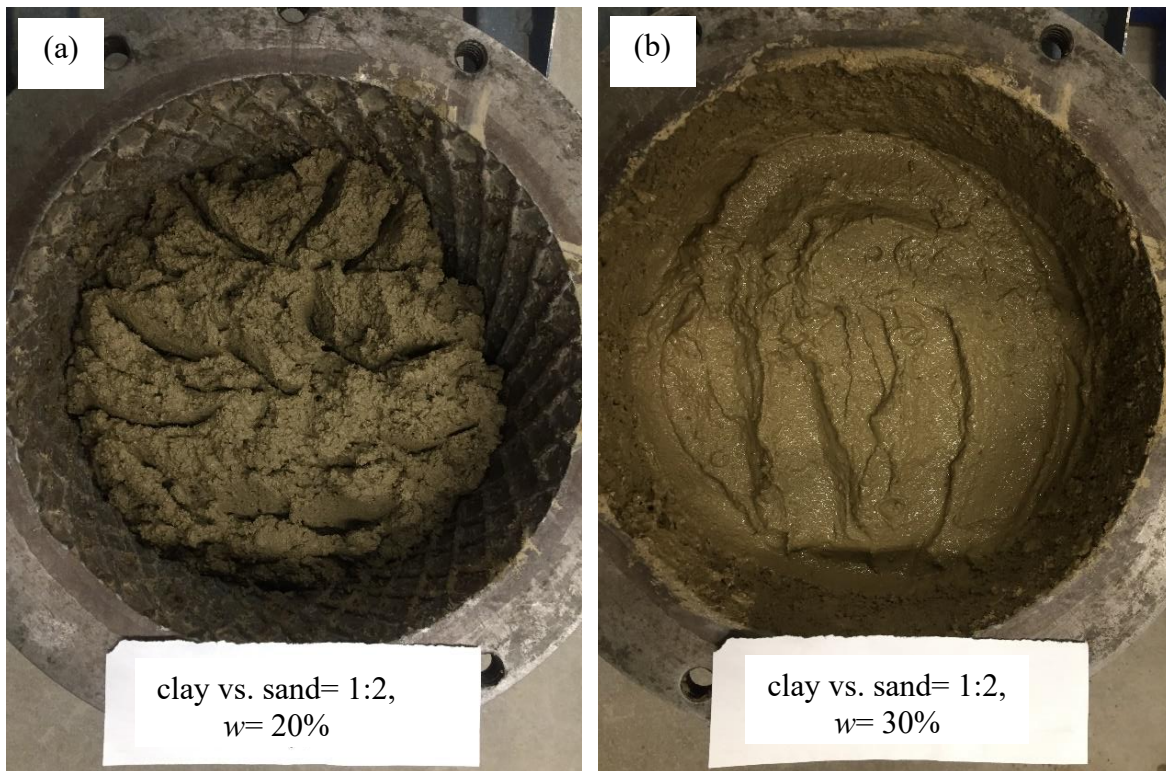


Figure 6.5 Comparison of flow capability for clay vs. sand ratio of 1:2 between: (a) $w=20\%$; and (b) $w=30\%$.

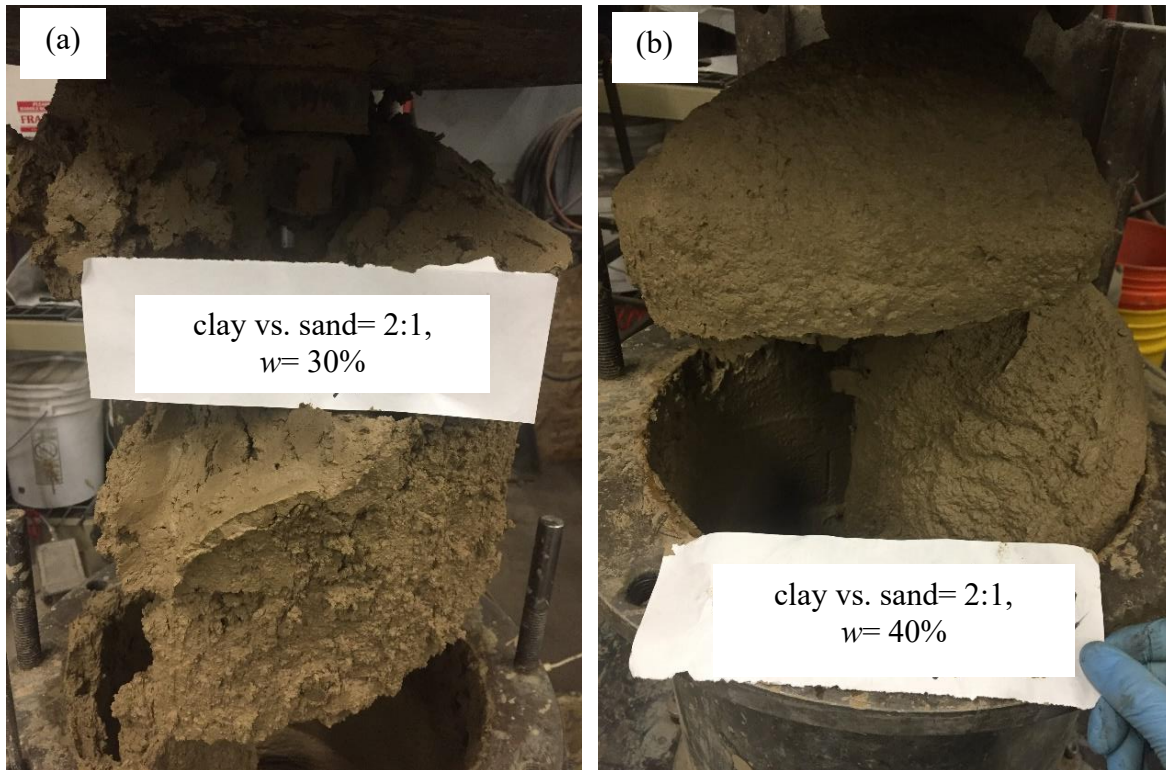


Figure 6.6 Comparison of flow capability for clay vs. sand ratio of 2:1 between: (a) $w=30\%$; and (b) $w=40\%$.

6.4 Evaluation of clay clogging potential

6.4.1 Consistency Index approach

The clay clogging potential was first evaluated via the Consistency Index approach proposed by Hollmann and Thewes (2013), as shown in Figure 6.7. The key concepts and boundaries in this approach include natural water content (w_n), plastic limit (w_P), liquid limit (w_L), plasticity index (I_P) and consistency index (I_C). I_P and I_C are defined by the following equations:

$$I_P = \omega_L - \omega_P \quad (6.1)$$

$$I_C = (\omega_L - \omega_n)/I_P \quad (6.2)$$

All of these concepts are associated with water content, demonstrating the dominating impact of water content on clay clogging. As the water content of Denver clay increased from the plastic limit of 23% to the liquid limit of 50%, as shown in Figure 6.7, the clogging potential initially increased, and then reached the peak at a water content level between 30% and 35%, followed by a reduction afterward. From pure anti-clogging perspective, the optimal water content is above 35%. The muck at this stage, however, is too liquid and does not live up to other muck requirements such as face pressure control. A common practice to balance anti-clogging and other

muck requirements is to control the water content to the range which falls within “strong clogging” category and add anti-clay agent or foam to control the other properties of the mix.

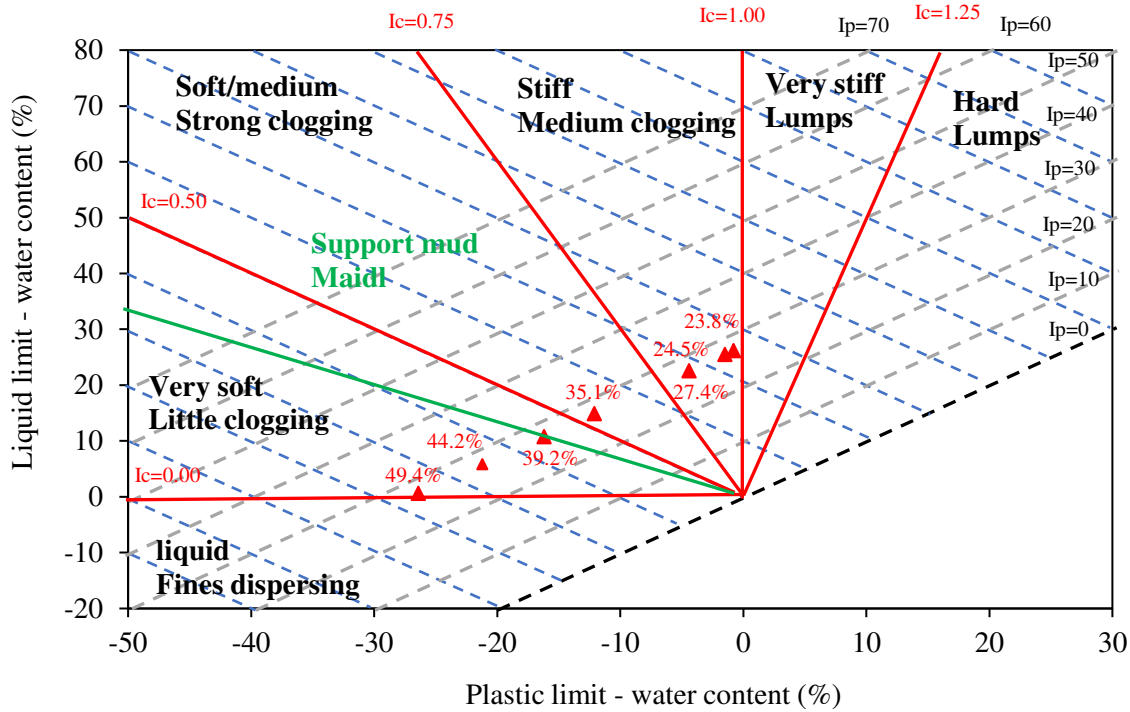


Figure 6.7 Evaluation of clogging potential of Denver clay based on the Consistency Index approach for EPB supporting mud (Hollmann and Thewes, 2013). Data from this study are overlaid in the graph as triangular markers.

6.4.2 Empirical Stickiness Ratio approach

The clogging potential of Denver clay was also assessed via the Empirical Stickiness Ratio (λ) approach proposed by Zumsteg and Puzrin (2012). It is based on the mixing test using dough mixers and defined by the following equation:

$$\lambda = G_{MT}/G_{TOT} \quad (6.3)$$

In this equation, G_{MT} is the soil sticking to the mixing tool and G_{TOT} is the total weight of soil in the mixer. The bigger the ratio, the higher the clogging potential is. Zumsteg and Puzrin (2012) did not specify the size of the mixing tool, however, G_{MT} is expected to be dependent on the tool size. As an empirical method, the concept still owns merit as a semi-quantitative approach of stickiness evaluation. It was found that clay clogging evaluation by the Empirical Stickiness Ratio method had good agreement with that by the Consistency Index approach, while advancing the definition to a quantitative level (Zumsteg et al., 2013). In current study, a KitchenAid mixer

with a volume of 4.5 quart, as shown in Figure 6.8 (a), was used to mix the pulverized clay powders with calculated amount of water to achieve the desired water content condition until a homogeneous state was reached. The mixing time to ensure this satisfactory homogeneity was observed to be within 2 min for preliminary testing. To ensure parallel testing conditions, the standard mixing time thereafter was fixed at 2 min. After mixing, the flat beater was taken out for weight measurement for each water content, as shown in Figure 6.8 (b). The testing results depicting λ versus w relationship, shown in Figure 6.9, echo the results of evaluation of clay clogging potential by the Consistency Index method. Note that the dashed line in the figure is meant to offer readers a probable overall trend of λ with regards to the change of water content. It is shown that two water content thresholds for Denver clay exist, i.e., 20% and 40%. The ratio, λ , is negligible when the water content is lower than 20%, followed by a drastic increase as the water content rises from 20% to 30%. λ remains at a high value as the water content further increases from 30% to 40%. Subsequently, the ratio plunges as the water content keeps increasing towards the liquid limit. That said, it is recommended that EPB operation should avoid running into the problematic region with high Empirical Stickiness Ratio values.

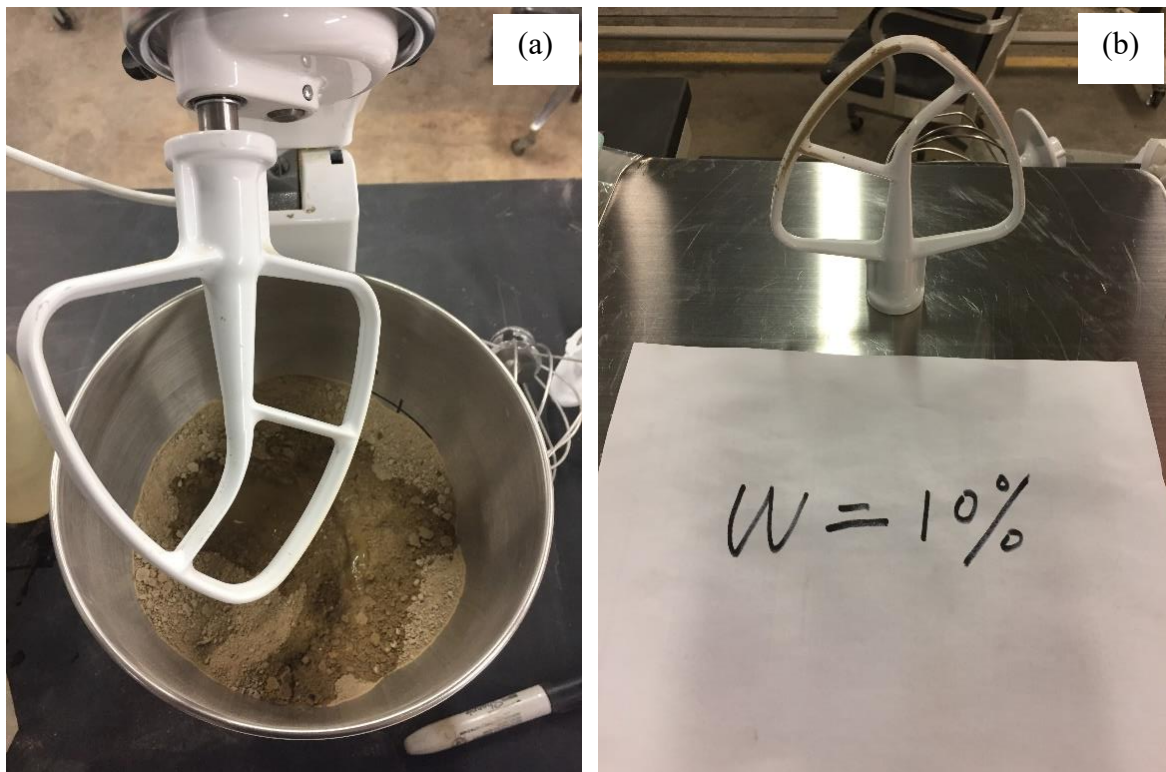


Figure 6.8 Evaluation of clay clogging based on Empirical Stickiness Ratio approach: (a) testing device; and (b) weight measurement.

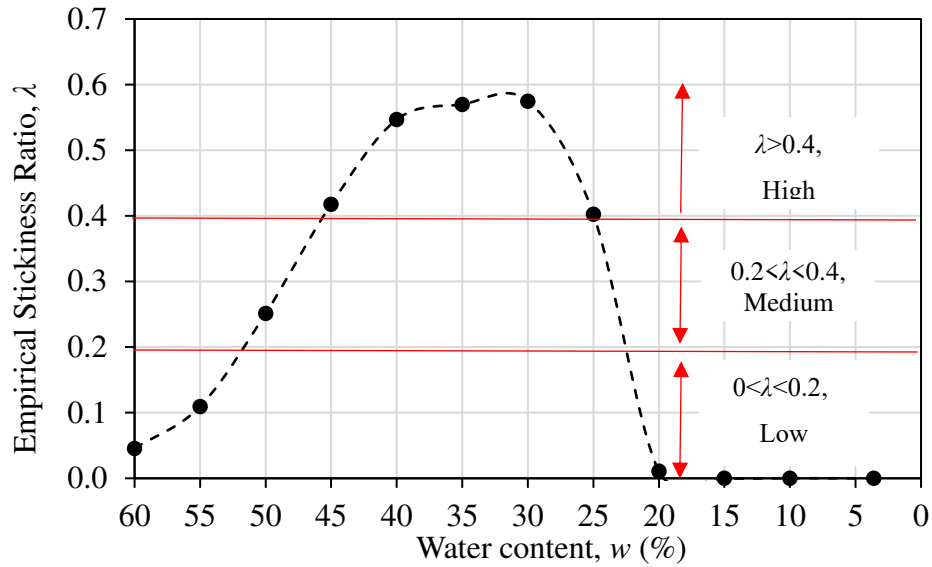


Figure 6.9 Empirical Stickiness Ratio vs. water content curve. The boundaries were suggested by Zumsteg, Plötze, and Puzrin (2013).

To examine how anti-clogging agent can change clogging behavior of clay, Empirical Stickiness Ratio experiments were also conducted on mixtures of foam solution and Denver clay at different c_f . BASF MasterRoc ACP 127 was mixed with water to achieve designated c_f before being poured into dry Denver clay. The mixture was manually mixed to homogeneity before being stirred by the mixer for 2 min. A total of eight tests were carried out with the same ultimate water content of 40%. The λ vs. c_f curve, as shown in Figure 6.10, demonstrates that λ shows no change between 0% and 2% of c_f and stays in the “High” zone. It starts to plunge at $c_f = 2\%$ and reaches the High-Medium and Medium-Low boundaries at $c_f = 4\%$ and 6% , respectively. Because of the extreme difficulties to mix clay and foam, this series of testing reveals that it could be possible to inject only anti-clogging conditioner solution to mitigate the clogging problem in EPB machines.

6.4.3 Proposed evaluation approach using torque as an indicator

Both the Empirical Stickiness Ratio and the Consistency Index methods only consider the water content in the evaluation of clay clogging. The feasibility of these practices is uncertain because in addition to water content, other factors can also influence clogging of the machine such as in situ stress conditions and machine operational parameters. In this study, the impact of water content on clay clogging potential was explored by using the Soil Abrasion Index (SAI) testing machine equipped with the 10 degree pitched propeller with three blades. Evidence of the potential impact from pressure conditions was subsequently investigated.

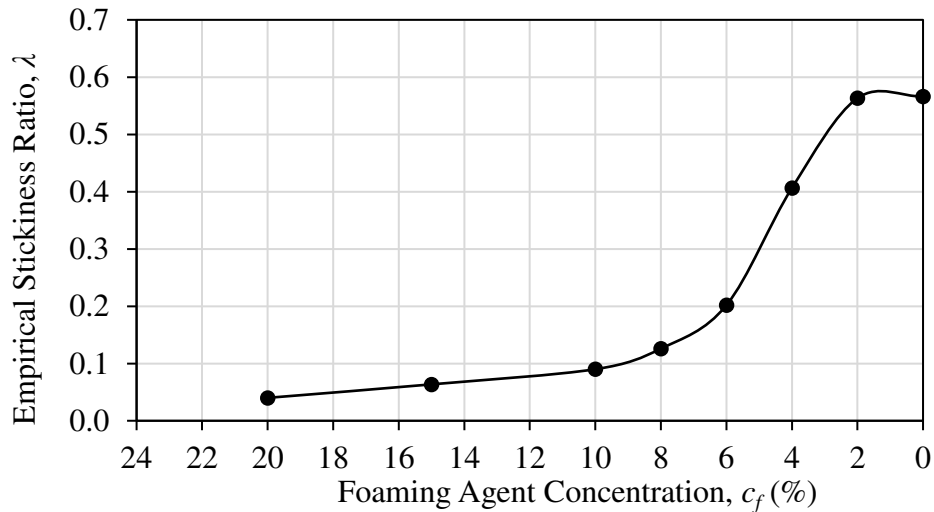


Figure 6.10 Empirical Stickiness Ratio vs. Foaming Agent Concentration curve at $w=40\%$ while mixing Denver clay with conditioner solution.

The drill mixing tool shown in Figure 6.2 (c) was used to prepare the clay and water mixture with designated water content. The homogeneous clay and water mixture was then placed into the SAI testing chamber layer by layer to assure least voids in the chamber. The propeller with 10 deg pitched blades was used to test at the rotational speed of 60 rpm. A total of five SAI tests were conducted for five designated water content conditions. At each water content, the testing was run until a steady torque vs. time curve was obtained.

The maximum torque was obtained for each water content and was plotted against corresponding water content, as shown in Figure 6.11. The curve has a bi-linear feature with $w=27.4\%$ being the transition point between the two linear sections. Starting from the liquid limit state at the right end of the curve, the maximum torque increases very gently from 40 N·m at the liquid limit state to 103 N·m at $w =27.4\%$, and then drastically rises to 555 N·m at $w =23.8\%$, which is the plastic limit state. In EPB machine tunneling, the cutterhead torque can be considered as an indicator for clay clogging. This index system is proven to be suitable based on the SAI testing study, where higher torque means higher clay clogging potential. This idea was further confirmed by observation of the clay structure after testing, as shown in Figure 6.12. As seen in these two pictures, the clay in both scenarios endured compaction due to high contact stress imposed by the propeller with 10 deg pitched blades. The difference is that the plastic yet stiff clay

at $w = 23.8\%$ showed significant compaction which would cause severe clogging issues, while the compaction at $w = 49.4\%$ was low resulting in significantly reduced clogging potential.

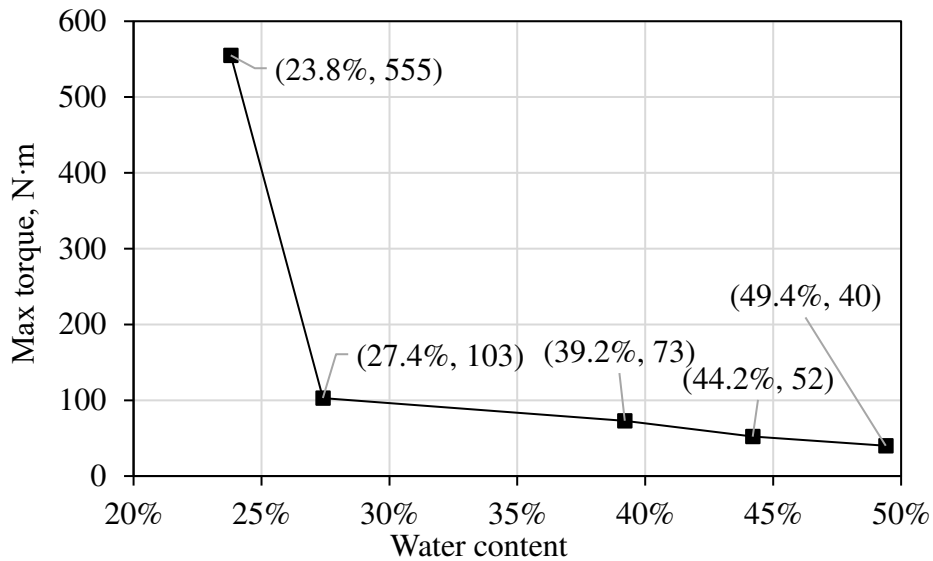


Figure 6.11 Measured maximum torque vs. water content curve for Denver clay using SAI testing machine with 10 deg pitched propeller.

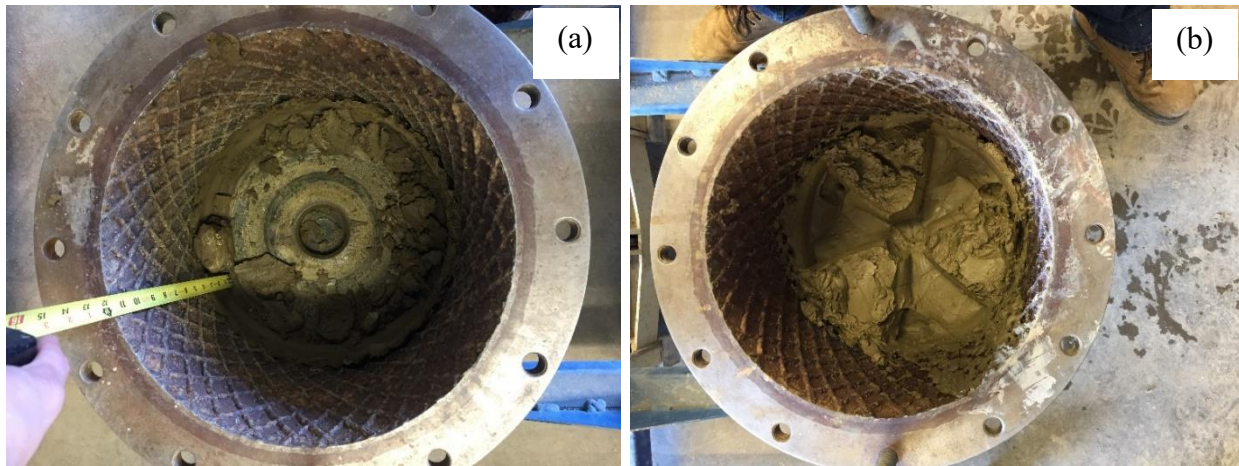


Figure 6.12 Compaction of Denver clay at the end of SAI testing without surcharge loading: (a) significant compaction at $w = 23.8\%$; and (b) slight compaction and signs of plastic deformation at $w = 49.4\%$.

To further prove the necessity of incorporating the effect of pressure into clogging evaluation, three types of experiments were carried out. First, Proctor compaction tests and subsequent uniaxial compressive strength (*UCS*) measurements were conducted, as shown in Figure 6.13(a) and (b). The results are shown in Figure 6.15 and Figure 6.15, respectively. Both results confirm that the clay with close initial loose structure is most susceptible to density and/or strength change when the water content is close to the plastic limit state of the clay, i.e., $w = 23\%$.



Figure 6.13 Compaction and UCS measurement using: (a) Proctor compaction; and (b) Penetrometer.

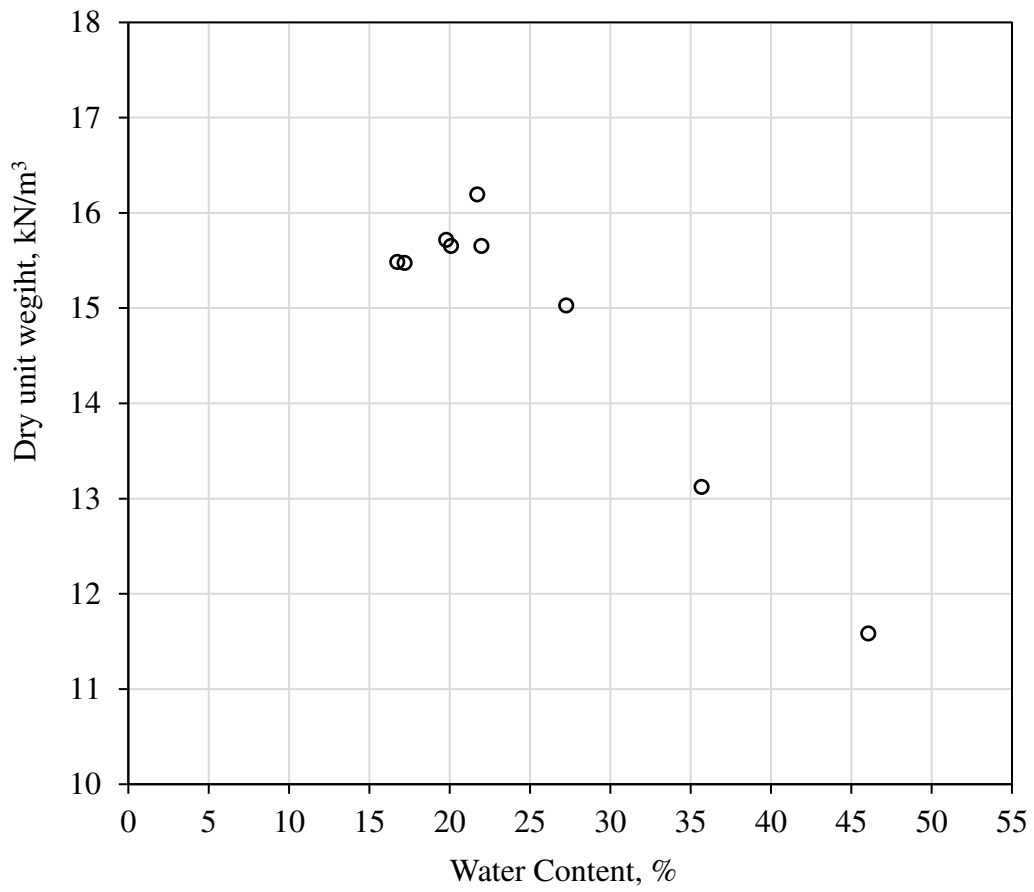


Figure 6.14 Dry unit weight vs. water content measurements using Proctor compaction.

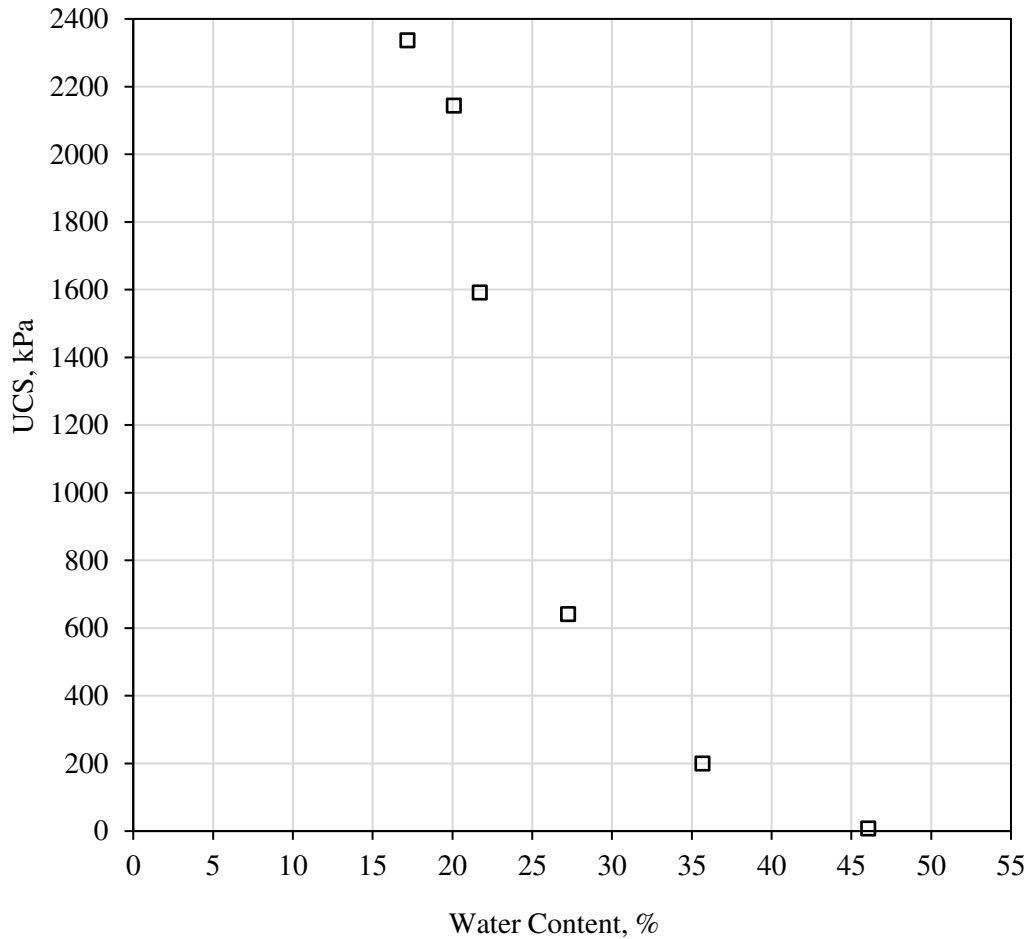


Figure 6.15 UCS vs. water content measurements using Penetrometer.

Secondly, a surcharge loading component, as shown in Figure 6.16 (a), was added to the SAI testing machine to explore the torque response with respect to the changes of surcharge loading and water content. The results are shown in Figure 6.16 (b) and (c), respectively. Figure 6.16 (b) clearly demonstrates that the system torque increased significantly when the surcharge pressure increased from 1 bar to 3 bar. Meanwhile, Figure 6.16 (c) verifies the potential impact of surcharge loading on torque responses, and consequently, clogging potential. Note that due to the limitation of the machine motor capacity, some critical portion of the curves are missing and are represented by the dashed lines in the plot. Modification of the motor and the gear box to provide higher torque output capacity is essential to proceed with a comprehensive study on the impact of pressure on clay clogging.

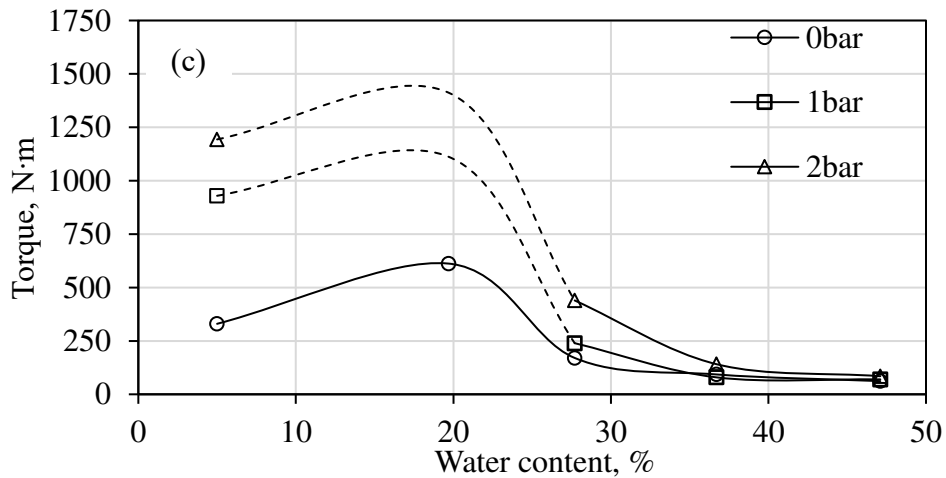
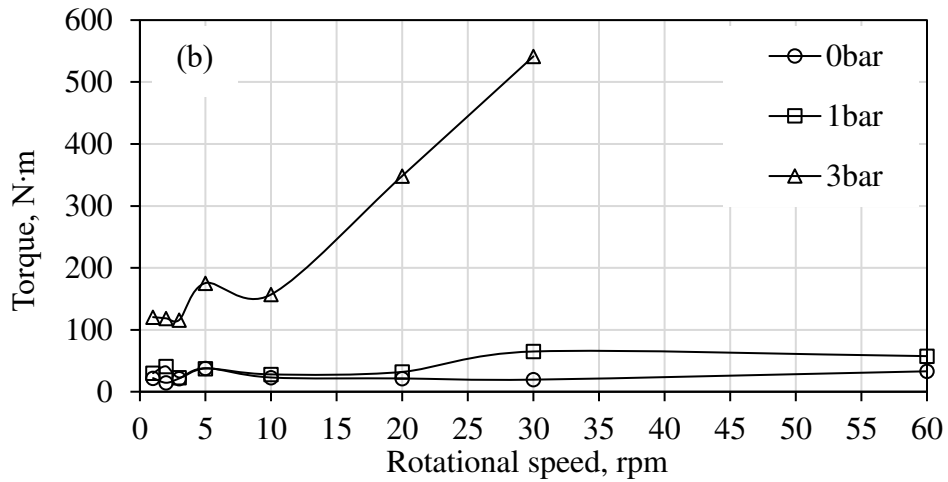


Figure 6.16 Torque measurement on Denver clay using SAI testing machine with surcharge loading: (a) surcharging loading component; (b) torque vs. rotational speed curves for three surcharge loading pressures at $w=27.3\%$; and (c) torque vs. water content curves for three surcharge loading pressures at a rotational speed of 60 rpm. The dashed lines indicate missing data due to limitation of the machine motor capacity.

6.5 Conclusions

A viable mixing method needs to be developed to generate sufficiently homogeneous foam conditioned clay. The chapter started with the effort to mix Denver clay with liquid and expanded it to mixing the clay with foam. The results show that there is no problem to mix Denver clay with liquid provided the clay is pulverized before mixing. On the contrary, the clay and the foam do not mix well using the current mixing tools. This is partially due to the low permeability of the clay and partially because of the drastic contrast of density between the clay and the foam. In addition, time constraint also adds to the difficulty of mixing.

Rheology testing results of Denver clay and CSM sand mixture show that the higher clay vs. sand ratio, the higher water content is required to achieve the expected rheological response of the mixture. Although it is not practical or recommended to inject sand to the cutting face and TBM chamber while tunneling in clayey ground, it is possible to do it in the reversed way, i.e., to inject slurry to the muck during tunneling in sandy ground to achieve desired flowability and viscosity.

It is important to note that the most severe clogging region revealed by torque measurement using the 10 deg. pitched propeller does not directly overlap the areas identified by the Consistency Index and the Empirical Stickiness Ratio approaches. While this observation requires additional investigation and comparison with field observations, it still shows the possibility of encountering severe clogging even outside of the critical ranges predicted by the Consistency Index and the Empirical Stickiness Ratio methods. This difference implies that more influencing factors, especially face pressure, should be considered for evaluating clay clogging although water content is still one of the dominant factors.

CHAPTER 7

CONCLUSIONS, CONTRIBUTIONS AND RECOMMENDATIONS

This thesis aimed to advance the knowledge of soil property evaluation as a function of various conditioning methods by offering a quantitative measurement system for application in the range of soil conditions as encountered in EPBM tunneling. The major contribution of the thesis is the development of a new large-scale rheology measurement system of conditioned soil in a step-by-step approach involving the design of experiments, implementation, and validation. The thesis also explores the measures to tackle challenges of characterizing properties of conditioned sand and clay in the same application. The achievement of this thesis is expected to be extended in the future to establish an on-site intelligent EPB shield operating system with both predictive and real-time assessment capabilities which could help manufacturers to design optimal configurations of cutterhead and excavation chamber, screw conveyor, and conditioning system. It also allows contractors to reasonably control machine operational parameters before the start of tunneling, or during the course of construction. Such a system can ideally assist the operators to make proper decisions about machine operational and soil conditioning parameters. With such an intelligent system together with experienced crews, EPB machine advance rate is expected to improve due to optimal operation of the machine, reduced power consumption and less wear on the machine, and hence reduced downtime. The following summarizes concluding remarks and major contributions from this thesis and proposes some recommendations for future work.

7.1 Conclusions from each chapter

Brief review of the available literature showed the knowledge gaps in the field of quantitative assessment of rheology of conditioned soil, which is an essential component of numerical modeling of material flow in the cutterhead, cutting chamber, and screw conveyor of EPB machines.

This study examined the feasibility of using existing small-scale rheometers to measure yield stress and viscosity of conditioned soils. The rheometers are TA Instruments products named ARES-G2 and HR-3. The gaps between the vane and the cell of the two rheometers are 6.5 mm and 1 mm, respectively. The testing proved that torque and axial force capacities of these rheometers are limited for study of the conditioned soil, which further restricted their applications

in testing rheology of soils. Therefore, it was deemed necessary to develop large-scale rheology measurement systems for application in EPB tunneling.

Investigating the viability of converting the Soil Abrasion Index testing machine to a desired large-scale rheometer for measuring rheology of conditioned soil was accomplished in this study. A Variable Frequency Drive was incorporated into the existing Soil Abrasion Index Testing Machine, which allows for the propeller to spin at a rotational speed range between 0 rpm and 1000 rpm. The pitched propeller with 10 deg inclination angle was used as a preliminary propeller geometry. Calibration of the device in air and water demonstrated that negligible torque was generated, and the device is capable of measuring the required torque at required accuracy for the purposes of evaluating soil properties. Testing on CSM sand indicated that a rotational speed greater than 3 rpm should be used, and that the Bingham plastic model is applicable to describe soil rheological behaviors. Also, differences between ramping up and ramping down the speed are negligible. The proposed method for determining yield stress and viscosity includes combination of experimental work and CFD modeling and a subsequent back calculation. The experimental work generates torque vs. rotational speed relationships while the rheology is still unknown. The CFD modeling generates torque vs. rotational speed relationships for specific soil rheology. A combination of both physical measurement and numerical modeling allows for the derivation of yield stress and viscosity of corresponding soil conditions.

A parametric study using CFD modeling proved that an auger geometry with a similar diameter to the 10 deg pitched propeller is the preferred geometry for development of the rheology measurement system.

The ability and validity of the proposed large-scale rheology measurement system was examined as a follow up to the original design and fabrication, along with calibration of the testing unit and combined modeling efforts. The system is based on the components from the preliminary unit or SAI testing system, using the optimized auger geometry to offer higher level of sensitivity towards variations in properties of conditioned soil, namely viscosity and yield strength. A parametric study and related experiments showed better performance of the auger propeller configuration as compared to the original 10 degree pitched propeller. The optimized auger is a single-flight setting with a diameter and a height of 296 mm and 292 mm, respectively. Depending on the magnitude of the torque response, another flight could be added to generate more sensitivity to torque when testing soil samples conditioned by foam. The standard procedure of the experiment

work includes ramping up and ramping down the rotational speed once for eight different speeds, including 3 rpm, 5 rpm, 10 rpm, 20 rpm, 30 rpm, 40 rpm, 50 rpm and 60 rpm. For testing on foam conditioned soils, the testing duration of 1 min at each rotational speed seems to be sufficient. For testing on soils without foam, the testing duration of 2 min can produce enough data points for averaging in highly variable conditions. The interval between adjacent rotational speeds is suggested to be 1 min.

The effects of eight influencing factors on soil rheology were investigated. These include auger geometry, water content, soil type, foam conditioning, passing of time, ambient pressure, ramping sequence, and compressibility setting. The proposed auger with similar dimensions was confirmed to be suitable for testing conditioned soil by generating sensible and distinguishable torque values while allowing the materials to circulate within the chamber. With the change of water content, yield stress and viscosity peak at water content of 7.5% for CSM sand and drop by either increasing or decreasing water content from the peak. The relationships between soil rheology, including slump value, and foam conditioning parameters were established for CSM sand and work as a successful demonstration for future testing on other granular soils. The stability of conditioned soil was studied by comparing the rheology response at different time intervals. The results show that the torque values overlap within 2h, indicating that the foam conditioned granular soil can sustain its rheological behaviors for a sufficient amount of time, and consequently, allow for the testing window to live up to the requirements of testing different impacting factors with the same batches of conditioned soil.

This study also explored the challenges related to testing conditioned clay and the potential tackling measures moving forward. The primary challenge was to find a way to mix the clay and foam homogeneously and quickly. The results show that none of the six methods tested is able to provide satisfactory clay-foam mixture for large-scale testing, while the clay and any form of liquid can be mixed with reasonable results.

Rheology testing results of clay and sand mixture show that the higher clay vs. sand ratio, the higher water content is required to achieve the desired rheological response of the mixture. In addition, it is a viable solution to inject slurry to the muck during tunneling in sandy ground to achieve desired flowability and viscosity.

Lastly, the study of conditioned clay showed the evidence of severe clay clogging at a water content range different from that estimated by the existing Consistency Index and Empirical

Stickiness Ratio approaches. It is suggested that the face pressure is an important missing factor to be considered for clogging evaluation even though water content is still one of the dominant factors. The clogging potential of conditioned fine-grained soil and clays can also be assessed with our proposed new soil rheology testing unit through the monitoring of torque. The advantage of this approach is the ability to incorporate the impacts of pore pressure and surcharge stresses in the ground on the clogging behavior of the native or conditioned soil.

To summarize, the primary contribution of this thesis is the development of a large-scale soil rheology measurement system for application in EPBM tunneling. The proposed new system is capable of quantifying the impact of soil conditioning on rheology of conditioned soil and deriving the critical rheological parameters including viscosity and yield stress of the mixture that are essential for modeling of material flow in the machine during the operation. In addition, the impacts of c_f , FIR , and FER on the behaviors of selected sand samples were examined and characterized. Moreover, while various methods for mixing of the clay and foam were tested, the ability of the proposed soil rheometry in characterizing the properly mixed samples of clay-liquid and clay-sand was demonstrated.

With the current version of the newly developed measurement system, however, there are also several limitations for measuring rheology of conditioned soil, as summarized in Table 7.1. These include limitation in the operational range of the rotational speed, a gap to readily apply total pressure, limited torque output to test firm soils, and no viable means to prepare foam conditioned clay for rheology testing.

7.2 Recommendations for future work

This thesis is an early stage study of developing an on-site intelligent EPB shield operating system. So far, the newly developed large-scale rheology measurement system with the proposed rheology characterization method has demonstrated its capability in evaluating rheology of conditioned soil while some limitations need to be addressed. To reach the ultimate goal of having such an intelligent system, however, more work needs to be conducted in the future. Some of the highlights of required future research on this topic and recommended follow-up work are offered as follows.

(1) One of the priorities is to keep trying to find a solution to mix foam and clay homogeneously and quickly for the purpose of rheology testing of conditioned clay using the measurement system in this thesis.

Table 7.1 Limitations of the current version of the newly developed rheology measurement system.

Category	Limitations
1. Experimental component	<p>(1) A rotational speed smaller than 3 rpm is deemed beyond the measurement accuracy of the device.</p> <p>(2) Total pressure, i.e., the sum of pore pressure and effective pressure, is not readily applied on the conditioned soil even though a makeshift surcharge loading plate can apply pressure on relatively firm soils.</p> <p>(3) The power of the rheometer's motor is 3.7 kW. Based on current gear box configuration, it offers limited torque output to test some difficult soil conditions such as very abrasive sand and compacted firm clay.</p>
2. Testing material	<p>(1) The system is likely to run into difficulty when testing very abrasive sand.</p> <p>(2) Clay with very high stickiness is not readily tested because of difficulties in the loading operation.</p> <p>(3) The system has not tested foam conditioned clay due to obstacle in mixing clay and foam.</p>

(2) Once such a desired mixing solution is found, a series of rheology measurement tests need to be conducted in foam conditioned clay. The suggested experimental program includes similar evaluation matrix presented in this study where pertinent c_f , FIR , and FER values are changed and the impacts of these parameters on the soil behaviors are assessed.

(3) Clay clogging evaluation considering potential impact of pressure conditions should be further explored. This may include an upgrading of the current device motor or gear box to enable higher torque output to test firmer soil conditions under compaction.

(4) More rheology testing of different types of soils at different water content levels and foam conditioning parameters need to be conducted. This includes not only obtaining new types of soils for rheology testing but extending the existing foam conditioning parameter ranges to investigate the boundary of rheological properties and phases, as well as repeating experiments with existing conditions to develop a statistically meaningful database for evaluation of the rheology of conditioned soils and variations with soil conditioning parameters.

(5) With the expanded soil rheology database, the relationships between soil rheology, i.e., yield stress and viscosity, and soil conditioning settings such as w , c_f , FER , FIR need to be further established. Subsequently, a classification system of conditioned soils based on rheology can be established. The concept and model correlating soil conditioning settings and soil rheology would help for optimization of proper soil conditioning.

(6) Lastly, effort shall be further extended to modeling material flow and EPB machine cutterhead and screw conveyor response during certain machine operations, including the required torque on the cutterhead and screw conveyor, pressure and flow velocity of the muck at various locations in the machine, contact stress between the muck and machine components, and optimal operating conditions for the machine. The results of such modeling should be validated with field data and observations.

REFERENCES

- ASTM Standard D2487, 2017, "Standard Practice for Classification of Soils for Engineering Purposes (Unified Soil Classification System)," ASTM International, West Conshohocken, PA, 2018, DOI: 10.1520/D2487-17E01, www.astm.org.
- Alavi, E., J. Rostami, and A. M. Palomino. 2011. "New Soil Abrasion Testing Method for Soft Ground Tunneling Applications." *Tunnelling and Underground Space Technology*, 26: 604–613. Elsevier Ltd. <https://doi.org/10.1016/j.tust.2011.04.003>.
- Alavi, E. 2013. "Development of A Soil Abrasion Test and Analysis of Impact of Soil Properties on Tool Wear for Soft-ground Mechanized Tunneling." PhD diss., *Pennsylvania State University*.
- Alavi, E., T. Qiu, and J. Rostami. 2013. "Evaluation of Granular Soil Abrasivity for Wear on Cutting Tools in Excavation and Tunneling Equipment." *Journal of Geotechnical and Geoenvironmental Engineering*, 139: 1718–26. [https://doi.org/10.1061/\(ASCE\)GT.1943-5606.0000897](https://doi.org/10.1061/(ASCE)GT.1943-5606.0000897).
- Alavi, E., J. Rostami, and K. Talebi. 2014. "Experimental Study of the Effect of Conditioning on Abrasive Wear and Torque Requirement of Full Face Tunneling Machines." *Tunnelling and Underground Space Technology*, 41: 127–136. Elsevier Ltd. <https://doi.org/10.1016/j.tust.2013.12.003>.
- Ball, R. P. A., D. J. Young, J. Isaacson, et al. 2009. "Research in Soil Conditioning for EPB Tunneling through Difficult Soils." In *Rapid Excavation & Tunneling Conference (RETC)*, Las Vegas, USA, June 14-17, 2009, 1–16.
- Barzegari, G., A. Uromeihy, and J. Zhao. 2013. "A Newly Developed Soil Abrasion Testing Method for Tunnelling Using Shield Machines." *Quarterly Journal of Engineering Geology and Hydrogeology*, 46: 63–74. <https://doi.org/10.1144/qjegh2012-039>.
- BASF. 2018. "Technical Data Sheet of MasterRoc ACP 127." BASF Corporation. 2018.
- Bhattacharai, A., S. K. Chatterjee, and T. P. Niraula. 2013. "Effects of Concentration, Temperature and Solvent Composition on Density and Apparent Molar Volume of the Binary Mixtures of Cationic-Anionic Surfactants in Methanol – Water Mixed Solvent Media." *SpringerPlus*, 2 (280): 1–9. <https://doi.org/10.1186/2193-1801-2-280>.
- Borio, L., and D. Peila. 2010. "Study of the Permeability of Foam Conditioned Soils with Laboratory Tests." *American Journal of Environmental Sciences*, 6 (4): 365–370. <https://doi.org/10.3844/ajessp.2010.365.370>.
- Budach, C., and M. Thewes. 2015. "Application Ranges of EPB Shields in Coarse Ground Based on Laboratory Research." *Tunnelling and Underground Space Technology*, 50: 296–304. <https://doi.org/10.1016/j.tust.2015.08.006>.
- Comsol Inc. 2018. *COMSOL Multiphysics Reference Manual*.
- Oliveira D. G. G., M. S. Diederichs, M. Thewes, et al. 2017. "EPB Conditioning of Mixed

- Transitional Ground: Investigating Preliminary Aspects.” In *Proceedings of the World Tunnel Congress 2017 – Surface Challenges – Underground Solutions*. Bergen, Norway.
- Djeran-Maigre, I., P. Dubujet, and T. M. Vogel. 2018. “Variation over Time of Excavated Soil Properties Treated with Surfactants.” *Environmental Earth Sciences*, 77: 67. Springer Berlin Heidelberg. <https://doi.org/10.1007/s12665-018-7230-z>.
- Duarte, M. Á. P. 2007. “Foam as a Soil Conditioner in Tunnelling: Physical and Mechanical Properties of Conditioned Sands.” PhD diss., *University of Oxford*.
- EFNARC. 2005. “Specification and Guidelines for the Use of Specialist Products for Mechanised Tunnelling (TBM) in Soft Ground and Hard Rock.” Vol. 44.
- Ewoldt, R. H., M. T. Johnston, and L. M. Caretta. 2015. “Experimental Challenges of Shear Rheology: How to Avoid Bad Data.” In *Complex Fluids in Biological Systems: Experiment, Theory, and Computation*, edited by S. E. Spagnolie, 207–241. New York: Springer New York. https://doi.org/10.1007/978-1-4939-2065-5_6.
- Farrokh, B., and A. S. Khan. 2010. “A Strain Rate Dependent Yield Criterion for Isotropic Polymers : Low to High Rates of Loading.” *European Journal of Mechanics A/Solids*, 29 (2): 274–282. <https://doi.org/10.1016/j.euromechsol.2009.08.004>.
- Feinendegen, M., M. Ziegler, G. Spagnoli, et al. 2011. “Evaluation of the Clogging Potential in Mechanical Tunnel Driving with Evaluation of the Clogging Potential in Mechanical Tunnel Driving with EPB-Shields.” In *Proceedings of the 15th European Conference on Soil Mechanics and Geotechnical Engineering*, 1633–1637. <https://doi.org/10.3233/978-1-60750-801-4-1633>.
- Ferraris, C. F. 1999. “Measurement of the Rheological Properties of High Performance Concrete: State of the Art Report.” *Journal of Research of the National Institute of Standards and Technology*, 104 (5). <https://doi.org/10.6028/jres.104.028>.
- Freimann, S., M. Galli, and M. Thewes. 2017. “Rheology of Foam-Conditioned Sands : Transferring Results from Laboratory to Real-World Tunneling.” In *9th International Symposium on Geotechnical Aspects of Underground Construction in Soft Ground IS – Sao Paulo, 2017*.
- Hollmann F. S., M. Thewes, and M. Weh. 2014. “Influence of Clogging on Muck Transport in Shield Machines.” *Tunnel*, 3: 10–19.
- Galli, M. 2016. “Rheological Characterization of Earth-Pressure-Balance (EPB) Support Medium Composed of Non-cohesive Soils and Foam.” PhD diss., *Ruhr-Universität Bochum*.
- Galli, M., and M. Thewes. 2014. “Investigations for the Application of EPB Shields in Difficult Grounds (Untersuchungen für den Einsatz von Erddruckschilden in schwierigem Baugrund)” *Geomechanics and Tunneling*, 7 (1): 31–44. <https://doi.org/10.1002/geot.201310030>.
- Galli, M., and M. Thewes. 2016. “Rheology of Foam - Conditioned Sands in EPB Tunneling.” In *World Tunnel Congress San Francisco*, 1–10.
- Galli, M., and M. Thewes. 2019. “Rheological Characterisation of Foam-Conditioned Sands in EPB Tunneling.” *International Journal of Civil Engineering*, 17(1): 145–160.

<https://doi.org/10.1007/s40999-018-0316-x>.

- Godinez, R., H. Yu, M. Mooney, et al. 2015. "Earth Pressure Balance Machine Cutterhead Torque Modeling: Learning from Machine Data." In *Proceedings of the Rapid Excavation and Tunneling Conference 2015*, 1261–1271.
- Graco. 2019. *Instructions on ToughTek CM-Series Continuous Mixers, 3A4350J*.
- Hedayatzadeh M., J. Rostami, D. Peila, et al. 2017. "Development of a Soil Abrasion Test and Analysis of Impact of Soil Properties on Tool Wear for Soft-Ground Mechanized Tunneling Using EPB Machines." In *Proceedings of the World Tunnel Congress 2017*, 1–6.
- Hollmann, F. S., and M. Thewes. 2013. "Assessment Method for Clay Clogging and Disintegration of Fines in Mechanised Tunnelling." *Tunnelling and Underground Space Technology*, 37: 96–106. Elsevier Ltd. <https://doi.org/10.1016/j.tust.2013.03.010>.
- Hu, W., and J. Rostami. 2020. "A New Method to Quantify Rheology of Conditioned Soil for Application in EPB TBM Tunneling." *Tunnelling and Underground Space Technology*, 96: 103192. <https://doi.org/10.1016/j.tust.2019.103192>.
- Jakobsen, P. D., A. Bruland, and F. Dahl. 2013. "Review and Assessment of the NTNU/SINTEF Soil Abrasion Test (SATTM) for Determination of Abrasiveness of Soil and Soft Ground." *Tunnelling and Underground Space Technology*, 37: 107–114. Elsevier Ltd. <https://doi.org/10.1016/j.tust.2013.04.003>.
- Jakobsen, P. D., L. Langmaack, F. Dahl, et al. 2013. "Development of the Soft Ground Abrasion Tester (SGAT) to Predict TBM Tool Wear, Torque and Thrust." *Tunnelling and Underground Space Technology*, 38: 398–408. <https://doi.org/10.1016/j.tust.2013.07.021>.
- Kundu, P. K., I. M. Cohen, and D. R. Dowling. 2012. *Fluid Mechanics*. Fifth Edition. Elsevier. <https://doi.org/10.1016/B978-0-12-382100-3.10010-1>.
- Langmaack, L. 2000. "Advanced Technology of Soil Conditioning in EPB Shield Tunnelling." In *North American Tunneling Proceedings*, 1–16.
- Lu, N., W. J. Likos. 2006. "Suction Stress Characteristic Curve for Unsaturated Soil." *Journal of Geotechnical and Geoenvironmental Engineering*, 132 (February): 131–142. [https://doi.org/10.1061/\(ASCE\)1090-0241\(2006\)132](https://doi.org/10.1061/(ASCE)1090-0241(2006)132).
- Lu, N., and W. J. Likos. 2004. *Unsaturated Soil Mechanics*. John Wiley & Sons, Inc.
- Malvern Instruments Worldwide. 2016. *A Basic Introduction to Rheology*.
- Meng, Q., F. Qu, and S. Li. 2011. "Experimental Investigation on Viscoplastic Parameters of Conditioned Sands in Earth Pressure Balance Shield Tunneling." *Journal of Mechanical Science and Technology*, 25: 2259–2266. <https://doi.org/10.1007/s12206-011-0611-9>.
- Merritt, A. S., and R. J. Mair. 2006. "Mechanics of Tunnelling Machine Screw Conveyors: Model Tests." *Géotechnique*, 56: 605–615. <https://doi.org/10.1680/geot.2008.58.2.79>.
- Merritt, A. S., and R. J. Mair. 2008. "Mechanics of Tunnelling Machine Screw Conveyors: A Theoretical Model." *Géotechnique*, 58: 79–94. <https://doi.org/10.1680/geot.2008.58.2.79>.

- Merritt, A. S. 2004. “Conditioning of Clay Soils for Tunnelling Machine Screw Conveyors.” PhD diss., *University of Cambridge*.
- Messerklinger, S., R. Zumsteg, and A. M. Puzrin. 2011. “A New Pressurized Vane Shear Apparatus.” *Geotechnical Testing Journal*, 34: 112–121. <https://doi.org/10.1520/GTJ103175>.
- Mitsoulis, E. 2007. “Flows of Viscoplastic Materials: Models and Computations.” *Rheology Reviews*, 135–178. [https://doi.org/10.1016/S0045-7949\(96\)00167-8](https://doi.org/10.1016/S0045-7949(96)00167-8).
- Mori, L. 2016. “Advancing Understanding of the Relationship between Soil Conditioning and Earth Pressure Balance Tunnel Boring Machine Chamber and Shield Annulus Behavior.” PhD diss., *Colorado School of Mines*.
- Mori, L., E. Alavi, and M. Mooney. 2017. “Apparent Density Evaluation Methods to Assess the Effectiveness of Soil Conditioning.” *Tunnelling and Underground Space Technology*, 67:175–186. Elsevier. <https://doi.org/10.1016/j.tust.2017.05.006>.
- Mori, L., Y. Wu, M. Cha, et al. 2015. “Measuring the Compressibility and Shear Strength of Conditioned Sand under Pressure.” In *Proceedings of the Rapid Excavation and Tunneling Conference 2015*.
- Mosleh, M., W. Hu, and J. Rostami. 2019. “Introduction to Rock and Soil Abrasivity Index (RSAI).” *Wear*, 432–433: 202953. <https://doi.org/10.1016/j.wear.2019.202953>.
- Nazem, A. 2017. “Mixing Mechanism.” *Personal Correspondence*.
- Nazem, A., M. Mooney, and Y. Wu. 2018. “Experimental Evaluation of Soil-Foam Mixing under Pressure.” In *World Tunnel Congress*.
- Nelson, S. 2006. “The Time of Sands: Quartz-Rich Sand Deposits as a Renewable Resource.” *Electronic Green Journal*, 1 (24).
- Nilsen, B., F. Dahl, J. Holzhäuser, et al. 2007. “New Test Methodology for Estimating the Abrasiveness of Soils for TBM Tunneling.” In *Proceedings of the Rapid Excavation and Tunneling Conference 2007*, 104–116.
- Oliva, A. M., N. R. Hargrave, D. Feys, et al. 2015. “Simulation of Yield-Stress Fluid in a Rotational Rheometer: The Effect of Vane Geometry on the Accuracy of Measured Properties.” In *Proceedings of the 2015 COMSOL Conference*.
- Oliveira, D. G. G. 2018. “EPB Excavation and Conditioning of Cohesive Mixed Soils: Clogging and Flow Evaluation.” PhD diss., *Queen’s University*.
- Papanastasiou, T. C. 1987. “Flows of Materials with Yield.” *Journal of Rheology*, 31 (5): 385–404. <https://doi.org/10.1122/1.549926>.
- Paul, E. L., V. A. Atiemo-Obeng, and S. M. Kresta, eds. 2004. *Handbook of Industrial Mixing: Science and Practice*. Hoboken, New Jersey, Wiley-Interscience.
- Pei, X., X. Zhang, B. Guo, et al. 2017. “Experimental Case Study of Seismically Induced Loess Liquefaction and Landslide.” *Engineering Geology*, 223: 23–30. <https://doi.org/10.1016/j.enggeo.2017.03.016>.

- Peila, D. 2014. “Soil Conditioning for EPB Shield Tunneling.” *Journal of Civil Engineering*, 18 (3): 831–836. <https://doi.org/10.1007/s12205-014-0023-3>.
- Peila, D., A. Picchio, D. Martinelli, et al. 2016. “Laboratory Tests on Soil Conditioning of Clayey Soil.” *Acta Geotechnica*, 11:1061–1074. Springer Berlin Heidelberg. <https://doi.org/10.1007/s11440-015-0406-8>.
- Peila, D., C. Oggeri, and R. Vinai. 2007. “Screw Conveyor Device for Laboratory Tests on Conditioned Soil for EPB Tunneling Operations.” *Journal of Geotechnical and Geoenvironmental Engineering*, 133: 1622–1625. [https://doi.org/10.1061/\(ASCE\)1090-0241\(2007\)133:12\(1622\)](https://doi.org/10.1061/(ASCE)1090-0241(2007)133:12(1622)).
- Peila, D., A. Picchio, A. Chierigato, et al. 2012. “Test Procedure for Assessing the Influence of Soil Conditioning for EPB Tunneling on the Tool Wear.” In *World Tunnel Congress*.
- Plötze, M., R. Zumsteg, and A. M. Puzrin. 2013. “Effects of Dispersing Foams and Polymers on the Mechanical Behaviour of Clay Pastes.” *Géotechnique*, 63: 920–933. <https://doi.org/10.1680/geot.12.P.044>.
- Psomas, S. 2001. “Properties of Foam / Sand Mixtures for Tunnelling Applications.” Master's thesis, *University of Oxford*.
- Quebaud, S., M. Sibai, and J. P. Henry. 1998. “Use of Chemical Foam for Improvements in Drilling by Earth-Pressure Balanced Shields in Granular Soils.” *Tunnelling and Underground Space Technology*, 13 (2): 173–180. [https://doi.org/10.1016/S0886-7798\(98\)00045-5](https://doi.org/10.1016/S0886-7798(98)00045-5).
- Roby, J., and D. Willis. 2014. “Achieving Fast EPB Advance in Mixed Ground: A Study of Contributing Factors.” In the *Proceedings of North American Tunneling Conference*, 182–194.
- Rostami, J., E. Alavi, A. M. Palomino, et al. 2012. “Development of Soil Abrasivity Testing for Soft Ground Tunneling Using Shield Machines.” *Tunnelling and Underground Space Technology*, 28: 245–256. <https://doi.org/10.1016/j.tust.2011.11.007>.
- Roussel, N., and P. Coussot. 2005. “‘Fifty-Cent Rheometer’ for Yield Stress Measurements: From Slump to Spreading Flow.” *Journal of Rheology*, 49 (3): 705–718. <https://doi.org/10.1122/1.1879041>.
- Samaniuk, J. R., C. T. Scott, T. W. Root, et al. 2012. “Rheological Modification of Corn Stover Biomass at High Solids Concentrations.” *Journal of Rheology*, 56 (3): 649–665. <https://doi.org/10.1122/1.3702101>.
- Samaniuk, J. R., T. W. Shay, T. W. Root, et al. 2014. “A Novel Rheometer Design for Yield Stress Fluids.” *AIChE Journal*, 60: 1523–1528. <https://doi.org/10.1002/aic>.
- TA Instruments. 2017. *ARES-G2 Rheometer*.
- TA Instruments. 2019. *The Discovery Hybrid Rheometer*.
- Talebi, K., H. Memarian, J. Rostami, et al. 2015. “Modeling of Soil Movement in the Screw Conveyor of the Earth Pressure Balance Machines (EPBM) Using Computational Fluid Dynamics.” *Tunnelling and Underground Space Technology*, 47: 136–142. Elsevier Ltd.

<https://doi.org/10.1016/j.tust.2014.12.008>.

- Thewes, M. 1999. “Bergische Universität Gesamthochschule Wuppertal Fachbereich Bauingenieurwesen Bodenmechanik Und Grundbau Beim Tunnelvortrieb Mit Flüssigkeitsschilden.” PhD diss., *Bergische Universität*.
- Thewes, M., and W. Burger. 2004. “Clogging Risks for TBM Drives in Clay.” *Tunnels & Tunneling International*, 2004.
- Thewes, M., and F. Hollmann. 2016. “Assessment of Clay Soils and Clay-Rich Rock for Clogging of TBMs.” *Tunnelling and Underground Space Technology*, 57: 122–128. Elsevier Ltd. <https://doi.org/10.1016/j.tust.2016.01.010>.
- Thuro, K., J. Singer, H. Kasling, et al. 2007. “Determining Abrasivity with the LCPC Test.” In *1st Canada - U.S. Rock Mechanics Symposium, 27-31 May, Vancouver, Canada, 1973–1980*. <https://doi.org/10.1201/NOE0415444019-c103>.
- Chen, T. 2000. “Rheological Techniques for Yield Stress Analysis.” TA Instruments.
- Vinai, R., C. Oggeri, and D. Peila. 2008. “Soil Conditioning of Sand for EPB Applications: A Laboratory Research.” *Tunnelling and Underground Space Technology*, 23: 308–317. <https://doi.org/10.1016/j.tust.2007.04.010>.
- Vipulanandan, C., and A. S. Mohammed. 2014. “Hyperbolic Rheological Model with Shear Stress Limit for Acrylamide Polymer Modified Bentonite Drilling Muds.” *Journal of Petroleum Science and Engineering*, 122: 38–47. <https://doi.org/10.1016/j.petrol.2014.08.004>.
- Wright, A. J., M. G. Scanlon, R. W. Hartel, et al. 2001. “Rheological Properties of Milkfat and Butter Concise Reviews in Food Science.” *Journal of Food Science*, 66 (8): 1056–1071. <https://doi.org/10.1111/j.1365-2621.2001.tb16082.x>.
- Wu, Y. 2018. “Investigation on Foam Stability and Foam-Conditioned Soil Properties under Pressure in EPB TBM Tunneling.” PhD. diss., *Colorado School of Mines*.
- Zhong, Q. 2019. *Chapter 18. Food Rheology. Handbook of Farm, Dairy and Food Machinery Engineering*. Elsevier Inc. <https://doi.org/10.1016/B978-0-12-814803-7.00018-X>.
- Zumsteg, R., M. Plötze, and A. M. Puzrin. 2012. “Effect of Soil Conditioners on the Pressure and Rate-Dependent Shear Strength of Different Clays.” *Journal of Geotechnical and Geoenvironmental Engineering*, 138: 1138–1146. [https://doi.org/10.1061/\(ASCE\)GT.1943-5606.0000681](https://doi.org/10.1061/(ASCE)GT.1943-5606.0000681).
- Zumsteg, R., M. Plötze, and A.M. Puzrin. 2013. “Reduction of the Clogging Potential of Clays: New Chemical Applications and Novel Quantification Approaches.” *Geotechnique*, 63: 276–286. <https://doi.org/10.1680/geot.SIP13.P.005>.
- Zumsteg, R., and A. M. Puzrin. 2012. “Stickiness and Adhesion of Conditioned Clay Pastes.” *Tunnelling and Underground Space Technology*, 31: 86–96. Elsevier Ltd. <https://doi.org/10.1016/j.tust.2012.04.010>.

Personal correspondences:

- Rostami, J. 2019. Exchange notes when visiting China Railway Engineering Equipment Group

(CREG), China Railway Construction Heavy Industry (CRCHI), and communication with Herrenknecht.

Rostami, J., and W. Hu. 2019. Exchange notes on “clay clogging mechanisms and solutions” with Normet International Ltd.

Hu W. 2019. Exchange notes on “negative viscosity at high shear rate” with Dr. Joseph Samaniuk from Department of Chemical and Biological Engineering at Colorado School of Mines.

Web sources:

Kinnane P. 2013. <https://www.comsol.com/blogs/new-mixer-module-showcases-capabilities-comsol/>.

Wollblad C. 2018. <https://www.comsol.com/blogs/how-to-set-up-a-mesh-in-comsol-multiphysics-for-cfd-analyses/>.

Washington State Department of Transportation Flickr, n.d., Bertha – SR 99 Tunneling Machine, <<https://www.flickr.com/photos/wsdot/albums/72157675202550505/>>.

CONDAT, n.d., Foaming agents for EPB, <<https://www.condat-lubricants.com/product/sealant-foam-lubricant-tunnel-boring/foaming-agents-epb/>>.